Combined optogenetic and pharmacological analysis of 5-HT control of cortical microcircuitry

Cheryl So

Wolfson College

University of Oxford

A thesis submitted for the degree of

Doctor of Philosophy

Hilary 2023

Abstract

5-HT (5-hydroxytryptamine, serotonin) powerfully influences cognition and mood regulation. In the medial prefrontal cortex (mPFC), the intricate balance between excitation and inhibition in celluar microcircuits allow the generation of network oscillations that encode behaviour and cognition. In particular, parvalbumin-expressing interneurons (PVINs) act as key regulators of the excitatory/inhibitory balance. The precise interactions between the 5-HT system and these PVINs, however, are little understood. Using an array of modern neuroscience tools, this thesis provides a comprehensive report of interactions between the 5-HT system and different neuron subtypes in the mPFC, including PVINs.

In slice electrophysiology experiments, local application of 5-HT greatly increased the intrinsic excitability of genetically labelled PVINs in the mPFC via the 5-HT_{2A} receptor. Such 5-HT_{2A} receptor-mediated activation of PVINs was then demonstrated in *in vivo* silicon probe multi-unit recordings following the systemic administration of the 5-HT_{2A} receptor agonists DOI and psilocin. Pharmacological activation of the 5-HT_{2A} receptor suppressed slow wave oscillations and elevated multi-unit activity in the mPFC, possibly via the excitation of putative PVINs and the disruption of their correlated activity with neighbouring neurons.

With an optogenetic approach, the effects of physiologically evoked 5-HT on neural activity in the mPFC were determined. This methodology was first verified with immunohistochemistry as well as *in vitro* and *in vivo* electrophysiology, which revealed diverse firing properties of optotagged 5-HT neurons. Specifically, optotagged regular-firing 5-HT neurons tended to fire action potentials following light stimuli up to 20 Hz, whereas optotagged irregular-firing 5-HT neurons were unlikely to sustain spiking at higher frequencies. Optogenetic activation of 5-HT neurons induced frequency-dependent suppression of slow wave oscillations and increase in UP state duration. Changes in the firing rate of individual neurons, including PVINs, were mainly inhibitory, although excitatory effects and non-responders were also observed. Notably, optogenetic activation of 5-HT neurons at high frequencies disrupted the spiking correlation between putative PVINs and other neurons, once again providing a potential mechanism for 5-HT modulation of excitatory-inhibitory balance and local oscillations in the mPFC.

Collectively, this thesis presents concrete evidence for 5-HT modulation of microcircuit activity, including PVINs, in the mPFC. These findings highlight the importance of elucidating the actions of 5-HT on a cellular level in gaining a better understanding of how 5-HT shapes cortical network output and, ultimately, cognition.

Acknowledgements

First and foremost, I must express my sincerest thanks to Prof Trevor Sharp for his guidance and support throughout this project. I will always be grateful for his invaluable advice and insights that shaped my skills and perspective as a scientist. My gratitude extends to past and current members of the Sharp lab for the great company and all the knowledge they shared with me. Thanks to Dr Raquel Pinacho, Dr Helen Collins, and Sophie Gullino for sharing their statistical analysis and animal management expertise with me; to Dr Judith Schweimer and Ruairi O'Sullivan for showing me animal surgery and electrophysiology techniques; to Cara Fuller for helping me with immunohistochemistry experiments.

I wish to thank Dr Ed Mann for his help during my time in the Mann lab and for teaching me all things slice electrophysiology. Special thanks to Dr Julien Carponcy, who gifted me with electrophysiology equipment and shared valuable experimental knowledge with me.

Above all, I must thank those closest to me, without whom I would not have made it through the toughest times in the past few years. While my colleagues helped me grow as a scientist, my friends and family made all the personal and emotional growth throughout this journey possible.

To John, the rock in my life, thank you for being by my side through all the joyous and challenging moments. Thank you for believing in me when I forgot how to.

To Anita and Jeffrey, I would not be where I am today without your unwavering love and support. Thank you for always making me feel unconditionally loved, even from the other side of the world.

Contents

List of Figures

List of Abbreviations

5-HT 5-hydroxytryptamine

5-HTT . . . . . 5-HT transporter, also SERT

AAV . . . . . Adeno-associated virus

aCSF . . . . . Artificial cerebrospinal fluid

AHP . . . . . Afterhyperpolarisation

ANOVA . . . . Analysis of variance

auROC . . . . Area under the receiver operator characteristic curve

BW . . . . . Broad waveform

CCK . . . . . Cholecystokinin

Cg1 . . . . . Cingulate area 1

Cg2 . . . . . Cingulate area 2

ChR2 . . . . . Channelrhodopsin 2

cKO . . . . . Conditional knockout

CNS . . . . . Central nervous system

CV2 . . . . . Coefficient of variation between adjacent inter-spike intervals

DOI 2-5-dimethoxy-4-iodoamphetamine

DRD . . . . . Dorsal portion of the dorsal raphe nucleus

DRN . . . . . Dorsal raphe nucleus

DRV . . . . . Ventral portion of the dorsal raphe nucleus

EEG . . . . . Electroencephalography

eYFP . . . . . Enhanced yellow fluorescent protein

FDR . . . . . False discovery rate

FF . . . . . Fast-firing

GABA . . . . . γ-Aminobutyric acid

GAD . . . . . Glutamate decarboxylase

HHW . . . . . Half-hyperpolarisation width

i.p. . . . . . Intraperitoneal

IL . . . . . Infralimbic cortex

ISI . . . . . Inter-spike interval

LFP . . . . . Local field potential

LSD . . . . . Lysergic acid diethylamide

mPFC . . . . . Medial prefrontal cortex

MRN . . . . . Median raphe nucleus

MUA . . . . . Multi-unit activity

PBS . . . . . Phosphate-buffered saline

PFA . . . . . Paraformaldehyde

PFC . . . . . Prefrontal cortex

PHP . . . . . Prehyperpolarisation

PrL . . . . . Prelimbic cortex

PSD . . . . . Power spectral density

PTT . . . . . Peak-to-trough time

PV . . . . . Parvalbumin

PVIN . . . . . Parvalbumin-expressing interneuron

RMP . . . . . Resting membrane potential

ROC . . . . . Receiver operator characteristic

s.c. . . . . . Subcutaneous

SEM . . . . . Standard error of the mean

SERT . . . . . Serotonin (5-HT) transporter, also 5-HTT

SIR . . . . . Slow irregular

SR . . . . . Slow regular

SWA . . . . . Slow wave activity

TPH2 . . . . . Tryptophan hydroxylase 2

VGLUT3 . . . Vesicular glutamate transporter 3

VIP . . . . . Vasoactive intestinal peptide

1 General Introduction

1.1 Scope

The 5-HT (5-hydroxytryptamine; serotonin) system is critically involved in cortical function. 5-HT plays a key role in cognition and mood regulation, and represents a significant target for many psychiatric treatments such as antidepressants and antipsychotics. In particular, ascending 5-HT projections from the midbrain dorsal raphe nucleus (DRN) directly modulate and influence neuronal activity in the medial prefrontal cortex (mPFC), a cortical region associated with high-level cognitive functions in rodents and of high research interest.

Within the mPFC, intricate interactions between the excitatory output from pyramidal neurons and the inhibitory control of local circuits by GABAergic interneurons are thought to form the electrophysiological basis of cognition. In particular, parvalbumin-expressing interneurons (PVINs) represent a major class of cortical interneurons that are important for the generation of neurophysiological changes in the mPFC, such as high-frequency local oscillations thought to be crucial for cognitive performance. These PVINs have been reported to express 5-HT receptors, although their exact interactions with 5-HT *in vitro* and *in vivo* remain poorly understood.

As such, a central theme of this thesis is to investigate the interactions between

5-HT and the mPFC *in vitro* and *in vivo* with a focus on PVINs. Using recent technology, including targeted transgenic reporter mouse lines, multi-unit recording electrophysiology, and optogenetics, this thesis aims to address gaps in our knowledge and further advance the understanding of how 5-HT modulates the activity of mPFC neurons, in particular PVINs.

1.2 Medial prefrontal cortex

1.2.1 Medial prefrontal cortex and cognition

The prefrontal cortex (PFC) is a collection of interconnected neocortical areas that processes incoming sensory information and executes outgoing behaviour (Miller and Cohen, 2001). The PFC orchestrates executive functions associated with higher order cognitive tasks, such as behavioural flexibility, impulse control, decision making, sustained attention, and reversal learning (Funahashi and Andreau, 2013; Hardung et al., 2017).

The mPFC plays a vital role in coordinating "top-down" executive functions and is the most commonly featured subregion in rodent studies of the PFC (Miller and Cohen, 2001; Laubach et al., 2018). The mPFC consists of three subdivisions – the prelimbic, infralimbic, and anterior cingulate areas (Figure 1.1; Franklin and Paxinos, 2013). The prelimbic area is especially associated with cognitive flexibility, defined as the ability to alter one's behaviour in response to dynamic environmental conditions (Waltz, 2017). Impairments in cognitive flexibility are commonly observed in psychiatric disorders and often persist after treatment in depression and schizophrenia patients (Spellman et al., 2021).

Early lesion studies of the rat prelimbic/infralimbic cortex showed impaired behavioural flexibility (Ragozzino et al., 1999). Moreover, pharmacological inactivation of the rat prelimbic cortex was subsequently shown to impair the ability of

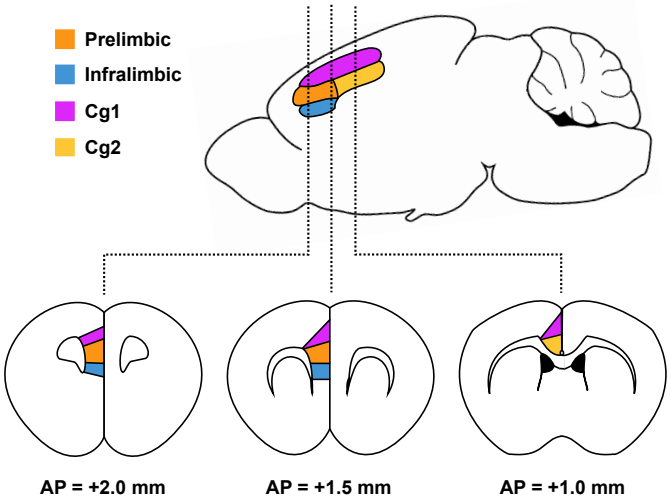

Figure 1.1: Schematic of anatomical subdivisions of the medial prefrontal cortex (mPFC) across the coronal plane. The prelimbic region is shown in orange, the infralimbic region is shown in blue, and the anterior cingulate areas Cg1 and Cg2 are shown in magenta and yellow, respectively. AP, anteroposterior coordinates from bregma. Anatomical areas were defined according to Paxino's Mouse Brain Atlas (Franklin and Paxinos, 2013). Image adapted from Francis-Oliveira et al. (2022).

animals to use contextual cues to resolve response conflict, a readout of cognitive flexibility (Marquis et al., 2007). More recently, Sharpe and Killcross (2015) showed that inactivation of the rat prelimbic cortex disrupted behavioural flexibility in an aversive setting, in which animals had to modulate their response towards stimuli in a fear conditioning context. Taken together, this evidence points to the importance of the integrity of mPFC function in cognitive processes that shape key executive functions. These functional studies, alongside the cytoarchitecture and anatomy of the rodent mPFC, provide evidence for homology with the primate dorsolateral PFC. As such, the rodent mPFC serves as a valuable model system for studying the precursors of higher level cognitive processes (Granon and Poucet, 2000).

1.2.2 Medial prefrontal cortex microcircuits and oscillations

At a cellular level, PFC activity is broadly defined by the interaction of local pyramidal cells and GABAergic interneurons, glutamatergic input from other

limbic structures, and neuromodulatory input by the 5-HT, catecholamine, and acetylcholine systems (Robbins, 2005; Caballero et al., 2021). Pyramidal cells are glutamatergic excitatory neurons that represent the majority of cortical neurons, whereas GABAergic inhibitory interneurons extensively innervate local circuits and shape the dynamics of the local network (Somogyi and Klausberger, 2005; Tremblay et al., 2016). Complex ensembles of excitatory and inhibitory neurons form microcircuits in the PFC and constitute the cellular basis of cognition. The resulting output of the mPFC therefore reflects the balance between these excitatory and inhibitory signals.

Excitatory signals from pyramidal neurons drive the entire local network, and in turn, rhythmic inhibition by interneurons synchronises the activity of pyramidal neurons to generate neural network oscillations of different frequencies, typically ranging from 0.1 to 100 Hz. These oscillations can encode behaviour by allowing efficient communication in local and distant neural circuits (Buzsáki and Draguhn, 2004; Jung and Carlén, 2021). In the mPFC, oscillations in the gamma range (30 − 80 Hz) are thought to be fundamental for the normal processing of executive functions (Fries, 2009). Abnormal oscillatory activities in the gamma band have been observed in the mPFC of psychiatric patients such as those with schizophrenia, who show clear cognitive impairment (Uhlhaas and Singer, 2010). Impairment of gamma oscillations has also been observed in patients with autism spectrum disorder, attention deficit hyperactive disorder, major depression, epilepsy, and Alzheimer's disease (Herrmann and Demiralp, 2005; Fitzgerald and Watson, 2018; Kayarian et al., 2020).

1.2.3 Medial prefrontal cortex architecture

In the mPFC, neurons are organised and distributed in layers that compute and integrate different inputs in specialised manners. The mPFC comprises layers I, II, III, V, and VI, as layer IV is absent (Merre et al., 2021).

Pyramidal projection neurons are distributed across layers II to VI, while layer I comprises axonal projections from other brain regions and sparsely arranged interneurons (Wu et al., 2009). Layer II/III pyramidal neurons receive inputs from layer I and send output to layer V/VI pyramidal neurons, which compute the incoming information from the cortical network and the thalamus (Francis-Oliveira et al., 2022). In rodent studies, layers V and VI are often combined and referred to as "deep layers" (Baker et al., 2018). These deep layer pyramidal neurons represent the primary source of output from the mPFC and project to many limbic and subcortical structures, including but not limited to the DRN, ventral tegmental area, amygdala, basal ganglia, and thalamus (Caballero et al., 2021). Deep layer prefrontal neurons are of particular research interest, as a recent study by Spellman et al. (2021) showed that projections from deep layers of the mPFC, mainly located in the prelimbic cortex, play a key role in enabling cognitive flexibility. Finally, long-range inputs from other brain regions arrive across all layers, fine tuning the excitatory/inhibitory balance in the PFC and sculpting its output (Anastasiades and Carter, 2021).

1.3 Cortical PV interneurons

1.3.1 Inhibitory neurons in the cortex

GABAergic inhibitory neurons represent approximately 15% of all neurons in the rodent cerebral cortex (Meyer et al., 2011). Despite being few in number, cortical interneurons are highly heterogeneous and their axons branch extensively throughout

local networks (Tremblay et al., 2016). There is a large diversity of cortical interneurons that differ in their morphology, electrophysiological properties, and biological markers (Klausberger and Somogyi, 2008). Thus far, more than 15 classes of interneurons have been identified in cortical brain circuits, and more subtypes may remain to be discovered (Sultan and Shi, 2018; Fishell and Kepecs, 2020).

In the rodent PFC, GABAergic interneurons are divided by their non-overlapping biological markers into three main categories: the calcium-binding protein parvalbumin (PV), the neuropeptide somatostatin (SST), and the ionotropic serotonin receptor (5-HT_3R; Llorca and Deogracias, 2022, see Figure 1.2). Parvalbumin-expressing interneurons (PVINs) constitute a major class of inhibitory neurons that target perisomatic regions and are typically characterised by their fast-spiking properties (Hu et al., 2014). SST interneurons, on the other hand, are dendrite-targeting and have heterogeneous firing characteristics (Lim et al., 2018). Finally, 5-HT_3R interneurons that also express vasoactive intestinal peptide (VIP) preferentially target other cortical interneurons and potentially modulate pyramidal neuron ensembles via disinhibitory mechanisms (Pi et al., 2013; Kullander and Topolnik, 2021). Alongside VIP, other notable cortical interneuron biomarkers include cholecystokinin (CCK), neuropeptide Y, calretinin, and calbindin. These biomarkers, except for VIP, are expressed in overlapping subpopulations of cortical interneurons (Tremblay et al., 2016).

1.3.2 PVINs in the mPFC

PVINs comprise about a third of the cortical interneuron population and represent the classical interneuron subtype, recognisable by their characteristic high-frequency firing and narrow action potentials (Bartos et al., 2001; Hu et al., 2014). PVINs can be subdivided into PV-expressing basket cells and PV-expressing chandelier cells,

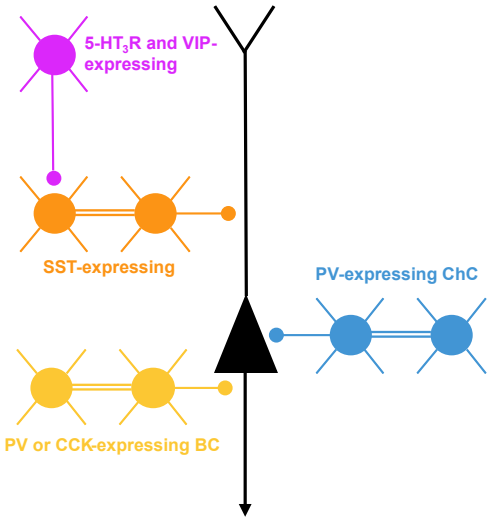

Figure 1.2: Schematic showing the broad subtypes of GABAergic interneurons in the mPFC, distinguished by their molecular markers and intercellular innervation targets. Double lines between interneurons represent electrical coupling. Circles represent synapses onto other interneurons or pyramidal cells (black). Modified with information taken from Hestrin and Galarreta (2005) and Taniguchi (2014). 5-HT: 5-hydroxytryptamine; VIP: vasoactive intestinal peptide; SST: somatostatin; PV: parvalbumin; BC: basket cell; CCK: cholecystokinin; ChC: chandelier cell.

also known as axo-axonic cells, based on their morphology and subcellular targeting domains. PV-expressing basket cells target the soma and proximal dendrites of pyramidal neurons and other interneurons, whereas PV-expressing chandelier cells exclusively target the axon initial segment of pyramidal cells (Somogyi and Klausberger, 2005). PV-expressing basket and chandelier cells are both reported to be fast-spiking interneurons despite subtle differences in their electrophysiological properties (Woodruff et al., 2009). It is, however, important to note that PV-expressing basket cells represent the majority, but not all, basket cells. A small basket cell subpopulation includes interneurons that express CCK rather than PV, which can be distinguished from their PV-expressing counterparts by their regular-spiking phenotype (Tremblay et al., 2016).

PV-expressing basket cells are found across layers II to VI but are most enriched in layer V. Some basket cells have largely local axons, while others have local and translaminar axons, enabling interlaminar interactions with neighbouring layers

(Tremblay et al., 2016). PV-expressing chandelier cells, on the other hand, are found in layers II and V/VI. They are highly specialised in their postsynaptic target and innervate multiple pyramidal cells at their axon initial segment (Blazquez-Llorca et al., 2015). Finally, a third type of PVIN has been identified as multipolar bursting cells located in superficial layers. They differ in morphology and electrophysiological characteristics from PV-expressing basket and chandelier cells but have not been studied as extensively (Blatow et al., 2003).

Owing to their fast-spiking phenotype and specialised axonal targeting of perisomatic regions, PVINs exert a significant influence on the output of pyramidal neurons by producing hyperpolarising and/or shunting inhibition (Cardin, 2018). Additionally, PVINs form a mutually connected network via gap junctions for enhanced synchronisation (Hestrin and Galarreta, 2005). Extensive gap junction coupling between interneurons is commonly observed in PVIN and SST interneuron populations, but only between cells of the same subtype and not across different classes (Cardin, 2018). There is evidence that PV-expressing basket and chandelier cells are electrically connected, however such connections are not as widespread as PV-expressing basket-to-basket connections (Hestrin and Galarreta, 2005).

1.3.3 PVINs and gamma oscillations

Inhibition is crucial in the generation of gamma range oscillations ($30 - 80$ Hz), which facilitate the transfer of information both within the mPFC and between the mPFC and other brain regions (Mann and Paulsen, 2007; Sohal et al., 2009; Buzśaki and Wang, 2012). PVINs, in particular, are the inhibitory neuron class known to contribute most to gamma oscillation generation (Sohal et al., 2009; Hu et al., 2014). PVINs are optimally positioned to powerfully regulate local network activities due to a combination of their fast-spiking characteristics, perisomatic-targeting axons,

and electrically connected network that enables high levels of synchrony (Naka and Adesnik, 2016). Indeed, PVINs have been shown in large-scale extracellular recordings to exhibit uniform and transient inhibition on pyramidal cells (Kvitsiani et al., 2013). PVINs are therefore able to act as rapid signalling devices that transmit high-frequency inhibition, sustaining synaptic transmission at gamma frequencies (Bartos et al., 2001). CCK-expressing basket cells, in contrast, do not fire fast enough to sustain gamma frequencies even though their axons also target perisomatic sites (Bartos et al., 2001).

Electrophysiological studies of PV-expressing basket cells revealed their participation in nearly every gamma cycle during kainite- and carbachol-induced oscillations in rat hippocampal slices (Hajós et al., 2004). In subsequent *in vivo* studies, PVINs were shown to be strongly phase-locked to gamma oscillations in awake mice (Hasenstaub et al., 2005; Perrenoud et al., 2016). In particular, the inhibition of PVIN activity suppressed gamma oscillations in the mouse mPFC *in vivo*, and the indirect optogenetic activation of PVINs was sufficient to initiate the generation of gamma-band rhythms (Sohal et al., 2009).

In a mouse model of impaired cognitive flexibility, abnormal function of PVINs and altered gamma oscillations were observed in the PFC (Cho et al., 2015). By pharmacologically enhancing fast GABAergic signalling, Cho et al. (2015) restored gamma oscillations and rescued the cognitive inflexibility phenotype. This adds to the evidence that PVIN synchronisation at gamma frequencies plays a crucial role in maintaining cognitive flexibility, one of the key functions of the mPFC. The close relationship between mPFC PVIN activity and elevated gamma-band oscillations is also demonstrated in attention control, another important cognitive process governed by the mPFC (Kim et al., 2016). Finally, post-mortem human brain studies of schizophrenic patients that showed molecular alterations and morphological deficiencies of PVINs in the PFC provide further evidence for the

importance of PVINs and gamma oscillations in normal prefrontal function (Lewis et al., 2012; Gonzalez-Burgos et al., 2015; Perlman et al., 2021). Lastly, it is necessary to note that PVINs are not the only class of interneurons that can contribute to gamma rhythms. While PVINs are uniquely positioned in their morphology, connectivity, and spiking characteristics for gamma rhythm generation, there is emerging evidence that other interneuron types, such as SST-expressing interneurons, may contribute to gamma oscillations (Antonoudiou et al., 2020).

1.4 The central 5-HT system

1.4.1 5-HT as a pharmacological target in psychiatric disorders

Dysregulation of the 5-HT system is widely implicated in neuropsychiatric disorders such as depression and anxiety and the cognitive impairments observed in these patients (Sharp and Cowen, 2011). The 5-HT system is strongly linked to mood regulation, and is targeted by a range of pharmacological treatments for mental disorders (Nemeroff and Owens, 2002; Cowen and Browning, 2015; Harmer et al., 2017). However, the exact role of 5-HT in mood disorders is unclear, and the longstanding theory of a causal relationship between low brain 5-HT levels and depression has been increasingly criticised (Moncrieff et al., 2022; Kendrick and Collinson, 2022).

More recently, emerging clinical research reports that psychedelic hallucinogens that are 5-HT_{2A} receptor agonists, such as psilocybin and lysergic acid diethylamide (LSD), have therapeutic potential in a wide range of psychiatric disorders, including major depression, addiction, and post-traumatic stress disorder (Nutt et al., 2020; Krediet et al., 2020). A recent clinical trial reported the rapid-onset antidepressant effects of a single dose of psilocybin in treatment-resistant depression (Goodwin

et al., 2022). In accordance with this, psychedelic drugs are reported to cause an increase in neural plasticity within 24 hours of a single dose (Kwan et al., 2022; Calder and Hasler, 2023).

Additionally, many atypical antipsychotic drugs act as dual dopamine and 5-HT_2 receptor antagonists (Pogorelov et al., 2017). It is hypothesised that dopamine antagonism is essential for treating positive symptoms in schizophrenia (e.g. hallucinations, psychosis), whereas 5-HT_{2A} antagonism is closely related to negative and cognitive symptoms such as social withdrawal as well as learning and attention deficits (Jones et al., 2020).

1.4.2 Neuroanatomical organisation of the 5-HT system

The mPFC receives ascending inputs from the major neuromodulatory 5-HT system, predominantly originating from the midbrain dorsal raphe nucleus (DRN; Michelsen et al., 2007). 5-HT neurons in the brain are organised in cell clusters, namely B1-B9, mostly along the midline and distributed across the midbrain and brainstem (Dahlström and Fuxe, 1964; Gaspar and Lillesaar, 2012). The caudal clusters (B1-B3) begin in the brainstem medulla oblongata and continue rostrally in the pons (B4-B5) and midbrain (B6-B9). Midbrain 5-HT neurons represent the majority of ascending projections of the 5-HT system, originating from the DRN (B6-B7) and median raphe nucleus (MRN; B5, B8, B9; Muzerelle et al., 2014). Of all raphe nuclei, the DRN is the largest and most enriched in 5-HT neurons, containing a third of all 5-HT neurons in the brain (Huang et al., 2019). Raphe nuclei consist of a heterogeneous population of neurons, with about 50% of DRN neurons being 5-HT containing (Deneris and Gaspar, 2018). Other neuron types present in the DRN include dopaminergic, GABAergic, glutamatergic, and peptidergic neurons

(Huang et al., 2019).

1.4.3 5-HT neuron connectivity

The 5-HT system projects extensively throughout the central nervous system (CNS), from the olfactory bulb to the spinal cord. Anatomical tracing studies showed that caudal raphe nuclei send descending 5-HT projections to the spinal cord, whereas rostral raphe nuclei represent the primary source of 5-HT inputs to the forebrain (Deneris and Gaspar, 2018).

Ascending 5-HT projections from the midbrain are topographically organised, with the DRN and MRN sending 5-HT axons that occupy complementary regions in the forebrain (Gaspar and Lillesaar, 2012). DRN 5-HT neurons preferentially project to the cortex, amygdala, locus coeruleus, and striatum, whereas MRN 5-HT neurons preferentially innervate limbic regions such as the septum and hippocampus (Muzerelle et al., 2014). Retrograde tracing of 5-HT efferents from the DRN showed that the mouse frontal cortex received 5-HT input primarily from the ventral subregion (DRV), whereas 5-HT projections to the amygdala originated from the dorsal subregion (DRD; Ren et al., 2018). This is supported by anterograde tracing studies that showed preferential targeting of the mPFC by the ventral but not dorsolateral B7 cluster in the mouse DRN (Muzerelle et al., 2014).

In turn, midbrain 5-HT neurons also receive dense inputs from the forebrain, including but not limited to the PFC, amygdala, nucleus accumbens, and hypothalamus (Deneris and Gaspar, 2018). PFC projections from the prelimbic cortex target 5-HT neurons (Dorocic et al., 2014; Weissbourd et al., 2014; Challis and Berton, 2015) as well as GABAergic interneurons (Varga et al., 2001; Jankowski and Sesack, 2004) in the DRN. Overall, anatomical evidence indicates that 5-HT neurons in the DRN form an intertwined network with the PFC via direct and indirect connections

through thalamocortical areas.

1.4.4 Chemical aspects of 5-HT neurotransmission

One of the common defining features of 5-HT neurons is their ability to synthesise 5-HT from the essential amino acid L-tryptophan. The biosynthesis of 5-HT involves the conversion of L-tryptophan to 5-hydroxytryptophan by the tryptophan hydroxylase (TPH), then to 5-HT by the aromatic L-amino acid decarboxylase. In the DRN, TPH2 represents the dominant isoform of TPH, although TPH1 is present during certain developmental stages (Gaspar and Lillesaar, 2012). Another critical feature of 5-HT neurons is the vesicular transport and reuptake of 5-HT. Once synthesised, 5-HT is packaged and stored in vesicles by the vesicular monoamine transporter 2 until release. Excess 5-HT in the extracellular space is then reabsorbed by the 5-HT transporter (5-HTT), also known as the serotonin transporter (SERT; Gaspar and Lillesaar, 2012).

Aside from the shared expression of essential markers described above, 5-HT neurons in the DRN demonstrate heterogeneity, and subpopulations express a number of different molecular markers (Okaty et al., 2020). Notably, some of these markers co-expressed by DRN 5-HT neurons are traditionally markers for neuronal cell types based on their neurotransmitter usage, such as vesicular glutamate transporter (VGLUT) for glutamatergic transmission and glutamate decarboxylase (GAD) for GABAergic transmission (Huang et al., 2019). Specifically, single-cell transcriptomic analysis of the mouse DRN revealed subpopulations of 5-HT neurons with non-overlapping expression of genetic markers for glutamatergic transmission (VGLUT3) and GABAergic transmission (GAD65 and GAD67; Huang et al., 2019). Anatomical studies show that these 5-HT neuron subtypes are spatially organised in a complementary fashion within the DRN. 5-HT/VGLUT3 neurons are enriched

in ventromedial, medial, and caudal parts of the DRN, whereas 5-HT/GAD neurons are preferentially distributed in the dorsal and lateral subregions of rostral DRN (Shikanai et al., 2012; Ren et al., 2018; Okaty et al., 2020).

Glutamate co-transmission represents an emerging area of research in 5-HT neuron function, as up to two-thirds of DRN 5-HT neurons also express VGLUT3 (Trudeau, 2004; Liu et al., 2014). Immunocytochemical evidence in mice demonstrated co-localisation of VGLUT3 in DRN 5-HT cell bodies and 5-HT axons in forebrain regions, including the PFC, hippocampus, and lateral septum (Amilhon et al., 2010). In particular, up to 60% of 5-HT varicosities in deep layers of the prelimbic cortex co-expressed VGLUT3 (Amilhon et al., 2010). In the same study, Amilhon et al. (2010) showed that VGLUT3 enhanced 5-HT neurotransmission by facilitating vesicular transport and release of 5-HT in these 5-HT/VGLUT3 terminals. In addition to simply facilitating 5-HT transmission, it has been demonstrated in electrophysiological and optogenetic studies that 5-HT neurons indeed functionally release glutamate and cause post-synaptic fast excitation via ionotropic glutamate receptors (Varga et al., 2009; Liu et al., 2014; Kapoor et al., 2016; Sengupta et al., 2017). The functional importance of VGLUT3 was highlighted in a VGLUT3-deficient mouse model with elevated anxiety-related behaviour and blunted amphetamine-induced locomotor effects (Amilhon et al., 2010; Mansouri-Guilani et al., 2019). However, the functional importance of VGLUT3, specifically in the context of 5-HT/glutamate co-transmission, is yet to be established (Mansouri-Guilani et al., 2019).

1.4.5 5-HT receptors

5-HT exerts its effects through 7 distinct families of receptors that comprise 14 subtypes (Barnes and Sharp, 1999; Sharp and Barnes, 2020). The majority of these

receptors are widely expressed in the central and peripheral nervous systems. 5-HT receptor subtypes differ in their pharmacology, distribution within the CNS, as well as actions at the molecular and whole organism levels (Barnes and Sharp, 1999). Other than the 5-HT_3 receptor, a pentameric ligand-gated ionotropic receptor, all 5-HT receptors belong to the G-protein coupled receptor family (Barnes and Sharp, 1999). Activation of these G-protein coupled 5-HT receptors results in modulatory actions on the resting membrane potential, in contrast to direct depolarisation and spiking caused by the 5-HT_3 receptor. Understanding the distinct roles of 5-HT receptor subtypes is therefore a key step to understanding 5-HT function and dysfunction. Table 1.1 provides a summary of 5-HT subtypes and their characteristics, and table 1.2 provides a summary of key pharmacological agents used in this thesis and their binding affinity at relevant 5-HT receptor subtypes.

1.5 5-HT and mPFC

1.5.1 5-HT receptor localisation in mPFC neurons, including PVINs

There is a plethora of evidence that 5-HT pathways originating in the DRN influence mPFC activity and are critically involved in the regulation of mPFC function. Evidence specified below suggests that both GABAergic interneurons and pyramidal neurons in the mPFC are modulated by distinct 5-HT receptor subtypes that can have opposing effects on a single neuron. The mPFC is particularly enriched in the metabotropic inhibitory 5-HT_{1A} receptor, metabotropic excitatory 5-HT_{2A} and 5-HT_{2C} receptors, and the ionotropic excitatory 5-HT_3 receptor (Mengod et al., 2015; Celada et al., 2013).

In situ hybridisation studies of the rat PFC showed that over 50% of pyramidal neurons express 5-HT_{1A} and 5-HT_{2A} receptors (Santana et al., 2004), and that

Table 1.1: Summary of properties of 5-HT receptors. Information collected from Barnes and Sharp (1999), Hoyer et al. (2002), Sharp and Barnes (2020).

Receptor subtype	**Distribution in the CNS**	**Localisation in neuron**	**Signalling type**	**Neurophysiological effects**
5-HT_{1A}	Cortex, hippocampus, lateral septum, raphe nuclei, thalamus	Somatodendritic, presynaptic, postsynaptic, extrasynaptic	$G_{i/o}$	Hyperpolarisation (K^+, Ca^{2+})
5-HT_{1B}	Basal ganglia, striatum, cortex, raphe nuclei	Presynaptic, postsynaptic	$G_{i/o}$	Hyperpolarisation
5-HT_{1D}	Basal ganglia, hippocampus, cortex, raphe nuclei, locus coeruleus, nucleus accumbens	Presynaptic	$G_{i/o}$	Hyperpolarisation
5-ht_{1e}	Cortex, caudate putamen, claustrum, hippocampus, amygdala, striatum	Postsynaptic	$G_{i/o}$	Hyperpolarisation
5-HT_{1F}	Cortex, hippocampus, claustrum, thalamus, caudate putamen	Presynaptic	$G_{i/o}$	Hyperpolarisation
5-HT_{2A}	Cortex, caudate nucleus, nucleus accumbens, olfactory tubercle, hippocampus, thalamus	Postsynaptic	$G_{q/11}$	Depolarisation (K^+, glutamate)
5-HT_{2B}	Cerebellum, lateral septum, hypothalamus, amygdala	Postsynaptic	$G_{q/11}$	Depolarisation
5-HT_{2C}	Cortex, nucleus accumbens, hippocampus, amygdala, basal ganglia	Postsynaptic	$G_{q/11}$	Depolarisation
5-HT_3	Brainstem, hippocampus, amygdala, cortex	Postsynaptic	Ionotropic	Depolarisation
5-HT_4	Striatum, hippocampus	Postsynaptic	G_s	Depolarisation (Ca^{2+})
5-HT_{5A}	Cerebellum, cortex, dentate gyrus, olfactory bulb, thalamus	Unknown	$G_{i/o}$	Hyperpolarisation
5-ht_{5b}	Hippocampus, habenula, DRN	Unknown	Unknown	Unknown
5-HT_6	Striatum, olfactory tubercles, nucleus accumbens, hippocampus	Postsynaptic	G_s	Depolarisation
5-HT_7	Thalamus, hypothalamus, hippocampus	Postsynaptic	G_s	Depolarisation

Table 1.2: Summary of 5-HT receptor binding affinities of key pharmacological agents. h: human, r: rodent, *bovine instead of rodent. Information collected from Hoyer et al. (1985)[a], Canal et al. (2013)[b], Wainscott et al. (1996)[c], Pehek et al. (2006)[d], Kehne et al. (1996)[e], Kennett et al. (1997)[f], Titeler et al. (1988)[g], Nelson et al. (1999)[h], Erkizia-Santamaría et al. (2022)[i], McKenna and Peroutka (1989)[j], using the NIMH Psychoactive Drug Screening Programme.

	K_i (nM) for 5-HT receptor subtypes							
Ligand	**h1AR**	**r1AR**	**h2AR**	**r2AR**	**h2BR**	**r2BR**	**h2CR**	**r2CR**
5-HT	1.68[a]	1.65[a]	128[b]	138[b]	9.46[c]	11.3[c]	15.4[b]	503.4[b]
MDL-100907 (volinaserin)	>10,000[d]	-	1.50[e]	1.92[d]	261[d]	-	-	88[e]
SB-242084	631[f]	-	158[f]	-	100[f]	-	1.00[f]	-
DOI	-	2355[g]	3.2[b]	4.0[b]	20[h]	27[h]	19[b]	47[b]
Psilocin	152[i]	146[i]	120[i]	173[i]	450[j]*	-	311[i]	79[i]

these receptors are highly co-localised in pyramidal neurons (Puig et al., 2010). 5-HT_{2C} receptors are also shown to be present in rat PFC pyramidal neurons in immunohistochemical studies (Clemett et al., 2000). *In situ* hybridisation studies also report the presence of other 5-HT receptor subtypes on rat PFC pyramidal neurons, such as the 5-HT_4 and 5-HT_7 receptors, although the latter was only observed during early postnatal days (Peñas-Cazorla and Vilaró, 2015; Béïque et al., 2004).

On the other hand, as reviewed earlier, 5-HT_3 receptors are expressed by slow-spiking interneurons located in superficial layers (Puig et al., 2004; Rudy et al., 2011). A subpopulation of 5-HT_3 receptor-expressing interneurons in the rat PFC were reported to also express the 5-HT_6 receptor in *in situ* hybridisation studies (Helboe et al., 2015). Subpopulations of GABAergic interneurons in the rodent mPFC have been demonstrated to express 5-HT_{1A} and 5-HT_{2A} receptors, although evidence specific to PVINs is scarce in comparison to that for pyramidal cells (Santana et al., 2004; Mengod et al., 2015). In one *in situ* hybridisation study, the expression of 5-HT_{1A} and 5-HT_{2A} receptors was demonstrated in about 35% and 25% of PVINs, respectively, with 5-HT_{1A} receptors most enriched in superficial layers and 5-HT_{2A}

receptors more abundant in deep layers (Puig et al., 2010). Notably, unlike pyramidal neurons, the co-expression of 5-HT_{1A} and 5-HT_{2A} receptors was not observed in PVINs (Puig et al., 2010). Evidence for 5-HT_{2C} expression in PVINs is contradicting, as while the same study by Puig et al. (2010) showed an absence of 5-HT_{2C} receptor mRNA in rat PFC PVINs, an immunohistochemical study by Liu et al. (2007) instead reported about 25% of 5-HT_{2C} receptor immunoreactivity in rat PFC PVINs.

Given the abundance of 5-HT_{1A} and 5-HT_{2A} receptors in the mPFC, their differential localisation in cellular compartments is hypothesised to play a key role in their functional effects. Immunohistochemical studies showed that 5-HT_{2A} receptors in the PFC were predominantly located on the apical dendrites of pyramidal neurons where they amplify excitatory synaptic currents (Jansson et al., 2001; Amargós-Bosch et al., 2004). 5-HT_{1A} receptors, on the other hand, were found to be expressed on somata and axon initial segments of pyramidal neurons, maximising their ability to suppress the generation of action potentials (DeFelipe et al., 2001).

The vast majority of 5-HT signalling to cortical neurons (including pyramidal neurons and deep layer PVINs) is thought to be via volume transmission, with only about 25% of synaptic 5-HT release sites innervating interneurons in superficial layers (Puig and Gulledge, 2011). Therefore, the influence of 5-HT on mPFC pyramidal neurons and PVINs may represent tonic control of neuron excitability and firing in contrast to the phasic activation of interneurons in superficial layers (Puig et al., 2010).

1.5.2 5-HT and mPFC neuronal activity, including PVINs

The effects of 5-HT on neurons in the rodent mPFC are most extensively studied in pyramidal neurons located in the deep layers, as they represent the majority of prefrontal output (Andrade, 2011). *In vitro* whole-cell patch-clamp recordings of

pyramidal neurons in rat PFC slices revealed a prominent hyperpolarising effect of 5-HT on pyramidal cells mediated by 5-HT_{1A} receptors (Araneda and Andrade, 1991; Béïque et al., 2004). In addition, a subpopulation of pyramidal cells was excited by 5-HT, which increased spontaneous excitatory post-synaptic currents in a 5-HT_{2A} receptor-dependent manner (Araneda and Andrade, 1991; Zhou and Hablitz, 1999; Avesar and Gulledge, 2012).

The evidence for 5-HT modulation of cortical interneuron excitability *in vitro* is very limited compared to that for pyramidal neurons, and few studies have focused specifically on PVINs. Earlier *in vitro* studies showed that 5-HT application in rat cortical slices enhanced spontaneous inhibitory synaptic transmission by exerting an excitatory effect on interneurons (Zhou and Hablitz, 1999). Subsequent *in vitro* studies using selective receptor antagonists found that these excitatory effects were mediated by 5-HT_{2A} and 5-HT_3 receptors, located on fast-spiking putative PVINs in deep layers of the mouse cortex (Weber and Andrade, 2010), and VIP/CCK-expressing interneurons in superficial layers of the rat cortex (Férézou et al., 2002), respectively.

The effects of physiologically released 5-HT on mPFC neuron firing *in vivo* have been explored using single-unit recordings in the mPFC combined with electrical stimulation of the DRN. These studies reported overwhelmingly inhibitory effects of DRN stimulation on cortical pyramidal neuron firing, although excitations and biphasic responses comprised of short-latency inhibition followed by excitation were also observed (Gartside et al., 2000; Puig et al., 2005). Experiments using selective receptor antagonists suggested that these inhibitory and excitatory effects were mediated by the 5-HT_{1A} and 5-HT_{2A} receptors, respectively (Amargós-Bosch et al., 2004). There is, however, a lack of PVIN focus in the literature much like the case for *in vitro* electrophysiology studies. One study investigated the effects of DRN stimulation on juxtacellularly labelled PVINs and found that the majority

of PVINs were inhibited (about 60%) with a small subset displaying excitation (about 10%) or biphasic responses (about 7%), and the remaining PVINs were unaffected (about 23%; Puig et al., 2010). Pharmacological analysis suggested that the short-latency inhibitory effects of DRN stimulation on PVINs were mediated by the 5-HT_{1A} receptor, whereas the long-latency excitatory effects were mediated by the 5-HT_{2A} but not the 5-HT_{2C} receptor (Puig et al., 2010).

A number of *in vivo* studies also investigated the effects of systemically administered 5-HT_{2A} receptor agonists, in particular DOI (2,5-dimethoxy-4-iodoamphetamine), on the activity of individual neurons in the rat PFC. These studies reported heterogeneous effects of DOI on pyramidal neuron firing, with pyramidal neurons being activated, inhibited, or unaffected (Puig et al., 2003; Celada et al., 2008). Similar to many electrophysiology studies reviewed above, these studies monitored the activity of pyramidal neurons and not PVINs or other interneuron types.

Altogether, the above evidence suggests that the 5-HT system modulates excitatory/inhibitory activity in the mPFC in a complex manner. Only one study in the literature reported the effects of 5-HT on putative cortical PVINs *in vitro* (Weber and Andrade, 2010), while another reported the effects of electrical stimulation of DRN on the activity of mPFC PVINs *in vivo* (Puig et al., 2010). However, the uncertainty of PVIN identity remains a key concern, as these studies assumed the identity of PVINs based on their fast-spiking characteristics rather than the genetic expression of PV (Weber and Andrade, 2010; Puig et al., 2010). While PV is a prominent marker for fast-spiking interneurons, not all PV-expressing cells are fast-spiking and not all fast-spiking cells are PV-expressing (Markram et al., 2004). Moreover, the majority of *in vivo* studies that investigated interactions between 5-HT and the mPFC utilised single-unit recordings in which neuronal identity can be difficult to establish.

1.5.3 5-HT and mPFC network oscillations

Network oscillations in the cortex play an important role in cognition, and abnormal cortical oscillations are observed in a wide range of psychiatric disorders. Given the abundance of 5-HT-targeting psychiatric medications, 5-HT's involvement in the generation and modulation of cortical oscillatory activities has been investigated (Celada et al., 2013).

It is believed that the 5-HT system plays a key role in the regulation of brain states, particularly in the context of arousal. Wakefulness is associated with high levels of 5-HT neuron activity, whereas sleep is associated with low levels of 5-HT transmission (Jacobs and Fornal, 1999). During natural sleep and under anaesthesia, networks of cortical neurons fire synchronously, generating low-frequency oscillations called slow wave activity (SWA; < 2 Hz; Puig and Gener, 2015). During SWA, neurons alternate between periods of activity and silence that correspond to periods of membrane depolarisation and hyperpolarisation, respectively (namely UP and DOWN states), which are not observed during wakefulness (Mukovski et al., 2007).

Electrical stimulation of the DRN *in vivo* has been reported to reduce SWA in the cortex and promote UP states (representing spontaneous epochs of desynchronisation) via the activation of 5-HT_{2A} receptors (Puig et al., 2010). Interestingly, this finding suggests that the inhibitory actions of 5-HT on individual cortical neuron activity may not correspond with its excitatory effects on neural network dynamics. In addition, pharmacological activation of the 5-HT_{2A} receptor with the hallucinogen DOI was found to suppress SWA in the rat PFC (Monti et al., 1990; Dringenberg and Vanderwolf, 1996; Celada et al., 2008). These findings suggest an important role for 5-HT_{2A} receptors in the modulation of cortical SWA.

Much less is known about the role of 5-HT in the modulation of oscillations in higher frequencies. During sleep and anaesthesia, spontaneous gamma oscillations (30 – 80 Hz) emerge in the cortex during UP states of SWA. In the study by Puig

et al. (2010), electrical stimulation of the DRN evoked a strong modulation of UP state gamma oscillations in the rat PFC. While evidence for 5-HT modulation of gamma frequencies in awake animals is limited, it was recently shown that psilocin, the active metabolite of psilocybin, increased oscillatory power in the gamma band and decreased low-frequency oscillations in the mPFC of awake mice (Thomas et al., 2022; Golden and Chadderton, 2022).

1.6 Aims

The mPFC is critically involved in higher executive functions. Despite this, interactions between 5-HT neurotransmission and microcircuits in the mPFC, in particular PVINs, are poorly understood and in need of investigation using advanced neuroscience techniques. The aim of this thesis is to investigate the interactions between 5-HT and neurons of the mPFC on a cellular level, with a focus on PVINs in the prelimbic cortex. The effects of 5-HT on mPFC PVINs and other neuron types were examined on multiple levels, ranging from passive membrane properties and single cell firing patterns, to pair-wise neuronal activity correlations and aggregate network level activity. This was achieved using a combination of *in vitro* patch-clamp and *in vivo* multi-unit electrophysiology combined with pharmacological and optogenetic manipulations of the 5-HT system.

Chapter 2 describes a set of experiments which characterised 5-HT modulation of the passive electrophysiological properties of mPFC PVINs *in vitro* and the 5-HT receptor subtypes involved. In contrast to previous studies that did not verify the identity of PVINs, these experiments utilised a transgenic reporter mouse line in which PVINs were genetically tagged with a fluorescent marker.

Informed by these results, the effects of 5-HT_{2A} receptor agonists on mPFC PVINs *in vivo* were subsequently investigated in Chapter 3. *In vivo* recordings were

obtained using silicon probe technology, which enabled the simultaneous recording of large numbers of neurons. Attempts were made to isolate putative PVINs by their waveform characteristics as described in recent reports. The experiments determined drug effects on firing rate as well as pair-wise interactions of putative PVINs and other simultaneously recorded neurons, which is not achievable with single-unit recordings that dominate the literature.

Next, experiments detailed in Chapter 4 established a protocol for the selective optogenetic activation of DRN 5-HT neurons *in vitro* and *in vivo*. This included the demonstration of optogenetic tagging (optotagging) of 5-HT neurons and the characterisation of their electrophysiological properties. Additionally, a transgenic mouse line which models the conditional knockout of 5-HT/glutamate co-transmission was tested in order to evaluate whether the absence of glutamate co-transmission altered the firing properties of 5-HT neurons and other neuron subpopulations in the DRN.

Finally, building on these findings, Chapter 5 explores the effects of optogenetic activation of DRN 5-HT neurons on the activity of mPFC neurons, especially PVINs, both *in vitro* and *in vivo*. Unlike most studies in the literature which evoked 5-HT release by non-specific electrical stimulation of the DRN, the usage of optogenetics here allowed more refined and selective activation of DRN 5-HT neurons. These experiments combined methodology from all previous chapters; whole-cell patch-clamp, optogenetic activation of DRN 5-HT neurons, and *in vivo* multi-unit silicon probe recording of mPFC neurons.

2

5-HT interactions with mPFC PVINs *in vitro*

2.1 Introduction

2.1.1 Effects of 5-HT receptor subtypes on cortical neurons

A number of 5-HT receptor subtypes are expressed by mPFC neurons and are implicated in the influence of 5-HT network activity and functional output (see Section 1.5). The 5-HT_{1A} receptor couples negatively via the $G_{i/o}$ protein to adenylate cyclase. Previous *in vitro* data show that in rodent PFC neurons, 5-HT_{1A} receptor activation induces membrane potential hyperpolarisation and decreases membrane input resistance by enhancing inward rectifying potassium conductance without the involvement of the intracellular messenger cAMP (Barnes and Sharp, 1999). As such, 5-HT_{1A} receptor activation reduces the overall probability of action potential firing (Aghajanian, 1995). 5-HT_{1A} receptors are also coupled to calcium channels and are reported to reduce overall calcium currents in 5-HT neurons in the rat DRN *in vitro* (Penington and Kelly, 1990). Additionally, in slices of the rat PFC, local application of 5-HT_{1A} receptor agonists reduces AMPA-evoked currents of pyramidal neurons via the inhibition of CAMKII (Cai et al., 2002), and also suppresses NMDA-mediated signalling (Zhong et al., 2008).

5-HT_{2A} and 5-HT_{2C} receptors are coupled positively to phospholipase C via

the $G_{q/11}$ protein, which leads to increased accumulation of inositol phosphate 3 and diacylglycerol as well as the mobilisation of intracellular calcium stores (Barnes and Sharp, 1999). In rat cortical slices, 5-HT is reported to evoke 5-HT_{2A} receptor-mediated neuronal depolarisation by reducing inward rectifying potassium conductance (Aghajanian, 1995; Zhou and Hablitz, 1999). *In vitro* electrophysiological evidence also suggests that in rat PFC pyramidal neurons, the 5-HT_{2A} receptor evokes excitatory effects through the release of glutamate and activation of AMPA receptors (Aghajanian and Marek, 1999). Additionally, 5-HT_{2A} and 5-HT_{2C} receptors were found to enhance NMDA-mediated signalling in rat PFC pyramidal neurons *in vitro*, an effect directly opposite to that of 5-HT_{1A} receptors (Zhong et al., 2008). The role of 5-HT_{1A}, 5-HT_{2A} and 5-HT_{2C} receptors in the control of pyramidal neuron activity is consistent with the evidence of their localisation on these neurons (Santana et al., 2004; Clemett et al., 2000).

2.1.2 *In vitro* evidence for interactions between 5-HT and cortical PVINs

The electrophysiological effects of locally applied 5-HT on cortical PVINs are much less studied compared to pyramidal neurons. In a study by Zhong and Yan (2011), direct 5-HT application to rat PFC slices greatly increased the firing rate of fast-spiking putative PVINs via 5-HT_2 receptors. This excitatory effect by 5-HT persisted in the presence of glutamate and GABA receptor blockade, indicating that 5-HT altered the intrinsic properties of fast-spiking interneurons and, in turn, increased their excitability (Zhong and Yan, 2011). In another study, Weber and Andrade (2010) showed that 5-HT depolarised fast-spiking putative PVINs in mouse cortical slices, with effects ranging from slight membrane depolarisation to large depolarisation that initiated sustained spiking activity. Activation of fast-spiking interneurons by 5-HT enhanced spontaneous inhibitory post-synaptic

currents in neighbouring pyramidal cells. This effect was blocked by the selective 5-HT_{2A} antagonist MDL-100907 but not the 5-HT_3 antagonist tropisetron, and it was abolished in the transgenic 5-HT_{2A} receptor knockout mice (Weber and Andrade, 2010). While the above studies only reported excitatory effects of 5-HT on cortical fast-spiking interneurons, a study by Foehring et al. (2002) demonstrated heterogeneous effects of 5-HT on fast-spiking basket cells in superficial layers of the rat sensorimotor cortex, with neurons being depolarised (67%), hyperpolarised (19%), or unresponsive (14%). The hyperpolarising effects of 5-HT were not blocked by the 5-HT_2 antagonist ritanserin but mimicked by the 5-HT_{1A} receptor agonist 8-OH-DPAT, suggesting the involvement of the 5-HT_{1A} receptor (Foehring et al., 2002). These effects of 5-HT on putative PVINs are in agreement with reports that they express both 5-HT_{1A} and 5-HT_{2A} receptors, albeit in separate populations (Puig et al., 2010). PVINs may also express 5-HT_{2C} receptors, although this is not a consistent finding (Puig et al., 2010; Liu et al., 2007). However, it is essential to note that the identity of putative PVINs in these studies was not verified, meaning the neurons were not confirmed to be PV-expressing using immunohistochemical or genetic means (Zhong and Yan, 2011; Weber and Andrade, 2010; Foehring et al., 2002).

2.1.3 Aims of this chapter

Evidence suggests that 5-HT directly influences the excitability of cortical pyramidal neurons via 5-HT_{1A} and 5-HT_{2A} receptors, although the role of the 5-HT_{2C} receptor remains unclear. There is also evidence that 5-HT_{1A} and 5-HT_{2A} receptors modulate cortical PVINs, although the involvement of PVINs in these studies was inferred via indirect methods rather than proved by chemical identification. In this chapter, the effects of 5-HT on the activity of identified PVINs in slices of the mouse mPFC

were investigated using a transgenic reporter mouse line with PVINs genetically tagged with a fluorescent marker. Using a whole-cell patch-clamp approach, the *in vitro* effects of bath application of 5-HT on the intrinsic firing properties of mPFC PVINs were determined, and the involvement of specific 5-HT receptor subtypes was characterised using selective 5-HT receptor antagonists.

2.2 Materials and Methods

2.2.1 Experiment animals

Transgenic PV-Cre::tdTomato mice (University of Oxford), which selectively express the fluorescent reporter tdTomato in PV-expressing cells, were used. Homozygous PV-Cre::tdTomato mice were obtained by crossing PV-Cre mice that express Cre recombinase in PV-expressing cells (JAX stock #008069; Hippenmeyer et al., 2005) with the Ai9 reporter line (JAX stock #007909; Madisen et al., 2010) that express tdTomato in a Cre-dependent manner. Mice were group housed in individually ventilated cages on a 12-hour light/dark cycle with lights on at 7 am. Food and water were provided *ad libitum*. Procedures were performed in accordance with the Animals (Scientific Procedures) Act 1986 and in line with the guidelines of the University of Oxford. Both male and female mice, between 12 to 18 weeks old, were used.

2.2.2 Acute brain slice preparation

PV-Cre::tdTomato mice were decapitated under deep isoflurane-induced anaesthesia (4% isoflurane), and brains were rapidly extracted and submerged in ice-cold artificial cerebrospinal fluid (aCSF) containing (in mM): 126 NaCl, 3.5 KCl, 1.25 NaH_2PO_4, 1 $MgSO_4$, 2 $CaCl_2$, 26 $NaHCO_3$ and 10 glucose, at pH 7.2-7.4, saturated with carbogen

gas (95% CO2, 5% O2). Coronal brain slices of the mPFC (350 μm, between +1.7 and +2.3 mm from bregma) were prepared in the same cutting solution using a vibratome (VT1200S, Leica Biosystems, UK). Slices were then transferred to a chamber superfused with carbogenated aCSF heated to 32-34°C to recover for at least an hour before recording.

2.2.3 *In vitro* electrophysiology

Immediately prior to recording sessions, brain slices were transferred to a submerged recording chamber mounted on the stage of a microscope (Wild Heerbrugg, Switzerland) and secured under a nylon mesh. The recording chamber was continuously perfused with carbogenated aCSF at 5 mL/min and maintained at 34°C. Deep layers of the prelimbic cortex were targeted using microscopic observation, and PVINs were visually identified by their fluorescence using a digital camera (Orca-ER, Hamamatsu, Japan).

Whole-cell patch-clamp recordings were obtained from mPFC deep layer PVINs using borosilicate glass micropipettes filled with 6-8 MΩ internal solution containing (in mM): 110 potassium gluconate, 40 HEPES, 2 ATP-Mg, 0.3 GTP-NaCl, 4 NaCl (pH 7.2, 270-290 mOsmol l^{-1}). Current-clamp recordings were carried out using an Axon Multiclamp 700B amplifier (Molecular Devices, CA, USA) and digitised using an ITC-18 A/D board (Instrutech, CO, USA). Data acquisition and stimulation protocols were controlled using custom-written procedures in IgorPro 6.37 (WaveMetrics, OR, USA). Recordings were low pass filtered at 3 kHz and acquired at 10 kHz.

After establishing a whole-cell patch-clamp, the resting membrane potential (RMP) was set to -70 mV by direct somatic current injections but no holding current was applied afterwards. Five current step sweep procedures were applied

consecutively to determine the cell's intrinsic firing properties throughout the course of the recording. Current step sweeps started with 11 incremental negative current steps (-2 pA steps, from 0 to -20 pA, each 10 seconds long), followed by 11 incremental positive current steps (20 pA steps, from 0 to 200 pA, each 10 seconds long). Each sweep lasted for 220 seconds in total. RMP drift throughout the recording was not corrected for; however, any neuron with a baseline RMP that fluctuated for more than 5 mV was excluded. Recordings were obtained from one cell per slice, varying from two to four slices per mouse.

2.2.4 *In vitro* pharmacology

After the first current step sweep, the recording chamber was perfused with carbogenated aCSF containing 50 μM 5-HT at a rate of 5 mL/min at 34°C. The concentration of 5-HT was chosen based on previous whole-cell patch-clamp studies involving bath application of 5-HT in PFC slices, where 5-HT concentrations ranged from 10 μM to 200 μM (20 μM: Zhong and Yan, 2011; 30 μM: Béïque et al., 2004; Weber and Andrade, 2010; Weber and Andrade, 2010; 100 μM: Avesar and Gulledge, 2012; 200 μM: Férézou et al., 2002). The amount of time required for the 5-HT-containing aCSF to saturate the recording chamber was tested before recording. The solution reached the recording chamber within 4 min and was fully submerged within 7 min. Since each current step sweep lasted for 220 seconds (i.e. 3.67 min), 5-HT was expected to take effect during the second current step sweep. By the start of the fourth current step sweep (time = 7.33 min after 5-HT application), the recording chamber would be saturated with 5-HT solution and likely have reached the target 5-HT concentration of 50 μM.

The involvement of 5-HT_2 receptor subtypes in 5-HT evoked responses was determined by the application of MDL-100907 (150 nM, Sigma-Aldrich, MO, USA)

and SB-242084 (100 nM, Tocris Bioscience, UK), selective antagonists at the 5-HT_{2A} and 5-HT_{2C} receptors, respectively. These concentrations were chosen based on previous whole-cell patch-clamp studies in which 5-HT_{2A} and 5-HT_{2C} receptor-mediated effects were blocked (Kennett et al., 1997; Bocchio et al., 2015; Sengupta et al., 2017). Brain slices were either (i) not pre-treated with any receptor antagonist, (ii) pre-treated with MDL-100907, (iii) pre-treated with SB-242084, or (iv) pre-treated with a mixture of MDL-100907 and SB-242084. For receptor antagonist studies, brain slices were incubated in carbogenated aCSF containing the respective receptor antagonist(s) for at least 30 min before the start of recording. 5-HT was applied after the first current sweep (Figure 2.1).

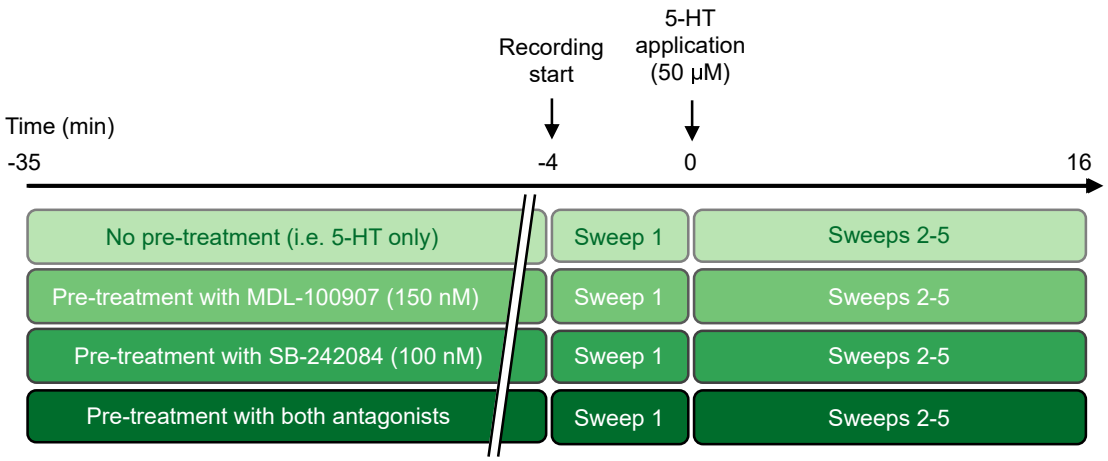

Figure 2.1: Schematic of experimental design. The experiment was carried out across four groups - (i) no pre-treatment (i.e. 5-HT application only), (ii) pre-treatment with MDL-100907, (iii) pre-treatment with SB-242084, and (iv) pre-treatment with both MDL-100907 and SB-242084.

2.2.5 Data analysis

The intrinsic firing properties and membrane excitability of PVINs were quantified using the following parameters: RMP, neural gain, rheobase, and input resistance. The effects of 5-HT were examined by comparing these parameters between the first and fourth current step sweeps. Data were first extracted from and processed

in IgorPro, then analysed using custom-written scripts in MATLAB (MathWorks, MA, USA). The neural gain was defined as the slope of a neuron's input-output (I/O) relationship and described the neuron's sensitivity to changes in current input. First, I/O analysis was performed by plotting the positive amplitude of each current step sweep (i.e. 0 to 200 pA) against the spike frequency of the neuron. The gain was calculated by fitting a straight line to the middle portion of the I/O curve (current amplitude between 60 and 140 pA) using the MATLAB function *polyfit* and computing its slope. Rheobase represents the minimum current amplitude required to initiate depolarisation of the neuron. To calculate rheobase, a straight line was fitted to the starting portion of the I/O curve using the first three points with non-zero spike frequency. The x-intercept of the fitted line was taken as the rheobase.

2.2.6 Statistical analysis

Statistical analyses were performed in MATLAB. Data normality was first determined using the Shapiro-Wilk test (using the MATLAB function *swtest*). Since all data presented in this chapter were normally distributed, paired two-tailed Student's t-tests (using the MATLAB function *ttest*) were used for comparisons between the baseline and 5-HT periods, and one-way analysis of variance (ANOVA) tests with Bonferroni's *post hoc* tests were used for comparisons across the four treatment groups (using the MATLAB functions *anova* and *multcompare*). Data are presented as mean ± standard error of the mean (SEM) values.

2.3 Results

2.3.1 Visualisation and targeting of PVINs

Whole-cell patch-clamp recordings were made in cortical slices of PV-Cre::tdTomato mice, with PVINs being visualised and targeted in deep layers of the prelimbic cortex (Figure 2.2A, B). Additionally, these cells had a small ovoid soma that distinguished them from larger and triangular pyramidal neurons. In line with well-documented PVIN firing properties, recording traces show that these neurons had a characteristic high spiking rate, short spike half-width, and fast afterhyperpolarisation in comparison to unlabelled putative pyramidal cells (Figure 2.2C; Booker et al., 2014).

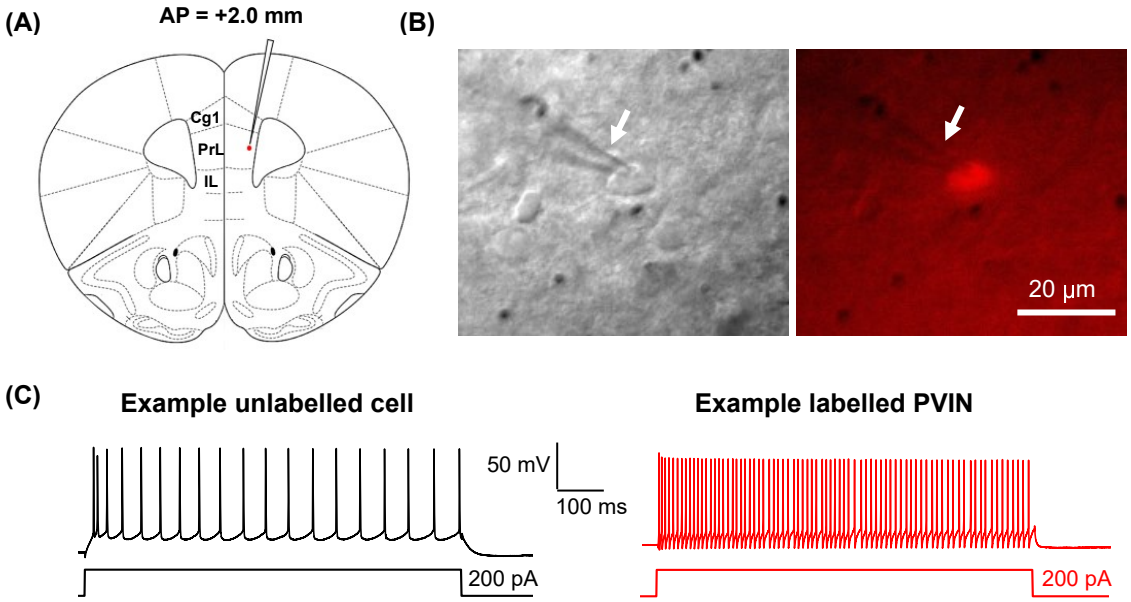

Figure 2.2: *In vitro* slice electrophysiology experiments targeting PVINs in the mPFC of PV-Cre::tdTomato mice. (A) Anatomical illustration of a coronal section (+1.8 mm from bregma) showing the location of target fluorescent PVIN (red) in deep layers of the prelimbic cortex. Atlas image adapted from Franklin and Paxinos (2013). (B) Fluorescent PVIN (red) during a whole-cell patch-clamp session, imaged at 20x. White arrow indicates the location of the recording electrode. (C) Example recording traces of an unlabelled cell (left) and labelled PVIN (right, in red) during 200 pA current injection. Cg1: cingulate area 1, PrL: prelimbic; IL: infralimbic.

2.3.2 5-HT induced changes in resting membrane potential

Once the whole-cell patch-clamp of a PVIN was achieved and its baseline firing properties established, the recording chamber was perfused with 5-HT-containing aCSF (50 μM).

5-HT application rapidly depolarised the resting membrane potential (RMP) of PVINs by around 4 mV within 5 min, followed by gradual and sustained depolarisation for the next 10 min. Comparison of the mean RMP during baseline and periods of 5-HT application showed a significant increase from -68.8 ± 1.16 mV to -64.4 ± 1.00 mV (Figure 2.3A, B; two-tailed paired t-test; t(7) = -3.364, p = 0.0120). The baseline (time = -4 to 0 min) and 5-HT application (time = 7 to 11 min) periods used for comparison were defined by the amount of time taken for aCSF in the recording chamber to reach target 5-HT concentration of 50 μM (see details in Section 2.2).

Given reports of 5-HT_{2A} and 5-HT_{2C} receptor expression in mPFC PVINs and their excitatory nature (Puig et al., 2010; Liu et al., 2007), the involvement of these receptors was tested. Interestingly, in slices pre-treated with MDL-100907, a selective 5-HT_{2A} receptor antagonist, the large initial depolarisation of the RMP induced by 5-HT was blocked, but the sustained rise was not. Pre-treatment with SB-242084, a selective 5-HT_{2C} receptor antagonist, had the opposite effect of blocking the gradual but not the initial depolarisation of RMP (Figure 2.3A). In both groups, statistical comparisons of the baseline and 5-HT application periods showed that changes in RMP induced by 5-HT were reduced by the antagonists (Figure 2.3B; two-tailed paired t-test, before vs. after 5-HT; 5-HT + MDL-100907, t(5) = -2.2571, p = 0.0736; 5-HT + SB-242084, t(8) = -0.0402, p = 0.9689). In brain slices that were pre-treated with both MDL-100907 and SB-242084, 5-HT-induced depolarisation of the RMP was completely abolished, and a small degree of membrane hyperpolarisation from -68.6 ± 0.67 mV to -70.2 ± 0.35 mV was

revealed (Figure 2.3B; two-tailed paired t-test, before vs. after 5-HT; $t(6) = 3.1996$, $p = 0.0186$). Finally, comparisons of the magnitude of RMP change across all four groups showed that the depolarising effects of 5-HT were indeed significantly reduced in all antagonist pre-treated slices (Figure 2.3C; one-way ANOVA, $F_{3,26} = 1648.5$, $p < 0.001$; Bonferroni's *post hoc* comparisons, 5-HT + MDL-100907, 5-HT+ SB-242084, and 5-HT + both antagonists vs. 5-HT only, $p < 0.001$).

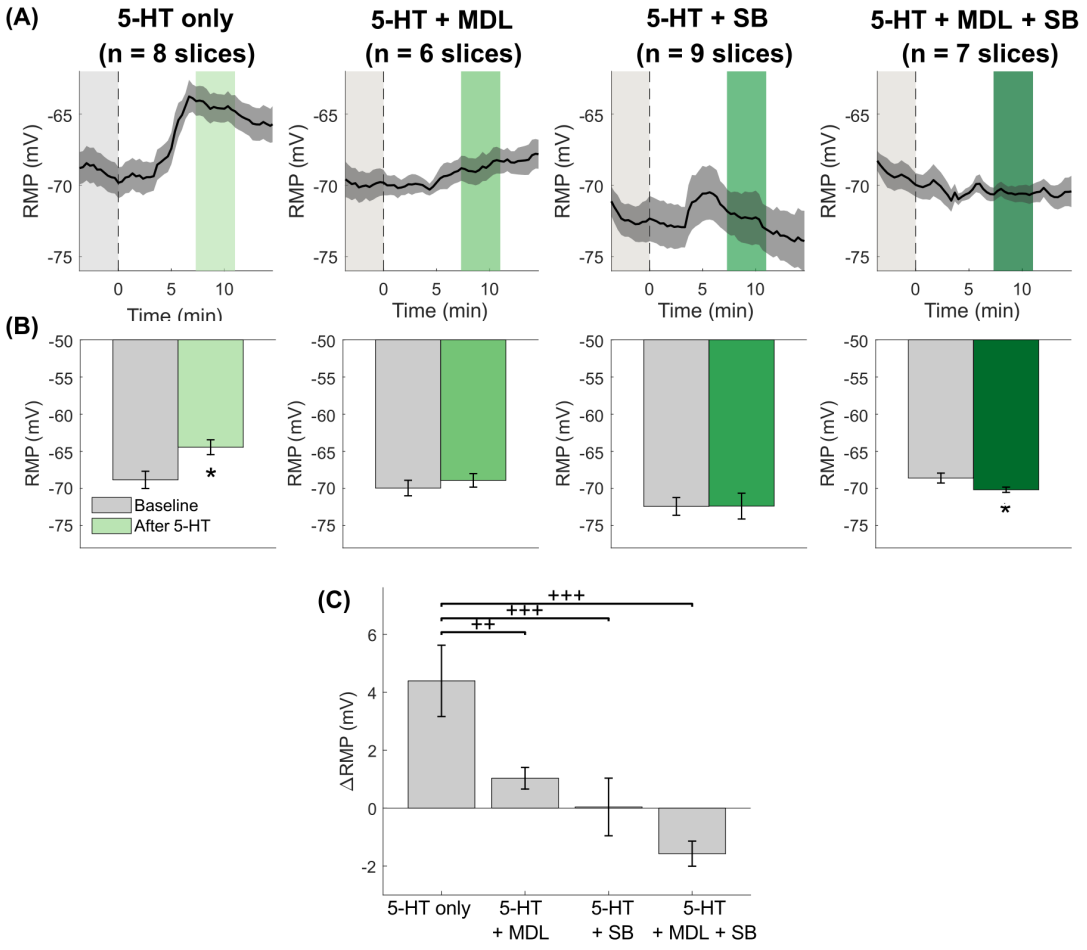

Figure 2.3: Effects of 5-HT on the resting membrane potential (RMP) of PVINs, with and without the 5-HT_{2A} and 5-HT_{2C} receptor antagonists MDL-100907 (abbreviated to MDL) and SB-242084 (abbreviated to SB), respectively. (A) Line plots showing the RMP (in mV) over the course of recording. Grey areas represent the baseline period before 5-HT application (black dotted lines). Green areas represent the 5-HT period used for comparison in subsequent panels. (B) Bar charts showing the change in RMP before (grey) and after (green) 5-HT application in each group. (C) Bar charts showing the magnitude of change in RMP for each group. Data are represented as mean ± SEM values. *$p<0.05$, two-tailed paired t-test; $^{++}p<0.01$, $^{+++}p<0.001$, one-way ANOVA with *post hoc* Bonferroni against 5-HT only group.

Altogether, these data suggest that 5-HT has a clear depolarising effect on the RMP of PVINs in the mPFC. The data suggest that 5-HT_{2A} receptors play a major role in the fast onset 5-HT-induced RMP depolarisation of PVINs, whereas 5-HT_{2C} receptors contribute via slow and sustained depolarisation. Blockade of both receptors revealed the potential involvement of other 5-HT receptors associated with a small degree of RMP hyperpolarisation.

2.3.3 5-HT induced changes in neural gain

The neural gain represents the sensitivity of a neuron to current input, and the gain of a neuron can be measured as the slope of the current-to-spike-frequency relationship over a given range of current inputs, namely the input-output (I/O) curve (Eldar et al., 2013). Here, patch-clamped PVINs were recorded in the current-clamp mode, and five consecutive current step sweeps were applied. In each sweep, increasing amounts of current were injected into the cell in 20 pA increments up to 200 pA (Figure 2.4A). Neural gain calculated from I/O curves at baseline and after 5-HT application (time = -4 to 0 min vs. 7 to 11 min relative to 5-HT application) were compared (Figure 2.4B).

Application of 50 μM 5-HT significantly increased the gain from 0.45 ± 0.14 to 1.01 ± 0.09, as evidenced in the change in slope of the I/O curve (Figure 2.4C; two-tailed paired t-test, before vs. after 5-HT; t(7) = -3.116, p = 0.0169). MDL-100907 pre-treatment blocked this effect (two-tailed paired t-test, before vs. after 5-HT; t(5) = -1.118, p = 0.3146), whereas pre-treatment with SB-242084 did not (two-tailed paired t-test, before vs. after 5-HT; t(8) = -3.019, p = 0.0194). In the presence of both antagonists, the increase in neural gain caused by 5-HT application was also significantly reduced (two-tailed paired t-test, t(6) = -1.882, p = 0.1018). Of all treatment groups, only MDL-100907 caused a statistically significant reduction in

the magnitude of 5-HT-induced gain (Figure 2.4D; one-way ANOVA, $F_{3,26} = 4.64$, $p = 0.0107$; Bonferroni's *post hoc* comparisons, 5-HT + MDL-100907 vs. 5-HT only, $p = 0.0138$).

2.3.4 5-HT induced changes in rheobase

The rheobase, another measure of membrane excitability extracted from the I/O curve, is defined as the minimal current amplitude that results in an action potential of a neuron. Application of 50 μM 5-HT decreased the rheobase of PVINs from 100.0 ± 22.7 pA at baseline to 30.7 ± 7.92 pA (Figure 2.5B, two-tailed paired t-test; $t(7) = 3.880$, $p = 0.0061$). Pre-treatment with MDL-100907, but not SB-242084, blocked this effect of 5-HT (Figure 2.5B; two-tailed paired t-test, before vs. after 5-HT; 5-HT + MDL-100907, $t(5) = 1.180$, $p = 0.2913$; 5-HT + SB-242084, $t(8) = 4.345$, $p = 0.0025$). When both antagonists were applied, changes in rheobase after 5-HT application were again blocked (two-tailed paired t-test, $t(6) = 1.491$, $p = 0.1795$). Across all antagonist groups, only MDL-100907 pre-treatment significantly reduced the magnitude of reduction in rheobase caused by 5-HT (Figure 2.5C; one-way ANOVA, $F_{3,26} = 3.12$, $p = 0.0426$; Bonferroni's *post hoc* comparisons, 5-HT + MDL-100907 vs. 5-HT only, $p = 0.0471$). Alongside the measurement of neural gain, these data add further evidence for the modulatory effects of 5-HT on PVIN excitability, as well as the involvement of 5-HT_{2A} but not 5-HT_{2C} receptors in this modulation.

2.3.5 5-HT induced changes in input resistance

Input resistance is another readout of membrane excitability and reflects the extent to which membrane channels are open. A low membrane resistance implies high

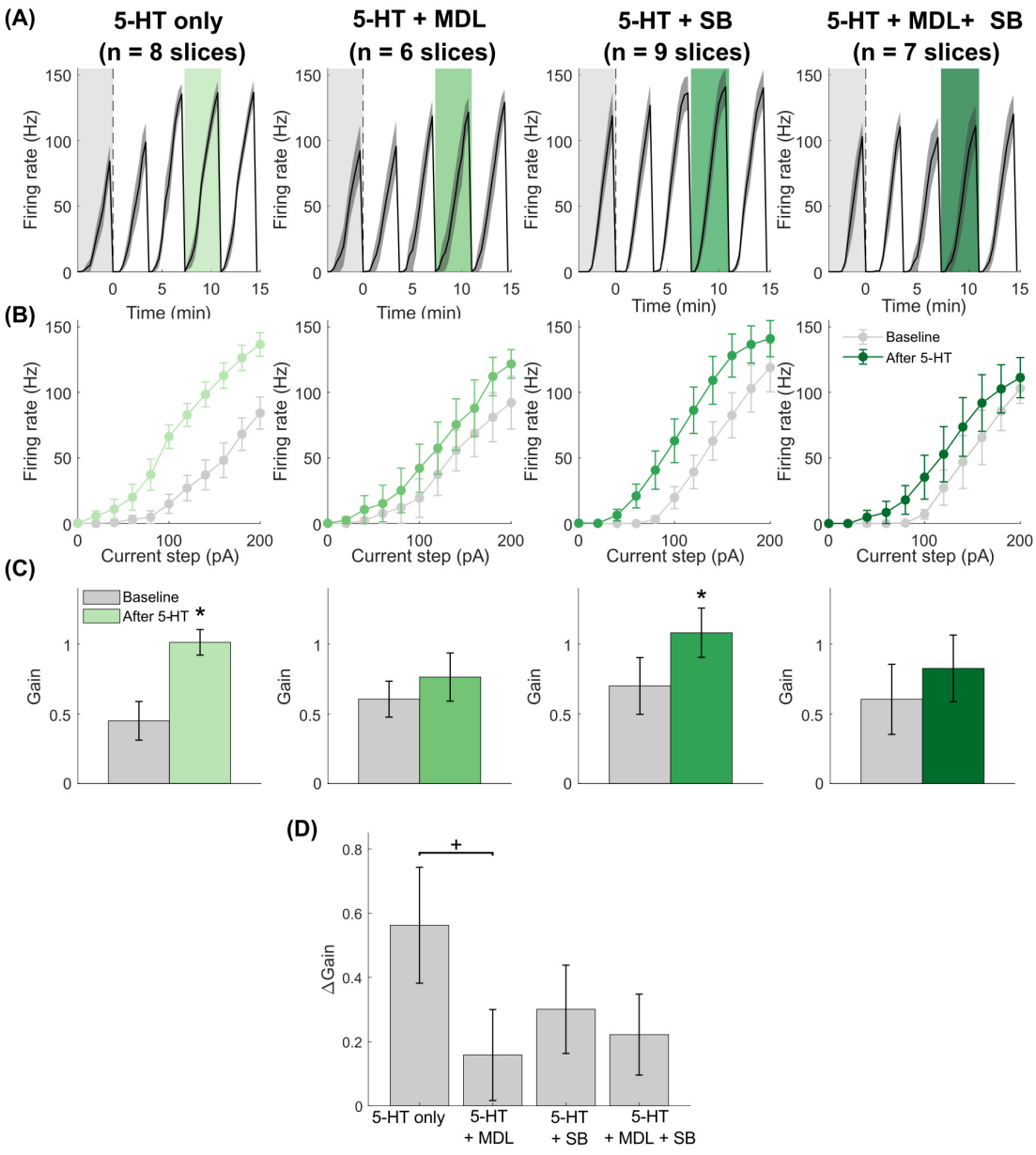

Figure 2.4: Effects of 5-HT on the gain of PVINs, with and without the 5-HT_{2A} and 5-HT_{2C} receptor antagonists MDL-100907 (abbreviated to MDL) and SB-242084 (abbreviated to SB), respectively. (A) Line plots of firing rate (Hz) of PVINs over the course of recording. Each peak corresponds to one current step sweep. 5-HT application is represented by the black dotted lines. Grey and green shaded areas represent the baseline and 5-HT current steps used for comparison in subsequent panels. (B) I/O analyses showing the firing rate (Hz) of PVINs versus current step amplitude (pA). Grey lines represent the I/O during baseline (first current step procedure) and green lines represent the I/O after 5-HT application (fourth current step procedure). (C) Bar charts showing the change in gain before and after 5-HT application in each group. (D) Bar chart showing the magnitudes of increase in gain after 5-HT application across each group. Data are represented as mean ± SEM values. *$p<0.05$, two-tailed paired t-test; $^{+}p<0.05$, one-way ANOVA with *post hoc* Bonferroni against 5-HT only group.

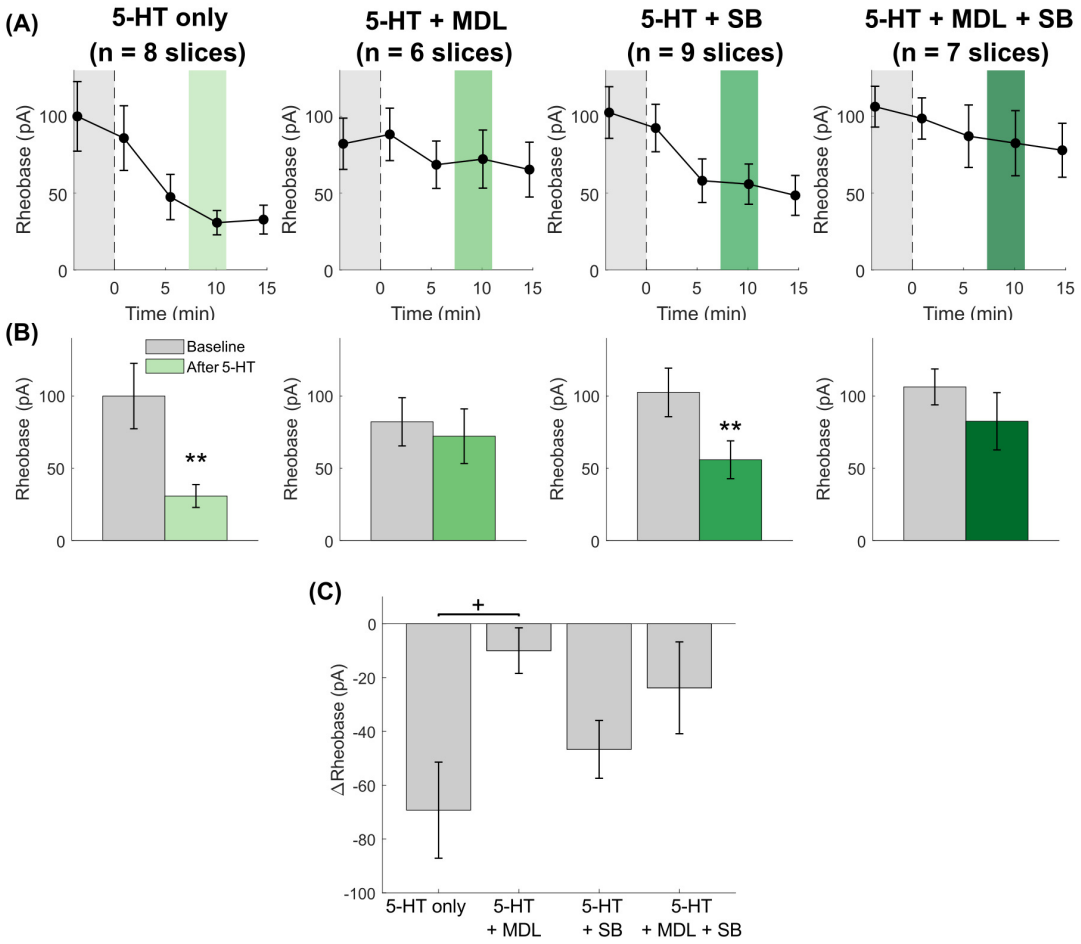

Figure 2.5: Effects of 5-HT on the rheobase (pA) of PVINs, with and without the 5-HT_{2A} and 5-HT_{2C} receptor antagonists MDL-100907 (abbreviated to MDL) and SB-242084 (abbreviated to SB), respectively. (A) Line plots showing the rheobase in each current step sweep. Black dotted lines indicate 5-HT application. Grey and green shaded areas represent the rheobase values used for comparison in the next panels. (B) Bar charts showing the decrease in rheobase caused by 5-HT application in each group. (C) Bar chart showing the magnitude of change in rheobase for each group. Data represented as mean ± SEM values. **p<0.01, two-tailed paired t-test; $^{+}$p<0.05, one-way ANOVA with *post hoc* Bonferroni against 5-HT only group.

conductance and open channels, whereas high resistance implies closed channels (Li et al., 2020).

In response to the application of 50 μM 5-HT, the input resistance of PVINs increased from 125.9 ± 10.18 MΩ to 145.8 ± 9.84 MΩ (Figure 2.6A, B, two-tailed paired t-test, t(7) = -5.503, p < 0.001). Similar to earlier observations, this effect of 5-HT was blocked in slices that were pre-treated with MDL-100907 as well as

MDL-100907 plus SB-242084, but not SB-242084 alone (Figure 2.6B; two-tailed paired t-test of before vs. after 5-HT; 5-HT + MDL-100907, t(5) = -1.208, p = 0.2811; 5-HT + SB-242084, t(8) = -2.699, p = 0.0271; 5-HT + MDL-100907 + SB-242084, t(6) = -0.4099, p = 0.6941). According to Ohm's Law ($V = I * R$ where V = voltage, I = current, and R = resistance), a higher input resistance indicates that any given depolarising current will produce a greater increase in voltage, hence a greater chance of evoking an action potential and higher excitability.

2.4 Discussion

Experiments in this chapter investigated the effects of 5-HT on the passive biophysical properties of mPFC PVINs *in vitro*. During whole-cell patch-clamp sessions of genetically labelled PVINs, 5-HT was bath applied and selective antagonists of 5-HT_{2A} and 5-HT_{2C} receptors were used to characterise the receptor subtypes involved. Results from these experiments showed that the application of 5-HT (50 μM) caused a robust increase in the excitability of PVINs by modulating their intrinsic membrane properties, specifically the RMP, gain, rheobase, and input resistance. Blockade of 5-HT_{2A} receptors abolished the effects of 5-HT on all parameters tested, indicating that the excitatory effects of 5-HT on mPFC PVINs were primarily mediated by the 5-HT_{2A} receptor.

2.4.1 5-HT increased mPFC PVIN excitability via the 5-HT_{2A} receptor

Results presented here are in agreement with previous *in vitro* studies that reported a 5-HT_{2A} receptor-mediated increase in excitability of a subpopulation of putative PVINs evoked by bath applied 5-HT ($20 - 30$ μM; Zhong and Yan, 2011; Weber and Andrade, 2010). The findings are also consistent with *in situ* hybridisation studies

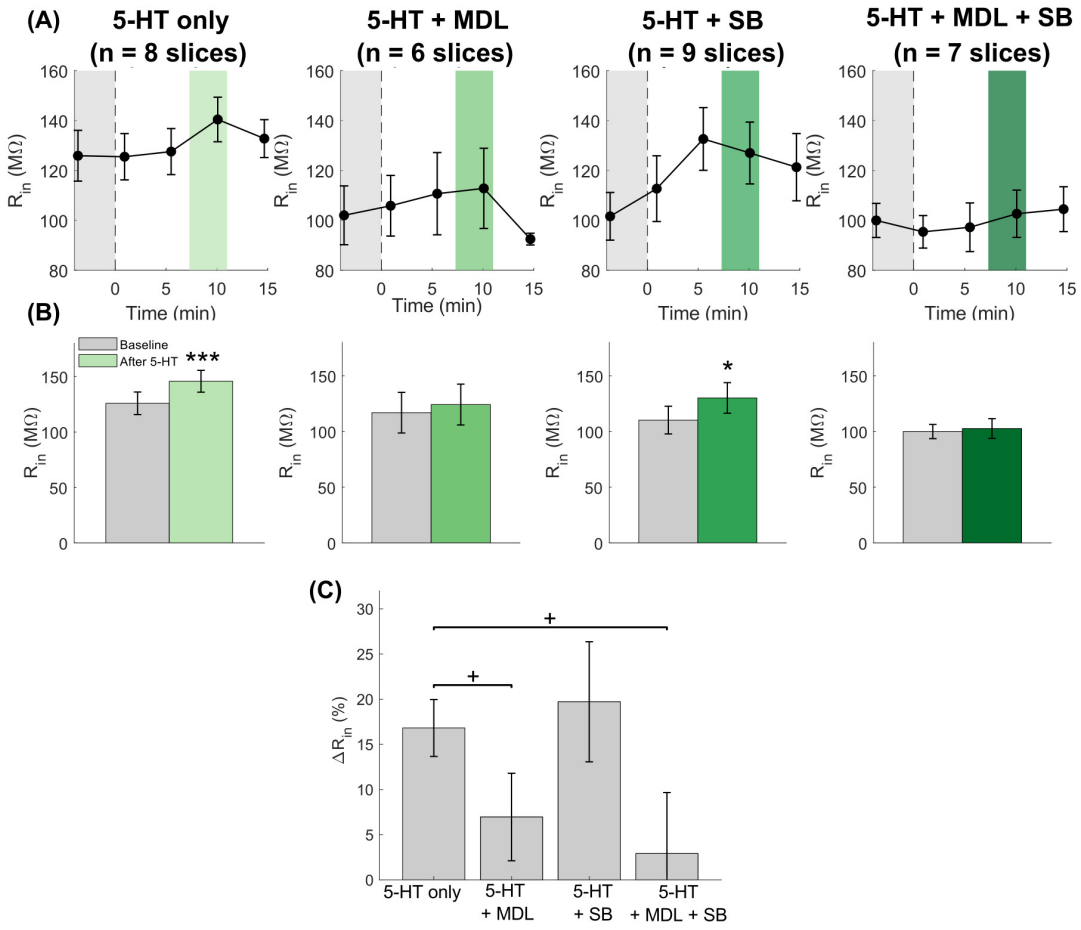

Figure 2.6: Effects of 5-HT on the input resistance (R_{in}, MΩ) of PVINs, with and without the 5-HT_{2A} and 5-HT_{2C} receptor antagonists MDL-100907 (abbreviated to MDL) and SB-242084 (abbreviated to SB), respectively. (A) Line plots showing the input resistances in each current step sweep. Grey areas represent the baseline periods before 5-HT application (black dotted line). Green areas represent the drug effect periods used for comparison in subsequent panels. (B) Bar charts showing the change in input resistance after 5-HT application in each group. (C) Bar chart showing the change in input resistance after 5-HT application for each group. Data are represented as mean ± SEM values. *$p<0.05$, ***$p<0.001$, two-tailed paired t-test; $^{+}p<0.05$, one-way ANOVA with *post hoc* Bonferroni against 5-HT only group.

demonstrating 5-HT_{2A} receptor expression in PVINs in the prelimbic cortex (Puig et al., 2010). Using the PV-Cre::tdTomato mouse line, the current study confirmed the genetic identity of recorded PVINs which was not achieved in previous studies (Zhong and Yan, 2011; Weber and Andrade, 2010). However, contrary to reports of inhibitory effects of bath applied 5-HT (30 μM) on putative PVINs *in vitro* (Foehring et al., 2002), results here indicated that the effects of 5-HT on mPFC PVINs were

overwhelmingly excitatory. This discrepancy could be due to the misidentification of PVINs in previous studies, or a regional difference in 5-HT receptor expression as Foehring et al. (2002) targeted putative PVINs in the sensorimotor cortex.

An important study by Athilingam et al. (2017), published after experiments in this chapter commenced, investigated the effects of bath applied 5-HT on mPFC PVINs which were genetically targeted using a similar PV-Cre::tdTomato mouse line (PV-Cre crossed with Ai14 instead of Ai9). In line with the results presented here, 5-HT_{2A} receptor-mediated excitatory effects of 5-HT were reported, including RMP depolarisation, a decrease in rheobase, and an increase in input resistance (Athilingam et al., 2017). Both the current study and Athilingam et al. (2017) observed excitatory effects of 5-HT in all recorded PVINs, whereas previous studies reported subpopulations of putative PVINs unaffected by 5-HT (Zhong and Yan, 2011; Weber and Andrade, 2010). Since those studies did not confirm the identity of recorded cells, it is possible that a subpopulation of fast-spiking SST-expressing interneurons was mistakenly identified as PVINs, as SST-expressing interneurons were shown to be unresponsive to bath applied 5-HT *in vitro* (Athilingam et al., 2017).

2.4.2 Involvement of the 5-HT_{2C} and 5-HT_{1A} receptors

Given that PVINs in the mPFC were reported to express 5-HT_{1A} and maybe 5-HT_{2C} receptors alongside 5-HT_{2A} receptors (Puig et al., 2010; Liu et al., 2007), it is surprising that mostly 5-HT_{2A} receptor-mediated effects were observed. The current study also tested the involvement of 5-HT_{2C} receptors, which are little studied in the context of mPFC PVIN electrophysiology. Results here suggest that the 5-HT_{2C} receptor is involved in the modulation of RMP of mPFC PVINs, albeit in a distinct manner compared to 5-HT_{2A} receptors. Thus, while 5-HT_{2A}

receptor-mediated effects had a rapid onset, effects mediated by 5-HT_{2C} receptors were more sustained and gradual. All other parameters of 5-HT-induced excitability, specifically the gain, rheobase, and input resistance, were unaffected by 5-HT_{2C} receptor blockade. On the other hand, a hyperpolarising effect of 5-HT was observed when both 5-HT_{2A} and 5-HT_{2C} receptors were blocked, indicating the potential (albeit minor) involvement of the 5-HT_{1A} receptor in the modulation of RMP of mPFC PVINs. However, this was not pharmacologically confirmed and it is unclear whether these effects resulted from direct modulation of PVINs. Both the 5-HT_{2C} receptor-mediated slow depolarisation and putative 5-HT_{1A} receptor-mediated hyperpolarisation of RMP may have been mediated indirectly via the action of 5-HT on other neurons in local circuits. This is supported by the fact that Athilingam et al. (2017) did not observe effects of 5-HT in the presence of synaptic blockers and MDL-100907, suggesting that 5-HT exerted direct effects on mPFC PVINs via 5-HT_{2A} receptors and potentially indirect effects via the 5-HT_{2C} and 5-HT_{1A} receptors.

2.4.3 Pharmacological versus physiological effects of 5-HT

A potential drawback of the current pharmacological approach is that direct local application of 5-HT may not evoke the same effects as physiologically released 5-HT, as a recent study by Unal et al. (2015) found that the effects of optogenetic activation of cholinergic terminals on amygdalar neurons were different from previously reported canonical responses to bath applied acetylcholine. This difference could be due to various factors, such as a mismatch between pharmacological and physiological 5-HT concentrations. Dose response experiments by Athilingam et al. (2017) showed that 30 μM 5-HT elicited about 80% of maximal response, suggesting that the effects of 50 μM 5-HT observed in the current study may represent near-maximal responses. As reviewed in Section 2.2, this concentration of 5-HT was selected based

on previous whole-cell patch-clamp studies in which 5-HT was bath applied in PFC slices. While it is reassuring that other studies which used lower concentrations of 5-HT ($20 - 30$ μM) observed similar results (Zhong and Yan, 2011; Weber and Andrade, 2010; Athilingam et al., 2017), it is important to note that physiological concentrations of 5-HT likely vary with behavioural state, and a single concentration of 5-HT may not be representative of physiological conditions.

Another limitation of the current study is that bath applied 5-HT likely misses the role of any physiologically released co-transmitters. As reviewed in Section 1.4, emerging evidence suggests that a sizable subpopulation of 5-HT neurons can co-release glutamate. For example, a recent study demonstrated that optogenetic activation of 5-HT afferents in amygdala slices evoked glutamate-mediated ionotropic excitation that would not have been observed with bath applied 5-HT (Sengupta et al., 2017). As such, while the current study provided valuable insight into how 5-HT modulates mPFC PVINs *in vitro*, the effects of bath applied 5-HT may not accurately reflect the actions of physiological 5-HT.

2.4.4 Specificity and efficiency of the PV-Cre::tdTomato mouse

A fundamental assumption in the current study is that PVINs were specifically and efficiently labelled in the PV-Cre::tdTomato mouse. Early studies showed that the PV-Cre mouse line, first introduced in 2005 by Hippenmeyer et al., indeed targeted PVINs with a high degree of specificity (i.e. the proportion of tdTomato-expressing neurons that also express PV) and efficiency (i.e. the proportion of PVINs labelled by tdTomato) in the neocortex and cingulate cortex (Tanahira et al., 2009), visual cortex (Atallah et al., 2012), medial entorhinal cortex (Martínez et al., 2017), and somatosensory cortex (Vascak et al., 2018). In particular, double immunofluorescence data in the somatosensory cortex of PV-Cre::tdTomato mice

showed that 90-95% of td-Tomato-expressing soma were PV-immunoreactive, and over 90% of PV-immunoreactive soma were tdTomato-expressing (Vascak et al., 2018). It should be noted that a small number of cortical pyramidal neurons can express PV, and it was demonstrated in PV-Cre::GFP mice that a small number of Cre-expressing pyramidal neurons were present in the cortex (Tanahira et al., 2009). To avoid the inclusion of PV-expressing pyramidal neurons in the current study, all patch-clamped neurons were tested both for their fluorescence and fast-spiking properties to ensure they were PVINs before proceeding with the experiment.

However, recent studies highlighted regional efficiency issues in PV-Cre::tdTomato mice. Two key immunohistochemical studies reported high levels of specificity (about 95%) but variable levels of efficiency (ranging from 40% to 90%) in PVIN labelling depending on the brain region (Nigro et al., 2021; Gradwell et al., 2022). In particular, Nigro et al. (2021) demonstrated high specificity (>90%) of PVIN labelling in the mPFC except for layer II of the infralimbic region (about 50%). However, the efficiency was only 60-70% in the prelimbic cortex, which was higher than some cortical regions, such as the perirhinal cortex (about 45%), but lower than others, such as the barrel cortex (about 90%; Nigro et al., 2021). It was suggested that this issue of low efficiency resided in the PV-Cre mouse line rather than the reporter line (Nigro et al., 2021), implying that this issue likely extends beyond the PV-Cre::tdTomato mouse line. Overall, much evidence demonstrates a low false positive rate of PVIN labelling in the PV-Cre::tdTomato mouse line, indicating that the vast majority, if not all recorded cells in the current study are likely genuine PVINs.

2.4.5 Conclusions

Altogether, the current study provided one of the first pieces of concrete evidence that 5-HT modulates genetically identified mPFC PVINs *in vitro* by increasing their excitability via the 5-HT_{2A} receptor. The current data also indicated that 5-HT_{2C} and 5-HT_{1A} receptors were involved to a lesser extent in the effects of 5-HT, perhaps indirectly, although further pharmacological analysis is required to confirm their exact roles. With the 5-HT_{2A} receptor identified as a key player in 5-HT modulation of mPFC PVINs *in vitro*, the effects of 5-HT_{2A} receptor agonists on mPFC single-unit and network activity *in vivo* are explored in the next chapter.

3

Effects of 5-HT_{2A} receptor agonist administration on neural activity in the mPFC *in vivo*

3.1 Introduction

With findings from Chapter 2 establishing an excitatory influence of the 5-HT_{2A} receptor on mPFC PVINs *in vitro*, the effects of systemic administration of 5-HT_{2A} receptor agonists on mPFC neurons, including PVINs, were explored *in vivo* in this chapter.

3.1.1 *In vivo* effects of 5-HT_{2A} receptor agonists on mPFC neurons

A number of earlier studies have reported the effects of 5-HT_{2A} receptor agonists on cortical neuronal activity *in vivo*, specifically that of pyramidal neurons, with DOI being a commonly used agent. Single-unit extracellular recording studies in anaesthetised rats by Puig et al. (2003); Celada et al. (2008) reported heterogeneous effects of DOI ($0.05 - 0.6$ mg/kg, *i.v.*) on pyramidal neurons recorded from the prelimbic cortex. Thus, in response to the systemic administration of DOI, subgroups of pyramidal neurons displayed firing rates that either increased, decreased, or remained unaffected (Puig et al., 2003; Celada et al., 2008). Both excitatory and

inhibitory effects of DOI were reversed by MDL-100907, and DOI's inhibitory effects were additionally reversed by picrotoxin, a GABA antagonist, suggesting that DOI's inhibitory effects were at least partially indirect and mediated by local GABAergic interneurons (Puig et al., 2003). DOI also reduced cortical low-frequency oscillations by desynchronising pyramidal neuron discharge, likely via 5-HT_{2A} receptors (Celada et al., 2008). Both studies showed that thalamic lesions had little impact on DOI's actions, indicating that DOI's effects were likely intracortical and independent from thalamocortical afferents (Puig et al., 2003; Celada et al., 2008).

A further study by Wood et al. (2012) in awake rats, however, showed that higher doses of DOI ($3 - 5$ mg/kg, *s.c.*) caused a sustained reduction in the population activity of mPFC pyramidal neurons, while lower doses of DOI (1 mg/kg, *s.c.*) failed to produce a significant effect. Such differences in DOI's actions on mPFC activity could be due to intrinsic differences in the awake and anaesthetised brain states. In addition, DOI consistently disrupted correlations between neuronal spiking and oscillatory power in the gamma band (Wood et al., 2012). Inhibitory effects of DOI ($0.3 - 1$ mg/kg, *i.p.*) on population activity of PFC neurons were also demonstrated in awake mice by Gener et al. (2019). Interestingly, DOI was reported to selectively enhance high gamma synchronization in the PFC (Gener et al., 2019). A recent study by Golden and Chadderton (2022) also demonstrated psilocybin's ability to reduce low-frequency oscillatory power and neural phase locking in the mPFC of awake mice. This disruption of oscillatory activity by DOI and similar agents seemingly contribute to their psychotropic actions, as supported by human studies that demonstrated cortical desynchronisation in subjects that were given psilocybin (Muthukumaraswamy et al., 2013).

3.1.2 Multi-unit recordings using silicon probes

The majority of electrophysiological studies of the effects of 5-HT_{2A} receptor agonists on cortical neurons are based on single-unit recordings, typically using glass micropipettes (Puig et al., 2003; Celada et al., 2008). Recording using micropipettes allows the detection of extracellular action potentials from single neurons at a high signal-to-noise ratio, as well as the summated synaptic activity of nearby neurons in the form of the local field potential (LFP; Buzsáki et al., 2015). However, while single-unit recordings can provide valuable insights into a single neuron's spiking activity *in vivo*, they generate small datasets that provide little information on different neuron subtypes and local interactions within the neural network. It is therefore important to increase the number of simultaneously recorded neurons in order to better understand neural microcircuits that underlie network computations and brain function.

The development of silicon probe technology over the past decade has enabled the large-scale recording of spiking activity from multiple neurons that can be separated to single-unit resolution through a "spike sorting" process (Buzsáki et al., 2015; Chaure et al., 2018). Silicon probes feature large and dense arrays of micron-scale recording sites, designed to achieve a balance between the maximisation of the number of recording locations and the minimisation of the probe width so as to reduce brain tissue damage (Steinmetz et al., 2018). Due to the invasive nature of these electrical recordings, silicon probes also provide an important feature of decreasing the number of animals used, in line with the goal of 3Rs (replacement, refinement, reduction) of animals in research, while at the same time increasing statistical power.

3.1.3 Identification of PVINs in *in vivo* electrophysiology

The diversity of cortical interneurons and their complex connectivity with neighbouring pyramidal neurons means that the ability to distinguish between different neuron types is crucial to interpreting data obtained from silicon probe recordings. In this regard, silicon probe recordings can provide a highly valuable readout of multiple electrophysiological parameters that reportedly allows the distinction of interneurons from pyramidal neurons (Barthó et al., 2004).

PVINs are often identifiable by their high firing rate, short spike duration, and narrow afterhyperpolarisation in the spike waveform, as supported by *in vitro* intracellular recording evidence in the rat and mouse cortex (Kawaguchi and Kubota, 1993; Avermann et al., 2012). In particular, the identification of putative PVINs by their narrow spike waveform characteristics is commonly seen in multi-unit extracellular recording studies of the mouse PFC (Tseng and Han, 2021), motor and barrel cortices (Mahrach et al., 2020), and hippocampus (Medrihan et al., 2017). Narrow waveforms of PVINs were also consistently observed in *in vivo* intracellular recordings of PVINs in the rat hippocampus (Sik et al., 1995; Henze et al., 2000), as well as *in vivo* juxtacellular recordings of PVINs in the rat mPFC (Schweimer et al., 2022) and mouse barrel cortex (Yu et al., 2019). Other interneuron subtypes, such as SST-expressing and VIP-expressing interneurons, had intermediate waveform durations that distinguished them from PVINs (Yu et al., 2019). In agreement with this, optotagging studies verified that the narrow waveforms of extracellularly recorded PVINs are distinct from the broader waveforms of pyramidal neurons in the mouse mPFC (Kvitsiani et al., 2013) as well as the barrel cortex (Cardin et al., 2009), hippocampus (Royer et al., 2012), and visual cortex (Senzai et al., 2019).

Other studies have also highlighted the importance of additional factors in the identification of PVINs, such as the waveform peak asymmetry (Barry, 2015) and the presence of putative monosynaptic interactions in pair-wise cross-correlograms

(Fujisawa et al., 2008). The peak asymmetry of a spike waveform represents the extent to which a waveform is triphasic and is important in the distinction of units generated by axons. This is because the narrow waveforms of axon units are even narrower than that of PVINs, and can often be mistaken as interneurons (Barry, 2015). However, axon units have triphasic waveforms that are unlikely generated by interneurons, which have waveforms shown to be more biphasic in comparison to pyramidal neurons (Royer et al., 2012; Robbins et al., 2013; Sirota et al., 2008). As such, by examining spike waveform width in addition to peak asymmetry, putative axon units can be appropriately identified and excluded.

On the other hand, the presence of putative inhibitory synaptic connections in cross-correlograms has been shown to match the waveform-based classification of PVINs with high fidelity in the rat mPFC (Insel and Barnes, 2015), rat parietal cortex (Sirota et al., 2008), mouse neocortex and hippocampus (Stark et al., 2013), as well as mouse visual cortex (Senzai et al., 2019). Millisecond synchronous spiking in the cross-correlogram can also serve as an indication for interneuronal coupling via gap junctions, which are commonly observed between interneurons of the same class including PV-expressing basket cells (Hestrin and Galarreta, 2005; Cardin, 2018). These cross-correlogram features can therefore serve as additional markers in the identification of PVINs.

Finally, it is necessary to note that even though the waveform-based identification of PVINs is widely used, it does not unequivocally identify all PVINs. Rather, it serves as a robust method to identify neurons that resemble PVINs enough to conclude with high confidence that they belong to the PVIN subtype.

3.1.4 Aims of this chapter

The aims of this chapter were to examine the *in vivo* effects of 5-HT_{2A} agonists, DOI and psilocin (4-hydroxy-dimethyltryptamine; 4-OH-DMT), on mPFC neuronal activity in anaesthetised mice. While DOI was chosen due to its selectivity at the 5-HT_{2A} receptor and well-documented status in the literature, psilocin, as the active metabolite of psilocybin, represents an emerging area of clinical research that could provide key insights into the relationship between the 5-HT system, cognition, and mental disorders (Daniel and Haberman, 2017; Nutt et al., 2020). Through a multi-unit recording approach, analytical methods in this chapter aimed to establish electrophysiological parameters that enable the identification of putative PVINs from the recorded mPFC neuronal population. To this end, experiments in this chapter investigated whether the 5-HT_{2A} receptor-mediated excitation of mPFC PVIN activity, demonstrated *in vitro* in Chapter 2, could be detected *in vivo*.

3.2 Materials and methods

3.2.1 Experiment animals

C57BL6/J wildtype mice (Charles River, UK) were group housed in individually ventilated cages, on a 12-hour light/dark cycle (lights on at 7:00 am) at constant temperature and humidity. Food and water were provided *ad libitum*. Mice were habituated to handling for at least three days prior to experiments. All experiments were conducted in two-to-four-month-old mice, both male and female. All procedures were performed in accordance with the Animals (Scientific Procedures) Act 1986 and in line with the guidelines of the University of Oxford.

3.2.2 *In vivo* recording devices

Neuronal recordings were made from a 32-channel silicon probe electrode (ASSY-37 H-Series 6b, Cambridge Neurotech, UK) consisting of one shank with two columns of 16 contact points clustered at the tip (Figure 3.1A). Each contact point was 25 μm apart, spanning over 400 μm. A stainless steel screw of 1 mm diameter was implanted into the skull over the cerebellum and used as ground and reference (Figure 3.1B).

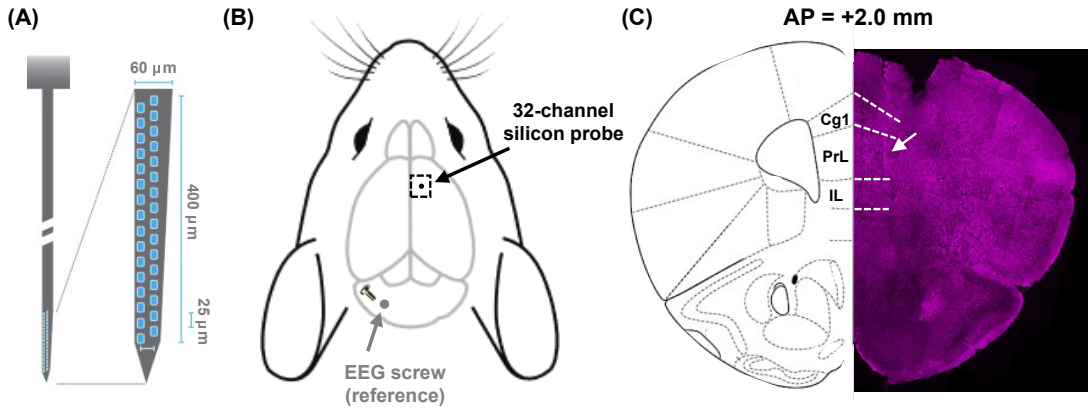

Figure 3.1: Schematic showing the experimental set up for investigation of effect of 5-HT_{2A} receptor agonists on neuronal activity in the mPFC of anaesthetised mice. (A) Layout of a 32-channel silicon probe. Image was taken and adapted from Cambridge Neurotech, UK. (B) A top-down illustration showing the locations of surgically implanted 32-channel silicon probe (black) in the right mPFC (black dotted line shows craniotomy) and ground EEG screw (grey) in the cerebellum. Images adapted from SciDraw (`doi.org/10.5281/zenodo.3925903`). (C) Anatomical atlas demonstrating the silicon probe target site in deep layers of the prelimbic cortex. Coronal section corresponds to 2.0 mm anterior of bregma, adapted from Franklin and Paxinos (2013). Cg1: cingulate area 1; PrL: prelimbic; IL: infralimbic.

3.2.3 Data acquisition

The electrode was connected via an A32-Omnetics32 headstage adaptor (NeuroNexus, MI, USA) to an RHD 32-channel headstage preamplifier (Intan Technologies, CA, USA), which was in turn connected via an Intan SPI cable to an OpenEphys acquisition box (Siegle et al., 2017). The reference screw was connected

to the reference input of the adaptor. The OpenEphys acquisition box was connected to a laptop computer via a USB-C connector where the raw signals were stored. All recordings were sampled at 30 kHz. The signals were monitored on the laptop in real time using the OpenEphys GUI (Figure 3.2).

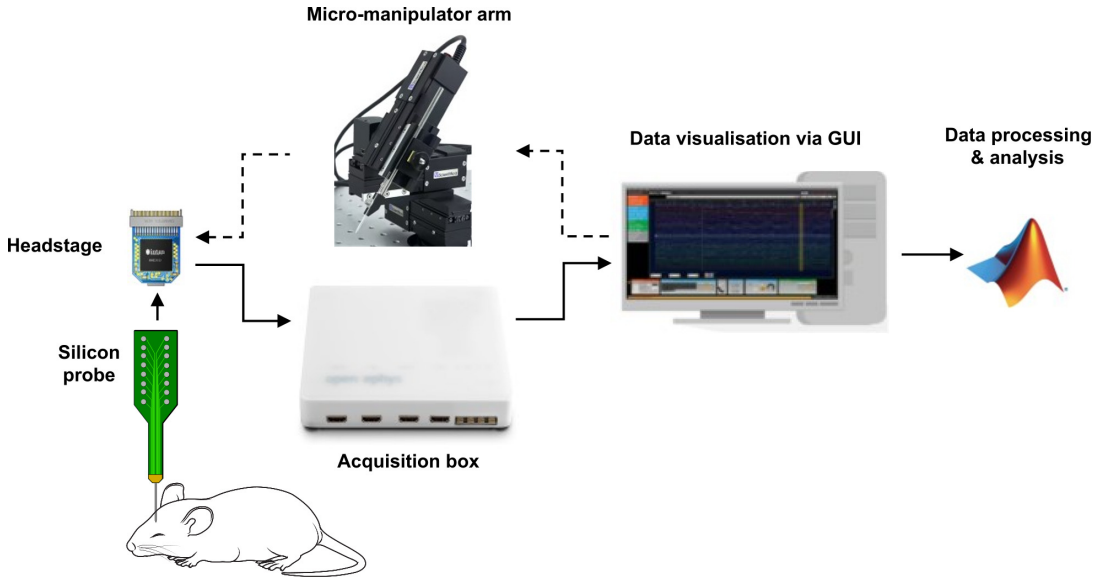

Figure 3.2: Schematic showing the data acquisition pipeline for *in vivo* multi-unit silicon probe recordings. The silicon probe was connected to an Intan headstag that was in turn connected to the micro-manipulator arm by Scientifica and acquisition box by Open Ephys. Both the micro-manipulator arm and acquisition box were connected to a computer for data visualisation on the Open Ephys GUI. Data were then exported, processed and analysed in MATLAB. Black arrows indicate the flow of information, with solid lines as output and dotted lines as input. Images were taken and adapted from SciDraw (`doi.org/10.5281/zenodo.3925977`; `doi.org/10.5281/zenodo.5749462`), Open Ephys (Siegle et al., 2017), Scientifica, and MATLAB.

3.2.4 Terminal recording procedure

Electrophysiology procedures were performed in aseptic conditions with mice under urethane anaesthesia (1.5 g/kg, *i.p.*). Top-ups of 0.01 ml 12.5% urethane were delivered as needed to maintain appropriate anaesthetic depth during the surgery. Anaesthetic doses of urethane potentiate the functions of neuronal nicotinic acetylcholine, $GABA_A$, and glycine receptors, while inhibiting NMDA and AMPA receptors (Hara and Harris, 2002). As a result, electrophysiological

measurements from urethane-anaesthetised animals may be complicated by the molecular mechanisms of urethane (Hara and Harris, 2002). After receiving a dose of 5% glucose-saline for rehydration (*s.c.*) and bupivicane (Marcain) for local anaesthesia in the scalp (*s.c.*), mice were secured to a standard stereotaxic frame (David Kopf Instruments, CA, USA). A liquid gel (Viscotears, Alcon Laboratories Ltd, UK) was locally applied to keep the animal's eyes hydrated. Body temperature was maintained at 35 ± 1°C using a homeothermic heating mat until completion of the surgery, then switched to microwaveable heating pads for the duration of the recording to reduce electrical noise.

The skull was exposed and ensured level in the dorsoventral plane, and a reference screw was implanted over the cerebellum. After a craniotomy (2×2 mm) was made above the right mPFC, the recording electrode was stereotaxically implanted into the prelimbic subregion of the mPFC (coordinates relative to bregma: +2.0 mm anteroposterior, AP; +0.4 mm mediolateral, ML; -1.3 mm and -1.7 mm dorsoventral, DV, from the brain surface). An incision was made in the dura mater to create two flaps, which were subsequently folded back over the edge of the craniotomy. The silicon probe, coated in a fluorescent dye (DiI, Thermo Fisher Scientific, MA, USA) prior to the procedure for verification of the recording site (see Figure 3.1C for example), was inserted using a micro-manipulator stereotaxic arm (LinLab 2, Scientifica, UK) at 2 μm/s, then 1 μm/s as the probe approaches within 200 μm of the target area to minimise tissue damage and improve quality of the recording (Fiáth et al., 2019). Once the recording probe was implanted, signals were allowed to stabilise for 20 min before the recording was started.

3.2.5 Experimental design

Following 15 min of baseline recording, mice were injected *i.p.* with either vehicle (1% acetic acid in 5% glucose-saline) or 0.3 mg/kg MDL-100907 (Tocris Bioscience, UK). Recordings were continued for another 15 min, before mice were injected with 2 mg/kg DOI (Sigma-Aldrich, MO, USA) or 2 mg/kg psilocin (Cayman Chemical Company, MI, USA). An additional group of mice were injected with saline alone. Recordings were continued for a further 30 min. Doses of 2 mg/kg for DOI and psilocin were chosen based on previous studies that increased head-twitch responses in mice (Jennings et al., 2008; Antoniadou et al., 2018).

DOI was dissolved in saline, whereas psilocin was first dissolved in 50 µM tartaric acid, then diluted 1:20 using 5% glucose-saline as an acidity buffer. MDL-100907, on the other hand, was first dissolved in 100% acetic acid, then diluted 1:100 in 5% glucose-saline.

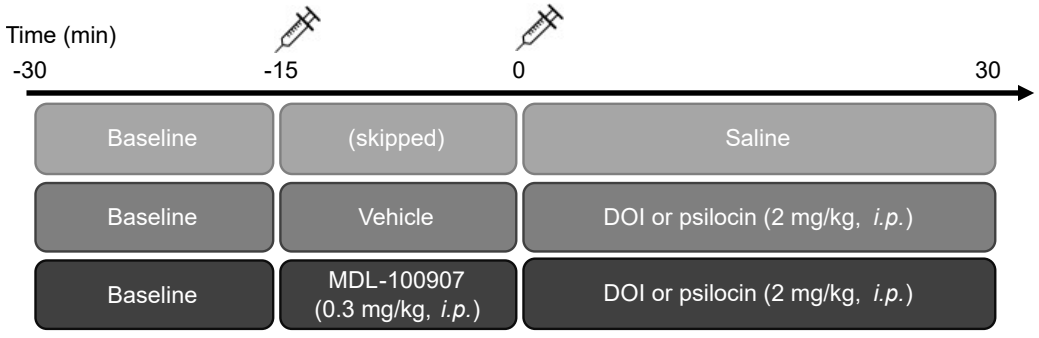

Figure 3.3: Schematic showing the experimental design for investigation of effects of 5-HT_{2A} receptor agonists on neural activity in the mPFC of anaesthetised mice. Time represented in min relative to DOI/psilocin/saline injection.

3.2.6 Histology

Immediately following the termination of recording protocols, mice were euthanised with an overdose of pentobarbitone (Euthanal, *i.p*) and perfused transcardially to achieve brain fixation. Mice were first perfused with 0.1M phosphate-buffered

solution (PBS) until exsanguinated, followed by a fixative solution containing 4% paraformaldehyde (PFA) in 0.1M PBS until the body was fully rigidified. Brains were extracted and post-fixed overnight at 4°C in the same fixative solution and then submerged in a cryoprotective solution containing 30% sucrose in 0.1M PBS for at least 48 hours. 30 μm coronal slices were sectioned using a cryostat at -21°C, and mPFC slices were mounted for *post hoc* verification of silicon probe location.

3.2.7 Data processing and spike sorting

Raw data were exported in flat binary format (.dat) and processed using a custom-written MATLAB script. Data were first processed with a 2nd order bandpass Butterworth filter (high pass at 5000 Hz, low pass at 300 Hz, using the MATLAB *butter* and *filter* functions), then rearranged according to a channel map specified by the recording probe, headstage adaptor, and headstage.

Filtered recording data were processed using the automatic spike sorting algorithm KiloSort2 (Pachitariu et al., 2016) to generate a list of clusters that represent putative single units. These were then manually classified to identify well-sorted single units using Phy (open-source programme available at `https://github.com/cortex-lab/phy`; spike sorting guide available at `https://github.com/kwikteam/phy-contrib/blob/master/docs/template-gui.md`).

Clusters were first assessed by their waveforms for a distinct shape, as well as a large and stable spike amplitude relative to baseline (i.e. good signal-to-noise ratio) over the course of the recording (using WaveformView and AmplitudeView on Phy). Auto-correlograms were then examined for a clear refractory period (using CorrelogramView). Units with poor signal-to-noise ratio, noise-like waveforms, or no indication of refractory periods were classified as noise and discarded. The remaining single units were then compared to each other pair by pair to evaluate

whether they were well-isolated. If the auto-correlograms were the same and looked similar to the cross-correlogram, the two units were then examined by their principal component features for the presence of any overlap (using FeatureView). Clusters that overlap were merged, and the assessment process was repeated from the start. Alternatively, if the original cluster had two distinct waveforms in the same channel or if it showed non-overlapping sub-clusters in its principal component features, it was split into two clusters accordingly and the assessment process was repeated.

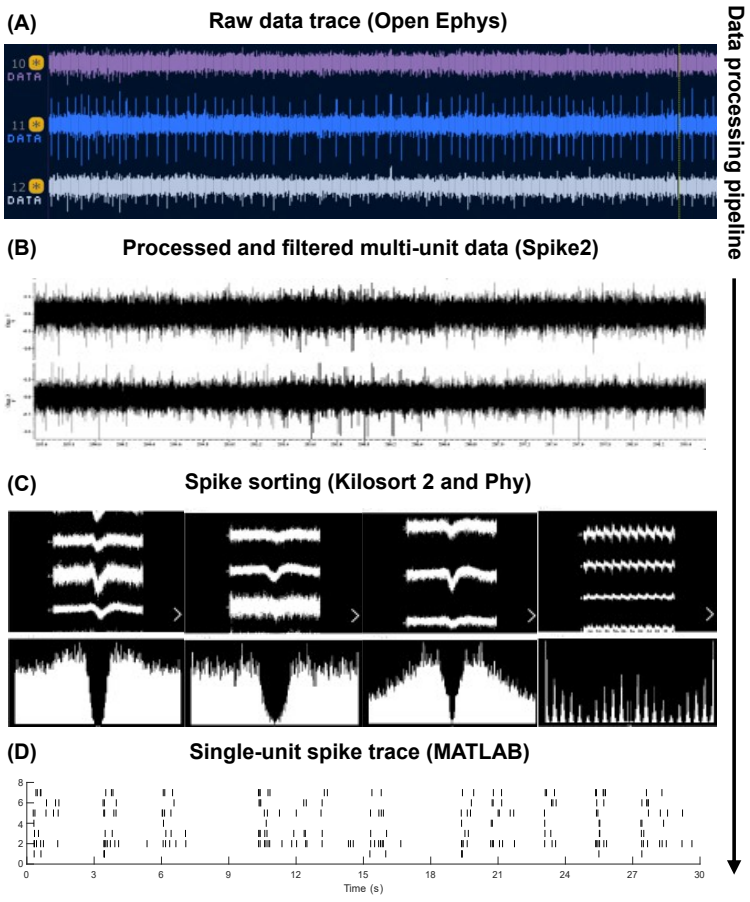

Figure 3.4: Schematic showing the data processing pipeline for *in vivo* multi-unit recordings. This consists of: (A) acquisition of raw data using Open Ephys; (B) processed and filtered multi-unit data via MATLAB, visualised using Spike2; (C) spike sorting process using Kilosort2 and Phy, showing example well-isolated units (first three panels) and noise artefact (fourth panel); (D) final spike trace with each row representing a single unit, visualised and analysed using MATLAB.

After all potential assessments were made, units that satisfied all criteria were classified as well-sorted single units and used for subsequent data analysis. Any

units that were unclear were classified as multi-unit and discarded. At the end of the spike sorting process, spike events of confirmed single units were exported for further analysis. A .csv copy of these files was imported into Spike2 (Cambridge Electronic Design Ltd, UK) for spot-checking against the raw recording trace to ensure that exported units were well-isolated.

3.2.8 Firing rate analysis

The effects of DOI and psilocin on neuronal firing rate were analysed by comparing the data collected 15 min before drug administration (i.e. after administration of either vehicle or MDL-100907) with that collected over the 30 min post-drug period. First, arrays of spike events were binned over 60 sec and converted to arrays of spike counts. Spike count arrays of raw firing rate (Hz) were smoothed with a Gaussian filter (using the MATLAB function *movmean*) and converted to firing rate z-scores. All z-scores were normalised against the 15 min pre-drug period. Firing rate heat maps were generated using these z-scores, with rows sorted in descending order of summed z-scores over the 30 min post-drug period.

Significant responses to the administration of DOI and psilocin were determined by comparing 10 min periods directly before and after drug injection. Data were organised in 60 sec bins. The magnitude of response was quantified in the form of the area under the receiver operator characteristic curve (auROC). Unlike % change calculations, the auROC value is independent of the amplitude of the baseline firing rate (Chance, 2007). Such quantification of firing rate change has been utilised in other multi-unit electrophysiological studies (Cohen et al., 2015; Lottem et al., 2016).

The ROC curve represents the ability of a binary classifier to distinguish between two distributions, as the detection threshold is varied. The ROC curve was generated by plotting the true positive rate (i.e. the rate of correctly identifying the distribution

a given data point belongs to) against the false positive rate (i.e. the rate of mistakenly identifying a given data point as part of the other distribution). The auROC of a perfect detector would be 1, as the curve would traverse the y-axis (100% true positive rate and 0% false positive rate) then horizontally across the x-axis (100% for both true positive and false positive rates). If detection were random, the auROC would be 0.5, as the true positive rate would be equivalent to the false positive rate under all conditions. auROC values can therefore be used as a numerical representation of the degree of overlap between two distributions. An auROC close to 0.5 indicates perfect overlap (i.e. zero or negligible difference between two groups), whereas auROC values close to 0 or 1 indicate little to no overlap between the two groups (i.e. statistically different distributions).

Conventional calculation of the ROC curve involves fitting two normal distributions. However, since the firing rate data did not follow a normal distribution, auROC values were assessed using the Mann-Whitney U / Wilcoxon rank sum test as the nonparametric equivalent (see Section 3.2.13 for more detail). Neurons that showed a statistically significant change in firing rate z-score with an auROC value > 0.5 were labelled as activated units, and those with auROC < 0.5 were labelled as inhibited units.

3.2.9 Unit classification using spike waveform properties

Units identified through spike sorting were classified into putative neuronal types on the basis of their spike waveform properties during the baseline period. For each unit, raw extracellular waveforms were extracted from bandpass-filtered data using the first 300 spikes in the baseline period. These were then normalised and upsampled (using MATLAB *fit* function) to 30,000 kHz to allow for higher-resolution analyses. Key waveform parameters, including peak-to-trough time

(PTT), half-hyperpolarisation width (HHW), and peak asymmetry ratio (PAR), were selected based on literature that identified putative PVINs and verified their identities with optotagging, as reviewed in Section 3.1 (Royer et al., 2012; Senzai et al., 2019, see Figure 3.5). All waveform parameters were calculated using a custom-written MATLAB script. Peak-to-trough time was defined as the time between the maximum amplitude of depolarisation (peak) to the maximum amplitude of afterhyperpolarisation (AHP, trough). Half-hyperpolarisation width referred to the time between the two points of the afterhyperpolarisation at which the amplitude is half the maximum amplitude. The peak asymmetry ratio was calculated using Equation 3.1 and represents the ratio between the amplitude of prehyperpolarisation (PHP) and afterhyperpolarisation. Biphasic waveforms with little to no prehyperpolarisation have peak asymmetry ratio values close to 1, whereas triphasic waveforms have peak asymmetry ratio values close to -1.

$$\text{Peak Asymmetry Ratio (PAR)} = \frac{\text{AHP amplitude - PHP amplitude}}{\text{AHP amplitude + PHP amplitude}} \tag{3.1}$$

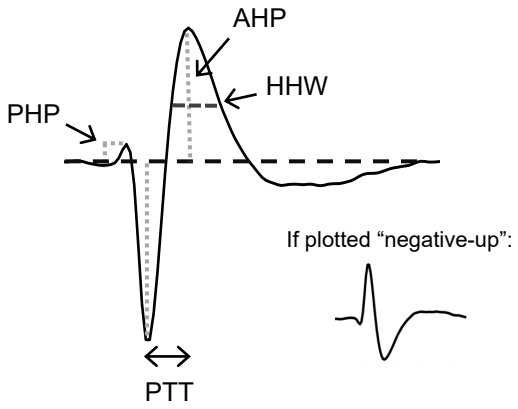

Figure 3.5: Example waveform showing key parameters used in the classification of putative PVINs. PPT: peak-to-trough time, HHW: half-hyperpolarisation width, PHP: prehyperpolarisation, AHP: afterhyperpolarisation.

Using the peak-to-trough time and half-hyperpolarisation width, hierarchical clustering analysis (using MATLAB functions *cluster* and *dendrogram*) was performed to identify two main clusters comprising neurons with narrow waveforms

and broad waveforms. In particular, units of peak-to-trough time ≤ 200 μs and peak asymmetry ratio ≤ 0.5 (i.e. triphasic waveform with prehyperpolarisation amplitude greater than a third of afterhyperpolarisation amplitude) were considered putative axon units and excluded from subsequent analyses (Barry, 2015). Narrow waveform units identified with this method were labelled putative PVINs based on evidence reviewed in Section 3.1. Units were pooled across all experiments for the clustering analysis.

3.2.10 Spike timing correlation analysis using cross-correlograms

The correlation of spike timing between simultaneously recorded pairs of neurons was investigated to identify putative synaptic connections or gap junctions between neurons. Cross-correlograms of spike trains of neuron pairs from the same recording session were constructed using their spike times during the baseline period. To correct for spike rate drift over time, a shift predictor was generated by constructing cross-correlograms where one unit's spike times were kept constant and the other's were shuffled in random order. This process was repeated 1,000 times, and the average shift predictor was subtracted from the raw cross-correlogram to obtain the corrected cross-correlogram.

Clearly defined narrow peaks or troughs in the cross-correlogram between 1.5 and 4.5 ms are suggestive of direct excitatory or inhibitory synaptic connections (Barthó et al., 2004), whereas synchronous firing with zero-lag on a millisecond timescale can indicate putative interneuron coupling via gap junctions (van Welie et al., 2016; Peyrache and Destexhe, 2019).

Cross-correlograms were binned in 0.5 ms windows, and a Poisson distribution was fitted over a moving 7-ms Gaussian window to calculate the moving mean and standard deviation (Senzai et al., 2019). A putative connection was considered

significant when at least two consecutive 0.5 ms bins within the target window fell above or below the statistical threshold of mean ± 4 standard deviations (Insel and Barnes, 2015). The target window was defined as +1.5 to +4.5 ms for putative post-synaptic connections and -1.0 to +1.0 ms for putative gap junctions. The magnitude of spike time correlation was computed as the % change in area under the curve during the target window compared to the threshold.

The proportions of significantly correlated neuronal pairs, as well as the magnitude of spike time correlation, were compared between neuron pair types. For putative post-synaptic connections, correlation values were unidirectional, and four neuron pair types were considered: between two putative PVINs (PV→PV), putative PVIN to broad waveform unit (PV→BW), broad waveform unit to putative PVIN (BW→PV), and between two broad waveform units (BW→BW). For putative gap junctions, there were only three neuronal pair types (PV↔PV, PV↔BW, BW↔BW) as the target window (-1.0 to +1.0 ms) is symmetrical.

3.2.11 Spike count correlation analysis

To investigate neuronal correlations on a longer timescale (i.e. spike count level), Pearson correlation coefficients (r values) were computed using spike count arrays (organised in 60 sec bins) of neuron pairs from simultaneous recording sessions (using the MATLAB function *corrcoef*). To test for the statistical significance of r values, a null distribution was generated for each recording session in a process similar to that described in Section 3.2.10. Correlation coefficients were calculated using inter-spike-interval-shuffled spike time data, and the resulting null distribution was compared to the observed r values. This process was repeated 1,000 times, and r values with $p < 0.05$ were considered statistically significant.

The effects of DOI and psilocin on spike count correlations were evaluated by repeating the Pearson correlation coefficient calculation for pre-drug and post-drug windows. The magnitude of correlation before and after drug injection, in terms of absolute r values, were compared for neuron pairs involving a putative PVIN (i.e. PV-PV and PV-BW).

3.2.12 LFP and spectral analysis

To analyse cortical LFP signals, raw multi-unit data were first downsampled to 1,000 Hz, then processed with a 2^{nd} order bandpass Butterworth filter between 0.5 and 150 Hz for low frequencies. Short-time Fourier transform was applied to the data in 10 sec segments with 50% overlap, and the power spectral density (PSD, power/frequency in dB/Hz) in the slow wave activity (SWA) range ($0.1 - 2$ Hz) was calculated (using the MATLAB functions *spectrogram* and *fft*). PSD values were subsequently converted to z-scores normalised to the pre-drug time window.

3.2.13 Statistical analysis

All statistics were carried out in MATLAB. The normality of data was first determined using the Shapiro-Wilk test (using the MATLAB function *swtest*). For normally distributed data, two-tailed Student's t-tests were performed when comparing two groups (using the MATLAB functions *ttest2* for unpaired data and *ttest* for paired data), while one-way ANOVA tests with *post hoc* Bonferroni comparisons were performed when comparing more than two groups (using the MATLAB functions *anova* and *multcompare*). For nonparametric data, the Mann Whitney-U test was performed (using the MATLAB functions *ranksum*). The Wilcoxon rank sum W value was first converted to the U value and subsequently to

auROC values using Equations 3.2-3.3 , where n denotes the sample number of the datasets x and y.

$$W = U - \frac{n_x(n_x + 1)}{2} \tag{3.2}$$

$$auROC = \frac{U}{n_x n_y} \tag{3.3}$$

Where more than five statistical tests were carried out in the same dataset, the Benjamini-Hochberg procedure with a false discovery rate (pFDR) of 5% was applied to correct for multiple testing errors.

3.3 Results

To determine the effects of DOI and psilocin on the activity of mPFC neurons *in vivo*, silicon probe multi-unit recordings were performed in urethane-anaesthetised mice, targeting deep layers of the prelimbic cortex. Prior to each recording session, the silicon probe was coated with a fluorescent dye to allow for *post hoc* confirmation of probe localisation (Figure 3.1, see Section 3.2 for detail). Recordings were performed in 19 wildtype mice.

3.3.1 Effects of DOI and psilocin on network oscillations

First, spectral analysis was performed to isolate LFP signals from each recording session. Since these recordings were obtained from urethane-anaesthetised mice, LFP spectra were dominated by sleep-like slow wave activity (SWA) oscillations in the $0.1 - 2$ Hz range (Figure 3.6A).

Administration of 2 mg/kg *i.p.* DOI (n = 4 mice) or 2 mg/kg *i.p.* psilocin (n = 5 mice), but not saline (n = 3 mice), disrupted LFP oscillations in SWA range (Figure 3.6A). Pre-drug and post-drug windows used for statistical comparisons were defined as the 10 min periods immediately before and after drug injection, and were selected based on the duration of SWA disruption caused by DOI and psilocin (Figure 3.6B). Within-animal statistical analyses comparing the mean LFP power in SWA range before and after drug injection showed that both DOI and psilocin, but not saline, significantly reduced SWA (Figure 3.6C; two-tailed paired t-test; saline, $t(2) = -0.2078$, $p = 0.8455$; DOI, $t(3) = 2.530$, $p = 0.0447$; psilocin, $t(4) = 2.937$, $p = 0.0425$).

To confirm that the effects of DOI and psilocin were 5-HT_{2A} receptor-mediated, additional experiments were conducted where 0.3 mg/kg *i.p.* MDL-100907, a selective 5-HT_{2A} receptor antagonist, was given 15 min prior to DOI or psilocin. In

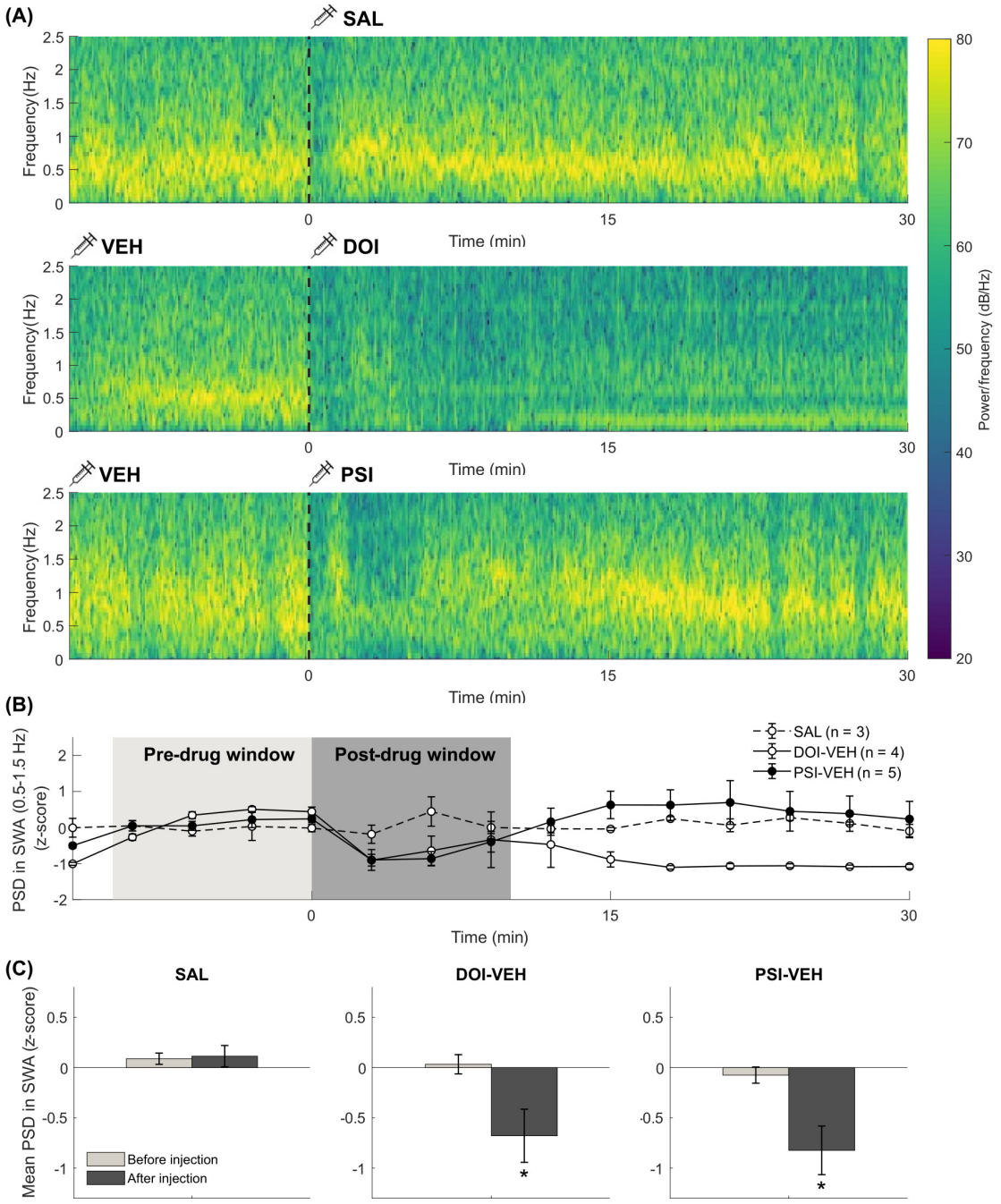

Figure 3.6: Effect of DOI (2 mg/kg *i.p.*), psilocin (PSI, 2 mg/kg *i.p.*), and saline (SAL) on LFP power in SWA range (0.1 − 2 Hz) in the mPFC. (A) Example spectrograms from mice that received a dose of saline (top), DOI after vehicle (middle), and psilocin after vehicle (bottom). Black dotted line indicates time of injection. (B) Change in relative power spectral density (PSD, z-score) over time in 3-min bins in mice that received saline (SAL, n = 3), DOI after vehicle (DOI-VEH, n = 4), and psilocin after vehicle (PSI-VEH, n = 5). Highlighted areas in light and dark grey represent the time windows used for pre-drug and post-drug comparisons. (C) Change in mean PSD (z-score) 10 min prior to injection compared to 10 min immediately after injection for each group. Data are presented as mean ± SEM. *p<0.05.

mice pre-treated with MDL-100907, the reduction in SWA immediately after DOI or psilocin injection was blocked (Figure 3.7A, B). Within-animal statistical analyses further confirmed that MDL-100907 blocked the suppression of SWA induced by DOI and psilocin (Figure 3.7D, F; two-tailed paired t-test, pre-drug vs. post-drug; DOI-MDL, t(2) = 0.2964, p = 0.7949; PSI-MDL, t(3) = -1.447, p = 0.1982).

3.3.2 Isolation of single-unit signals from multi-unit recordings

Having confirmed the 5-HT_{2A} receptor-mediated effects of DOI and psilocin on local network oscillations in the prelimbic region of the mPFC, the effects of DOI and psilocin were next examined at a higher spatial resolution by isolating single-unit signals.

A multi-step data processing and analysis pipeline utilising various programmes and custom-written scripts was developed throughout the course of the project (see Section 3.2 for more detail). First, raw data exported from the Open Ephys acquisition system were filtered and processed. Putative single-unit signals in the filtered data were identified through an automatic spike sorting process using KiloSort 2, followed by manual filtering in Phy. Noise artefacts and any units with unclear signal-to-noise indicators were discarded. The resulting single-unit data were analysed in MATLAB (n = 443 units across 19 mice). Examples of final single-unit recording traces are shown in Figure 3.8.

3.3.3 Effects of DOI and psilocin on multi-unit activity

Multi-unit activity over time, as a read-out of the aggregate firing activity of the local neuronal population, was computed as the sum of all single-unit activity in the mPFC from each mouse. The net effects of DOI and psilocin on the overall

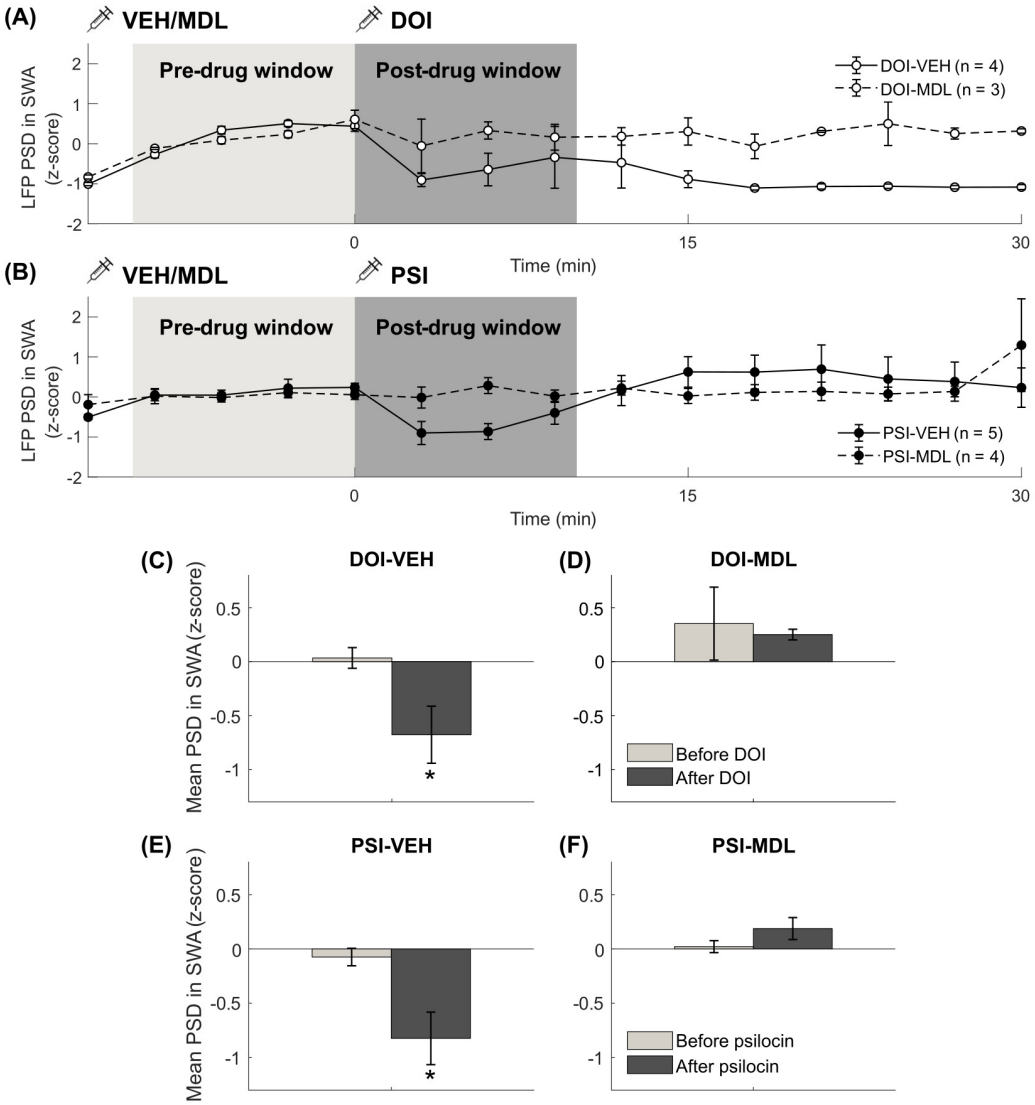

Figure 3.7: Effects of pre-treatment with MDL-100907 (abbreviated to MDL) on the suppression of LFP power in SWA frequencies (0.1 − 2 Hz) by DOI and psilocin (PSI). Line plots showing the change in mean PSD of LFP in SWA range over time, in (A) mice that received vehicle dose prior to DOI (DOI-VEH, n = 4) and MDL-100907 prior to DOI (DOI-MDL, n = 3), and (B) mice that received vehicle prior to psilocin (PSI-VEH, n = 5) and MDL-100907 prior to psilocin (PSI-MDL, n = 3). Comparison of mean PSD (z-score) in SWA range in mice that received (C) vehicle before DOI, (D) MDL-100907 before DOI, (E) vehicle before psilocin, and (F) MDL-100907 before psilocin. Data are represented as mean ± SEM. *p<0.05.

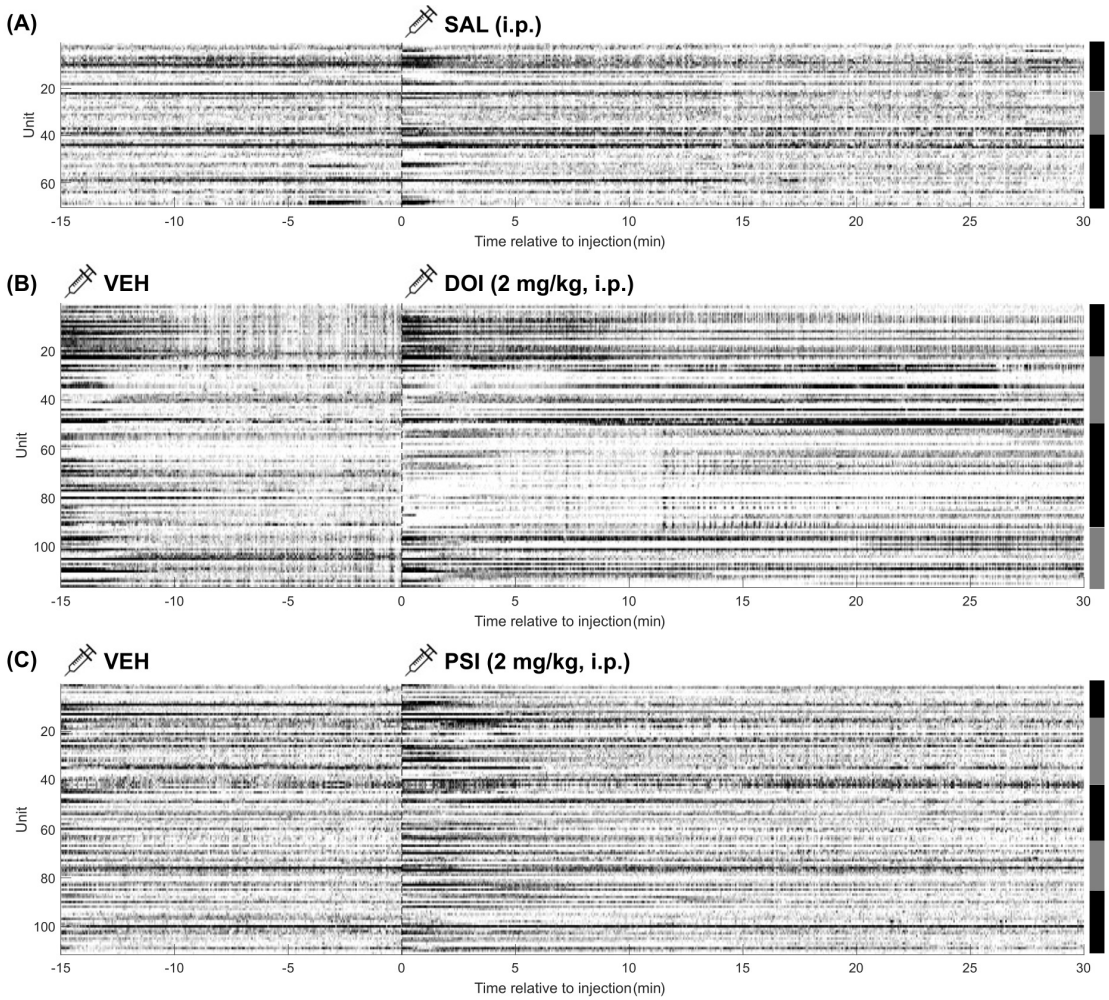

Figure 3.8: Spike traces from (A) saline (SAL), (B) DOI after vehicle (DOI-VEH), and (C) psilocin after vehicle (PSI-VEH) recordings. Each row represents a single unit, and alternating black/grey bars on the right hand side indicate neurons recorded simultaneously from the same mouse. (A) n = 70 neurons from 3 mice (21, 18, 31 from each mouse). (B) n = 116 neurons from 4 mice (23, 27, and 43, 23 from each mouse). (C) n = 111 neurons from 5 mice (15, 28, 22, 19, 27 from each mouse).

activity of mPFC neurons were first determined using this parameter (Figure 3.9A). Despite providing less spatial resolution than single-unit activity analysis, multi-unit activity analysis allows for the compartmentalisation of data obtained from different mice and serves as a key step to provide confidence that the effects of DOI and psilocin were observed across all mice before proceeding to single-unit analysis.

As predicted by DOI and psilocin's SWA-suppressing effects, DOI and psilocin significantly increased multi-unit activity in the mPFC compared to pre-drug levels

(Figure 3.9B; two-tailed paired t-test; DOI, t(3) = -6.903, p = 0.0023; psilocin, t(4) = -4.073, p = 0.0152), whereas saline had no significant effect in the post-injection compared to the pre-injection period (Figure 3.9B; two-tailed paired t-test; saline, t(2) = -2.271, p = 0.0856).

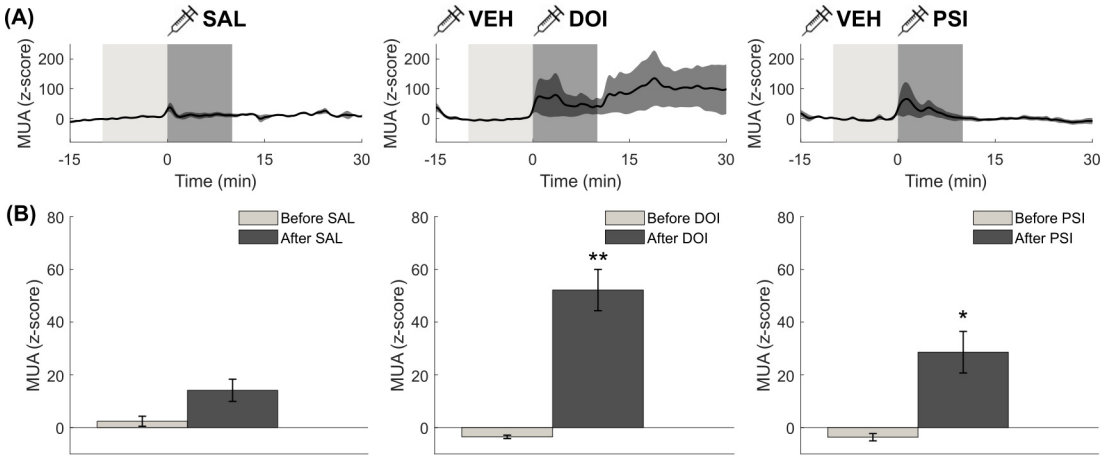

Figure 3.9: Effects of saline, DOI (2 mg/kg, *i.p.*), and psilocin (2 mg/kg, *i.p.*) on mPFC multi-unit activity. (A) Multi-unit activity (MUA) of all units that received a dose of saline (SAL, n = 70 neurons across 3 mice, DOI after vehicle (VEH) (n = 116 neurons across 4 mice), and psilocin (PSI) after vehicle (VEH) (n = 111 neurons across 5 mice). Shaded areas indicate time windows used for statistical analysis (i.e. time = -10 to 0 v. 0 to 10 min). (B) Bar charts showing the effects of saline (left), DOI (middle), and psilocin (right) on the mean MUA between pre-drug and post-drug windows. Data are represented as mean ± SEM. *p<0.05, **p<0.01.

In experiments where mice were pre-treated with MDL-100907, the increase in multi-unit activity caused by DOI injection was blocked and even reversed (Figure 3.10B; two-tailed paired t-test, pre-drug vs. post-drug; DOI-MDL, t(3) = 8.249, p = 0.001). Unlike the case for DOI, MDL-100907 did not completely reverse the effects of psilocin on overall neuronal activity in the mPFC (Figure 3.10C). A within-animal two-tailed paired t-test showed that psilocin administration had no effect on multi-unit activity in mice pre-treated with MDL-100907 (Figure 3.10D; PSI-MDL, t(3) = -1.311, p = 0.2601).

Between-animal statistical analyses showed that both DOI and psilocin increased multi-unit activity in the mPFC compared to pre-drug control levels (Figure 3.11;

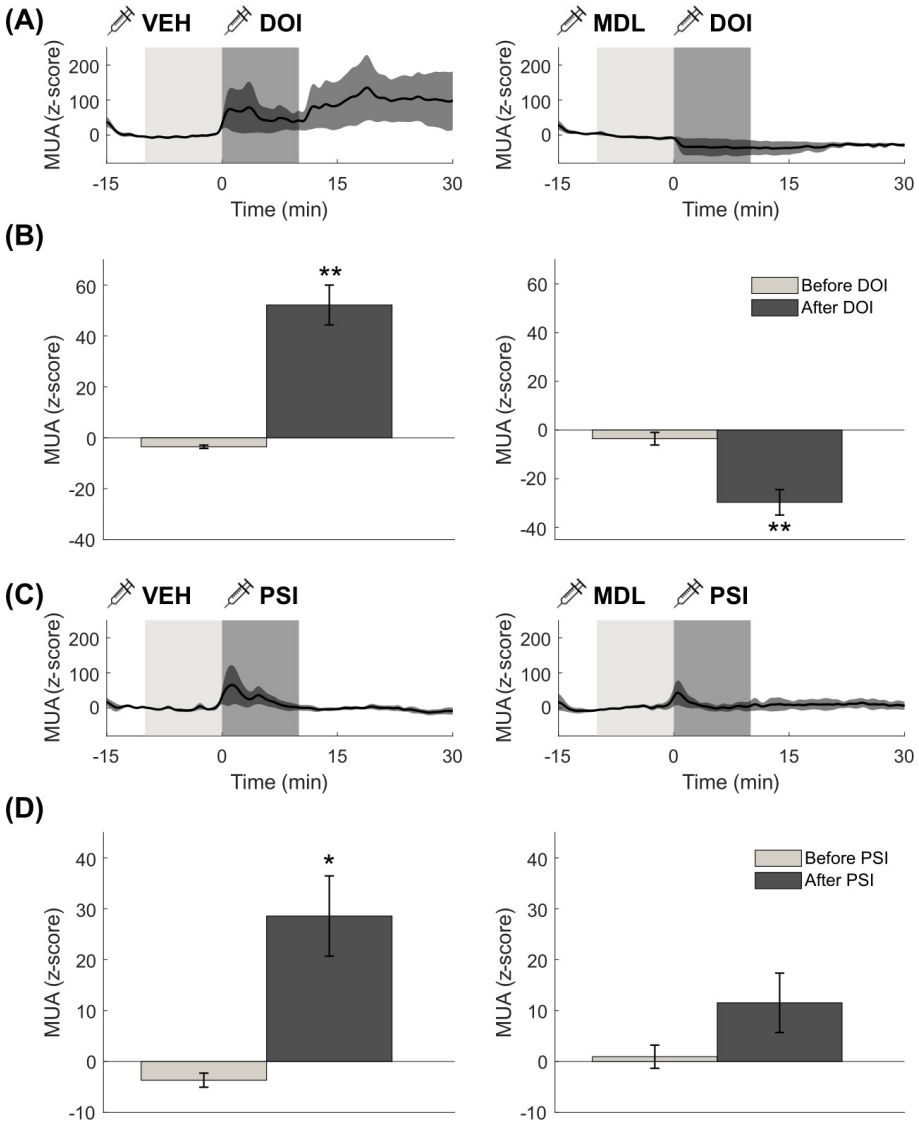

Figure 3.10: Effects of MDL-100907 (abbreviated to MDL) pre-treatment on the effects of DOI and psilocin on multi-unit activity in the mPFC. Relative multi-unit activity (MUA, *z*-score) over time for units that received (A) DOI after vehicle (left panel, n = 116 neurons across 4 mice) and DOI after MDL-100907 (right panel, n = 67 neurons across 3 mice), and (C) psilocin after vehicle (left panel, n = 111 neurons across 5 mice) and psilocin after MDL-100907 (right panel, n = 79 neurons across 4 mice). Shaded areas indicate time windows used for statistical analysis (i.e. time = -10 to 0 vs. 0 to 10 min). Bar charts showing the change in relative MUA between the vehicle group (left) and MDL-100907 group (right) before and after (B) DOI injection and (D) psilocin injection. Data are represented as mean ± SEM. *p<0.05, **p<0.01.

one-way ANOVA; $F_{4,14} = 33.26$, $p < 0.001$; Bonferroni's *post hoc* comparisons; DOI vs. SAL, $p < 0.001$; psilocin vs. SAL, $p = 0.0155$). These effects were attenuated, and in the case of DOI, reversed, by pre-treatment with MDL-100907

(Figure 3.11; Bonferroni's *post hoc* comparisons; DOI vs. DOI-MDL, $p < 0.001$; PSI vs. PSI-MDL, $p = 0.0075$).

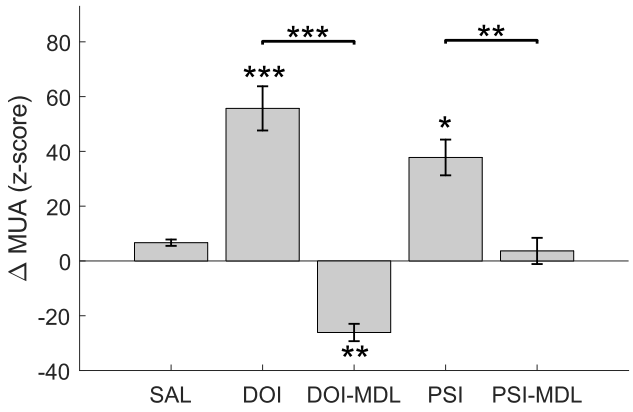

Figure 3.11: Comparison of magnitude of change in multi-unit activity (MUA) after saline (SAL), DOI alone (DOI), DOI after MDL-100907 (DOI-MDL), psilocin alone (PSI), and psilocin after MDL-100907 (PSI-MDL). Data are represented as mean ± SEM. *p<0.05, **p<0.01, ***p<0.001.

3.3.4 Effects of DOI and psilocin on the single-unit activity of mPFC neurons

Next, the effects of DOI and psilocin on single-unit activity were examined, initially with recorded units from all mice in each experiment pooled for analysis. The relative firing rates over time (z-scores) of individual neurons were visualised as heat maps, where each row represents one unit (see top panels of Figure 3.12A-C). Each neuron was classified by its response to drug injection as activated, inhibited, or unchanged. The firing rate of each neuron between the pre-drug and post-drug windows (t = -10 to 0 min vs. t = 0 to 10 min) was statistically compared using the Mann-Whitney U test to identify significant responders ($p < 0.05$), and the Benjamini-Hochberg procedure was applied to correct for false positives from multiple comparisons (false discovery rate, pFDR = 0.05). As shown in Figure 3.12, DOI and psilocin significantly altered the firing rate of a subpopulation of

mPFC neurons, with both excitatory and inhibitory effects being detected, whereas saline had no significant effect.

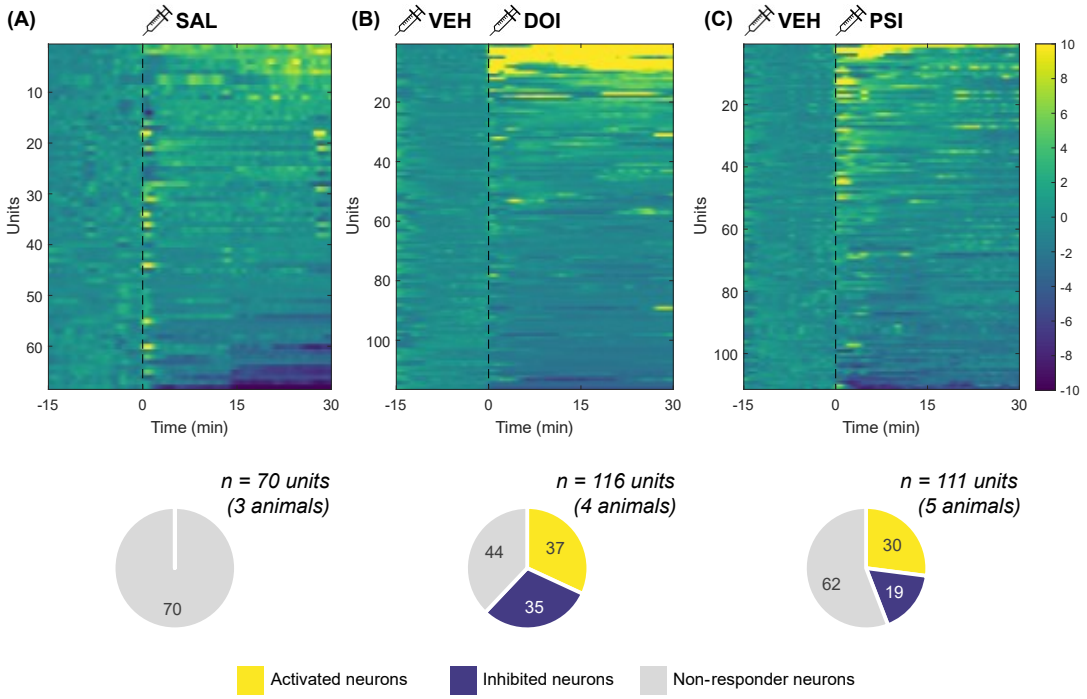

Figure 3.12: Effects of (A) saline, (B) DOI (2 mg/kg, *i.p.*), and (C) psilocin (2 mg/kg, *i.p.*) on single-unit activity in the mPFC. Top panels show heat maps of firing rate z-scores over time for each experiment. Each row represents one unit, and rows were sorted in descending order according to their z-scores after drug injection. Bottom panels display pie charts showing proportions of units in each experiment that were significantly activated (yellow) and inhibited (blue) after drug injection. Non-responder units are in grey.

Additionally, DOI appeared to act on a different timescale compared to psilocin (Figure 3.13A, B). In the case of DOI, both activations and inhibitions were long-lasting and sustained until the end of the recording. In contrast, the excitatory and inhibitory effects of psilocin were more acute and returned to pre-drug levels by the end of the recording (see Figure 3.13C for example neuron traces). This difference is consistent with the earlier observations of psilocin's short-lasting effects on SWA and multi-unit activity compared to DOI (see Figure 3.6 and Figure 3.9).

Overall, single-unit analysis revealed heterogeneous effects of DOI and psilocin on the firing rate of individual mPFC neurons on varying timescales. To further investigate the actions of DOI and psilocin, the role of 5-HT_{2A} receptors was determined.

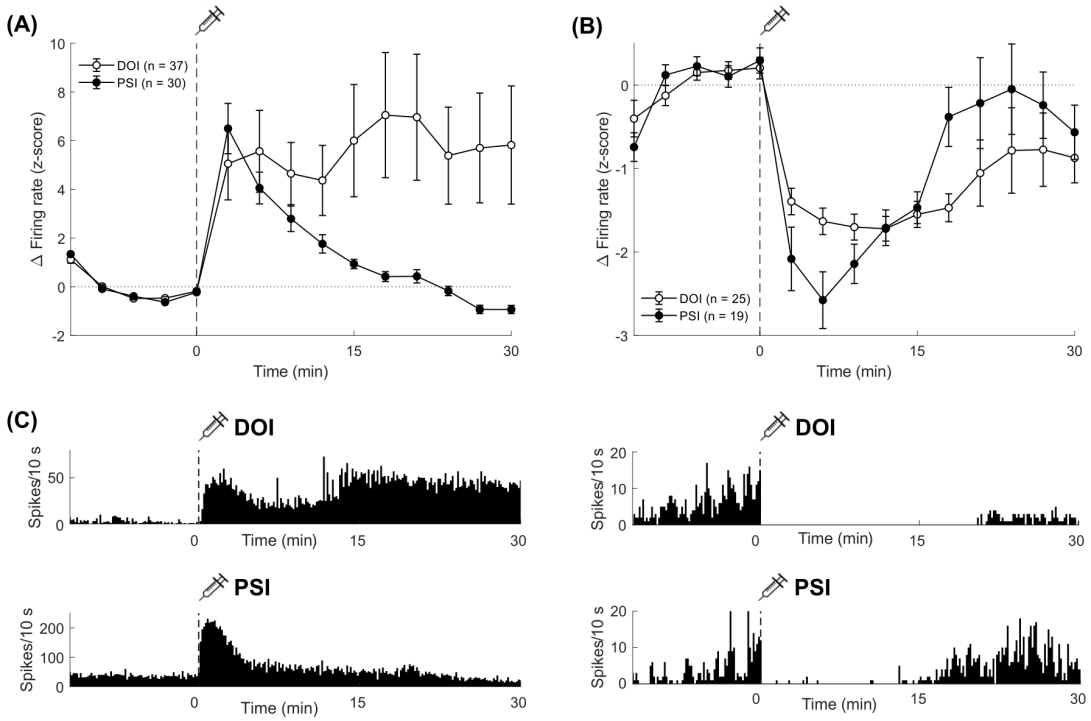

Figure 3.13: The timescale of DOI and psilocin's effects on firing rates. (A) Line plots of normalised firing rate of units activated by DOI (n = 37) and psilocin (n = 30) in z-scores over time. (B) Line plots of normalised firing rate of units inhibited by DOI (n = 25) and psilocin (n = 19) in z-scores over time. (C) Example spike traces of neurons activated by DOI (top left) and psilocin (bottom left), as well as neurons inhibited by DOI (top right) and psilocin (bottom right), with black dotted lines indicating time of injection. Data are represented as mean ± SEM.

At a single-unit level, heat maps were produced (top panels of Figure 3.14A, B) and responder neurons were again identified with Mann-Whitney U tests ($p < 0.05$) alongside the Benjamini-Hochberg procedure (pFDR = 0.05). Subsequently, the U value was converted to auROC (middle panels of Figure 3.14A, B). ROC analysis is traditionally used to distinguish two distributions of responses, and is particularly useful here as its area under the curve provides a measure for the magnitude of change that is independent of the scale of baseline values (Chance, 2007, see Section 3.2 for more detail). Activated neurons had auROC values trending towards 1 (i.e. pre-drug and post-drug distributions were statistically different in the positive direction), whereas inhibited neurons had auROC values close to 0 (i.e. pre-drug and post-drug distributions are statistically different in the negative direction).

auROC values close to 0.5, on the other hand, represent those with no significant difference between pre-drug and post-drug distributions.

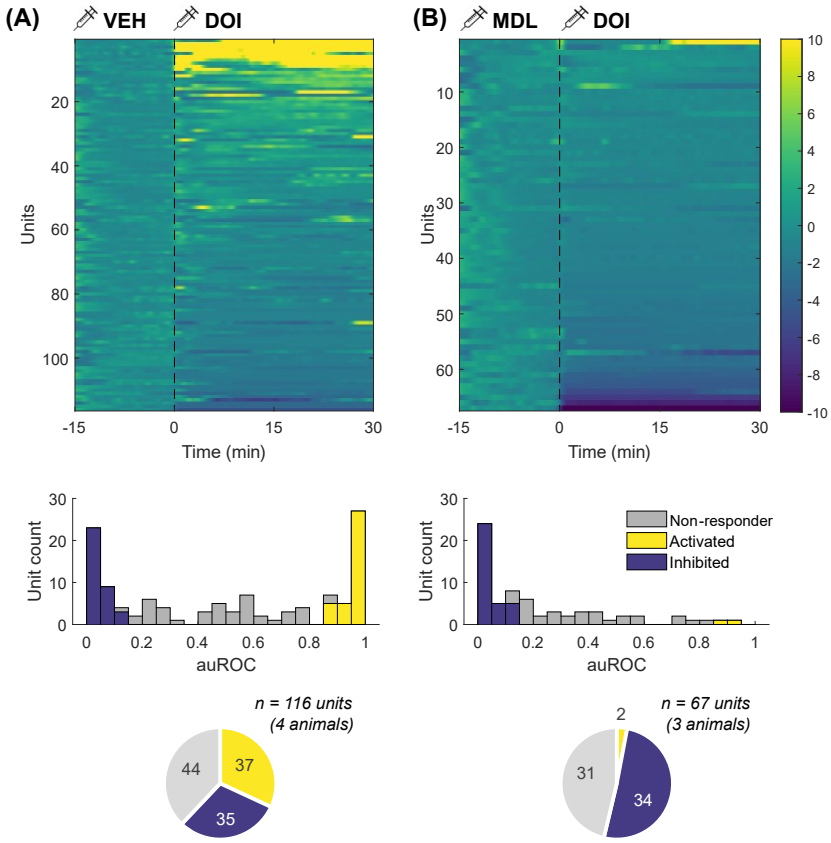

Figure 3.14: Effects of DOI on single-unit activity in mice treated with (A) DOI + vehicle versus (B) DOI + MDL-100907 (abbreviated to MDL). Top panels show firing rate heat maps of neurons that received a pre-treatment dose with (A) vehicle solution (n = 116 neurons across 4 mice) and (B) MDL-100907 (n = 67 neurons across 3 mice) prior to DOI (black dotted line). Middle panels are histograms showing the area under receiver operator characteristic curve (auROC), a measure of magnitude of change, of neurons that received (A) vehicle and (B) MDL-100907 prior to DOI. Activated neurons are highlighted in yellow, and inhibited neurons are highlighted in blue. Grey neurons were non-responders. Bottom panels display pie charts showing the proportion of neurons in each experiment that were activated (yellow) or inhibited (blue) by DOI.

Statistical testing revealed an almost completely abolished population of activated neurons (2.99%, 2/67) in the DOI + MDL-100907 group compared to the DOI + vehicle group (31.9%, 37/116; bottom panels of Figure 3.14A, B). In the DOI + MDL-100907 group, the proportion of inhibited neurons increased from 30.2% (35/116) to 50.7% (34/67), reflecting the earlier observation that MDL-100907 reversed the excitatory effects of DOI on multi-unit activity. Single-unit analyses in

Figure 3.15 showed that MDL-100907 attenuated the number of neurons excited by psilocin, with the psilocin + MDL-100907 group showing a decreased proportion of activated units (11.4%, 9/79) compared to mice receiving psilocin + vehicle (27.0%, 30/111). The number of inhibited neurons was similar across both groups (psilocin + vehicle, 17.1%, 19/111; psilocin + MDL-100907, 15.2%, 12/79).

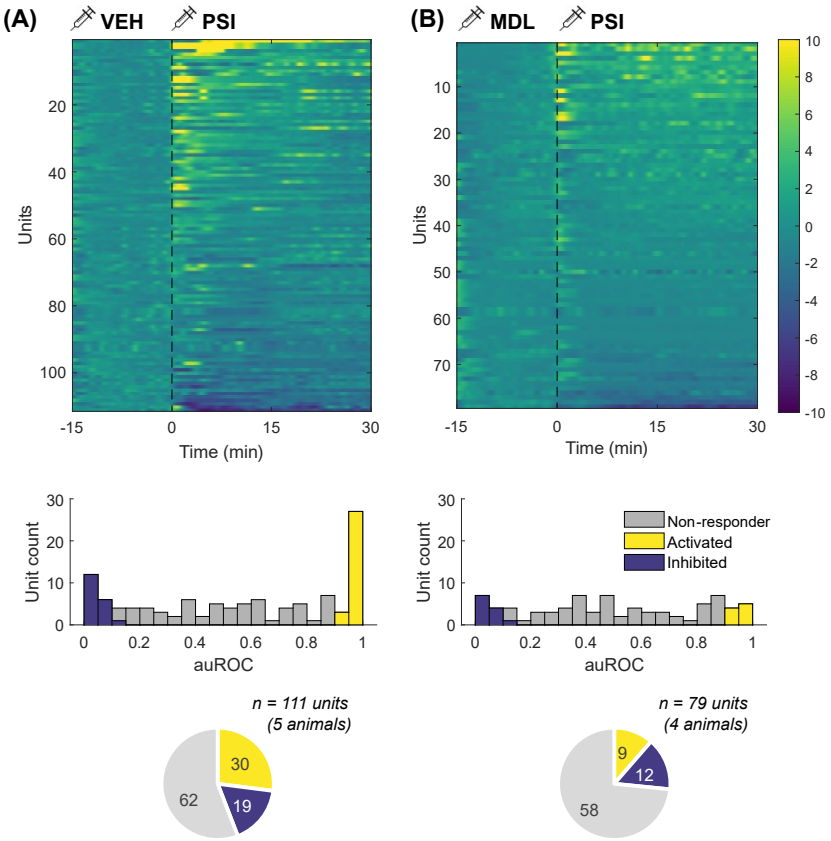

Figure 3.15: Effects of psilocin (PSI) on single-unit activity in mice treated with (A) psilocin + vehicle versus (B) psilocin + MDL-100907 (abbreviated to MDL). Top panels show firing rate heat maps of neurons that received a pre-treatment dose with (A) vehicle (n = 119 neurons across 5 mice) and (B) MDL-100907 (n = 79 neurons across 4 mice) prior to psilocin (black dotted line). Middle panels are histograms showing the area under receiver operator characteristic curve (auROC), a measure of magnitude of change, of neurons that received (A) vehicle and (B) MDL-100907 prior to psilocin. Activated neurons are highlighted in yellow, and inhibited neurons are highlighted in blue. Grey neurons were non-responders. Bottom panels display pie charts showing the proportion of neurons in each experiment that were activated (yellow) or inhibited (blue) by psilocin.

Overall, higher resolution analysis revealed heterogeneous effects of DOI and psilocin at a single-unit level. Pre-treatment with MDL-100907 reduced the excitatory effects of psilocin and DOI. On the other hand, the number of neurons

inhibited by DOI was increased by pre-treatment with MDL-100907, whereas the number of neurons inhibited by psilocin remained similar.

3.3.5 Identification of putative PVINs via unit clustering

To determine whether DOI and psilocin affected the firing rates of mPFC PVINs specifically, the electrophysiological parameters of individual neurons were more closely examined to differentiate putative PVINs from other neuronal types present in the dataset. Hallmark electrophysiological features are reported to distinguish PVINs from other neuron types, including other interneuron subtypes. These characteristic features include their fast-spiking phenotype and narrow spike waveforms resulting from brief action potentials and fast afterhyperpolarisation, as discussed in Chapter 2 and Section 3.1 (see also Booker et al., 2014; Hu et al., 2014).

First, firing rate was investigated as a potential PVIN classification parameter. However, it became clear from the dataset that in the presence of urethane anaesthesia, fast-spiking neurons were rarely detected in these silicon probe recordings. Next, extracellular spike waveforms were extracted from the raw data, and the average waveform of each unit was computed using its first 300 spikes during the baseline period. These waveforms were quantified by two width measures, namely peak-to-trough time (PTT) and half-hyperpolarisation width (HHW). The peak-to-trough time describes the duration from a waveform's peak (depolarisation) to its trough (afterhyperpolarisation), whereas the half-hyperpolarisation width describes the width between the two points of afterhyperpolarisation at which the amplitude equals half of the maximum amplitude (Figure 3.16A). Half-hyperpolarisation widths followed a bimodal distribution, a characteristic often used for the classification of interneurons versus pyramidal neurons in the literature (Figure 3.16B; Senzai et al., 2019; Tseng and Han, 2021). However, it has been suggested that neuron

classification based on a single waveform feature may be inaccurate, as neurons of different types may appear to overlap in one feature but be dissimilar in another (Robbins et al., 2013).

As a next step, hierarchical clustering was performed using both peak-to-trough time and half-hyperpolarisation width based on Euclidean distances between each point (Figure 3.16C). Two clusters were identified, one of which consisted of narrow waveform (NW) spikes with peak-to-trough time and half-hyperpolarisation width dimensions of < 0.55 ms (n = 95 neurons, 21.4% of the population), and the other of broad waveform (BW) spikes (n = 346 neurons, 78.1%; Figure 3.16D). According to this classification, narrow waveform units exhibited a higher median firing rate than broad waveform units (Figure 3.16E; 2.47 ± 0.43 Hz vs. 1.39 ± 0.10 Hz; Mann-Whitney U test, Z = 2.493, p = 0.0127). This is consistent with the corresponding characteristics of PVINs and non-fast-spiking neurons, even though the differences were smaller than expected. These narrow waveform units will be referred to as putative PVINs from now on.

Notably, four main types of waveforms were observed – biphasic putative PVIN, biphasic broad waveform, triphasic putative PVIN, and triphasic broad waveform (see Figure 3.16F for examples). The peak asymmetry ratio (PAR) was evaluated as the ratio between the afterhyperpolarisation and prehyperpolarisation peaks. The majority of units had high peak asymmetry trending towards one (Figure 3.17A, n = 225, 50.8% with peak asymmetry ratio > 0.75), representing biphasic waveforms with afterhyperpolarisation at least seven times larger than prehyperpolarisation. A small number of units are highly triphasic (n = 37, 8.35% with peak asymmetry ratio < 0, i.e. prehyperpolarisation was greater than afterhyperpolarisation) but have a broad waveform. These triphasic broad waveform units were not considered putative axon units, as axon waveforms have a much shorter average peak-to-trough time of 172 μs (Barry, 2015). Overall, units with peak-to-trough time ≤ 200 μs and peak

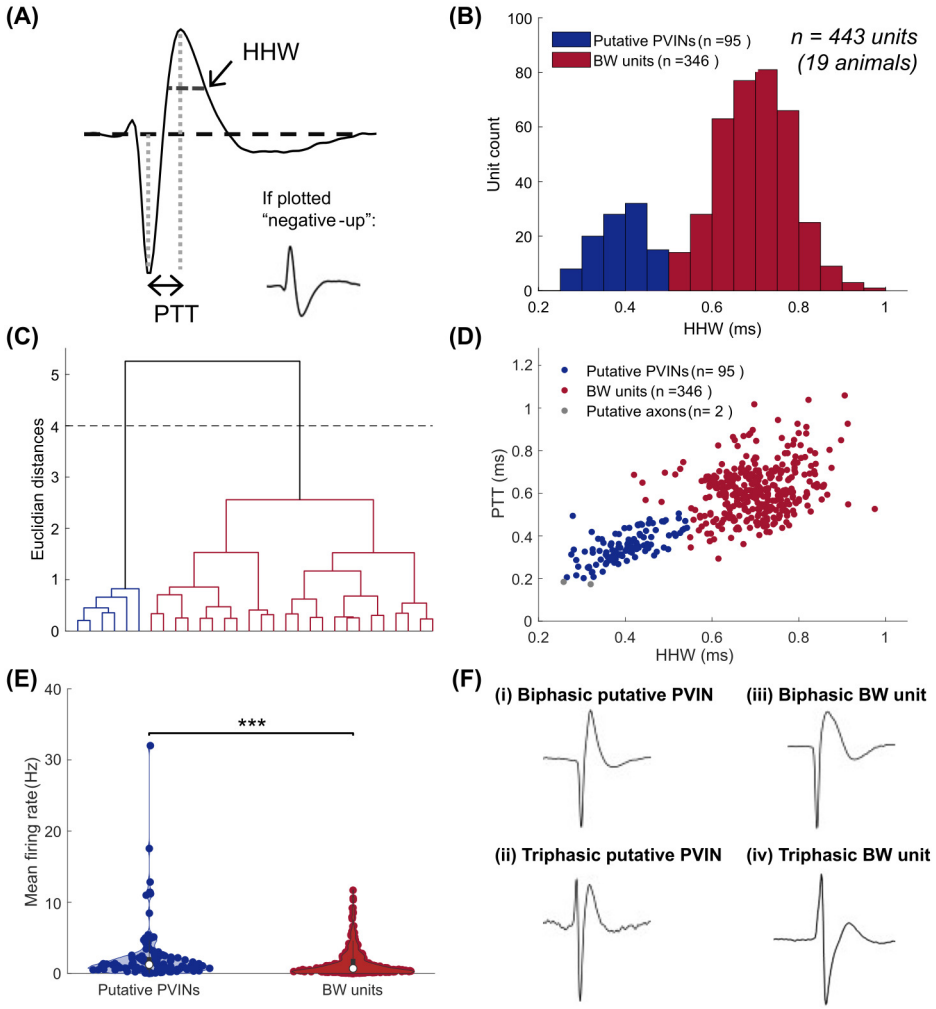

Figure 3.16: Classification of putative PVINs (narrow waveform, NW units) based on their waveform properties. (A) Example waveform showing how peak-to-trough time (PTT) and half-hyperpolarisation width (HHW) were calculated. (B) Histogram showing the bimodal distribution of HHW of units (n = 443 neurons across 19 mice), with putative PVINs highlighted in blue and other broad waveform (BW) units in red. (C) Dendrogram showing the hierarchical clustering and classification of neurons according to their PTT and HHW. Black dotted line represents the clustering threshold used to generate the scatter plot in (D). (D) Scatter plot showing the distribution of putative PVINs (blue), BW neurons (red), and putative axonal units (grey), allocated according to the dendrogram shown in (C). (E) Baseline firing rate (Hz) of putative PVINs (n = 95) compared to other BW units (n = 346). ***p<0.001. (F) Example waveforms showing (i) biphasic putative PVIN, (ii) triphasic putative PVIN, (iii) biphasic BW unit, (iv) triphasic BW unit.

asymmetry ratio ≤ 0.5 (i.e. prehyperpolarisation peak of amplitude greater than or equal to a third of afterhyperpolarisation amplitude) were considered putative axon units and discarded from analysis going forward (Figure 3.17B, n = 2, 0.45%).

$$\text{Peak Asymmetry Ratio (PAR)} = \frac{\text{AHP amplitude} - \text{PHP amplitude}}{\text{AHP amplitude} + \text{PHP amplitude}} \tag{3.4}$$

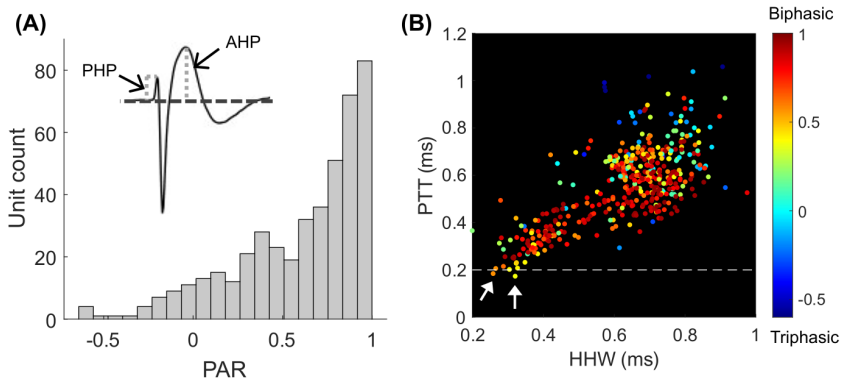

Figure 3.17: Identification of putative axon units for exclusion based on their peak asymmetry ratio (PAR) and peak-to-trough time (PTT). (A) Histogram showing the distribution of PAR of units (n = 443 neurons from 19 mice), with an example waveform showing how PAR was calculated. (B) Scatter plot showing the distribution of neurons according to their PTT and HHW. White dotted line indicates the exclusion threshold of PTT < 200 μs. White arrows point at neurons that are classified as putative axon units and hence excluded from analysis.

Altogether, 95 narrow waveform units were classified as putative PVINs out of 443 neurons in total. The remaining 346 broad waveform units likely represent mostly pyramidal neurons, but also other interneuron subtypes that have intermediate waveforms such as SST-expressing interneurons.

3.3.6 Putative PVIN interactions in cross-correlograms

In addition to single-unit electrophysiological features, PVIN identity could be further verified by examining their short-latency interactions with other neurons, as they are known to be powerful inhibitors of local neurons and form an extensive electrically coupled network with other PVINs (Tremblay et al., 2016; Hestrin and Galarreta, 2005). Spike timing correlation analysis was performed using cross-correlograms of activity between putative PVINs and other simultaneously

recorded neurons. This allowed the examination of pair-wise interactions on a millisecond timescale, in the form of putative post-synaptic inhibitory connections or putative gap junctions (Insel and Barnes, 2015; Peyrache and Destexhe, 2019; Senzai et al., 2019).

Using the cluster classification described in Section 3.3.5, spike timing correlations between simultaneously recorded neuron pairs were evaluated. In cross-correlograms, putative monosynaptic connections are well-defined in the form of significant peaks (excitatory) or troughs (inhibitory) with a short latency offset (< 5 ms) between two neurons (Barthó et al., 2004). On the other hand, cross-correlograms that show a symmetric peak at zero-lag indicate synchronous activity likely attributed to inter-neuronal coupling by gap junctions (van Welie et al., 2016). With PVIN characteristics in mind, this analysis aimed to detect putative monosynaptic inhibitory connections (significant trough in the window of +1.5 to +4.5 ms, see example in Figure 3.18B) and putative gap junctions (significant peak in the window of -1.0 to +1.0 ms, see example in Figure 3.18D). These connections were considered significant when two or more consecutive bins in the peak or trough exceed the statistical threshold of mean $\pm$ 4 standard deviations. There were 6135 unique neuron pairs across all recordings, of which 314 were putative PVIN pairs, 1751 were pairs of a putative PVIN and a broad waveform unit, and the remaining 4002 were pairs between broad waveform units.

Putative PVIN to broad waveform neuron pairs (PV$\rightarrow$BW, where the unidirectional arrow indicates the direction of putative synaptic connection) contained the highest proportion of significant putative post-synaptic inhibitory connections compared to other neuron pair types (Figure 3.18A; one-way ANOVA test, $F_{3,60} = 5.99$, $p = 0.0017$; Bonferroni's *post hoc* comparisons, PV$\rightarrow$BW vs. PV$\rightarrow$PV, $p = 0.0016$; PV$\rightarrow$BW vs. BW$\rightarrow$PV, $p = 0.0322$; PV$\rightarrow$BW vs. BW$\rightarrow$BW, $p = 0.0161$). On the other hand, putative PVIN pairs (PV$\leftrightarrow$PV, where the bidirectional arrow

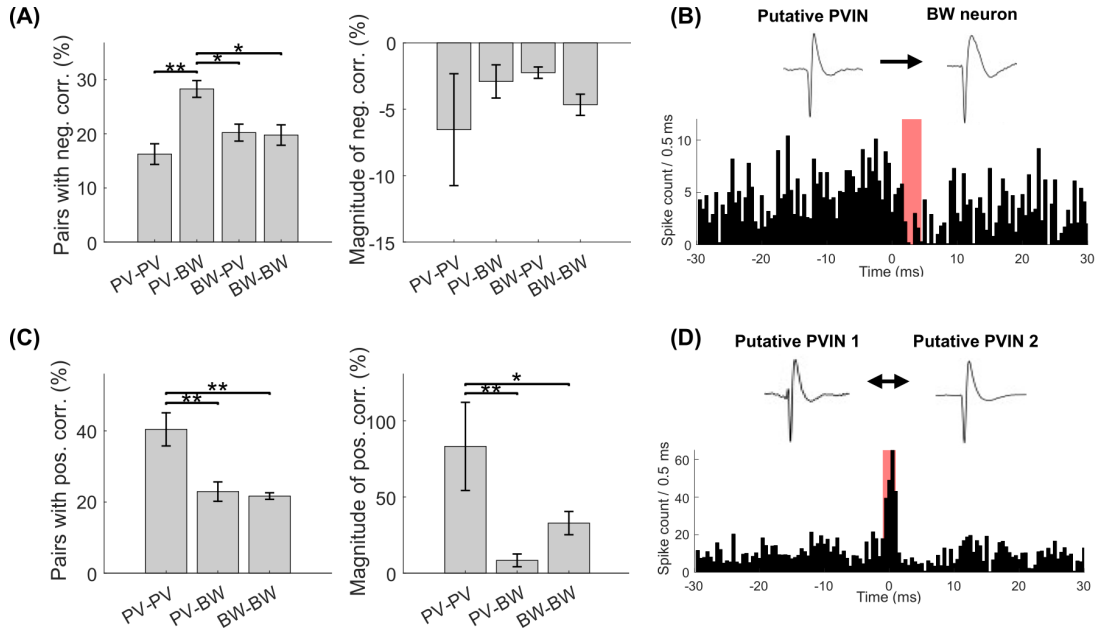

Figure 3.18: Cross-correlogram analysis of simultaneously recorded neuron pairs show distinct putative PVIN behaviour. (A) Proportion and magnitude (%) of neuron pairs with a significant negative spike timing correlation, i.e. putative post-synaptic inhibitory connection. Pairings include putative PVIN neuron pairs (PV-PV, n = 628 pairs), putative PVIN to BW neuron pairs (PV-BW, n = 1751 pairs), BW to putative PVIN pairs (BW-PV, n = 1751 pairs), and BW neuron pairs (BW-BW, n = 8004 pairs). (B) Example cross-correlogram of a putative PVIN to BW neuron pair with significant negative spike timing correlation in the +1.5 to +4.5 ms window (highlighted in red). (C) Proportion and magnitude (%) of putative PVIN neuron pairs (PV-PV, n = 314 pairs), putative PVIN to BW neuron pairs (PV-BW, n = 1751 pairs), and BW neuron pairs (BW-BW, n = 4002 pairs) that show significant positive spike timing correlation. (D) Example cross-correlogram of two putative PVINs with significant positive correlation in the -1.0 to +1.0 ms window (highlighted in red). Data are represented as mean ± SEM. *p<0.05, **p<0.01.

indicates symmetrical interaction) were most commonly synchronised with each other on a zero-lag millisecond timescale (Figure 3.18C; one-way ANOVA test, $F_{2,45}$ = 7.06, p = 0.0033; Bonferroni's *post hoc* comparisons, PV↔PV vs. PV↔BW, p = 0.008; PV↔PV vs. BW↔BW, p = 0.0052). In addition, comparisons of correlation magnitudes showed that putative PVIN pairs had the highest degree of positive synchronisation (Figure 3.18C; one-way ANOVA test, $F_{2,1463}$ = 6.54, p = 0.0015; Bonferroni's *post hoc* comparisons, PV↔PV vs. PV↔BW, p = 0.0012; PV↔PV vs. BW↔BW, p = 0.0327).

Here, cross-correlogram analyses provided added confidence in the current

classification of putative PVINs. These data showed that putative monosynaptic inhibitory connections were most likely found in pairs consisting of simultaneously recorded putative PVINs and broad waveform units. Putative PVIN pairs were also more likely synchronised via a putative gap junction than other neuron pair types. These characteristics are consistent with PVINs' inhibitory nature and highly synchronous activity patterns.

3.3.7 Effects of DOI and psilocin on putative PVIN activity

Once the classification of putative PVINs was established, single-unit analysis was reviewed to determine whether this subpopulation of mPFC neurons was affected by DOI and psilocin. To this end, earlier waveform scatter plots were revisited with a focus on putative PVINs, and the proportions of activated, inhibited, and non-responding PVINs were identified for each experiment (Figure 3.19).

As predicted by evidence from *in vitro* experiments presented in Chapter 2, DOI and psilocin significantly increased the firing rate of a subgroup of neurons with PVIN properties. An inhibitory effect of DOI and psilocin on the firing rate on this neuron population was also observed. Specifically, out of 26 putative PVINs, DOI activated 10 (38.5%) and inhibited 5 (19.2%), whereas 11 (42%) did not respond (Figure 3.19A). On the other hand, out of 30 putative PVINs, psilocin activated 10 (33.3%), inhibited 4 (13.3%), and 16 (53.3%) did not respond (Figure 3.19C). In the presence of MDL-100907, very few putative PVINs responded to DOI and psilocin with activation. In contrast, MDL-100907 increased the proportion of putative PVINs inhibited by DOI, whereas the proportion of putative PVINs inhibited by psilocin remained similar (Figure 3.19B, D). Next, the magnitude and timing of the effects of DOI and psilocin on putative PVINs, with and without MDL-100907, were examined.

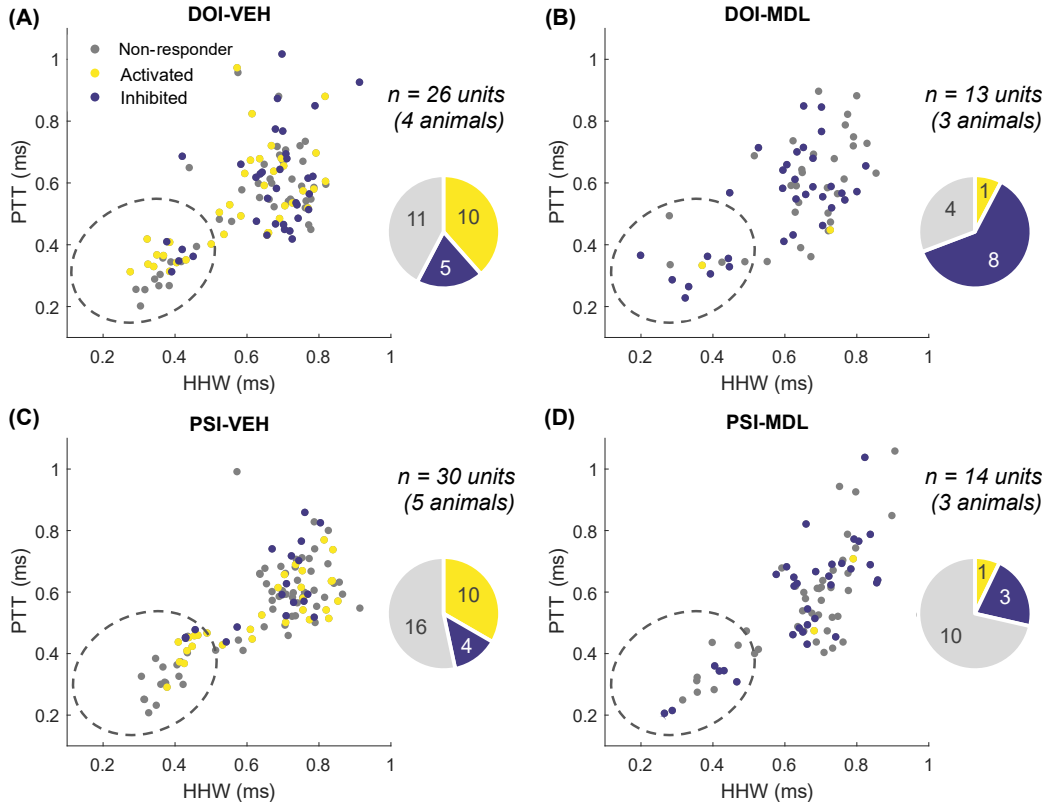

Figure 3.19: Effects of DOI and psilocin on firing rate of putative PVINs. Scatter plots showing the distribution of activated units (yellow), inhibited units (blue), and non-responder units (grey) according to their peak-to-trough time (PTT) and half-hyperpolarisation width (HHW). Putative PVINs are circled. Experiments shown are (A) DOI + vehicle (DOI-VEH), (B) DOI + MDL-100907 (DOI-MDL), (C) psilocin + vehicle (PSI-VEH), and (D) psilocin + MDL-100907 (PSI-MDL).

Utilising auROC analysis as a representation of the magnitude of change in firing rate caused by DOI, it was apparent that the auROC distribution was shifted to the left by pre-treatment with MDL-100907 (i.e. the number of activated neurons was greatly reduced; Figure 3.20A). A Mann-Whitney U test showed that the overall activation effects of DOI on putative PVINs were significantly reduced by MDL-100907 pre-treatment (Figure 3.20B; $Z = 3.448$, $p < 0.001$). Timescale analyses showed that the activation effects of DOI on putative PVINs were shorter-lasting and reduced in the presence of MDL-100907 (Figure 3.20C). On the other hand, the inhibitory effects of DOI on putative PVIN firing rate tended to be greater in the presence of MDL-100907 (Figure 3.20D).

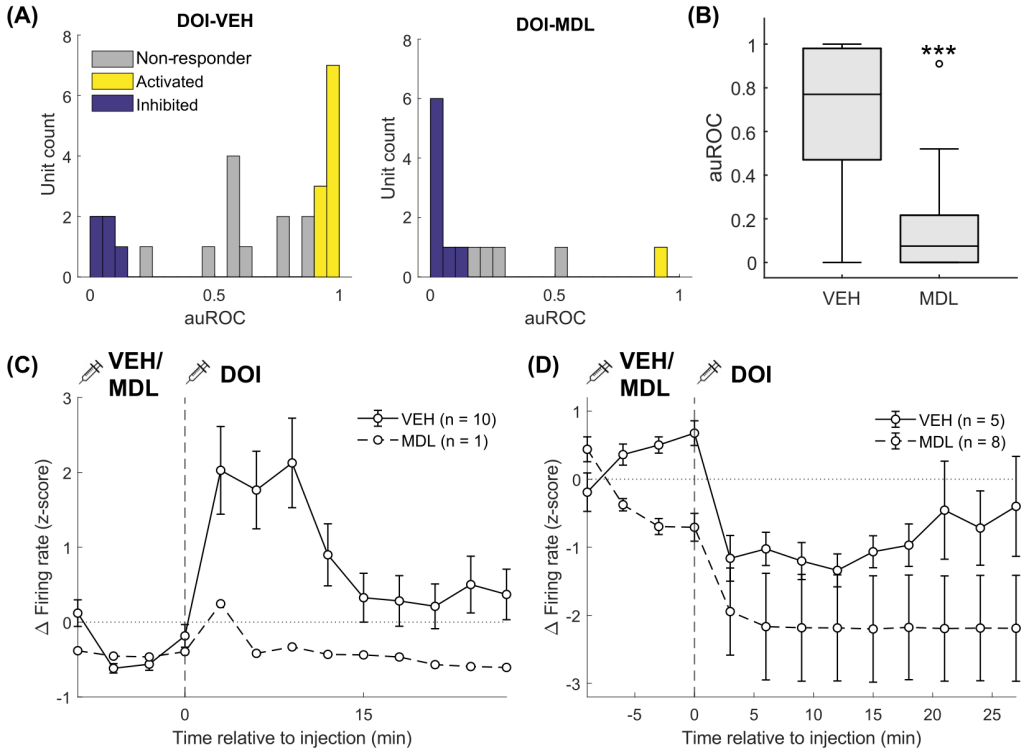

Figure 3.20: Effects of DOI on putative PVINs with and without MDL-100907 (abbreviated to MDL). (A) Histograms of the distribution of area under the receiver operator characteristic curve (auROC) of putative PVINs when given DOI + vehicle (DOI-VEH), and DOI + MDL-100907 (DOI-MDL). (B) Bar chart comparing the median auROC of putative PVINs with and without MDL-100907 pre-treatment. Line plots showing DOI's timescale of action on the mean relative firing rate (z-score) of (C) activated units and (D) inhibited units. Vehicle experiment is represented in solid lines, and MDL-100907 experiment is represented in dotted lines. Data are represented as median ± interquartile range in (B) and mean ± SEM in (C) and (D). ***p<0.001.

Similarly, MDL-100907 reduced the number of neurons activated by psilocin, although this effect did not reach statistical significance (Figure 3.21A, B; Mann-Whitney U test; Z = 1.190, p = 0.2343). Timescale analyses showed that both activation and inhibition effects of psilocin were reduced in the presence of MDL-100907 (Figure 3.21C, D).

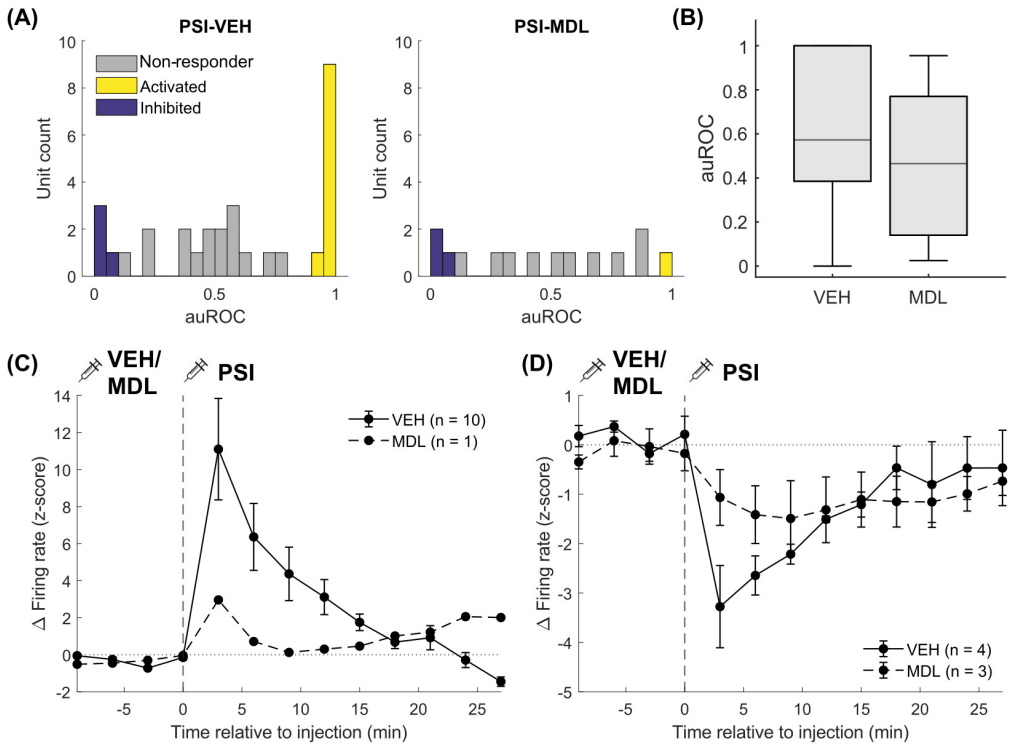

Figure 3.21: Effects of psilocin on putative PVINs with and without MDL-100907 (abbreviated to MDL). (A) Histograms of the distribution of area under the receiver operator characteristic curve (auROC) of putative PVINs when given psilocin after vehicle (PSI-VEH), and psilocin after MDL-100907 (PSI-MDL). (B) Bar chart comparing the median auROC of putative PVINs with and without MDL-100907 pre-treatment. Line plots showing psilocin's timescale of action on the mean relative firing rate (z-score) of (C) activated units and (D) inhibited units. Vehicle experiment is represented in solid lines, and MDL-100907 experiment is represented in dotted lines. Data are represented as median ± interquartile range in (B) and mean ± SEM in (C) and (D).

3.3.8 Effects of DOI and psilocin on correlation of neuron pairs

To test whether the actions of DOI and psilocin on PVINs contributed to the desynchronisation of mPFC neurons, spike count correlation analysis of neuron pairs was performed using the single-unit firing rate data. This analysis aimed to determine the strength of spike count correlations over time for given neuron pairs, and whether this shifted after drug administration. To this end, the Pearson correlation coefficient (r) was computed for simultaneously recorded neuron pairs using their spike counts in 1 sec bins in the pre-drug and post-drug windows (i.e. 10 min immediately prior to and after drug injection). Neuron pairs consisted of both

putative PVINs (PV-PV) or between a putative PVIN and a broad waveform unit (PV-BW). Significantly correlated pairs were identified through a bootstrapping procedure using $p < 0.05$. Correlation strength was measured in terms of absolute r values (see Section 3.2 for detail).

Examples of positively correlated and negatively correlated neuron pairs identified with this method are shown in Figure 3.22A and B, respectively. In all experiments, the proportion of correlated pairs was not significantly different between the pre-drug and post-drug periods (data not shown). Analysis of correlation strength, however, revealed the effects of DOI and psilocin administration on pairwise correlations. The correlation strength of PV-PV pairs significantly decreased after DOI administration, but that of PV-BW pairs was unaffected (Figure 3.22D; two-tailed Wilcoxon signed rank test; PV-PV, $Z = 3.423$, $p < 0.001$, $n = 92$ pairs; PV-BW, $Z = 1.675$, $p = 0.0939$, $n = 444$ pairs). Interestingly, pre-treatment with MDL-100907 reversed the effects of DOI, significantly increasing the correlation strength of both neuron pair types (Figure 3.22E; two-tailed Wilcoxon signed rank test; PV-PV, $Z = -3.695$, $p < 0.001$, $n = 26$ pairs; PV-BW, $Z = -10.45$, $p < 0.001$, $n = 276$ pairs). Psilocin, on the other hand, uniformly and strongly decreased the correlation strength of both neuron pair types (Figure 3.22F; two-tailed Wilcoxon signed rank test; PV-PV, $Z = 5.668$, $p < 0.001$, $n = 148$ pairs; PV-BW, $Z = 10.15$, $p < 0.001$, $n = 650$ pairs). Pre-treatment of MDL-100907 blocked the effects of psilocin (Figure 3.22G; two-tailed Wilcoxon signed rank test; PV-PV, $Z = 0.3385$, $p = 0.7350$, $n = 48$ pairs; PV-BW, $Z = 1.818$, $p = 0.0691$, $n = 449$ pairs).

Overall, both DOI and psilocin decreased the correlation strength of putative PVIN pairs via a 5-HT_{2A} receptor-mediated mechanism, in line with the hypothesis that SWA disruption caused by DOI and psilocin was, at least in part, due to cortical neuron desynchronisation.

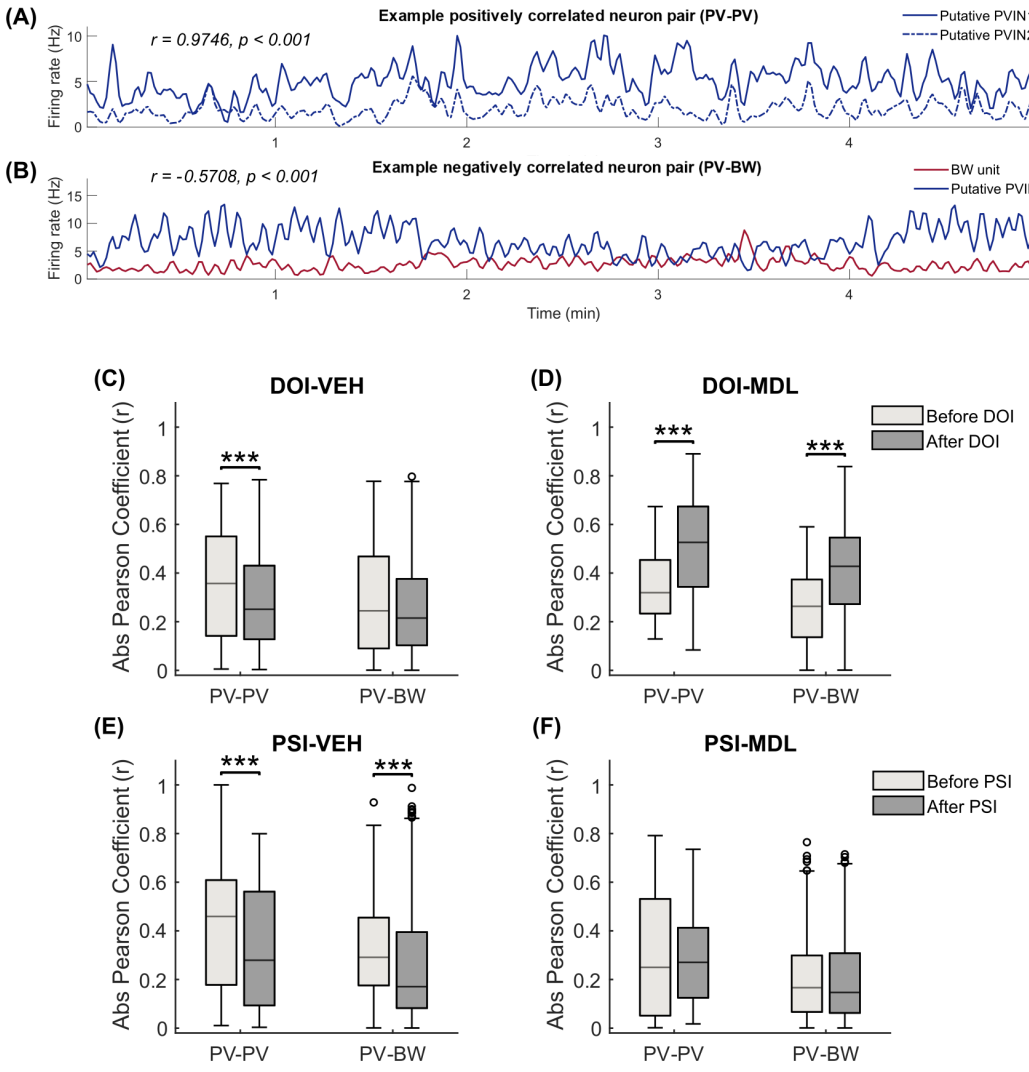

Figure 3.22: Effects of DOI and psilocin on spike count correlation between neuronal pairs, with and without MDL-100907. Firing rate over time of example neuron pairs that have (A) a positive spike count correlation between two putative PVINs (blue) and (B) a negative spike count correlation (between putative PVIN and BW unit, in blue and red respectively). Relative change in mean magnitude of correlation, in terms of absolute Pearson coefficient value (r), for each neuron pair type in mice treated with (C) DOI + vehicle (DOI-VEH), (D) DOI + MDL-100907 (DOI-MDL), (E) psilocin + vehicle (PSI-VEH), and (F) psilocin + MDL-100907 (PSI-MDL). Neuron pair types are (i) both putative PVINs (PV-PV) and (ii) between putative PVIN and another BW neuron (PV-BW). Data are represented as median ± interquartile range, with circles indicating outliers. ***p<0.001.

3.4 Discussion

Experiments in this chapter investigated the *in vivo* effects of systemic administration of the 5-HT_{2A} receptor agonists DOI and psilocin on the activity of mPFC neurons, including putative PVINs that were identified by their waveform characteristics. Multi-unit recordings were obtained from urethane-anaesthetised mice using silicon probes, and the effects of DOI and psilocin were tested in the presence of the selective 5-HT_{2A} receptor antagonist MDL-100907 or vehicle control. The neural activity of the mPFC was evaluated at multiple levels, ranging from local network oscillations and multi-unit activity to single-unit firing rates and pair-wise correlations.

3.4.1 Identification of PVINs by their waveform properties

A key aim of the current chapter was to identify putative PVINs using their spike waveform characteristics. While it remains a common approach to separate narrow and broad waveform units based on a single waveform parameter (Senzai et al., 2019; Garcia-Garcia et al., 2020; Mahrach et al., 2020; Tseng and Han, 2021), the importance of considering more than one waveform parameter has been highlighted (Barry, 2015). Here, clustering analysis was performed using peak-to-trough time and half-hyperpolarisation width, as described in reports by Medrihan et al. (2017) and Yu et al. (2019), and narrow waveform units were considered putative PVINs based on optotagging evidence reviewed in Section 3.1.

However, while there is clear evidence that PVINs have specific waveform characteristics, the question remains as to whether all narrow waveform units are PVINs. Using juxtacellular recording combined with immunostaining and optogenetics, Yu et al. (2019) showed that PVINs in the barrel cortex were the most well-separated interneuron class on the basis of their spike waveforms. Other

interneuron classes, such as SST-expressing and VIP-expressing interneurons, displayed intermediate waveform durations and were part of a broad waveform cluster. It is noteworthy that juxtacellular recordings provide cleaner waveform traces compared to extracellular recordings such as those used here, where physiological and external noise give rise to a broader distribution of waveforms. On the other hand, an optotagging study by Royer et al. (2012) in the mouse hippocampus demonstrated that extracellularly recorded waveforms of optotagged PVINs were still well-separated from pyramidal cells that have broad waveforms and SST-expressing interneurons that have intermediate waveforms. There was, however, a small degree of overlap between SST-expressing interneurons and PVINs (Royer et al., 2012) that was also observed in another PVIN optotagging study in the mouse mPFC (Kvitsiani et al., 2013). Altogether, juxtacellular labelling and optotagging evidence in the literature suggests that the waveform classification method can reliably separate PVINs from pyramidal cells and other neuron types, though there is a risk of contamination from neurons with intermediate waveforms, such as SST-expressing interneurons, that should not be overlooked.

As part of PVIN identification in the dataset, cross-correlograms were analysed to detect the presence of putative monosynaptic or gap junction coupling between simultaneously recorded neuron pairs. Indeed, in the current study, PV→BW neuron pairs were shown to contain the highest proportion of putative inhibitory synaptic connections, and putative gap junctions were most observed in PV↔PV neuron pairs. These findings provide further confidence to the waveform-based classification of PVINs.

Finally, the spontaneous firing rate of putative PVINs was compared to that of broad waveform neurons. Although the firing rate of putative PVINs was higher (2.47 ± 0.43 Hz vs. 1.39 ± 0.10 Hz), the difference was not as pronounced as expected given the fast-spiking nature of most PVINs. A likely explanation is that

the firing rate of PVINs varies with brain state and is most probably suppressed under urethane anaesthesia compared to awake conditions. In support of this, optotagged PVINs in the auditory cortex of ketamine-anaesthetised mice were shown to spontaneously fire at 5.5 ± 4.8 Hz and only went up to 30.3 ± 26.6 Hz when white noise stimuli were presented (Moore and Wehr, 2013). Optotagged PVINs in the mPFC of awake mice, on the other hand, displayed much higher spontaneous firing rates at 31 ± 3 Hz (Kvitsiani et al., 2013). Therefore, the lack of a fast-spiking phenotype in putative PVINs recorded here most likely reflects the urethane anaesthesia conditions.

Overall, 95 putative PVINs were identified out of 443 neurons in the dataset (i.e. 21%) using a comprehensive approach that considers a number of waveform parameters and cross-correlogram properties. Given that roughly 15% of cortical neurons are inhibitory and 40% of cortical interneurons are PV-expressing (Meyer et al., 2011; Tremblay et al., 2016), the expected population of cortical PVINs would be 6%, suggesting a potential over-representation of PVINs in the current dataset. However, as reviewed in Section 1.3, different interneuron subtypes are not evenly distributed across cortical layers, and PVINs are particularly enriched in deep layers of the cortex (Tremblay et al., 2016) where recordings were made in the current study. It is therefore likely that the waveform-based classification used here was able to capture a significant population of PVINs.

3.4.2 DOI and psilocin altered mPFC activity on multiple levels

The present LFP results showed that DOI and psilocin suppressed SWA in the mPFC via a 5-HT_{2A} receptor-mediated mechanism, in agreement with previous studies that observed a reduction in low-frequency oscillatory power in the PFC of anaesthetised rats in response to DOI (Celada et al., 2008) and awake mice in

response to psilocin (Golden and Chadderton, 2022). Mirroring the LFP results, DOI and psilocin administration also increased the multi-unit activity of mPFC neurons via a 5-HT_{2A} receptor mechanism. Further analysis at the single-unit level revealed heterogeneous changes in the firing rates of individual neurons in response to DOI and psilocin. This result is similar to earlier *in vivo* single-unit recording studies that reported both excitatory and inhibitory effects of DOI on rat PFC pyramidal neurons (Puig et al., 2003; Celada et al., 2008). Taken together with the current multi-unit activity data, these results indicate that the net effect of DOI and psilocin on mPFC activity was excitatory, in keeping with reports by Puig et al. (2003) that the excitatory effects of DOI were more common than its inhibitory effects.

Here, the single-unit results showed that the excitatory effects of DOI were mediated by the 5-HT_{2A} receptor, as pre-treatment with MDL-100907 greatly reduced the proportion of activated neurons (32% to 3%). The excitatory effects of psilocin were also reduced by MDL-100907 pre-treatment, albeit to a lesser extent (27% to 11%). While both DOI and psilocin are 5-HT_{2A} receptor agonists (Vollenweider et al., 1998; González-Maeso et al., 2007), they are also ligands at the 5-HT_{2C} receptor and, in the case of psilocin, 5-HT_{1A} and other 5-HT receptors (summarised in Table 1.2). DOI exhibits 5-to-10-fold higher selectivity at the 5-HT_{2A} receptor compared to the 5-HT_{2C} receptor and has little affinity at the 5-HT_{1A} receptor (K_i = 4, 47, and 2355 nM for the mouse 5-HT_{2A}, 5-HT_{2C}, and rat 5-HT_{1A} receptors, respectively; Canal et al., 2013; Titeler et al., 1988). Psilocin, on the other hand, acts as an agonist at 5-HT_{2A}, 5-HT_{2C}, and 5-HT_{1A} receptors with moderate affinities (K_i = 173, 79, 146 nM for the mouse 5-HT_{2A}, 5-HT_{2C}, and 5-HT_{1A} receptor, respectively; Erkizia-Santamaría et al., 2022). Results of the current study, alongside binding affinity evidence, indicate that the excitatory effects of DOI on mPFC activity that were apparent in measurements of single-unit, multi-unit, and local oscillations, were predominantly mediated via the 5-HT_{2A}

receptor. On the other hand, while the network excitatory effects of psilocin (multi-unit activity and LFP) were mediated by the 5-HT_{2A} receptor, the effects of psilocin on the firing rates of individual neurons were likely mediated by the 5-HT_{2A} receptor alongside other 5-HT receptor subtypes, since effects were not completely blocked by MDL-100907.

3.4.3 DOI and psilocin activated a subpopulation of putative PVINs

Importantly, the identification of putative PVINs in the dataset allowed the examination of the effects of DOI and psilocin on these neurons. Single-unit firing rate results showed that DOI and psilocin altered the activity of a subpopulation of putative PVINs in a heterogeneous manner (DOI, 39% activated, 19% inhibited; psilocin, 33% activated, 13% inhibited). As predicted by *in vitro* results in Chapter 2, the excitatory effects of DOI and psilocin on putative PVINs were mediated by the 5-HT_{2A} receptor, as these effects were greatly reduced by pre-treatment with MDL-100907.

It is, however, not certain whether the excitatory effects of DOI and psilocin on putative PVINs were direct, since the drugs were given by systemic injection. It is possible that these effects were partly mediated via other brain regions that are rich in 5-HT_{2A} receptors and project to the mPFC, such as the thalamus (Rodríguez et al., 2011). Previous *in vivo* studies showed that the effects of DOI on cortical activity, at least that of pyramidal neurons, were unaffected by thalamic lesions and thereby independent from thalamocortical afferents (Puig et al., 2003; Celada et al., 2008). The reciprocal connectivity between the mPFC and DRN should also be considered. For instance, the systemic application of DOI was shown to suppress DRN 5-HT neuron firing and reduce 5-HT release in the mPFC via the 5-HT_{2A} receptor (Boothman et al., 2003), but the local application of DOI in the

mPFC instead increased the firing of DRN 5-HT neurons and in turn increased 5-HT release (Martín-Ruiz et al., 2001). Therefore, systemic administration of DOI and psilocin may have caused a reduction in DRN 5-HT neuron activity and produced knock-on effects of reduced 5-HT levels on putative PVINs in the mPFC. Overall, evidence from *in vitro* experiments in Chapter 2, as well as previous studies involving thalamic lesions, suggests that the observed effects of DOI and psilocin on putative PVINs in the current study were at least partially directly exerted via postsynaptic 5-HT_{2A} receptors expressed by putative PVINs in the mPFC.

Finally, it is worth considering the effects of DOI and psilocin on local interactions within mPFC circuits. Results from correlation analysis showed that both DOI and psilocin caused a reduction in the strength of correlated spiking activity between putative PVINs and other neurons via the 5-HT_{2A} receptor. These findings are in support of the idea that a disruption in excitatory/inhibitory balance and desynchronisation of cortical neuron activity underlies the psychotropic actions of hallucinogens (Martín-Ruiz et al., 2001; Celada et al., 2008; Muthukumaraswamy et al., 2013), and are in keeping with reports that DOI reduced the correlation between spike rates and gamma range LFP power in awake rats (Wood et al., 2012). It is also noteworthy that PVINs are key regulators of cortical network oscillations and the maintenance of UP/DOWN state balance during SWA (Puig et al., 2008; Massi et al., 2012; Zucca et al., 2017, further discussed in Chapter 5). It is therefore plausible that the modulation of PVIN activity by DOI and psilocin underlies their effects on multi-unit activity and SWA observed in the current study. By altering the activity of PVINs and desynchronising their interactions with other neurons, the excitatory/inhibitory balance of the mPFC and as a result UP/DOWN state transitions were likely disrupted. This potentially led to overall elevated mPFC neuron activity, forming the electrophysiological basis for hallucination.

3.4.4 Conclusions

Overall, experiments in the current chapter demonstrate that both DOI and psilocin evoked marked effects on neural activity in the mPFC *in vivo* at multiple levels. While the excitatory effects of DOI were almost completely abolished by MDL-100907, the excitatory effects of psilocin were reduced by MDL-100907 to a lesser extent, indicating the potential involvement of other 5-HT receptor subtypes. Isolation of putative PVINs by their waveform characteristics revealed that DOI and psilocin evoked heterogeneous changes in firing rates and an overall reduction in their spiking correlation with other neurons. To further understand the relationship between 5-HT, PVINs, and overall mPFC activity, the effects of optogenetically-evoked release of 5-HT on mPFC neurons, including PVINs, were explored in the upcoming chapters.

4

Optogenetic activation of DRN 5-HT neurons *in vitro* and *in vivo*

4.1 Introduction

With the previous chapter demonstrating excitatory effects of the systemic administration of 5-HT_{2A} receptor agonists on mPFC neurons, including PVINs, *in vivo*, the following chapters investigated the interactions between physiologically released 5-HT and mPFC neurons, including PVINs, *in vitro* and *in vivo* with optogenetics. In order to optogenetically evoke 5-HT release in the mPFC, the optogenetic methodology was first established and tested in this chapter.

4.1.1 Utility of optogenetics in multi-unit recordings

The emerging field of optogenetics combines optical and genetic methodology to control neural activity in a spatially and temporally precise manner. With genetic modification approaches, microbial light-activated opsins can be selectively expressed in neurons of interest. These opsins can then be controlled with light pulses of specific wavelengths, in turn rapidly activating or inhibiting the genetically transduced cells (Han, 2012). In particular, channelrhodopsin-2 (ChR2) is a widely used light-gated ion channel in optogenetic studies for the optical activation of neurons. When

illuminated with blue light, conformational changes in ChR2 allow the inward flow of cations such as Na^+, K^+, H^+, and Ca^{2+}, leading to rapid depolarisation and action potential firing (Nagel et al., 2003). Other commonly used opsins include halorhodopsin and archaerhodopsin for the selective silencing of neurons (Han, 2012).

The integration of multi-unit electrophysiology and optogenetics offers a powerful toolbox for modern neuroscience. In particular, this technology enables two important goals: the identification of genetically labelled neurons among the recorded population (optical tagging or optotagging), and the determination of the causal roles of genetically defined neurons in brain circuits and behaviour (Buzsáki et al., 2015). To achieve optotagging, opsins are expressed in genetically targeted neurons and light pulses are applied during a multi-unit recording session to drive or suppress the activity of such neurons (depending on the excitatory or inhibitory nature of the opsins used). Individual neurons that express the opsin can then be detected by their short-latency light-induced activity, providing a "tag" for their genetic identity (Buzsáki et al., 2015). The main goal of optotagging, rather than to manipulate neuronal activity and observe downstream effects, is to identify a subset of neurons by their genetic identity and monitor their natural activity and physiological properties (Deubner et al., 2019).

4.1.2 Electrophysiological properties of DRN 5-HT neurons

The DRN comprises a heterogeneous neuronal population of which about 50% are 5-HT containing (Deneris and Gaspar, 2018). As reviewed in Section 1.4, while these 5-HT neurons share a common set of defining markers, subpopulations of 5-HT neurons express various additional markers. Given the heterogeneous nature of DRN 5-HT neurons, understanding their electrophysiological properties will further aid the overall understanding of 5-HT signalling.

Early *in vitro* and *in vivo* intracellular recordings of rat DRN 5-HT neurons, identified by histofluorescence or immunohistochemistry, reported that these neurons have characteristics such as the slow and regular firing of broad action potentials followed by a prominent afterhyperpolarisation, high input resistance, and suppression of action potentials by 5-HT_{1A} receptor activation (Aghajanian and Vandermaelen, 1982; Vandermaelen and Aghajanian, 1983; Li et al., 2001). Subsequently, *in vivo* extracellular recording studies of the rat DRN demonstrated that juxtacellularly labelled 5-HT neurons were slow and regular firing with clock-like characteristics and broad action potentials (Allers and Sharp, 2003). In the same study, most slow and irregular firing DRN neurons were immunonegative for 5-HT, whereas most fast-firing DRN neurons were immunoreactive for GAD (Allers and Sharp, 2003).

Abundant early evidence of a classical 5-HT neuron spiking phenotype formed the basis for putative 5-HT neuron identification in many subsequent studies. Putative 5-HT neurons were commonly identified by their slow (< 4 Hz) and regular (coefficient of variance of inter-spike interval, CV-ISI < 0.6) firing characteristics, while fast-firing ($5 - 40$ Hz) DRN neurons were generally considered putative GABAergic neurons (Hajós et al., 1995, 1998; Varga et al., 2003). However, this definition of DRN neuron electrophysiology is increasingly being questioned, with more recent studies revealing neurochemical and electrophysiological diversity in DRN 5-HT neurons. Additionally, it was reported in later *in vitro* studies that the firing properties of neurochemically or genetically identified 5-HT neurons in the rat DRN were similar and sometimes indistinguishable from those of non-5-HT neurons, suggesting that such classification criteria may not be entirely accurate (Beck et al., 2004; Calizo et al., 2011).

Non-classical electrophysiological properties of 5-HT neurons have been reported in *in vitro* and *in vivo* studies. In addition to classical 5-HT neurons, early *in vivo*

single-unit studies of the rat DRN reported the presence of burst-firing putative 5-HT neurons (Hajós et al., 1995; Hajós and Sharp, 1996), which were later confirmed as 5-HT-expressing via juxtacellular labelling (Schweimer et al., 2011). These burst-firing 5-HT neurons have similar characteristics to classical 5-HT neurons, except they regularly discharge two (sometimes up to four) action potentials in short succession. As such, a subpopulation of 5-HT neurons with low firing rates and broad spikes may instead display irregular firing patterns. The presence of fast-firing 5-HT neurons has also been reported in juxtacellular recording studies of the rat DRN, against the early consensus that 5-HT neurons are slow-firing (Allers and Sharp, 2003; Kocsis et al., 2004). Some of these neurons were shown to be uniquely phase coupled to hippocampal theta rhythm, suggesting that they represent an electrophysiologically and functionally distinct subpopulation of DRN 5-HT neurons (Kocsis et al., 2004). Later, an *in vitro* study identified a subpopulation of mouse DRN 5-HT neurons that lacked the 5-HT_{1A} autoreceptor, the expression of which was previously considered a common and defining characteristic of DRN 5-HT neurons (Kiyasova et al., 2013). In the same study, patch-clamp recordings of these 5-HT_{1A} receptor-lacking 5-HT neurons showed that, compared to 5-HT_{1A} receptor-expressing 5-HT neurons, they fired at higher frequencies in response to large depolarising currents. This is presumably due to the absence of autoinhibitory action of 5-HT_{1A} receptors (Kiyasova et al., 2013).

Finally, emerging evidence suggests that glutamate can be co-released by a subpopulation of 5-HT neurons that co-express the vesicular glutamate transporter VGLUT3 (Johnson, 1994; Trudeau, 2004; Sengupta et al., 2017). Increasing numbers of studies report the impact of 5-HT/glutamate co-release on 5-HT release and neurotransmission as well as 5-HT-related behavioural output, although the electrophysiological properties of these VGLUT3-expressing 5-HT neurons are not yet defined. VGLUT3-expressing 5-HT neurons represent up to two-thirds

of DRN 5-HT neurons as demonstrated in *in situ* hybridisation studies (Hioki et al., 2010), and may potentially account for subpopulations of 5-HT neurons of distinct firing properties.

Altogether, evidence in the literature suggests that while a significant proportion of DRN 5-HT neurons have the classical slow and regular firing phenotype, subpopulations of 5-HT neurons can have non-classical firing properties. These reports are based on patch-clamp or single-unit recording studies which do not provide a comprehensive overview of 5-HT neurons in the DRN. Moreover, the molecular identity of non-classical 5-HT neurons remains unknown, and could be 5-HT/glutamate co-releasing neurons. Despite the use of optogenetics in recent 5-HT research, most studies have focused on the causal role of 5-HT neurons in neural circuit function or behavioural performance. There are no studies combining optotagging and multi-unit recording approaches to determine the electrophysiological phenotype of DRN 5-HT neurons in the literature.

4.1.3 Aims of this chapter

The main objective of this chapter was to establish a methodology for the activation of DRN 5-HT neurons using optogenetics, such that the influence of selective 5-HT neuron activation on mPFC PVIN activity could be explored in future work (see Chapter 5). Using the transgenic SERT-Cre mice, DRN 5-HT neurons were transfected with ChR2 and the functionality of ChR2 was tested using *in vitro* whole-cell patch-clamp experiments and *in vivo* optotagging experiments. The latter used multi-unit silicon probe recording, and putative 5-HT neurons were first identified in a clustering approach based on their slow firing rate and spike regularity. 5-HT neurons were then identified with an optotagging approach, and the results were compared to the clustering analysis. Finally, to investigate whether

any DRN neuron cluster corresponded to a VGLUT3-expressing subpopulation, the firing properties of DRN neurons were investigated in a novel conditional knockout mouse in which VGLUT3 expression was selectively deleted from 5-HT neurons.

4.2 Materials and methods

4.2.1 Experiment animals

Experiments in this chapter utilised two types of transgenic mice, SERT-Cre and SERT-Cre::VGLUT3$^{LoxP/LoxP}$ (referred to as VGLUT3-cKO from now on). SERT-Cre mice express the CRE recombinase exclusively in 5-HT neurons, allowing the selective genetic targeting of 5-HT neurons. VGLUT3-cKO mice were bred by crossing the aforementioned SERT-Cre mice with VGLUT3$^{LoxP/LoxP}$ mice with a C57BL/6J background. In the latter mice, 5-HT neurons are deficient of VGLUT3 (Mansouri-Guilani et al., 2019).

All mice were group housed in individually ventilated cages. Mice were maintained on a 12-hour light/dark cycle (lights on at 7:00 am) at constant temperature and humidity, with food and water provided *ad libitum*. Male and female mice between the age of 2 to 4 months were used. Prior to any surgical procedure, mice were habituated to handling for at least three days. All procedures were performed in accordance with the Animals (Scientific Procedures) Act 1986 and in line with the guidelines of the University of Oxford.

4.2.2 Viral transfection

DRN 5-HT neurons of SERT-Cre and VGLUT3-cKO mice (8 to 12 weeks old, both male and female) were selectively transfected with ChR2 via stereotaxic injection of

a Cre-inducible recombinant viral vector (AAV5-EF1a-DIO-hChR2(E123T/T159C)-EYFP; UNC Vector Core, NC, USA) that carries a floxed ultrafast (E123T/T159C) ChR2 fused with eYFP (ChR2-eYFP). Intracerebral viral transfection was carried out under aseptic surgical conditions with mice under isoflurane anaesthesia (2% induction, 1-1.5% maintenance in 2 L/min oxygen). Anaesthetic depth was maintained by frequent monitoring of the animal's respiratory rate as well as occasional toe-pinch reflex checks.

Immediately before surgery, buprenorphine (Vetergesic, 0.1 mg/kg, *i.p.*) and a dose of 5% glucose-saline were given for analgesia and rehydration. Bupivacaine (Marcain, 2 mg/kg, *s.c.*) was applied locally under the scalp after wet shaving of the fur covering the head and neck. The scalp was then cleaned using an anti-microbial disinfectant, and the mice were secured in a standard stereotaxic frame (David Kopf Instruments, CA, USA). Liquid gel (Viscotears, Alcon Laboratories Ltd, UK) was applied as needed to keep the animal's eyes hydrated. Body temperature was maintained at 35 ± 1°C using a homeothermic heating blanket connected to a rectal thermometer. Subsequent surgical steps were performed under sterile conditions. An incision was made to expose the skull, and bregma and lambda were located to ensure the skull was level in the dorsoventral plane. A small craniotomy was made behind lambda and above the DRN. The viral vector was stereotaxically injected (1 μl at 100 nL/min, 500 nL each at two injection sites) into the DRN (-4.7 mm AP, -0.1 mm ML, -2.7 and -2.5 mm DV; coordinates in relation to bregma and brain surface). Two min were allowed between each injection for sufficient viral spread.

Upon recovery, mice were administered 5 mg/kg meloxicam and a final dose of 5% glucose-saline *i.p.* for postoperative analgesia and rehydration. Following the surgery, mice were closely monitored for at least five days and scored according to their weight, behaviour, general appearance, and wound recovery. Animals were then allowed to recover for 3 to 4 weeks. All drugs used in this section were provided

by Oxford University Veterinary Services.

4.2.3 *In vitro* electrophysiology and optogenetic stimulation

In vitro experiments in this chapter utilised SERT-Cre mice. After recovery from intracerebral viral transfection, acute coronal slices of the midbrain were obtained using the methodology described in Section 2.2. ChR2-expressing 5-HT neurons in the DRN were identified by visualising eYFP fluorescence, and whole-cell patch-clamp recordings were obtained from fluorescent cells (Figure 4.1A). After establishing a whole-cell patch-clamp, current-clamp recordings were obtained whilst pulses of optical stimuli were delivered through a fibre optic using a blue LED (473 nm, M470F3, Thorlabs, NJ, USA). Blue light pulses of 5 ms duration were delivered at 1, 5, 10, and 20 Hz. The maximum power at the optic fibre tip was 10 mW. With a light illumination area of 2 mm diameter, the light intensity was about 3.2 $mWmm^{-2}$. Current-clamp recording data were acquired, processed, and analysed as specified in Chapter 2.

4.2.4 *In vivo* electrophysiology and optogenetic stimulation

Multi-unit recordings were obtained from urethane-anaesthetised SERT-Cre as well as VGLUT3-cKO mice following viral transfection (Figure 4.1A). Experiments on SERT-Cre mice were performed using an optrode (custom A1x32 probe, NeuroNexus, MI, USA) kindly gifted by Dr Julien Carponcy from the MRC Brain Network Dynamics Unit, University of Oxford. Experiments on VGLUT3-cKO mice were performed using an optrode that consisted of a standard acute 32-channel silicon probe (H-Series 6b, Cambridge Neurotech, UK), identical to that used in Chapter 3, attached to a lambda-b optic fibre. The fibre diameter was 50 μm and had a 0.7 mm taper tip to deliver light along the length of the electrode array. A stainless

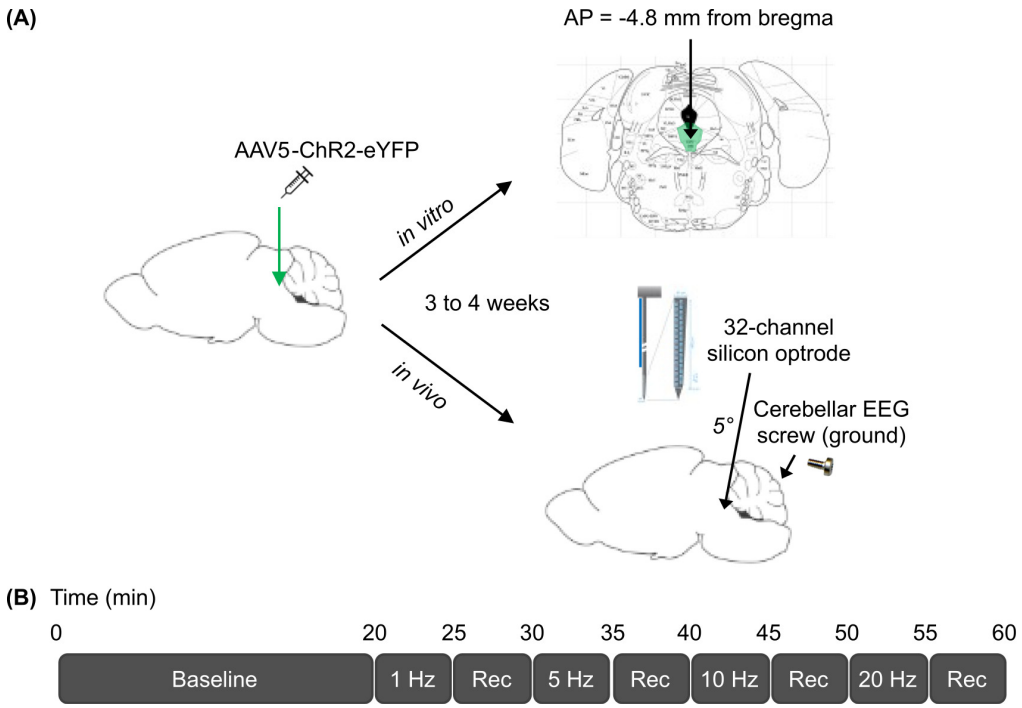

Figure 4.1: Schematic of experimental design. (A) A recombinant viral vector (AAV5) containing the ChR2-eYFP construct was first injected into the DRN of SERT-Cre mice to drive the targeted expression of ChR2-eYFP in 5-HT cells. After allowing 3 to 4 weeks for viral expression, animals were used for *in vitro* or *in vivo* experiments. In *in vitro* experiments, coronal slices of the DRN were taken, and patch-clamp recordings were taken from fluorescent cells. In *in vivo* experiments, multi-unit recordings were obtained using a 32-channel silicon optrode and cerebellar EEG screw as ground. (B) Timeline of *in vivo* recording. Baseline recording was obtained for 20 min before sequentially stimulating the DRN at 1, 5, 10, and 20 Hz. Each stimulation frequency was applied for 5 min and then stopped for 5 min to allow for recovery.

steel screw (1 mm diameter) was attached to the skull over the cerebellum for use as ground and reference. Recording devices were connected to the signal chain, and recordings were carried out as described in Section 3.2. The optrode was stereotaxically implanted into the DRN at -5.0 mm AP, -0.1 mm ML, -2.7 mm DV at a 5°angle along the AP axis.

4.2.5 Experimental design

Following 20 min of baseline recording, light pulses were delivered in 10 min blocks at 1, 5, 10, and 20 Hz, sequentially. In each 10 min block, 5 ms light pulses were

delivered for 5 min, followed by a 5 min recovery before the next block. Each recording ran for 60 min in total (Figure 4.1B).

4.2.6 Data acquisition

Data acquisition and hardware were as detailed in Chapter 3. For optical stimulation, the implanted optrode was connected to a 473 nm blue laser diode (Doric Lenses, Canada) with a zirconia sleeve. Light delivery was controlled using a Master-8 pulse generator (A.M.P.I., Israel) via a BNC digital input. Before each experiment, laser output was measured at the optical fibre tip with a power meter (Thor Labs, NJ, USA) and calibrated to 5 $mWmm^{-2}$ using the Master-8 pulse generator via an audio jack analogue input. The laser was connected to an Open Ephys acquisition box via a BNC input/output board to record the timestamps at which laser pulses were delivered in the form of .ttl files (Figure 4.2).

4.2.7 Immunohistological analysis

At the end of each recording session, mice were euthanised with an overdose of pentobarbitone (Euthanal, *i.p.*) and transcardial perfusion was performed to extract the brain. Brains were fixated, and 30 μm coronal slices were obtained as described in Chapter 3. Midbrain slices spanning across the area of interest (-4.4 to -5.0 mm AP from bregma) were selected for immunostaining. Sections were stained with goat anti-tryptophan hydroxylase 2 (TPH2) (1:1000 dilution, Abcam #Ab121013) and visualised with an Alexa Fluor 647-conjugated secondary antibody (1:1000 dilution, Abcam #Ab150131). Stained sections were mounted and visualised under a microscope to confirm the co-expression of ChR2-eYFP with DRN 5-HT cells. The latter staining was carried out by Cara Fuller from the Sharp Lab.

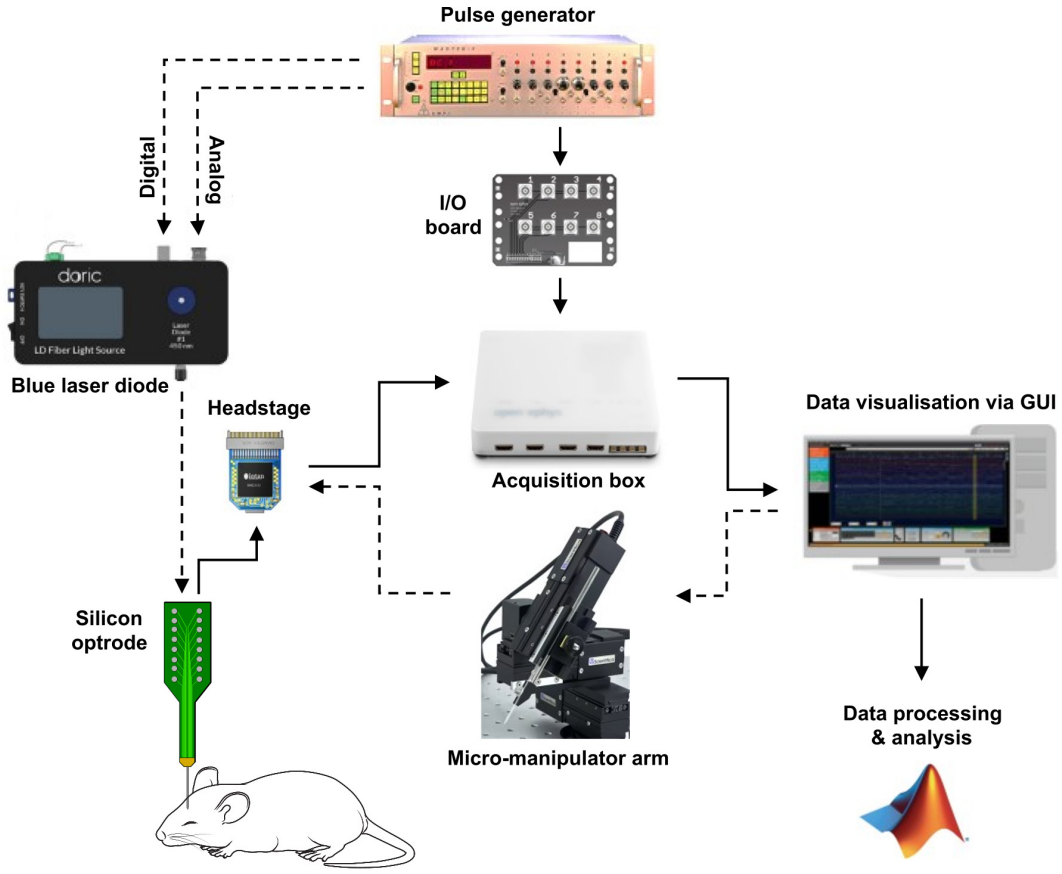

Figure 4.2: Schematic showing the data acquisition pipeline. The silicon optrode was connected to the headstage, acquisition box, micro-manipulator arm, and computer, as specified in Chapter 3. Additionally, the silicon optrode was connected to a Doric blue laser diode via a patch cord and zirconia sleeve. The laser diode output was controlled by a Master-8 pulse generator via a digital input, and the power of the light output was controlled by the same pulse generator via an analogue input. The pulse generator was, in turn, connected to an I/O board and the acquisition box, allowing the timestamps of laser pulses to be recorded. Data were visualised on the computer with the Open Ephys GUI and subsequently processed and analysed in MATLAB. Black arrows indicate the flow of information, with solid lines as output and dotted lines as input. Images were taken and adapted from SciDraw (`doi.org/10.5281/zenodo.3925977`; `doi.org/10.5281/zenodo.5749462`), Open Ephys (Siegle et al., 2017), Doric, Master-8, Scientifica, and MATLAB.

4.2.8 Baseline firing properties calculation

The baseline firing properties of DRN putative 5-HT neurons were determined using three metrics – firing rate, regularity, and spike width. The mean firing rate in Hz was calculated over the 20 min baseline period, and firing regularity was calculated as CV2 (adjacent coefficient of variation of inter-spike intervals).

Spike regularity is commonly measured in terms of the coefficient of variation

(CV) of the inter-spike interval (ISI), which evaluates the standard deviation relative to the mean of all ISIs of the entire spike train. Spike trains with low regularity or high variability have a high CV value, whereas spike trains that are highly regular have a low CV value. However, high CV artefacts are often observed in regular spike trains where the firing rate slowly changes over time. This is because the CV calculation evaluates the entire spike train at once and does not account for fluctuations in firing rate. In comparison, CV2 compares the relative difference of adjacent intervals and was used here to overcome the limitations of CV (Holt et al., 1996). CV2 has been used in place of CV in a number of electrophysiological studies as a clustering parameter for unit classification (Graf et al., 2020; Levenstein et al., 2022). A CV2 value was computed for each spike (apart from the first and last spikes) as the standard deviation of two adjacent ISIs divided by their mean and multiplied by $\sqrt{2}$. The median CV2 over time was then calculated, yielding a single measure of spike regularity that is independent of fluctuating firing rates.

$$\Delta t_i = t_i - t_{(i-1)} \tag{4.1}$$

$$CV = \frac{\sigma_{\Delta t}}{\mu_{\Delta t}} \tag{4.2}$$

$$CV2 = \frac{2|\Delta t_{(i+1)} - \Delta t_i|}{\Delta t_{(i+1)} + \Delta t_i} \tag{4.3}$$

Spike waveform width calculations were carried out as described in Chapter 3, using the peak-trough time, i.e. the time between the minimum and maximum amplitude of the average waveform from depolarisation to afterhyperpolarisation.

4.2.9 Unit classification using hierarchical clustering

To identify clusters of DRN neurons based on their baseline firing properties, hierarchical clustering was performed using values for firing rate (Hz) and spike regularity (CV2). These parameters were chosen based on previous studies characterising DRN 5-HT neurons. In particular, DRN 5-HT neurons are commonly reported to have slow and regular-firing characteristics. Previous multi-unit studies in the DRN by our lab identified three main clusters, namely slow regular firing (SR), slow irregular firing (SIR), and fast-firing (FF) neurons (O'Sullivan, 2022, *unpublished observations*). Here, clusters were identified via hierarchical clustering using a custom-written MATLAB script similar to that in Chapter 3. The analysis was performed separately for SERT-Cre and VGLUT3-cKO datasets. The Euclidean distance threshold was set such that units were divided into three clusters.

4.2.10 Identification of optotagged neurons

Peri-stimulus time histograms (PSTHs) and raster plots were constructed to identify optotagged neurons in each dataset. The firing rate of each unit was binned in consecutive 5 ms windows and summed across trials. Direct optogenetic activation of ChR2-expressing units resulted in sharp and narrow peaks in the 1 to 6 ms window immediately after light delivery in the PSTHs (Senzai et al., 2019). If the peak is more than 5 standard deviations larger than the baseline mean firing rate (-100 to 0 ms before light delivery), the unit was considered to be optotagged. PSTH analysis was performed for all neurons at 1 Hz stimulation, and subsequently performed at 5, 10, and 20 Hz stimulation for neurons that were optotagged at 1 Hz.

4.2.11 Statistical analysis

All data analysis and statistics were carried out in MATLAB. Data normality was first determined with the Shapiro-Wilk test (using the MATLAB function *swtest*). For parametric unpaired data, two-tailed Student's t-tests were performed (using the MATLAB function *ttest*). For nonparametric data, the Mann-Whitney U test was used (using the MATLAB function *ranksum*).

4.3 Results

4.3.1 Selective targeting of ChR2 expression in DRN 5-HT neurons

To optically activate 5-HT neurons in the DRN, a viral vector carrying a floxed recombinant ChR2 fused with eYFP was stereotaxically injected into the DRN of SERT-Cre mice (Figure 4.3A). Three weeks after injection, fluorescent microscopy and immunohistochemical analysis revealed an abundance of ChR2-eYFP-expressing cell bodies and axons in the DRN (example shown in Figure 4.3B). These ChR2-eYFP-expressing cell bodies were also positive for TPH2, the enzyme variant involved in the 5-HT synthesis pathway in the DRN (Figure 4.3C).

TPH2 staining revealed two distinct clusters of 5-HT cell bodies in the dorsal and ventral DRN subnuclei (DRD, DRV; Figure 4.3C). Since the goal of this project is to optically activate 5-HT projections to the mPFC, ChR2-eYFP injections were targeted to the DRV as these 5-HT neurons preferentially project to cortical regions (Ren et al., 2018, Figure 4.3B). Quantification in previous studies by the Sharp lab, utilising the identical transgenic mouse and recombinant viral vector, demonstrated 100% co-localisation of ChR2-eYFP and 5-HT in the DRN (Sengupta et al., 2017).

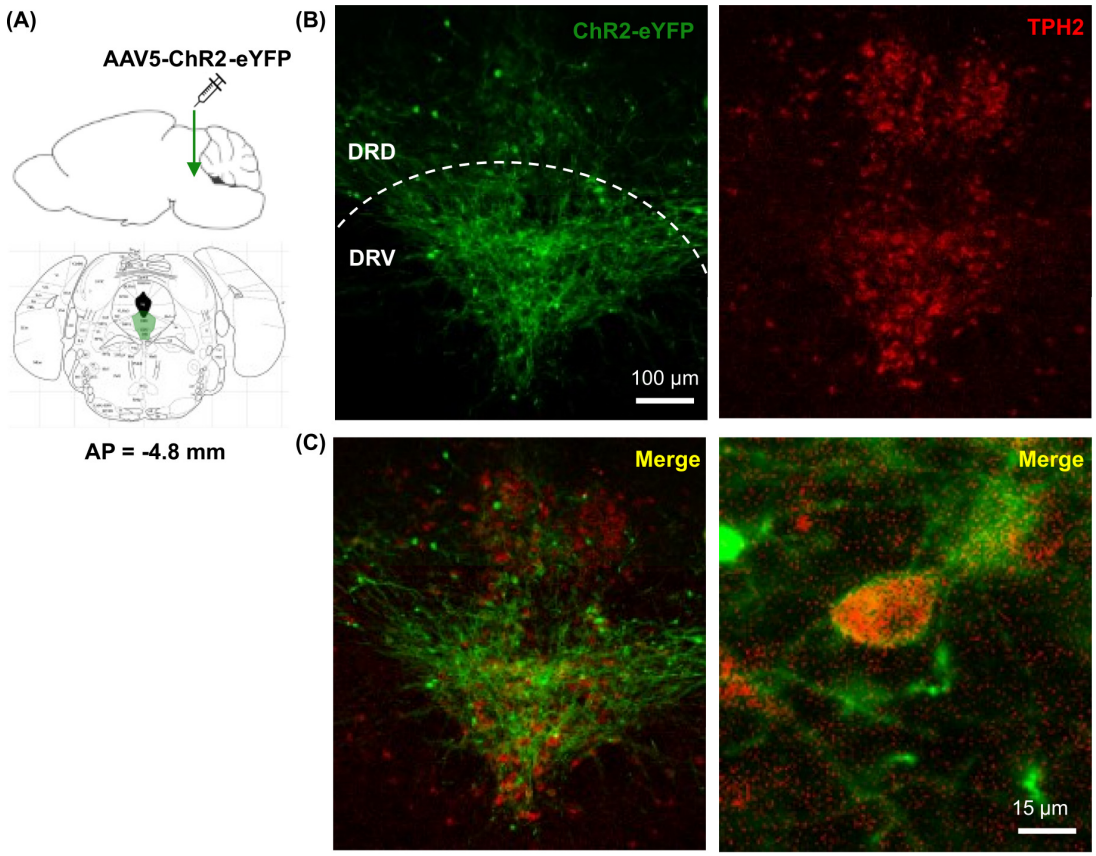

Figure 4.3: Expression of ChR2-eYFP in DRN 5-HT neurons. (A) Anatomical atlas illustrating the target site of ChR2-eYFP viral transfection. The coronal section corresponds to 4.8 mm posterior of bregma and is adapted from (Franklin and Paxinos, 2013). (B) Example Cre-dependent expression of ChR2-eYFP (green) and TPH2 expression (red) in the DRN of SERT-Cre mice. (C) Overlap between ChR2-eYFP (green) and TPH2 (red) expression in the DRN. Immunostaining experiments carried out and figures obtained by Cara Fuller, Department of Pharmacology, University of Oxford. DRD: Dorsal raphe dorsal subnucleus. DRV: Dorsal raphe ventral subnucleus.

4.3.2 Optogenetic activation of 5-HT neurons *in vitro*

Having verified targeted ChR2 expression in 5-HT neurons, the functionality of ChR2 was first tested *in vitro* by obtaining whole-cell patch-clamp recordings from ChR2-eYFP-expressing DRN neurons three weeks post-injection.

Recordings were obtained from 8 fluorescent neurons across three mice. Stimulation with light pulses at 1, 5, 10, and 20 Hz reliably evoked action potentials of these neurons in the current-clamp mode, demonstrating selective light-gated control of DRN 5-HT neuron activity in a frequency-dependent manner (examples

shown in Figure 4.4A-D).

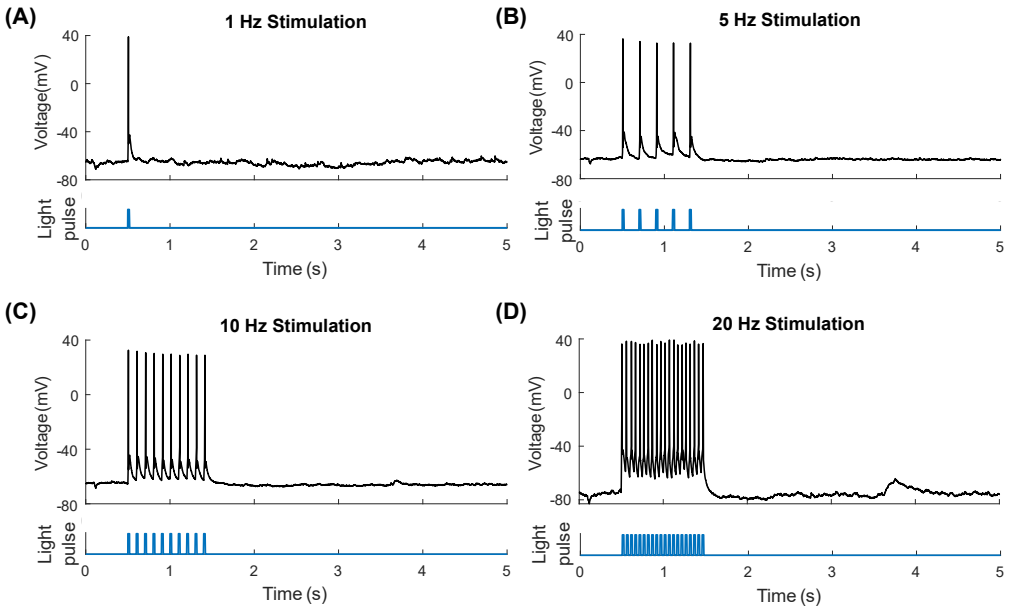

Figure 4.4: Example current-clamp recording traces during light stimulation of a ChR2-eYFP-expressing DRN 5-HT neuron *in vitro*, at (A) 1 Hz, (B) 5 Hz, (C) 10 Hz, and (D) 20 Hz. Square 5 ms light pulses are represented in blue in the bottom panels.

4.3.3 Firing properties of DRN neurons

With the functionality of ChR2 established *in vitro*, optical activation and tagging (optotagging) of DRN 5-HT neurons was next performed to confirm ChR2 functionality *in vivo*. Here, optotagging experiments utilised a dual optical and electrical silicon probe (optrode) that allows simultaneous illumination and extracellular recording of the local neuronal population. In these recordings, short-latency activation of cells following light stimuli enables the identification of their chemical nature, in this case, 5-HT neurons. To this end, multi-unit optrode recordings were obtained from the DRN of urethane-anaesthetised SERT-Cre mice three weeks after viral injection. Recordings were obtained from 11 mice, yielding 326 units in total. Abundant expression of ChR2-eYFP in the DRN was verified *post hoc* in all mice, with Figure 4.3 showing a typical example.

First, baseline firing properties of the recorded DRN neuron population were examined. This analysis aimed to identify putative 5-HT neurons by their electrophysiological characteristics described in the literature, as optotagged neurons were predicted to fall into this cluster. In rodent studies, classical firing properties of 5-HT neurons have been described as clock-like and slow-firing (Allers and Sharp, 2003). As such, spike regularity and firing rate over the 20 min baseline period were used to identify clusters of neurons present in the DRN. Spike regularity was computed as CV2, a measure of variability between adjacent inter-spike intervals, and firing rate was computed as the mean spike count per second (Hz) over the baseline period.

Using hierarchical clustering analysis based on standardised Euclidean distances between each point (Figure 4.5A, C), three clusters with the following properties were identified: slow regular firing (SR, n = 94, 28.8%), slow irregular firing (SIR, n = 174, 53.4%), and fast-firing (FF, n = 58, 17.8%; Figure 4.5B). Example spike traces of each neuron type are shown in Figure 4.5D. The slow regular cluster had regular spikes and low firing rates, which were in line with the firing properties of classical 5-HT neurons described in previous studies and were considered putative 5-HT neurons in this classification.

4.3.4 Optogenetic activation of 5-HT neurons *in vivo* and their firing properties

In this dataset, 32 neurons were optotagged out of 326 units tested, representing a 9.8% yield. Optotagged neurons were identified by their raster plots and peri-stimulus time histograms (PSTHs) at 1 Hz light stimulation (see examples in Figure 4.6). Neurons with a strong and narrow peak in the PSTH that occurred within 5 ms of light application and with an amplitude more than 5 standard deviations greater than the baseline mean (i.e. -100 to 0 ms before light application)

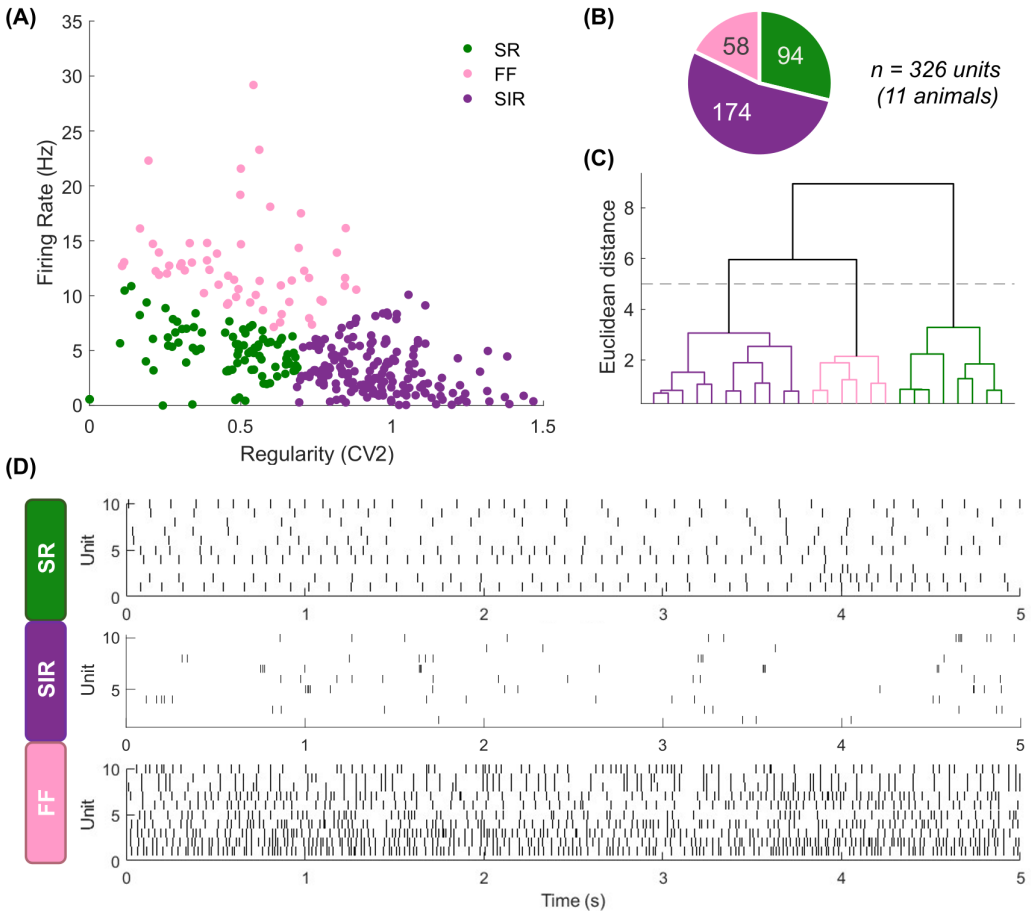

Figure 4.5: Clustering of DRN neurons in SERT-Cre mice based on their baseline firing properties (n = 326 units in total, across 11 mice). (A) Scatter plot showing the distribution of slow regular (SR, green, n = 94), slow irregular (SIR, purple, n = 174), and fast-firing (FF, pink, n = 58) neurons in the DRN, by their firing rate (Hz) and spike regularity (CV2). (B) Pie chart showing the proportion of each cell type in the DRN. (C) Dendrogram showing hierarchical clustering and classification of neurons. Black dotted line represents the clustering threshold used. (D) Example spike trains of SR (top), SIR (middle), and FF (bottom) neurons over 5 seconds (n = 10 each).

were considered optotagged. Raster plots and PSTHs at 5, 10, and 20 Hz were subsequently created for optotagged neurons.

Optotagged neurons were detected in each of the 11 mice (numbers ranging from 1 to 7), thereby indirectly verifying probe localisation in the DRN for all recordings. Unfortunately, direct staining and labelling of the optrode tract, as previously achieved in Chapter 3, was not possible because applying a strong fluorescent dye to the optrode risked distorting the colour of the blue light emitted at the optic fibre tip.

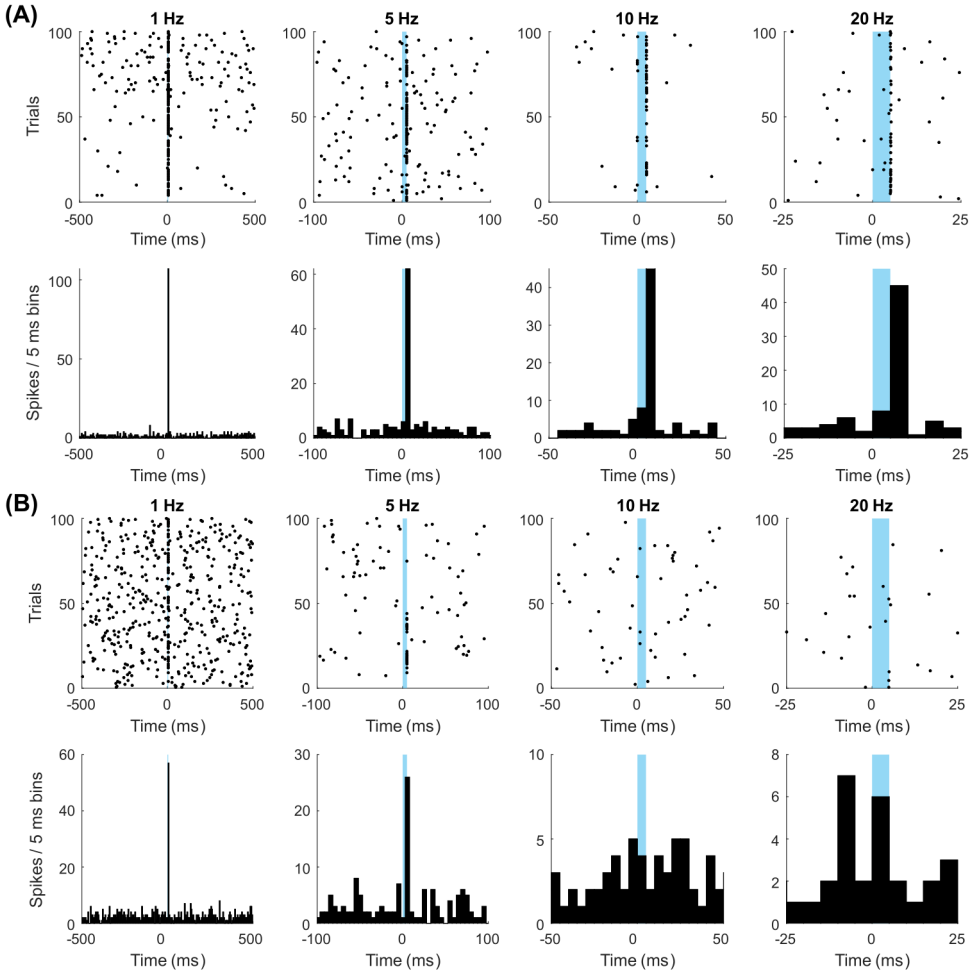

Figure 4.6: Example optotagged neurons that were (A) light-dependent and optically activated up to 20 Hz, and (B) light-independent and did not follow the light stimuli at all frequencies. Raster plots are shown in the top panel, and peri-stimulus time histograms (PSTHs) are shown in the bottom panel. Blue shaded area represents the duration of light stimuli (5 ms).

Notably, only a subpopulation of optotagged neurons (59.3%, 19/32) displayed light frequency-dependent properties. These light-dependent neurons followed the light stimuli up to 20 Hz, similar to the neurons that were optically activated in earlier *in vitro* slice experiments (see example in Figure 4.6A). Other optotagged neurons (40.6%, 13/32), however, were seemingly light-independent and only spiked with the light stimuli at 1 Hz, sometimes 5 Hz, but not at higher frequencies (see example in Figure 4.6B).

Next, optotagged units were located in the clustering map shown in Figure 4.5A.

In contrast to the earlier assumption that optotagged neurons would belong to the slow and regular firing cluster that resembled classical 5-HT neurons described in the literature, optotagged units were distributed across all three clusters of neurons (Figure 4.7A). Out of the total 32 optotagged neurons, 28% (9/32) were slow and regular firing, 50% (16/32) were slow and irregular firing, and the remainder (18.8%, 6/32) were fast-firing (Figure 4.7B). These results suggest the presence of 5-HT neurons that are not just the classical slow and regular firing phenotype (Table 4.1). The firing rate of optotagged neurons ranged from 0.0167 to 14.78 Hz, and the spike regularity (CV2) varied from 0.0002 to 1.242. The waveform length (ms, measured as time from peak to trough, PTT) and peak asymmetry ratio (PAR) of all recorded neurons were also examined to confirm that no putative axonal units were present in the recording (data not shown, see Chapter 3 for detail).

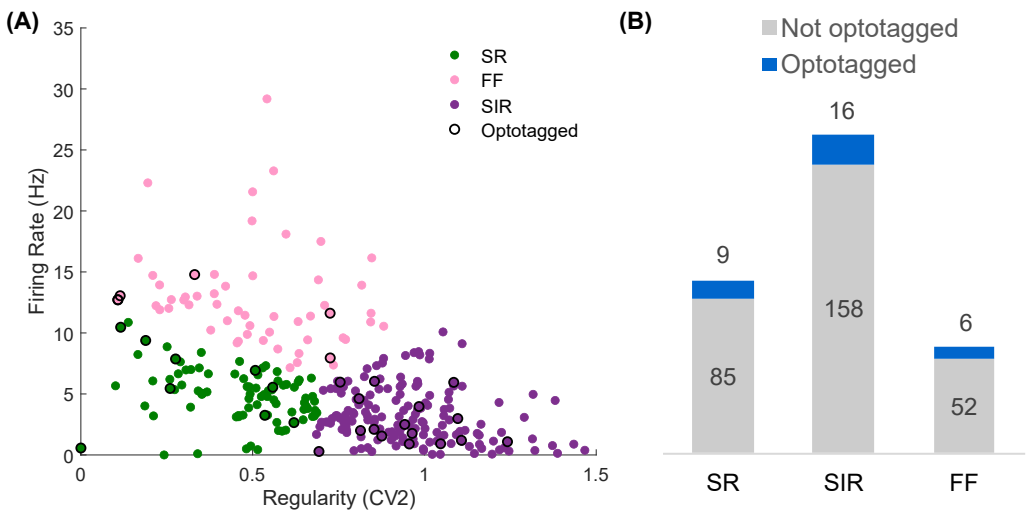

Figure 4.7: Distribution of optotagged 5-HT neurons in recorded DRN neuron population in SERT-Cre mice (n = 32 optotagged out of 326 total). (A) Scatter plot showing the distribution of optotagged units (circled in black) across slow regular (SR, green), slow irregular (SIR, purple), and fast-firing (FF, pink) clusters. (B) Bar charts showing the proportion of optotagged neurons in each cluster.

Altogether, these experiments verified the functionality of ChR2 *in vivo* as optical activation of 5-HT neurons in the DRN was achieved. These results also provided *in vivo* multi-unit evidence that 5-HT neurons in the mouse DRN have an

Table 4.1: Baseline firing properties of neuron clusters in the DRN of SERT-Cre mice. SR: slow regular, SIR: slow irregular, FF: fast-firing. Data are represented as mean ± SEM.

	SR: all	**SR: optotagged**	**SIR: all**	**SIR: optotagged**	**FF: all**	**FF: optotagged**
n	94	9	174	16	58	6
Firing rate (Hz)	4.85 ± 0.24	5.79 ± 1.08	3.14 ± 0.17	2.74 ± 0.49	12.9 ± 0.54	12.1 ± 0.94
Spike regularity (CV2)	0.45 ± 0.02	0.34 ± 0.07	0.97 ± 0.02	0.94 ± 0.04	0.52 ± 0.03	0.35 ± 0.12
Waveform width (ms)	0.50 ± 0.04	0.61 ± 0.08	0.48 ± 0.02	0.60 ± 0.05	0.40 ± 0.02	0.28 ± 0.06

unexpectedly high diversity of electrophysiological properties. Importantly, 5-HT neurons identified in this study spanned across a wide range of firing rate and spike regularity, much larger than the typical range used for putative 5-HT neuron classification in many previous studies (Varga et al., 2003; Allers and Sharp, 2003; Kocsis et al., 2004).

4.3.5 Light-dependent and light-independent optotagged 5-HT neurons

As described earlier, optotagged units in the dataset could be divided into light-dependent (Figure 4.6A) and light-independent (Figure 4.6B) types. Notably, there was no clear correlation between an optotagged unit's distance to the light source (i.e. channel location) and its frequency dependency (data not shown).

The baseline firing properties of the light-dependent and light-independent units were examined more closely to determine whether a 5-HT neuron's baseline behaviour could predict its frequency dependence. Visualisation of these units on the cluster map revealed differences in the distribution of light-dependent and light-independent units, with more of the former found on the left of the plot (i.e. lower CV2 value) and more of the latter found on the right of the plot (i.e. higher CV2 value; Figure 4.8A, B). Indeed, a two-tailed unpaired t-test revealed a significant difference in regularity between the two groups (Figure 4.8C; light-dependent vs. light-independent neurons, $t(29) = -4.146$, $p < 0.001$).

Interestingly, these results indicate that classical slow and regular firing 5-HT neurons are more likely to be light-dependent and able to follow light stimulation frequencies up to 20 Hz. Irregular firing 5-HT neurons, on the other hand, were more likely to be light-independent.

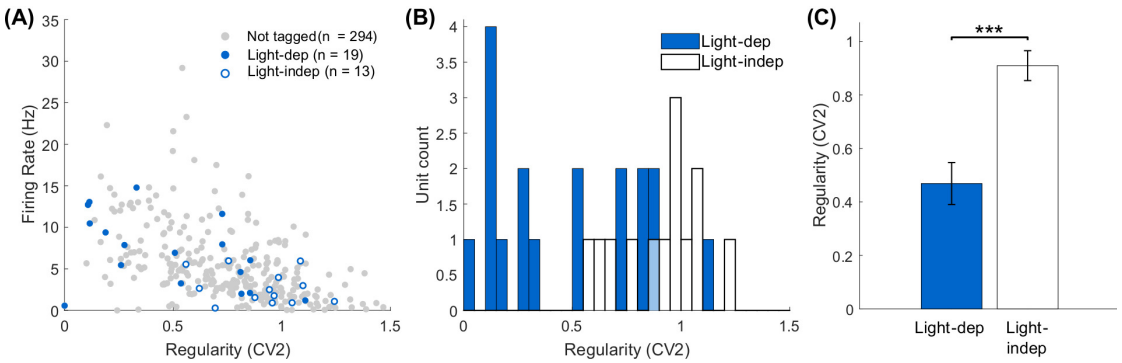

Figure 4.8: Distribution of optotagged 5-HT neurons that were light-dependent (light-dep) and light-independent (light-indep) in SERT-Cre mice. (A) Scatter plot of SERT-Cre DRN units, with light-dependent units highlighted in blue fill and light-independent units highlighted in blue outline. (B) Histogram and (C) bar chart showing the difference in regularity of light-dependent and light-independent units. Data are represented as mean ± SEM. ***p<0.001.

4.3.6 Optogenetic activation of 5-HT neurons in VGLUT3-cKO mice

The above *in vivo* optotagging results revealed that 5-HT neurons had a diversity of firing characteristics and did not belong to a single cluster. Recently, evidence has emerged that a subpopulation of 5-HT neurons in the DRN co-release glutamate (Amilhon et al., 2010). Here, follow-up experiments were conducted to determine whether 5-HT-glutamate co-releasing neurons might be represented by one of these clusters.

Optotagging experiments were repeated using a transgenic mouse line in which the vesicular glutamate transporter 3 (VGLUT3) is conditionally knocked out in 5-HT neurons (VGLUT3-cKO), providing a model of loss of 5-HT/glutamate co-transmission (Mansouri-Guilani et al., 2019). Indeed, in VGLUT3-cKO mice, DRN 5-HT neurons demonstrated a reduction in detectable immunoreactivity for VGLUT3 (Gullino, 2023, *unpublished observations*). It was predicted that these mice would demonstrate a different DRN cluster pattern and that lack of glutamate co-transmission would affect the baseline firing properties of 5-HT neurons.

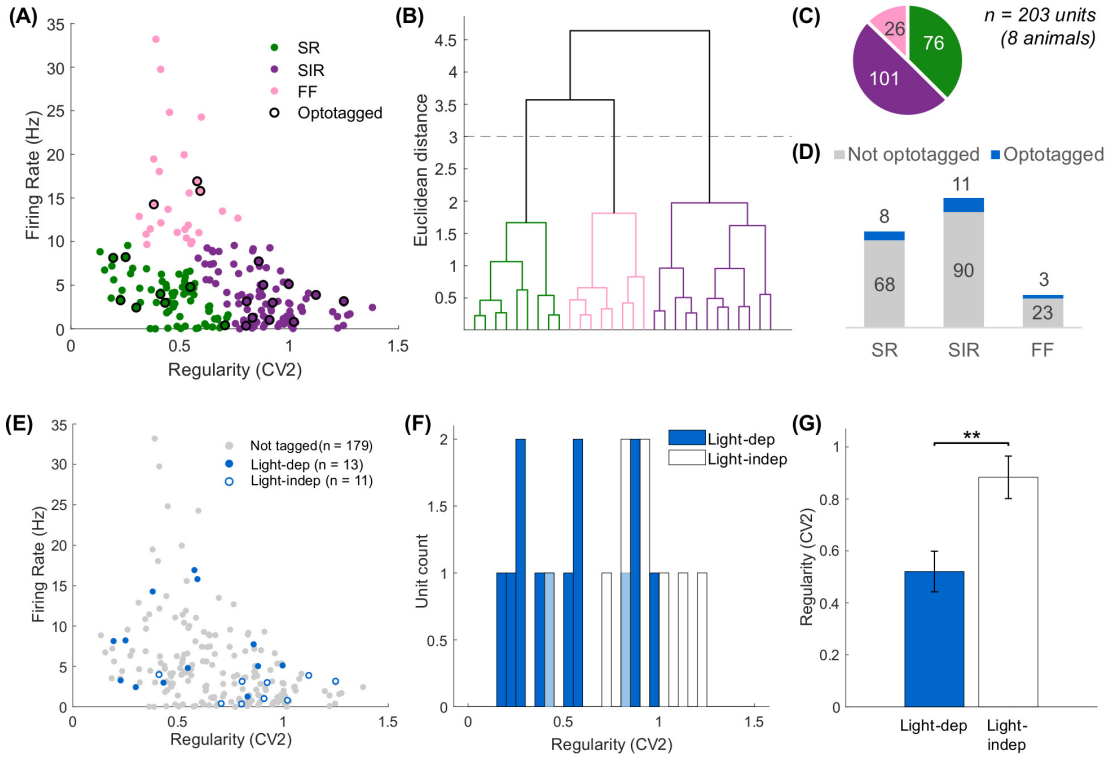

Figure 4.9: Distribution of optotagged 5-HT neurons in the DRN recorded population of VGLUT3-cKO mice (n = 8 mice). (A) Scatter plot showing slow regular (SR, green, n = 76), slow irregular (SIR, purple, n = 101), fast-firing (FF, pink, n = 26) groups of neurons. Optotagged units are circled in black. (B) Dendrogram showing hierarchical clustering and classification of neurons. Grey dotted line indicates clustering threshold. (C) Pie chart showing the proportion of each neuron type in the VGLUT3-cKO DRN. (D) Bar charts showing the proportion of optotagged neurons across SR, SIR, and FF clusters. (E) Scatter plot as in (A), with light-dependent (light-dep) units highlighted in blue fill and light-independent (light-indep) units highlighted in blue outline. (F) Histogram and (G) bar chart showing the difference in spike regularity (CV2) between light-dependent and light-independent units. Data are represented as mean ± SEM. **p<0.01.

To identify 5-HT neurons in the VGLUT3-cKO mice, optotagging experiments were performed three weeks after viral injection of ChR2-eYFP. A dataset of 203 units was obtained from 8 mice and subjected to hierarchical clustering, as previously carried out on the SERT-Cre dataset (Figure 4.9A, B). In the VGLUT3-cKO mice, 37.4% of neurons (76/203) were slow regular firing, 49.7% (101/203) were slow irregular firing, and the remaining 12.8% (26/203) were fast-firing (Figure 4.9C). The proportions of each cluster recorded in the VGLUT3-cKO mice were very similar to that of SERT-Cre mice.

Of 203 total units in VGLUT3-cKO mice, 22 (i.e. 10.8% yield) were optotagged. Again, similar to findings in the SERT-Cre mice, these optotagged units came from all three clusters; 36.3% of optotagged neurons (8/22) were slow regular firing, 50% (11/22) were slow irregular firing, and the remaining 13.6% (3/22) were fast-firing (Figure 4.9D). Light-dependent and light-independent optotagged neurons were also observed in the VGLUT3-cKO mice (Figure 4.9E). The distribution of these neurons was similar to that of SERT-Cre mice, with 59.1% (13/22) following light stimulation up to 20 Hz, and the remainder (40.9%, 9/22) only optically activated reliably at 1 Hz but not higher frequencies. Upon closer inspection, the distribution of light-dependent and light-independent VGLUT3-cKO neurons mirrored that of SERT-Cre neurons (Figure 4.9E, F); a two-tailed unpaired t-test showed that light-dependent neurons also displayed lower CV2 values than light-independent neurons (Figure 4.9G; $t(20) = -2.964$, $p = 0.0077$). Overall, these results showed that the electrophysiological properties of DRN neurons in VGLUT3-cKO mice were not detectably different from SERT-Cre mice. Therefore, the cluster classification described here was not sufficient to identify the subpopulation of 5-HT neurons involved in glutamate co-transmission.

Finally, the baseline firing parameters of DRN neurons in SERT-Cre and VGLUT3-cKO mice were compared to determine any influence of glutamate co-transmission. Interestingly, slow and irregular firing neurons in the VGLUT3-cKO mice fired less irregularly (i.e. lower CV2 values) compared to those in the SERT-Cre mice (Figure 4.10A; Mann-Whitney U test; $Z = 2.724$, $p = 0.0065$). Slow and regular firing neurons, on the other hand, had a significantly lower baseline firing rate in VGLUT3-cKO mice compared to SERT-Cre mice (Figure 4.10B; Mann-Whitney U test; $Z = 3.648$, $p < 0.001$). There was a trend for a higher firing rate of fast-firing neurons in VGLUT3-cKO versus SERT-Cre mice (Figure 4.10B; Mann-Whitney U test, $Z = -1.751$, $p = 0.0799$). All three neuron types from VGLUT3-cKO mice

displayed a greater spike width than those from SERT-Cre mice (Figure 4.10C; Mann-Whitney U test; SR, Z = -2.9284, p = 0.0034; SIR, Z = -2.9577, p = 0.0031; FF, Z = -3.1010, p = 0.0019). Since this difference occurred across all three neuron types, it could be due to the use of a different optrode of similar conformation, but from different manufacturers, in the two sets of experiments.

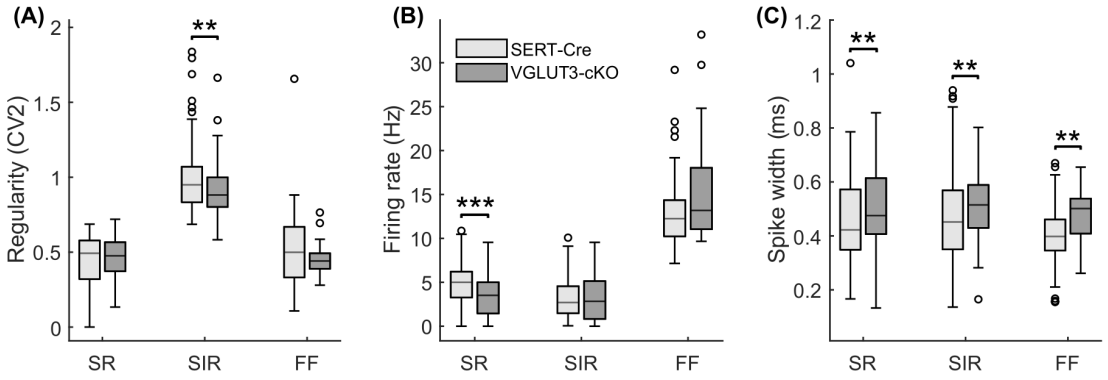

Figure 4.10: Differences in (A) spike regularity (CV2), (B) firing rate (Hz), (C) spike width (ms) of each DRN neuron cluster between SERT-Cre and VGLUT3-cKO mice. Data are represented as median ± interquartile range. Circles represent outliers. **p<0.01, ***p<0.001.

4.4 Discussion

Experiments in this chapter established a protocol to optically activate DRN 5-HT neurons *in vitro* then *in vivo*. Thus, ChR2-eYFP was selectively expressed in DRN 5-HT neurons of transgenic SERT-Cre mice, and the functionality of ChR2-eYFP was tested in *in vitro* whole-cell patch-clamp as well as *in vivo* optotagging experiments using silicon probe recordings. The results demonstrated abundant expression of ChR2-eYFP in TPH2-immunoreactive cells in the DRN and successful activation of DRN 5-HT neurons using light pulses *in vitro* and *in vivo*. Although quantification of ChR2-eYFP/TPH2 co-expression was not carried out in the current study, past studies by the lab using the same transgenic mouse line and viral vectors reported 100% co-localisation of ChR2-eYFP and 5-HT in the DRN (Sengupta et al., 2017).

4.4.1 5-HT neurons are comprised of heterogeneous sub-populations

As reviewed in Section 4.1, 5-HT neurons have long been agreed to exhibit a classical electrophysiological phenotype of slow and regular firing (Aghajanian and Vandermaelen, 1982; Vandermaelen and Aghajanian, 1983; Li et al., 2001; Allers and Sharp, 2003). In the present study, a novel clustering analysis of large numbers of simultaneously recorded DRN neurons was taken to identify three neuron clusters based on their baseline firing rate and regularity: slow regular firing, slow irregular firing, and fast-firing. While the slow regular firing cluster resembled classical 5-HT neurons described in the literature, optotagging results revealed the presence of 5-HT neurons in all three clusters, suggesting heterogeneity in the baseline properties of DRN 5-HT neurons *in vivo*.

This observation is in agreement with reports of diverse firing properties of juxtacellularly labelled 5-HT neurons in the rat DRN, including slow but burst-firing (i.e. slightly less regular compared to clock-like neurons) 5-HT neurons (Schweimer et al., 2011) and fast-firing 5-HT neurons (Allers and Sharp, 2003; Kocsis et al., 2004). While previous juxtacellular recording studies reported that most slow and irregular firing neurons in the rat DRN were immunonegative for 5-HT and tryptophan hydroxylase (Allers and Sharp, 2003; Schweimer et al., 2011), experiments here provided evidence that slow and irregular firing neurons in the mouse DRN can, in fact, be 5-HT containing. A recent optotagging study of mouse DRN 5-HT neurons also reported that the firing rate and spike regularity of optotagged 5-HT neurons were indistinguishable from that of non-optotagged neurons (Cohen et al., 2015), in support of an earlier *in vitro* report that 5-HT and non-5-HT neurons in the rat DRN were not distinguishable by their baseline firing characteristics (Beck et al., 2004). However, the study by Cohen et al. (2015) provided a superficial analysis of the electrophysiology of DRN 5-HT neurons, whereas the current study offers a

more extensive analysis of the baseline firing properties of optotagged 5-HT neurons. Current evidence of diverse electrophysiological properties amongst 5-HT neurons suggests that previous studies selecting DRN 5-HT neurons on the basis of slow and regular firing properties underestimated the true 5-HT neuron population.

4.4.2 A subpopulation of 5-HT neurons were light-independent

All recorded 5-HT neurons in slices reliably fired action potentials following optical stimuli up to 20 Hz. However, one notable observation in the current study is that while many optogenetically activated 5-HT neurons *in vivo* displayed light-dependent properties, a subpopulation instead displayed light-independent properties (i.e. fired at a lower rate even when light stimulation frequency increased to 20 Hz). Interestingly, further analysis showed that light-dependent 5-HT neurons were more regular firing compared to light-independent 5-HT neurons, suggesting that classical regular firing 5-HT neurons, as described by the literature, are more likely to fire at higher frequencies compared to irregular firing 5-HT neurons. It is possible that light-independent 5-HT neurons were present but undetected in slice experiments because the number of recorded neurons was too low (n = 8 neurons from 3 mice) in comparison to the *in vivo* recordings (n = 32 neurons from 11 mice). However, other optogenetic studies that activated 5-HT neurons in DRN slices also observed faithful action potential firing with light pulses up to 20 Hz (Liu et al., 2014; Grandjean et al., 2019).

A potential explanation for these different neuron types is that 5-HT neuron firing is intrinsically different in the slice compared to an *in vivo* setting. For instance, the *in vivo* activation of DRN 5-HT neurons might result in greater levels of extracellular 5-HT, leading to increased activation of 5-HT_{1A} receptors that limit the frequency responsivity of a subpopulation of 5-HT neurons via autoinhibition. Previous reports

of a subpopulation of DRN 5-HT neurons that do not express the 5-HT_{1A} receptor could correspond with the light-dependent 5-HT neurons that were able to fire at higher frequencies despite high levels of extracellular 5-HT (Kiyasova et al., 2013).

An alternative explanation is that some slow-firing 5-HT neurons may not have the natural capacity to fire at 20 Hz under physiological conditions, perhaps due to a lack of complementary ion channel expression, and therefore demonstrate light-independent properties. Although DRN 5-HT neurons are generally reported to fire at slow rates, their activity is known to change in relation to brain state. For instance, the activity of 5-HT neurons increases with wakefulness and arousal but decreases with sleep and rest (Jacobs and Fornal, 1999; Sakai, 2011). In recent optotagging studies of 5-HT neurons in awake mice, the firing rate of 5-HT neurons was shown to increase to $15 - 20$ Hz in response to aversive and rewarding stimuli (Cohen et al., 2015; Li et al., 2016), indicating that at least some 5-HT neurons physiologically fire up to 20 Hz during emotionally salient events. Thus, it is plausible that light-independent 5-HT neurons observed in the current study represent a subpopulation of 5-HT neurons that are not recruited during such events and therefore do not fire above about 10 Hz under physiological conditions.

4.4.3 Firing properties of 5-HT neurons in VGLUT3-cKO mice

Recent transcriptomic analyses of the mouse DRN revealed a high degree of heterogeneity and diversity in the molecular markers present in 5-HT neurons (Huang et al., 2019; Okaty et al., 2020), raising the possibility that these markers could represent subpopulations of DRN 5-HT neurons with distinct firing properties. Given that up to two-thirds of DRN 5-HT neurons express VGLUT3 (Hioki et al., 2010), this chapter explored whether VGLUT3-expressing 5-HT neurons might correspond to one of the DRN clusters. As such, optotagging experiments were

performed in VGLUT3-cKO mice in which VGLUT3 expression was selectively ablated in 5-HT neurons to model the absence of 5-HT/glutamate co-transmission (Mansouri-Guilani et al., 2019).

Although it was predicted that DRN neurons from VGLUT3-cKO mice might produce a different cluster pattern compared to SERT-Cre controls, results here showed no effect of genotype on DRN neuron clusters. Moreover, optotagged neurons were detected in similar proportions across the clusters in SERT-Cre and VGLUT3-cKO mice. Thus, the current clustering method was unable to identify VGLUT3-expressing DRN 5-HT neurons.

Interestingly, further analysis revealed differences in the baseline firing properties of DRN neurons from SERT-Cre and VGLUT3-cKO mice. In particular, slow regular firing neurons in VGLUT3-cKO mice had a significantly lower firing rate compared to SERT-Cre mice, while slow irregular neurons in the VGLUT3-cKO mice fired less irregularly compared to SERT-Cre mice. These results suggest that the loss of VGLUT3 from 5-HT neurons, and presumably loss of glutamate co-release, caused subtle shifts in the firing characteristics of DRN neuron subpopulations. The decrease in firing rate of DRN neurons in VGLUT3-cKO mice could be explained by a loss of glutamatergic input from VGLUT3-expressing 5-HT cells, as rat 5-HT neurons in microcultures have been shown to evoke glutamate-dependent excitatory potentials in neighbouring 5-HT neurons (Johnson, 1994).

Despite the growing interest in 5-HT/glutamate co-transmission, there are very few reports on the electrophysiological properties of identified VGLUT3-expressing 5-HT neurons in the DRN. A juxtacellular labelling study by Domonkos et al. (2016) reported the *in vivo* firing properties of VGLUT3-expressing 5-HT and non-5-HT neurons in the rat MRN and observed differences in firing characteristics between VGLUT3-expressing 5-HT neurons and VGLUT3-expressing non-5-HT neurons,

but no differences between VGLUT3-expressing 5-HT neurons and non-VGLUT3-expressing 5-HT neurons. More experiments will be required to characterise the molecular identity of subpopulations of DRN 5-HT neurons with different firing characteristics.

4.4.4 Conclusions

Overall, results presented in this chapter demonstrated successful optogenetic activation of DRN 5-HT neurons *in vitro* and *in vivo*. Additionally, results from optotagging studies provided new insights into the diverse firing characteristics of DRN 5-HT neurons and revealed subpopulations of DRN 5-HT neurons that exhibited light-independent responses to light stimuli. With the optogenetic methodology verified, experiments in the next chapter explored the effects of optogenetic activation of 5-HT neurons on mPFC neuron firing.

5

Effects of optogenetic activation of 5-HT neurons on neural activity in the mPFC *in vitro* and *in vivo*

5.1 Introduction

Thus far, experiments in this thesis have reported and characterised 5-HT_{2A} receptor-mediated interactions between 5-HT and genetically labelled PVINs in mPFC slices. The systemic administration of 5-HT_{2A} receptor agonists was also shown to greatly alter neural activity in the mPFC *in vivo*, including that of putative PVINs, at multiple levels. Here, the effects of physiologically released 5-HT on the neural activity in the mPFC *in vitro* and *in vivo* were investigated using the optogenetic methodology verified in Chapter 4.

5.1.1 Effects of electrical stimulation of the DRN on mPFC neurons *in vivo*

The earliest studies on the effects of physiologically released 5-HT on mPFC neurons were achieved by electrically stimulating the DRN and MRN (Mantz et al., 1990). Using glass micropipette recording technique, Mantz et al. (1990) reported the inhibition of spontaneous activity in 35% and 53% of rat PFC neurons tested following electrical stimulation of the DRN and MRN, respectively, suggesting an

inhibitory control of 5-HT neurons on spontaneous activity in the anaesthetised rat PFC. A subsequent study by Gartside et al. (2000) confirmed that electrical stimulation of DRN increased extracellular levels of 5-HT in the rat mPFC and that the majority of recorded mPFC neurons exhibited post-stimulus inhibition following electrical stimulation of the DRN at 1 Hz. These inhibitory effects of electrical stimulation of the DRN were shown to be abolished by the selective 5-HT_{1A} receptor antagonist WAY-100635, although the identity of these mPFC neurons was not confirmed (Hajós et al., 2003). Further single-unit recordings of pyramidal neurons in the rat mPFC during electrical stimulation of the DRN showed three different types of responses: inhibition (66%), excitation (13%), and biphasic responses (20%), in which excitation was preceded by inhibition (Puig et al., 2005). Although infrequent, excitatory effects of DRN stimulation on mPFC pyramidal neurons were blocked by the selective 5-HT_{2A} receptor antagonist MDL-100907, suggesting that endogenous 5-HT directly activated a subpopulation of mPFC pyramidal neurons via the 5-HT_{2A} receptor (Amargós-Bosch et al., 2004; Puig et al., 2005). On the other hand, inhibitory effects of DRN stimulation were partially antagonised by pharmacological blockade of 5-HT_{1A} and $GABA_A$ receptors, indicating the involvement of both direct inhibition of pyramidal neurons via the 5-HT_{1A} receptor as well as indirect inhibition via the activation of local interneurons (Puig et al., 2005). Interestingly, Amargós-Bosch et al. (2004) showed that excitatory or inhibitory responses could be induced in the same pyramidal neuron by stimulating the DRN at different sites, suggesting a precise spatial connectivity between the DRN and mPFC.

Electrical stimulation of the DRN was also reported to evoke short-latency excitation of putative GABAergic neurons in superficial layers of the rat mPFC, an effect blocked by the 5-HT_3 receptor antagonists (Puig et al., 2004). This finding was taken as evidence for an interaction between 5-HT and 5-HT_3R-expressing interneurons in the mPFC (Puig et al., 2004), which was recently confirmed in

an *in vivo* study demonstrating DRN-evoked excitation of juxtacellularly labelled 5-HT_3-expressing interneurons (Schweimer et al., 2022).

As noted in Section 1.5, few *in vivo* electrophysiological studies focused on PVINs. In one of the few such studies, Puig et al. (2010) monitored the effects of electrical stimulation of the DRN on putative PVINs in the rat mPFC and observed predominantly inhibitory effects (61%) via the 5-HT_{1A} receptor and a small degree of excitation (10%) via the 5-HT_{2A} but not 5-HT_{2C} receptor. In addition, Puig et al. (2008) identified two subpopulations of putative PVINs by their spiking activity patterns in relation to UP/DOWN states and later reported that both groups were mostly inhibited by DRN stimulation (Puig et al., 2010). More recently, juxtacellularly labelled PVINs in the rat mPFC were shown to exhibit mainly post-stimulus inhibition but also long-latency and short-latency excitation in response to electrical stimulation of the DRN (Schweimer et al., 2022). While the inhibitory and long-latency excitatory effects of 5-HT were consistent with that mediated by 5-HT_{1A} and 5-HT_{2A} receptors, the short-latency excitatory response (putatively ionotropic) was not blocked by the 5-HT_3 receptor antagonist vortioxetine and was theorised to be mediated by co-released glutamate (Schweimer et al., 2022).

Contrary to the above evidence that DRN stimulation inhibited mPFC neurons, LFP recordings suggest that electrical stimulation of the DRN led to an activated cortical brain state. Electrical stimulation of the DRN at 1 Hz was shown to modulate cortical network synchrony by reducing the amplitude of SWA and increasing the duration of UP states via the 5-HT_{1A} and 5-HT_{2A} but not the 5-HT_{2C} receptor (Puig et al., 2010). In addition, high-frequency stimulation of the DRN at 100 Hz completely suppressed cortical SWA for a few seconds, supporting the role of 5-HT in the modulation of cortical network oscillations and sleep-wake transitions (Puig et al., 2010).

5.1.2 Effects of optogenetically evoked 5-HT release on mPFC neurons *in vitro*

While the electrical stimulation of the DRN evoked physiological 5-HT release (Gartside et al., 2000), such stimulation is not specific to 5-HT neurons. Non-5-HT DRN projections, such as GABAergic projections (Bang and Commons, 2012), would also be activated. As such, recent advancements in optogenetic technique provide a valuable means for the selective activation of genetically targeted neurons, and have been used to characterise the dopaminergic modulation of mPFC neurons *in vivo* (Lohani et al., 2019).

Optogenetic characterisation of 5-HT interactions with mPFC neurons has been achieved *in vitro* but not *in vivo*. In a key study by Athilingam et al. (2017) reviewed in Chapter 2, the effects of physiologically released 5-HT on putative PVINs were investigated by optogenetically activating ChR2-expressing 5-HT afferents in mPFC slices. Replicating the effects of bath applied 5-HT, optogenetic activation of 5-HT terminals at 10 Hz increased the firing rate of putative PVINs via the 5-HT_{2A} receptor (Athilingam et al., 2017). Although not reported in the mPFC (Athilingam et al., 2017), other optogenetic studies have demonstrated 5-HT/glutamate co-transmission *in vitro* by optogenetically activating 5-HT afferents in slices of the mouse ventral tegmental area and nucleus accumbens (Liu et al., 2014), olfactory bulb (Kapoor et al., 2016), and amygdala (Sengupta et al., 2017). In particular, the co-release of glutamate by 5-HT terminals in the amygdala was shown to be frequency-dependent, as stimulation of 5-HT terminals at higher frequencies led to depression of glutamate-dependent fast excitatory postsynaptic currents (Sengupta et al., 2017).

Altogether, past *in vivo* studies provide predominant evidence for the inhibition of putative PVINs in the mPFC by DRN stimulation-evoked release of 5-HT (Puig et al., 2010; Schweimer et al., 2022). However, the exact actions of 5-HT are unclear, as *in vitro* experiments reported the excitation of putative PVINs following

optogenetic activation of 5-HT terminals in mPFC slices (Athilingam et al., 2017), an effect reminiscent of the excitatory effects on PVINs of locally applied 5-HT found in Chapter 2. The vast majority of *in vivo* studies reviewed here characterised the interactions between 5-HT and mPFC neurons by electrically stimulating the DRN, which nonselectively activates neurons in the DRN rather than 5-HT neurons themselves (Gartside et al., 2000; Amargós-Bosch et al., 2004; Puig et al., 2005, 2010), and there is a current lack of an optogenetic approach to investigate the interactions between 5-HT and mPFC neurons.

5.1.3 Aims of this chapter

With the functionality of ChR2 in genetically targeted DRN 5-HT neurons verified in Chapter 4, this chapter aims to determine the effects of optogenetically evoked 5-HT on mPFC neurons and PVINs in particular, *in vitro* and *in vivo*. 5-HT neurons in the DRN of SERT-Cre mice were selectively transfected with ChR2 or the control fluorophore mCherry as described in Chapter 4. First, slice experiments were performed to characterise the effects of optogenetically evoked 5-HT on mPFC neurons *in vitro*. ChR2-expressing 5-HT afferents in the mPFC were stimulated during whole-cell patch-clamp sessions of mPFC neurons, including putative PVINs. Next, *in vivo* experiments were performed in SERT-Cre mice, in which ChR2-expressing 5-HT neurons in the DRN were optogenetically activated during multi-unit recordings sessions in the mPFC. Neural activity in the mPFC was recorded using silicon probes and evaluated at multiple levels, ranging from LFP oscillations to multi-unit and single-unit spiking activity. As described in Chapter 3, a waveform-based clustering approach was used to identify putative PVINs and characterise their responses to optogenetically evoked 5-HT release.

5.2 Materials and Methods

5.2.1 Experiment animals

Transgenic SERT-Cre mice, which express the CRE recombinase in 5-HT neurons, were group housed with wildtype littermates in individually ventilated cages. Mice were maintained on a 12-hour light/dark cycle at constant temperature and humidity, with food and water provided *ad libitum*. Male and female mice between the age of two to four months were used. All procedures were performed in accordance with the Animals (Scientific Procedures) Act 1986 and in line with the guidelines of the University of Oxford.

5.2.2 Viral transfection

As described in Section 4.2.2, 5-HT neurons in the DRN of the SERT-Cre mice were selectively transfected with ChR2 via stereotaxic injection of a Cre-inducible recombinant viral vector that carries a floxed ultrafast (E123T/T159C) ChR2 fused with eYFP (AAV5-EF1a-DIO-hChR2(E123T/T159C)-EYFP; UNC Vector Core). Additionally, for *in vivo* experiments, a viral vector carrying the mCherry fluorescent reporter protein (AAV5-EF1a-DIO-mCherry; UNC Vector Core) was injected into a control group of mice. Viral transfection procedures were carried out as described in Section 4.2.2. Upon recovery, mice were allowed to recover for 3 to 4 weeks, and in some cases up to 16 weeks for *in vitro* electrophysiological experiments.

5.2.3 *In vitro* electrophysiology and optogenetic stimulation

After recovery of SERT-Cre mice from viral transfection surgeries, acute coronal slices of the mPFC were prepared using methodology described in detail in Section 2.2.2. In brief, whole-cell patch-clamp recordings were obtained from deep layer

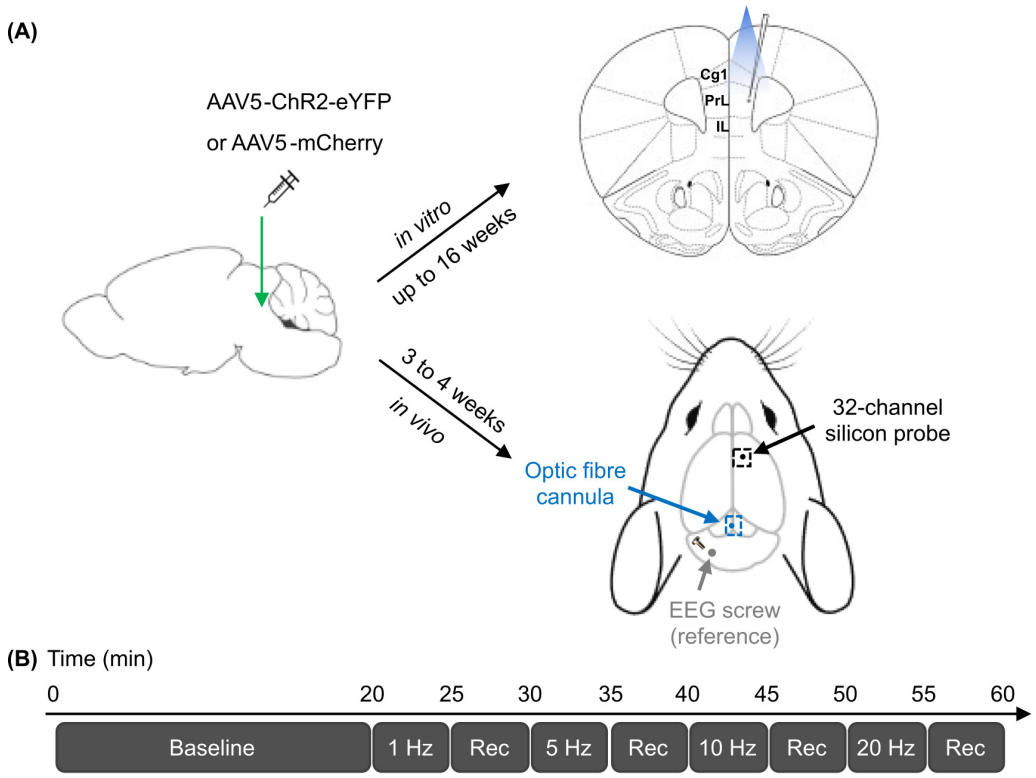

Figure 5.1: (A) Schematic of experimental design for the investigation of effects of optogenetically evoked 5-HT release on mPFC neurons *in vitro* and *in vivo*. (B) Timeline of *in vivo* recordings.

neurons in the prelimbic cortex, with a focus on cells with small and ovoid soma that did not resemble pyramidal neurons (Figure 5.1A). After establishing a whole-cell patch-clamp, current-clamp recordings were obtained as blue light pulses were delivered (473 nm, 5 ms duration) at 1, 5, 10, and 20 Hz. Current-clamp recording data were acquired, processed, and analysed as described in Chapter 2.

5.2.4 *In vivo* electrophysiology and optogenetic stimulation

Multi-unit recordings were obtained from urethane-anaesthetised SERT-Cre mice after recovery from viral transfection surgeries (Figure 5.1A). Experiments were performed using a 32-channel silicon probe electrode (ASSY-37 H-Series 6b, Cambridge Neurotech, UK) identical to that used in Chapter 3. In brief, the silicon probe was implanted into the right mPFC using a micro-manipulator stereotaxic

arm (LinLab 2, Scientifica, UK) at coordinates: AP +2.0 mm, ML +0.4 mm, DV -1.3 to -1.7 mm, relative to bregma and the brain surface. A stainless screw (1 mm diameter) was implanted into the skull over the cerebellum and used as ground and reference. Additionally, a fibre optic cannula of 200 μm diameter (ThorLabs, NJ, USA), connected to a 473 nm blue laser diode (Doric Lenses, Canada) via a zirconian sleeve and a patch cable, was implanted into the DRN (AP -5.0 mm, ML +0.1 mm, DV -2.7 mm) at a 5°angle relative to the AP axis. Prior to each experiment, the silicon probe was coated with a fluorescent dye for *post hoc* visualisation and the laser output was calibrated to 5 $mWmm^{-2}$. The silicon probe and laser diode were then connected to the signal chain (see Sections 3.2.3 and 4.2.6).

5.2.5 Experimental design

After 20 min of baseline recording, blue light pulses were sequentially delivered in 10 min blocks at 1, 5, 10, and 20 Hz. In each 10 min block, 5 ms pulses were continuously delivered for 5 min and the brain was allowed to recover for 5 min. The total length of each recording was 60 min (Figure 5.1B).

5.2.6 Immunohistological analysis

At the end of each recording session, brains were extracted from transcardially perfused mice, then fixated and cryoprotected as described in Section 3.2.6. Coronal slices of the mPFC were obtained and mounted for *post hoc* verification of silicon probe location. Midbrain coronal slices at the level of the DRN were also examined to confirm the expression of ChR2-eYFP in 5-HT neurons.

5.2.7 Data analysis

Firing rate analysis as well as putative PVIN identification based on spike waveform properties were carried out as described in Section 3.2.9. Peri-stimulus time histograms (PSTHs) and raster plots were subsequently constructed to examine short-latency responses of individual neurons to the optogenetic stimulation of the DRN at 1 Hz. The construction of PSTHs was performed as in Section 4.2.10. PSTHs were examined to determine the type of response, specifically no response, inhibition, slow excitation, inhibition followed by slow excitation, fast excitation, or both fast and slow excitations. Inhibition was characterised by a dip in spike rate within 50 ms after light stimulation, whereas fast and slow excitations were characterised by peaks in spike rate within 50 and 100 ms after light stimulation, respectively (Amargós-Bosch et al., 2004; Puig et al., 2004, 2005; Varga et al., 2009). Spike count correlation analysis was additionally carried out as described in Section 3.2.11.

5.2.8 UP and DOWN state detection

LFP data were obtained by downsampling and bandpass filtering raw multi-unit recording data, and spectrograms were computed as detailed in Section 3.2.12. To identify and assign UP and DOWN states, LFP data were processed to highlight instantaneous peaks in power in the gamma range ($30 - 80$ Hz) in multiple steps (Mukovski et al., 2007). First, fast Fourier transform (using the MATLAB function *fft*) was performed on the LFP signal. Coefficients corresponding to frequencies outside of the gamma range (i.e. $<$30 Hz and $>$80 Hz), as well as those within the mains noise frequency range ($49 - 51$ Hz), were set to zero. An inverse fast Fourier transform was then performed (using the MATLAB function *ifft*) to obtain the gamma component of the LFP signal.

The power spectral density in the gamma range was calculated using the filtered signal over 200 ms time bins with 50% overlap. Peaks of high gamma power were correlated with dips in the slow wave signal, as described in Mukovski et al. (2007) and Gretenkord et al. (2017). To accentuate the difference between phases of low and high gamma power, a moving standard deviation filter was applied over a 50 ms time bin. The resulting traces were reminiscent of rectangular shaped pulses, where each pulse represents a period of high instantaneous gamma power in the UP state. The amplitude distribution of the final trace was bimodal, allowing a UP/DOWN state threshold to be applied. The threshold was determined by fitting a polynomial curve to the histogram of 30 sec epochs and identifying the local minimum (using the MATLAB functions *polyfit*, *polyval*, and *islocalmin*). Using the bimodal distribution threshold, UP and DOWN states were assigned at a resolution of 0.1 ms, and percentage of time spent in UP state was quantified.

5.2.9 Statistical analysis

All statistical tests were performed in MATLAB. Data normality was first tested using the Shapiro-Wilk test (MATLAB function *swtest*). For parametric and paired data, two-tailed paired Student's t-tests were performed (using the MATALB function *ttest*). For nonparametric data, Mann-Whitney U tests were performed (using the MATLAB function *ranksum*). In situations where multiple comparisons were made, the Benjamini-Hochberg procedure was applied with a 5% false discovery rate to adjust the p-values. Where the frequency-dependency of light stimulation was examined, Pearson correlation coefficients were calculated using the MATLAB function *corrcoef*. Data are represented as mean ± SEM unless otherwise specified.

5.3 Results

5.3.1 Effects of optogenetic activation of 5-HT axons on mPFC neurons *in vitro*

To optogenetically activate 5-HT afferents in the mPFC, a recombinant viral vector containing ChR2-eYFP was injected into the DRN of transgenic SERT-Cre mice as described in Chapter 4 to achieve the selective expression of ChR2-eYFP in DRN 5-HT neurons. The presence of ChR2-eYFP in the DRN and mPFC was first examined in mice perfused between 3 to 6 weeks after viral transfection. In these mice, ChR2-eYFP-expressing 5-HT neurons in the DRN and ChR2-eYFP-expressing 5-HT axons in the mPFC were observed within 4 weeks of viral transfection (example shown in Figure 5.2A, B).

Whole-cell patch-clamp recordings were then obtained from neurons in deep layers of the prelimbic cortex in coronal slices of SERT-Cre mice (n = 8) between 4 to 6 weeks after viral injection to allow for adequate expression of ChR2-eYFP. In particular, neurons that were in proximity to ChR2-eYFP expression and with small ovoid soma that did not resemble pyramidal neurons were targeted. The brains of these mice were also harvested and ChR2-eYFP expression in the DRN was confirmed.

During these recordings, difficulties were encountered when locating and stimulating mPFC 5-HT terminals in the slice. Despite visualisation of ChR2-eYFP-expressing 5-HT axons at high resolution in fixed mPFC slices (80 μm) using strong fluorescence illumination (Figure 5.2B), it was not possible to visualise ChR2-eYFP-expressing 5-HT axons in fresh mPFC slices (350 μm) in the patch-clamp rig, even though *post hoc* histology confirmed that ChR2-eYFP was indeed present in the DRN of these mice. The recovery period was extended to up to 16 weeks in some mice (n = 4) to increase the time for ChR2 trafficking to mPFC terminals but ChR2-eYFP was still not observed in these mPFC slices during patch-clamp sessions.

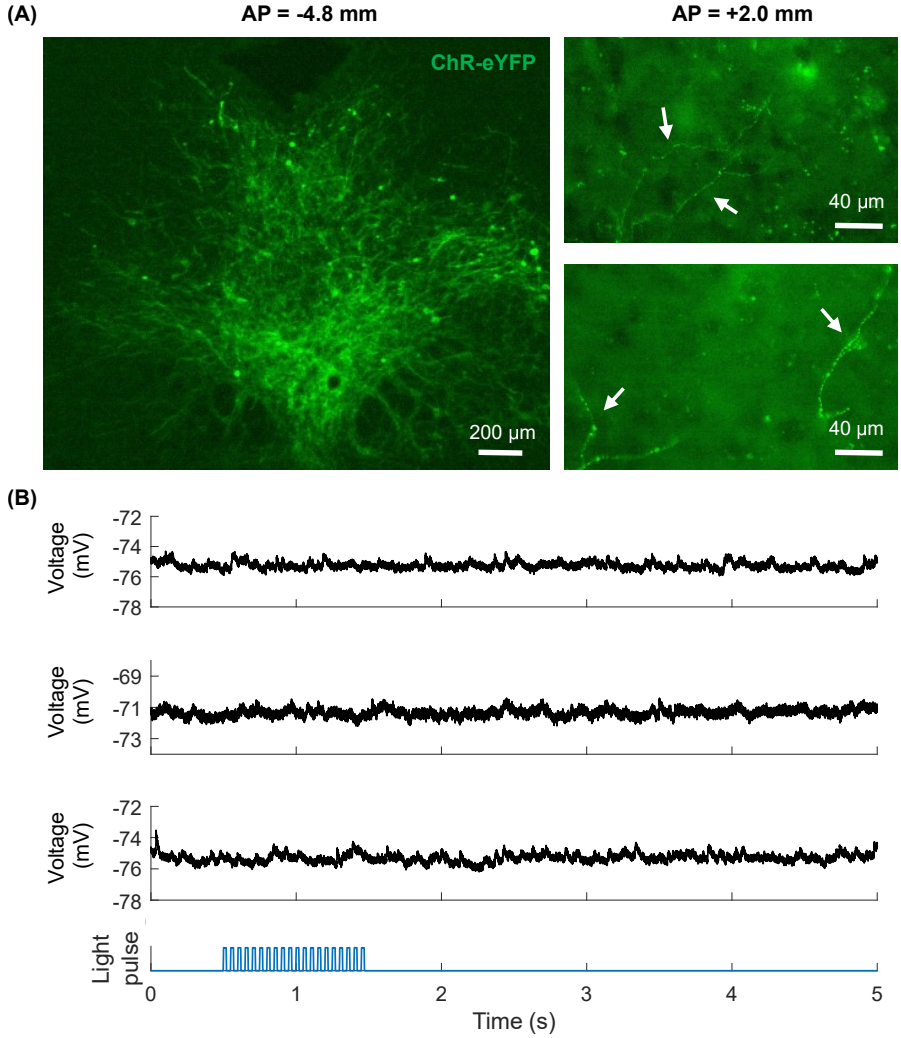

Figure 5.2: Effects of optogenetic activation of 5-HT terminals on mPFC neurons *in vitro*. (A) Demonstration of ChR2-eYFP expression in DRN 5-HT neurons (left) and mPFC 5-HT axons (right) of SERT-Cre mice 4 weeks after viral transfection. White arrows highlight axon locations. (B) Example current-clamp recording traces of the response in membrane potential (mV) of three mPFC neurons to the application of 20 Hz light pulses. All neurons featured were from different mice in which ChR2-eYFP expression was confirmed *post hoc* in the DRN.

Despite repeated attempts, light pulses applied (up to 20 Hz) during whole-cell patch-clamp recording sessions failed to evoke a response in any mPFC neuron examined (n = 39 neurons from 12 mice, example traces shown in Figure 5.2C). It was concluded from these experiments that whilst the optogenetic activation of ChR2-eYFP-expressing 5-HT cell bodies was successful (see Section 4.3.4), this did not extend to ChR2-eYFP-expressing 5-HT axons in the mPFC under current

experimental conditions.

5.3.2 Effects of optogenetic activation of DRN 5-HT neurons on network oscillations *in vivo*

Given the inconclusive *in vitro* results above, *in vivo* electrophysiology experiments were conducted to determine the effects of optogenetic activation of DRN 5-HT neurons on mPFC neurons, including PVINs. By activating 5-HT neuron cell bodies rather than terminals, it was theorised that sufficient 5-HT would be released in the mPFC to evoke detectable responses.

Multi-unit recordings targeting deep layers of the prelimbic cortex were performed in urethane-anaesthetised SERT-Cre mice between 3 and 4 weeks after viral injection. Recordings were obtained from 7 mice that were transfected with ChR2-eYFP and 3 control mice that were transfected with the fluorescent reporter mCherry. *Post hoc* histology was performed in all mice and demonstrated abundant expression of ChR2-eYFP or mCherry and localisation of optic fibre cannulae in the DRN (typical examples for each shown in Figure 5.3A), localisation of silicon probes in the mPFC (Figure 5.3B), and the presence of ChR2-eYFP-expressing 5-HT axons in the mPFC in ChR2-eYFP mice (Figure 5.3C). In these experiments, light pulses were applied in 5 min blocks at 1, 5, 10, and 20 Hz sequentially following 20 min of baseline recording to test the effects of optogenetically evoked 5-HT release.

LFP signals were first extracted for each recording session and the effects of optogenetic activation of 5-HT neurons on SWA oscillations ($0.1 - 2$ Hz) in the mPFC were examined. As reviewed in Chapter 1 and demonstrated in Chapter 3, electrical stimulation of the DRN as well as the application of 5-HT_{2A} receptor agonists resulted in a reduction of cortical SWA *in vivo* (Puig et al., 2010; Celada et al., 2008). It was therefore hypothesised that optogenetic activation of 5-HT neurons would reduce local oscillations in the SWA range in the mPFC.

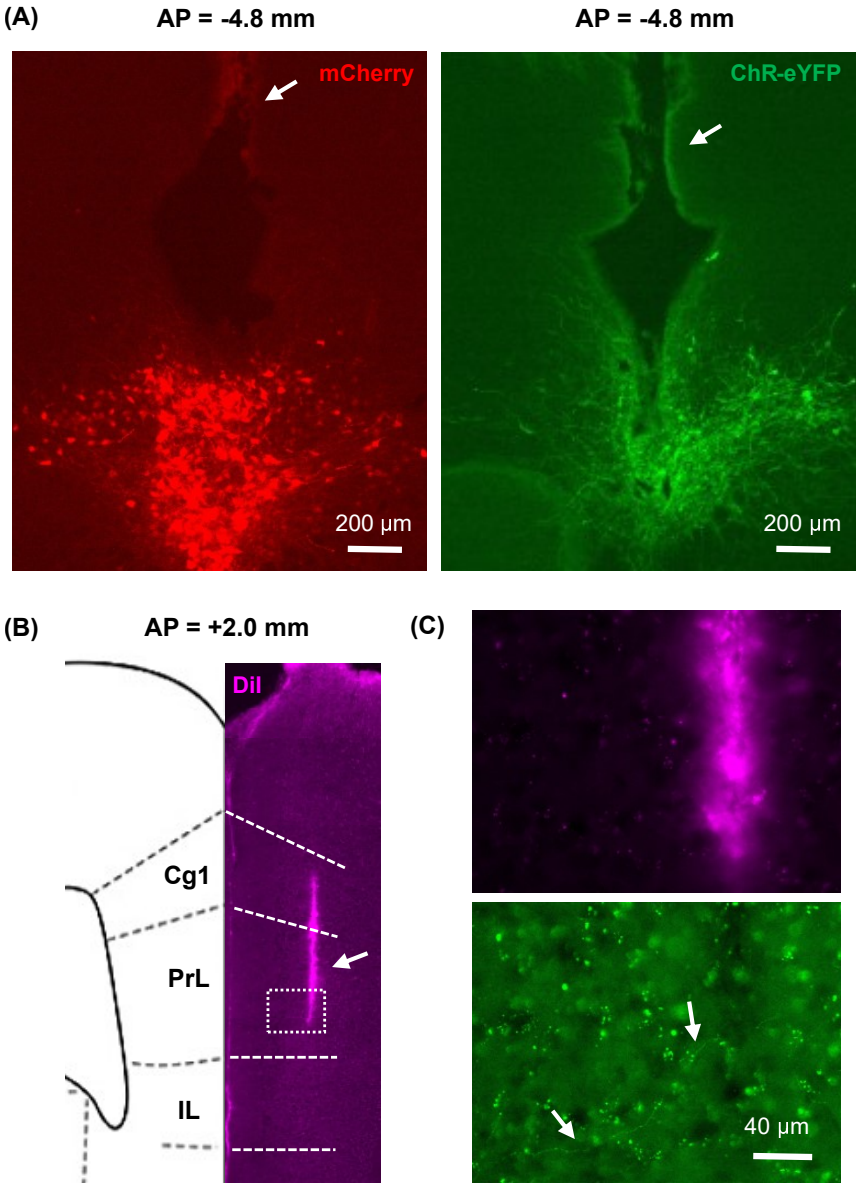

Figure 5.3: Expression of ChR2-eYFP and mCherry in DRN 5-HT neurons and mPFC 5-HT terminals. (A) Example Cre-dependent expression of ChR2-eYFP (green, left) and mCherry (red, right) in the DRN of SERT-Cre mice. Coronal sections correspond to 4.8 mm posterior of bregma. White arrows indicate the insertion tracts of optic fibre cannulae. (B) Example fluorescent tract (magenta) of DiI-coated silicon probe insertion in deep layers of the prelimbic (PrL) cortex. Anatomical atlas illustration on the left represents the mPFC subregions at 2.0 mm anterior of bregma and is adapted from Franklin and Paxinos (2013). White box indicates the area shown in (C). (C) Example expression of ChR2-eYFP (green, bottom) in 5-HT axons in the mPFC, in close proximity to silicon probe insertion tract (magenta, top). Cg1: Cingulate area 1. IL: Infralimbic.

Indeed, optogenetic activation of DRN 5-HT neurons reduced LFP power in SWA range in ChR2-eYFP mice but not control mice (spectrogram examples shown in Figure 5.4A and 5.5A, respectively). In ChR2-eYFP mice, 20 Hz light stimulation resulted in the longest-lasting and most pronounced reduction in SWA (Figure 5.4B, C; two-tailed paired t-test, $t(6) = 6.035$, $p = 0.0038$, $n = 7$ mice). A significant reduction in SWA was also observed at light stimulation frequencies of 5 and 10 Hz but not 1 Hz (Figure 5.4C; two-tailed paired t-test; 1 Hz, $t(6) = 1.598$, $p = 0.1853$; 5 Hz, $t(6) = 2.765$, $p = 0.0326$; 10 Hz, $t(6) = 2.524$, $p = 0.0450$). On the other hand, in control mice, LFP power in SWA range remained unaffected at all stimulation frequencies (Figure 5.5B, C; two-tailed paired t-test; 1 Hz, $t(2) = -0.2087$, $p =$ 08540; 5 Hz, $t(2) = 0.8139$, $p = 0.5012$; 10 Hz, $t(2) = 1.223$, $p = 0.3459$; 20 Hz, $t(2) = 0.5201$, $p = 0.6548$, $n = 3$ mice). Pearson correlation analyses revealed a positive correlation between the stimulation frequency and the degree of SWA reduction, indicating frequency-dependent effects of 5-HT on cortical SWA (Figure 5.4D; ChR2-eYFP, $r = -0.6756$, $p = 0.0080$; Figure 5.5D; control, $r = -0.0444$, $p =$ 0.8969).

5.3.3 Effects of optogenetic activation of DRN 5-HT neurons on UP states *in vivo*

It is known that neurons synchronously alternate between UP and DOWN states during SWA, which correspond to brief periods of activity and silence associated with membrane depolarisation and hyperpolarisation, respectively (Mukovski et al., 2007). In a previous study, the electrical stimulation of DRN at 1 Hz promoted the initiation and increased the duration of UP states in the mPFC (Puig et al., 2010). To this end, the effects of optogenetic activation of 5-HT neurons on UP state duration in the mPFC were examined.

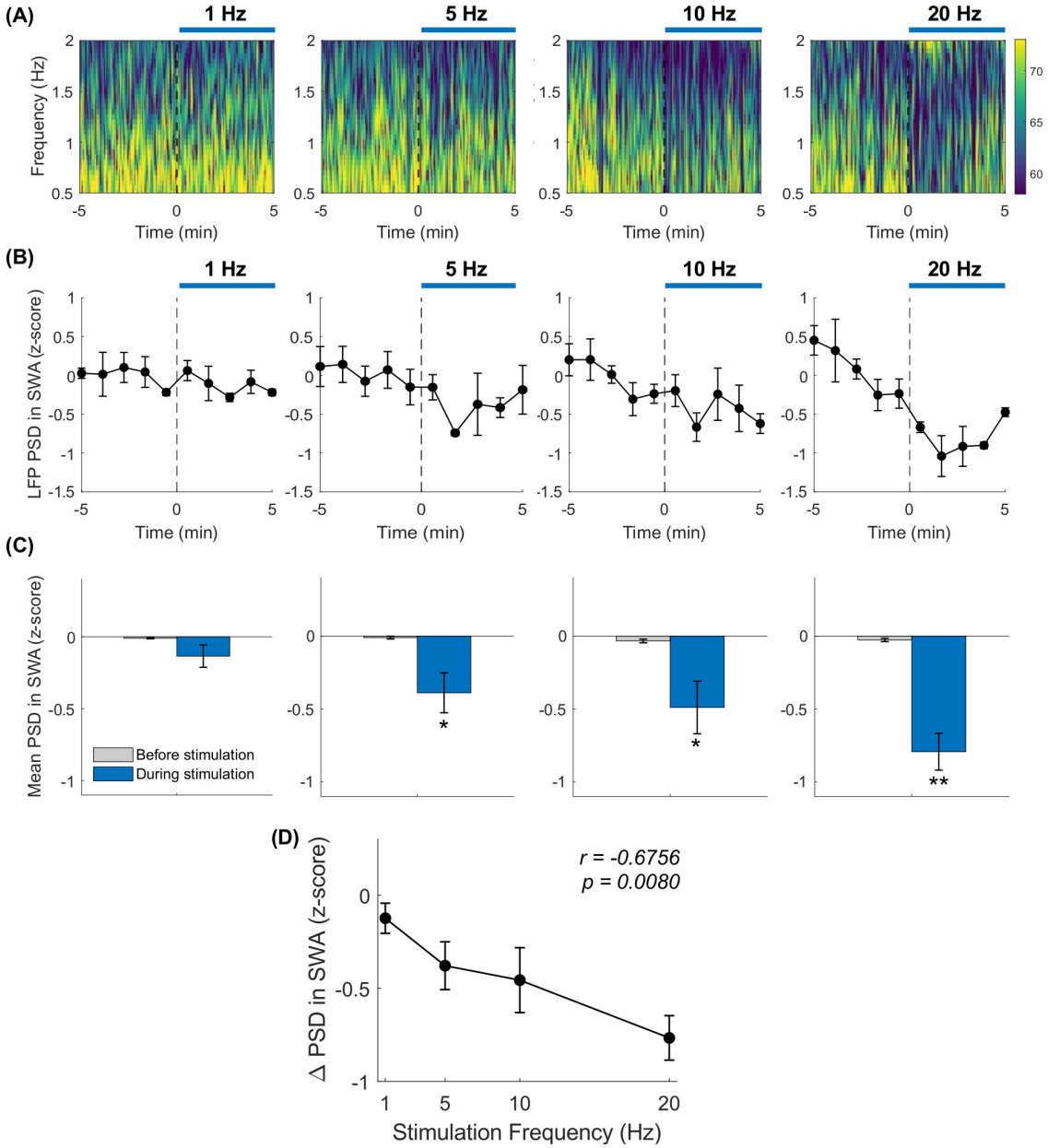

Figure 5.4: Effects of optogenetic activation of DRN 5-HT neurons on local slow wave activity (SWA, 0.1 − 2 Hz) in the mPFC of ChR2-eYFP mice (n = 7). (A) Example spectrograms of LFP power in SWA range at each light stimulation frequency, ordered from left to right: 1, 5, 10, and 20 Hz. (B) Line plots showing the change in relative power spectral density (PSD, z-scores) of LFP in SWA range over time, before and during stimulation at 1, 5, 10, and 20 Hz. (C) Bar charts showing the change in mean PSD of LFP in SWA range at each stimulation frequency. (D) Line plot showing the relationship between stimulation frequency (Hz) and the change in PSD of LFP in SWA range, with Pearson correlation coefficient and p-value. Data are represented as mean ± SEM. *p<0.05, **p<0.01.

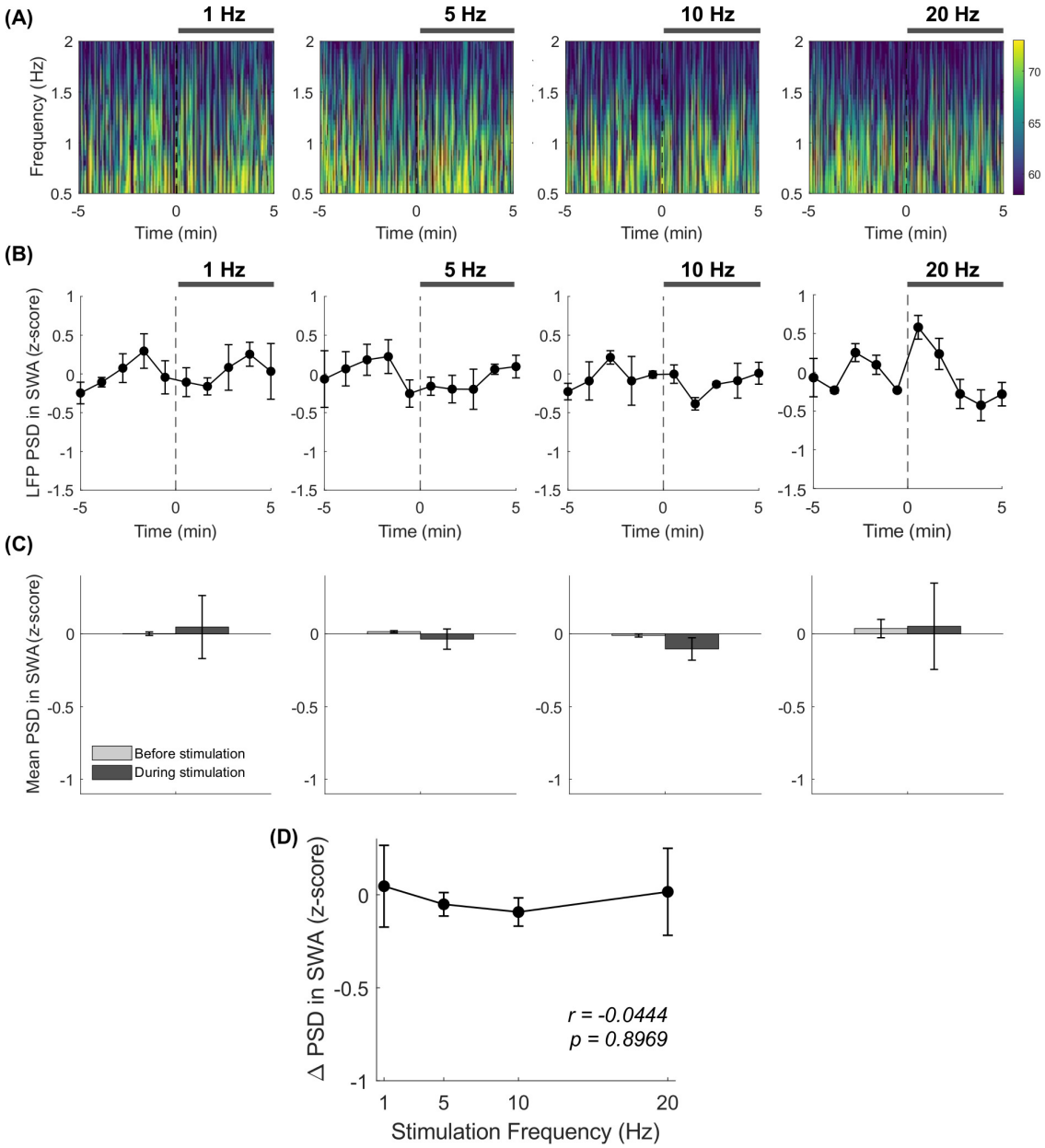

Figure 5.5: Effects of optogenetic activation of DRN 5-HT neurons on local slow wave activity (SWA, 0.1 − 2 Hz) in the mPFC of control mCherry mice (n = 3). (A) Example spectrograms of LFP power in SWA range at each light stimulation frequency, ordered from left to right: 1, 5, 10, and 20 Hz. (B) Line plots showing the change in relative power spectral density (PSD, z-scores) of LFP in SWA range over time, before and during stimulation at 1, 5, 10, and 20 Hz. (C) Bar charts showing the change in mean PSD of LFP in SWA range at each stimulation frequency. (D) Line plot showing the relationship between stimulation frequency (Hz) and the change in PSD of LFP in SWA range, with Pearson correlation coefficient and p-value. Data are represented as mean ± SEM.

To assign UP and DOWN states, a multi-step LFP signal filtering process based on that reported by Mukovski et al. (2007) was developed (see Section 5.2.8 for detail). First, the gamma component of the LFP (30 − 80 Hz) was extracted and the PSD in the gamma range was calculated. A moving standard deviation filter was then applied to obtain a final trace that resembled rectangular pulses and highlighted periods of elevated gamma power (Figure 5.6A). The histogram of this final trace was bimodal, allowing the placement of a threshold for UP-DOWN state detection in the local minimum point (Figure 5.6B). LFP signals from ChR2-eYFP mice were processed accordingly in 30 sec windows, allowing the calculation of time spent in UP state over time for each animal.

Mirroring the SWA power results, optogenetic activation of 5-HT neurons at 5, 10, and 20 Hz but not 1 Hz caused a frequency-dependent increase in time spent in UP state (Figure 5.7A; two-tailed paired t-test; 1 Hz, $t(6) = -0.9062$, $p = 0.3826$; 5 Hz, $t(6) = -2.300$, $p = 0.0402$; 10 Hz, $t(6) = -3.375$, $p = 0.0055$; 20 Hz, $t(6) = -4.609$, $p = 0.010$, $n = 7$ mice). Additionally, there was a significant positive correlation between light stimulation frequency and the magnitude of increase in UP state time, again suggesting a frequency-dependent relationship between 5-HT activation and UP state duration in mPFC neurons (Figure 5.7B; Pearson correlation coefficient, $r = 0.4311$, $p = 0.0354$).

5.3.4 Effects of optogenetic activation of DRN 5-HT neurons on multi-unit activity *in vivo*

Next, the effects of optogenetic activation of DRN 5-HT neurons on multi-unit activity, a representation of the neuronal population's aggregate firing activity, was tested. In ChR2-eYFP mice, optogenetic activation of DRN 5-HT neurons caused a significant change in mPFC multi-unit activity at 10 and 20 Hz but not lower frequencies (Figure 5.8A, B; two-tailed paired t-test; 1 Hz, $t(6) = 0.1239$, $p =$

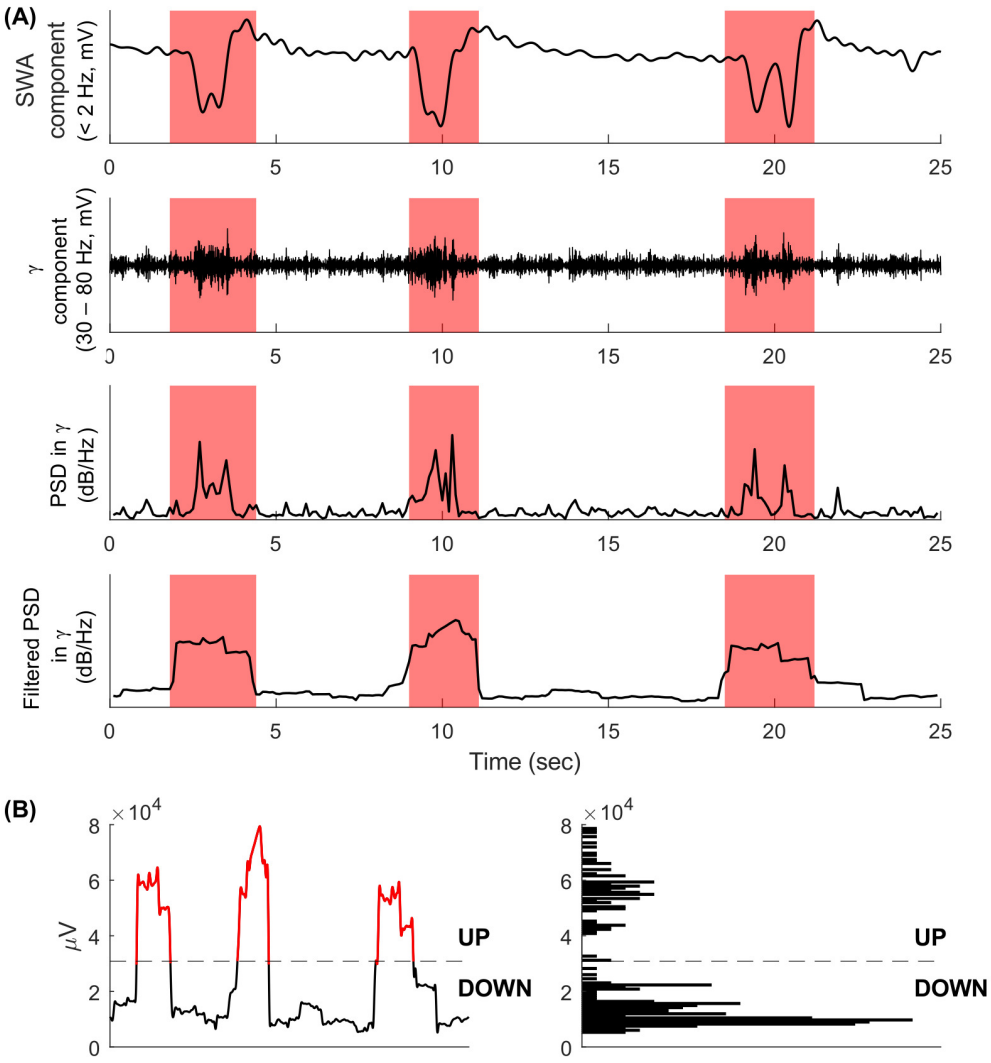

Figure 5.6: Processing steps of the LFP trace for UP and DOWN state assignment. (A) Example traces show from top to bottom: the filtered SWA component (0.1 − 2 Hz), filtered gamma component (30 − 80 Hz), power spectral density (PSD) of LFP power in gamma, and filtered PSD in gamma (using a moving standard deviation filter). Red shaded areas represent UP states. (B) Left panel shows the assignment of UP and DOWN states using the final filtered trace from (A), with UP state periods in red and DOWN state periods in black. Right panel demonstrates how the threshold was determined using the local minimum point in the histogram of values in the left panel. Black dotted line represents the threshold for UP and DOWN state assignments.

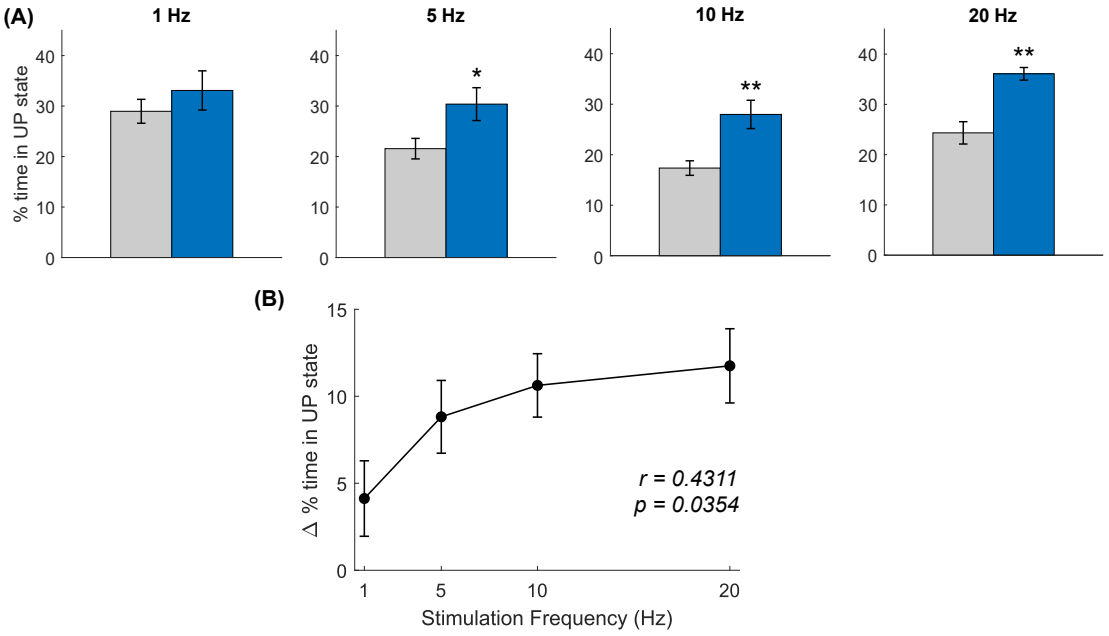

Figure 5.7: Effects of optogenetic activation of DRN 5-HT neurons on the percentage of time spent in UP state by neurons in the mPFC of ChR2-eYFP mice (n = 7). (A) Bar charts showing the change in percentage of time spent in UP state at each stimulation frequency, ordered from left to right: 1, 5, 10, and 20 Hz. (B) Line plot showing the relationship between change in percentage of time spent in UP state and light stimulation frequency (Hz) with Pearson correlation coefficient (r) and corresponding p-value. Data are represented as mean ± SEM. *p<0.05, **p<0.01.

0.9041; 5 Hz, t(6) = -0.5533, p = 0.5935; 10 Hz, t(6) = 6.893, p < 0.001; 20 Hz, t(6) = -2.617, p = 0.0279). Interestingly, 5-HT decreased the multi-unit activity at 10 Hz but increased the multi-unit activity at 20 Hz. In contrast, the multi-unit activity of control mice was unaffected by optogenetic activation of DRN 5-HT neurons, with the exception of a small decrease during 10 Hz stimulation (Figure 5.8C, D; two-tailed paired t-test; 1 Hz, t(2) = -1.883, p = 0.0923; 5 Hz, t(2) = -0.7396, p = 0.4784; 10 Hz, t(2) = 2.308, p = 0.0464; 20 Hz, t(2) = -0.0297, p = 0.9769). The effect at 10 Hz stimulation in the control dataset was small compared to that observed in ChR2-eYFP mice (15.34 ± 1.468 to 10.81 ± 2.461 for control vs. 15.24 ± 1.609 to -1.893 ± 1.250 for ChR2-eYFP). The lack of significant changes in multi-unit activity at other frequencies in the control experiments suggests that the effects caused by 10 Hz stimulation may be a false positive.

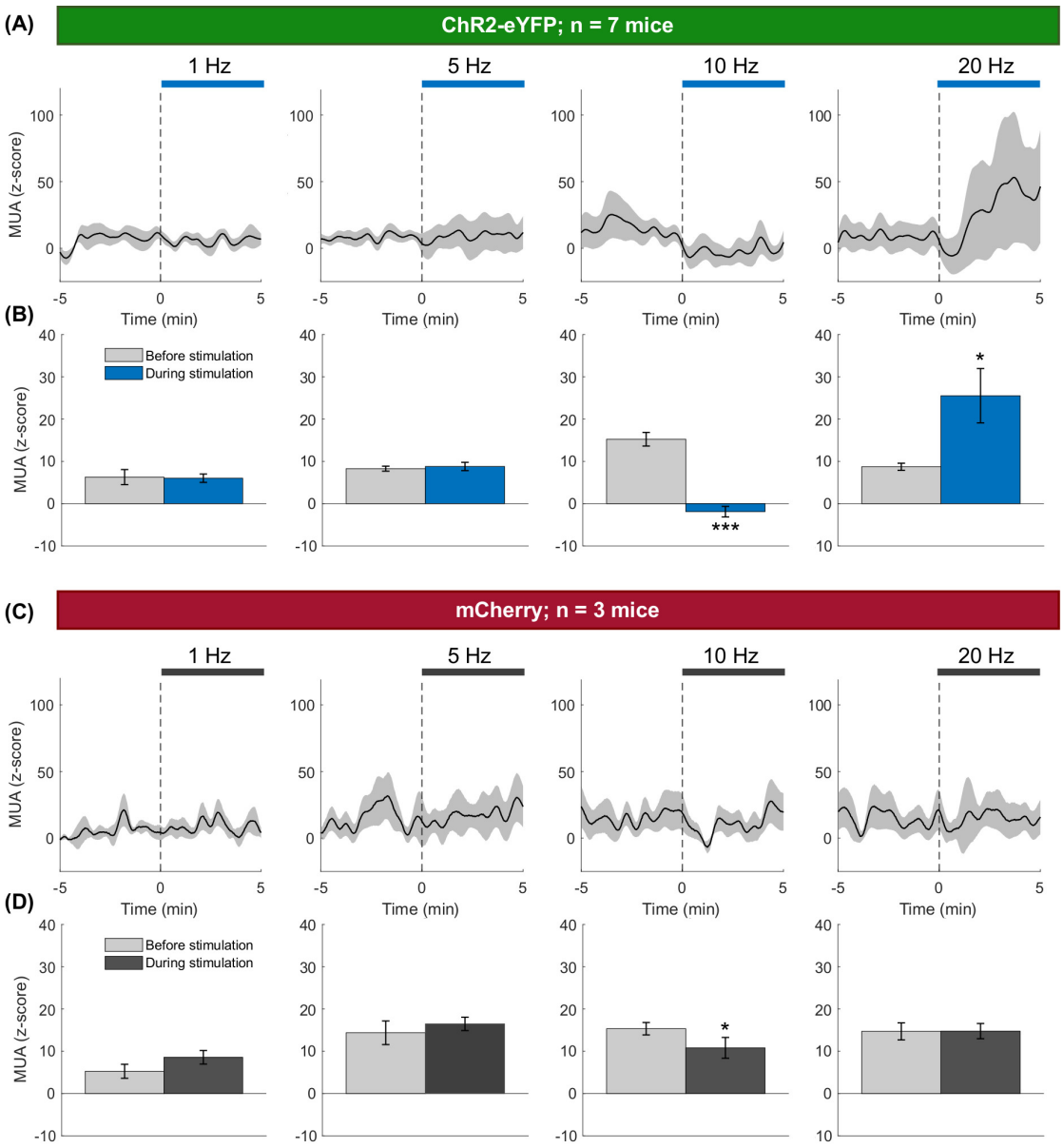

Figure 5.8: Effects of optogenetic activation of DRN 5-HT neurons on multi-unit activity (MUA) of mPFC recorded neuronal population in ChR2-eYFP mice (n = 7 mice) and control mCherry mice (n = 3 mice) at light stimulation frequencies 1, 5, 10, and 20 Hz (from left to right). Line plots showing the MUA over time for (A) ChR2-eYFP and (C) control mice. Bar plots showing the mean MUA before and during light stimulation periods for (B) ChR2-eYFP and (D) control mice. Data are represented as mean ± SEM. *p<0.05, ***p<0.001.

5.3.5 Effects of optogenetic activation of DRN 5-HT neurons on single-unit activity *in vivo*

Having established the effects of optogenetic activation of 5-HT neurons on network oscillations and aggregate multi-unit activity of the mPFC, single-unit activity in the mPFC was next examined with all recorded units in each group pooled for analysis (n = 190 from 7 ChR2-eYFP mice; n = 55 from 3 control mice). As previously described in Section 3.3.4, the relative firing rates of individual neurons over time were visualised in heat maps (z-scores; Figure 5.9A, C). Each neuron was then classified as activated, inhibited, or non-responding, using the Mann-Whitney U test ($p < 0.05$) with the Benjamini-Hochberg procedure (pFDR = 0.05) to correct for multiple comparisons.

Optogenetic activation of 5-HT neurons at all frequencies significantly altered the firing rates of a subpopulation of mPFC neurons in ChR2-eYFP mice, with some neurons activated and others inhibited (Figure 5.9A). As stimulation frequency increased, the proportion of inhibited neurons increased from 13.2% (25/190) at 1 Hz to 22.1% (42/190) at 5 and 10 Hz, and finally 24.7% (47/190) at 20 Hz (Figure 5.9B). Light stimulation also activated a small proportion of neurons (between 4.2 and 4.7%, 8 to 9/190) at all frequencies. On the other hand, light stimulation had little effect on single-unit activity of control mice (Figure 5.9D).

Using area under the operator characteristic curve (auROC) values calculated from Mann-Whitney U tests described above (see Section 3.3.4 for more detail), the magnitude of firing rate change in response to each light stimulation frequency in ChR2-eYFP and control mice was determined (Figure 5.10A, C). An auROC value close to 1 indicates a significant increase in firing rate, whereas that close to 0 indicate as significant decrease. Correlation analysis showed a significant negative relationship between stimulation frequency and the mean auROC of the mPFC neuronal population (Figure 5.10B; Pearson correlation coefficient, r = -0.1253, p =

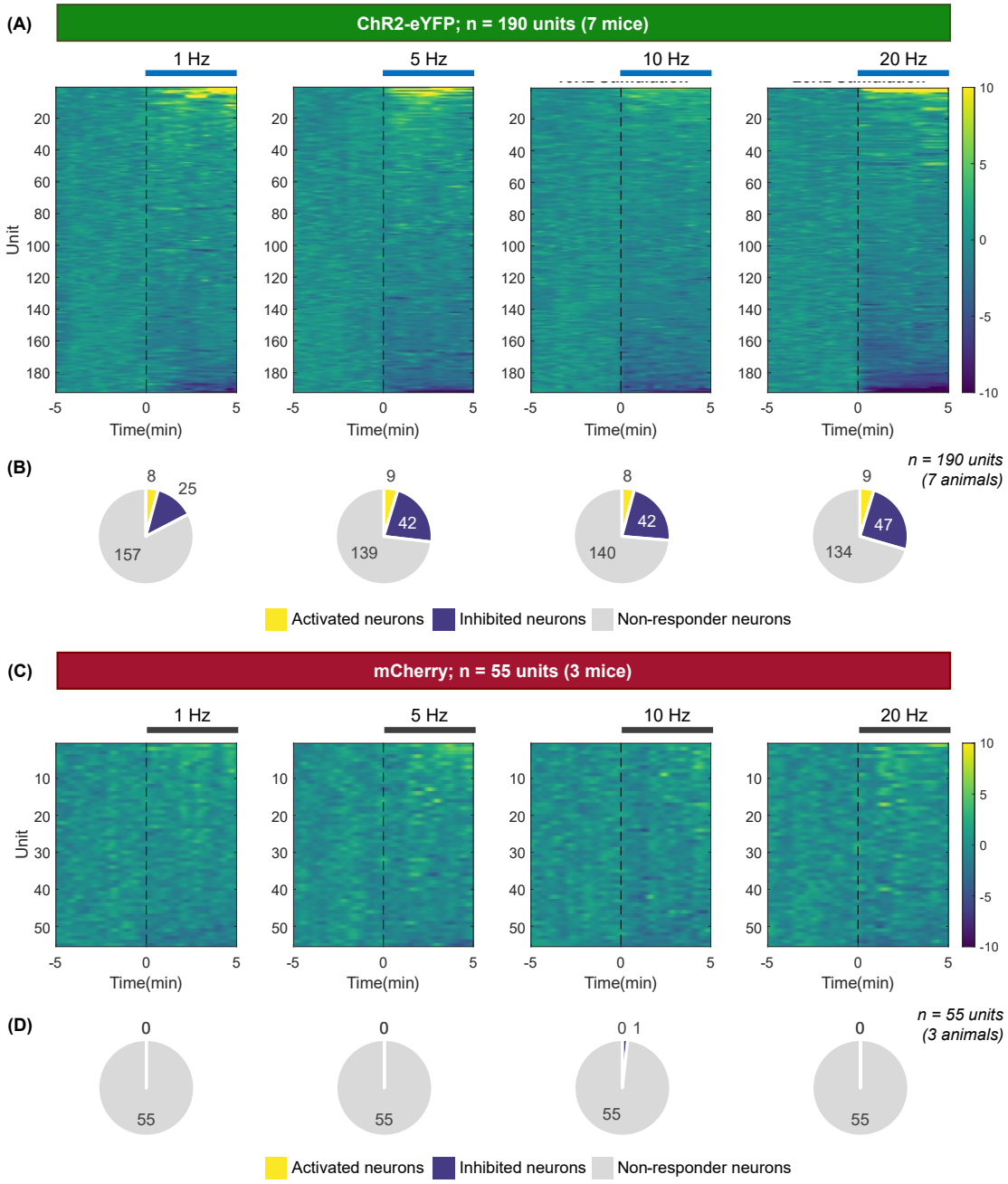

Figure 5.9: Effects of optogenetic activation of 5-HT neurons on single-unit firing rate in the mPFC. Heat maps of firing rate z-scores over time for (A) ChR2-eYFP mice (n = 190 units from 7 mice) and (C) control mCherry mice (n = 55 from 3 mice), ordered by light stimulation frequency from left to right: 1, 5, 10, and 20 Hz. Each row represents one unit, and rows were sorted in descending order according to their z-scores after drug injection. Pie charts of (B) ChR2-eYFP and (D) control experiments, showing the proportions of units that were activated (yellow) and inhibited (blue) at each light stimulation frequency. Non-responder units are in grey.

0.0005). On the other hand, there was no correlation between stimulation frequency and median auROC in control mice (Figure 5.10D; Pearson correlation coefficient, r = -0.0523, p = 0.4401).

5.3.6 Effects of optogenetic activation of DRN 5-HT neurons on putative PVINs *in vivo*

To determine the effects of optogenetic activation of DRN 5-HT neurons on the activity of PVINs specifically, waveform analysis using the baseline data was performed as detailed in Section 3.3.5 to identify putative PVINs in the dataset. Hierarchical clustering of two waveform parameters, peak-trough time (PTT) and half-hyperpolarisation width (HHW), revealed two distinct neuron clusters that resembled the putative PVINs (n = 43, 22.6%) and broad waveform neurons (n = 147, 77.4%) described in Chapter 3 (Figure 5.11A, B). The median baseline firing rate of putative PVINs was higher than that of broad waveform neurons (Figure 5.11C; 3.48 ± 0.45 Hz vs. 2.32 ± 0.18 Hz; Mann-Whitney U test, Z = 2.568, p = 0.0102), consistent with the expected characteristics of PVINs and non-PV-expressing neurons. Additionally, the peak asymmetry ratio (PAR) was evaluated to identify any putative axonal units present in the dataset (Figure 5.11D) using the same criteria as in Chapter 3 (PTT $\leq$ 200 μs and PAR $\leq$ 0.5). No putative axon units were identified and needed to be excluded.

With individual putative PVINs identified, their response to optogenetic activation of DRN 5-HT neurons was examined. Figure 5.12A shows a heat map in which each row represents a putative PVIN and their auROC values at each stimulation frequency. This demonstrates that the putative PVINs had heterogeneous responses to light stimulation. Not all putative PVINs responded at all stimulation frequencies, and in some cases, the direction of change in firing rate switched as stimulation frequency increased (Figure 5.12A).

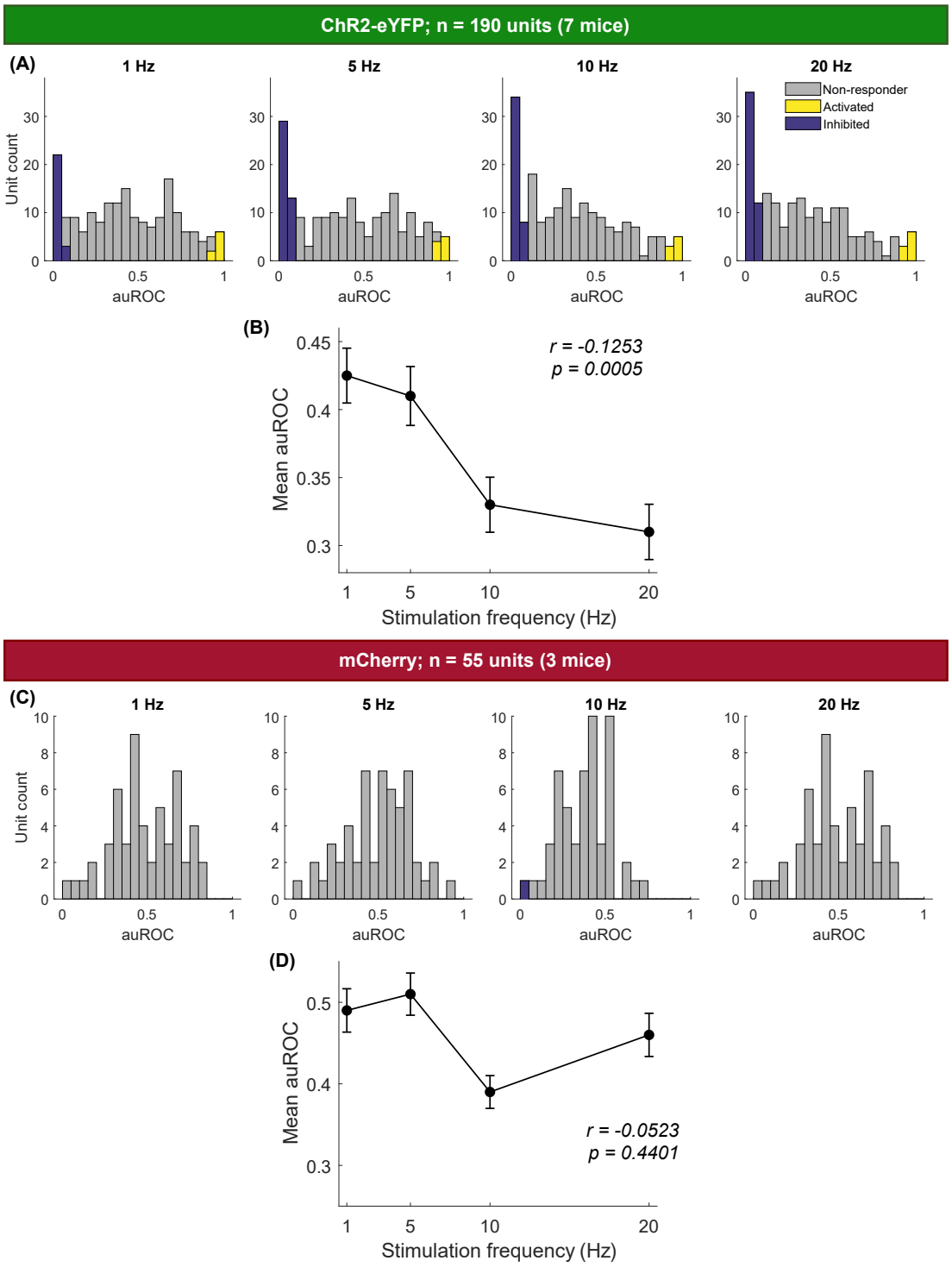

Figure 5.10: Distribution of area under the receiver operator characteristic curve (auROC) values for neurons in (A-B) ChR2-eYFP mice and (C-D) control mice at each stimulation frequency. (A, C) Histograms showing the auROC distribution of recorded neurons. Activated units are represented in yellow, inhibited units in blue, and non-responder units in grey. (B, D) Line plots showing the relationship between mean auROC and stimulation frequency (Hz), with the Pearson correlation coefficient (r) and p-value. Data are represented as mean ± SEM. *p<0.05, **p<0.01.

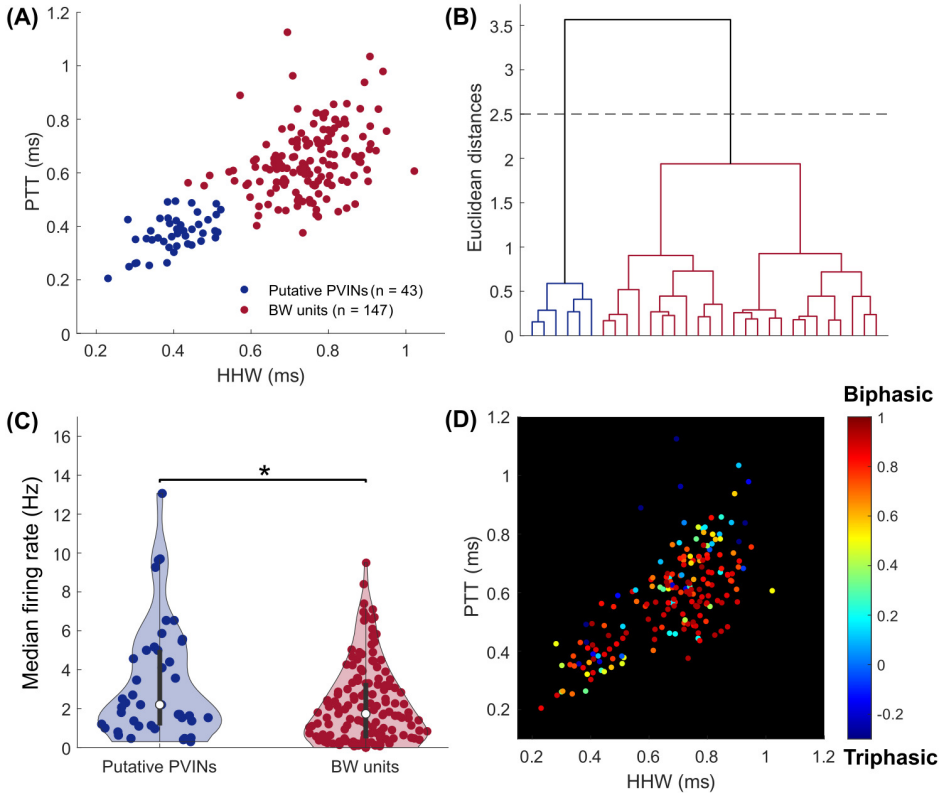

Figure 5.11: Classification of putative PVINs based on their waveform properties. (A) Scatter plot showing the distribution of peak-to-trough time (PTT) and half-hyperpolarisation width (HHW) of putative PVINs (blue; n = 43) and broad waveform (BW) neurons (red; n = 147). (B) Dendrogram showing the hierarchical clustering and classification of neurons according to their PTT and HHW. Black dotted line represents the clustering threshold used to generate the scatter plot in (A). (C) Mean baseline firing rate (Hz) of putative PVINs compared to other BW units. (D) Scatter plot identical to that shown in (A), with units additionally labelled in a colour scale demonstrating their PAR values ranging from blue for most triphasic waveforms to red for most biphasic waveforms. Data are represented as median ± SEM. *p<0.05.

The proportion of activated and inhibited putative PVINs also shifted as light stimulation frequency increased (Figure 5.12B). At 1 Hz, similar proportions of putative PVINs were activated (11.6%, 5/43) and inhibited (14.0%, 6/43). As stimulation frequency increased to 5 and 10 Hz, the proportion of activated neurons decreased (5 Hz and 10 Hz, 4.7%, 2/43) while that of inhibited neurons increased (5 Hz, 25.6%, 11/43; 10 Hz, 20.9%, 9/43). Finally, at 20 Hz stimulation, the proportion of activated neurons remained the same but inhibited neurons increased further, now representing over a third of the putative PVIN population (37.2%, 16/43).

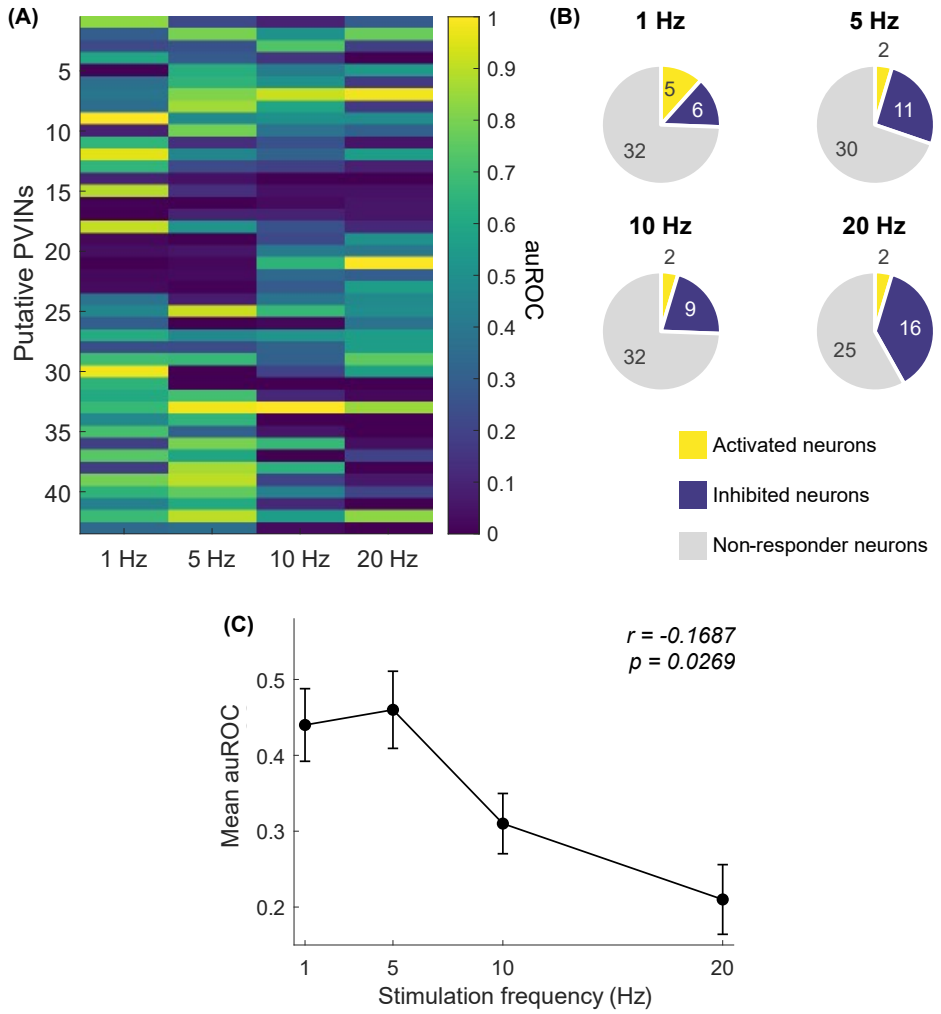

Figure 5.12: Effects of optogenetic activation of DRN 5-HT neurons on putative PVINs in the mPFC of ChR2-eYFP mice. (A) Heat map showing the auROC values of all putative PVINs across the light stimulation frequencies 1, 5, 10, and 20 Hz. Each row represents a putative PVIN. (B) Pie charts showing the proportion of activated (yellow), inhibited (blue), and non-responding (grey) putative PVINs at each stimulation frequency. (C) Line plot showing the relationship between light stimulation frequency and the median auROC of putative PVINs, with Pearson correlation coefficient (r) and p-value. Data are represented as mean ± SEM.

Results from correlation analysis showed a significant negative correlation between the mean auROC of putative PVINs and light stimulation frequencies (Figure 5.12C; Pearson correlation coefficient, r = -0.1687, p = 0.0269).

5.3.7 Peri-stimulus effects of the optogenetic activation of DRN 5-HT neurons *in vivo*

To investigate the effects of optogenetic activation of DRN 5-HT neurons on mPFC neurons at a higher temporal resolution, peri-stimulus time histograms (PSTHs) for the 1 Hz stimulation period were constructed as described in Chapter 4.

About two-thirds of mPFC neurons responded to light stimulation, but in five different ways: (i) inhibition (23%, 43/190), (ii) slow excitation (20%, 38/190), (iii) slow excitation preceded by fast inhibition (i.e. biphasic, 20%, 38/190), (iv) fast excitation (11%, 22/190), and (v) both fast and slow excitation (4%, 7/190; Figure 5.13A, B). Fast excitatory and inhibitory responses were classified on the basis of a short-latency onset of <50 ms from light stimulation, whereas slow excitatory responses were characterised by the long-latency onset of $50 - 100$ ms post-stimulation (Figure 5.13A). PSTH responses were also used to understand the effects of light stimulation on putative PVINs (Figure 5.13C). Putative PVINs responded to light stimulation in a similar fashion to other neurons, although there appeared to be an increased proportion demonstrating inhibition (37%, 24/43) and no PVINs exhibited a biphasic response.

5.3.8 Effects of optogenetic activation of DRN 5-HT neurons on correlation of neuron pairs *in vivo*

Finally, a pair-wise correlation analysis was performed as described in Section 3.3.8 to determine whether the optogenetic activation of DRN 5-HT neurons altered the synchrony of mPFC neuron spiking activity, specifically between neuron pairs involving putative PVINs. Simultaneously recorded pairs of two putative PVINs (PV-PV; n = 183) and pairs of one putative PVIN with one BW neuron (PV-BW; n = 1052) were evaluated for the strength of their spike count correlation before and during light stimulation at each frequency.

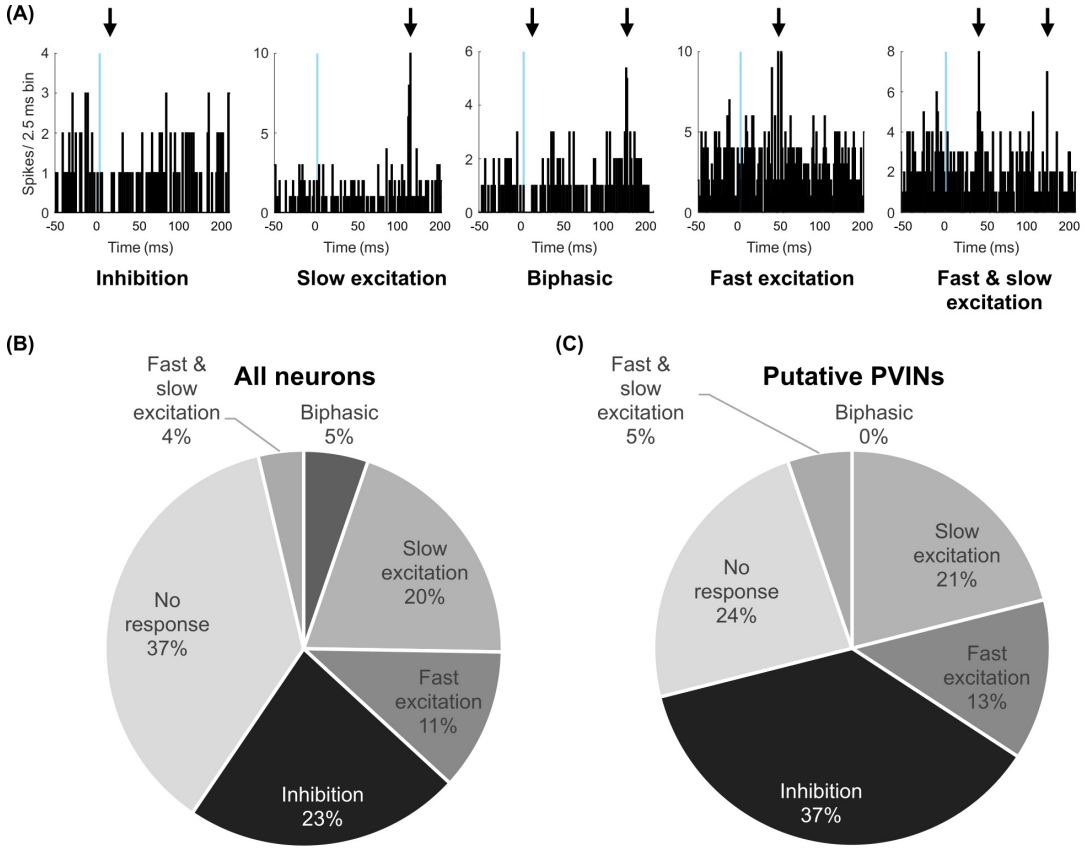

Figure 5.13: Peri-stimulus effects of optogenetic activation of DRN 5-HT neurons at 1 Hz on mPFC neurons in ChR2-eYFP mice. (A) Peri-stimulus time histograms (PSTHs) showing typical examples of the different types of responses observed. Pie charts showing the proportion of (B) all neurons and (C) putative PVINs only for each type of response.

Optogenetic activation of DRN 5-HT neurons at 1 and 5 Hz did not cause changes in the correlation strength of neuron pairs (Figure 5.14A, B; two-tailed Wilcoxon signed rank test, before vs during stimulation; 1 Hz, PV-PV, Z = 0.3591, p = 0.7195, PV-BW, Z = 1.3251, p = 0.1851; 5 Hz, PV-PV, Z = -0.0999, p = 0.9204, PV-BW, Z = -0.2961, p = 0.7671). Interestingly, when DRN 5-HT neurons were stimulated at 10 Hz, the correlation strength of all neuron pairs was significantly increased (Figure 5.14C; two-tailed Wilcoxon signed rank test; PV-PV, Z = -6.223, p $<$ 0.001; PV-BW, Z = -12.31, p $<$ 0.001). Finally, 20 Hz light stimulation decreased the correlation strength of PV-PV pairs but not that of PV-BW pairs (Figure 5.14D, two-tailed Wilcoxon signed rank test; PV-PV, Z = 2.539, p = 0.0111; PV-BW, Z = 0.0702, p = 0.9440).

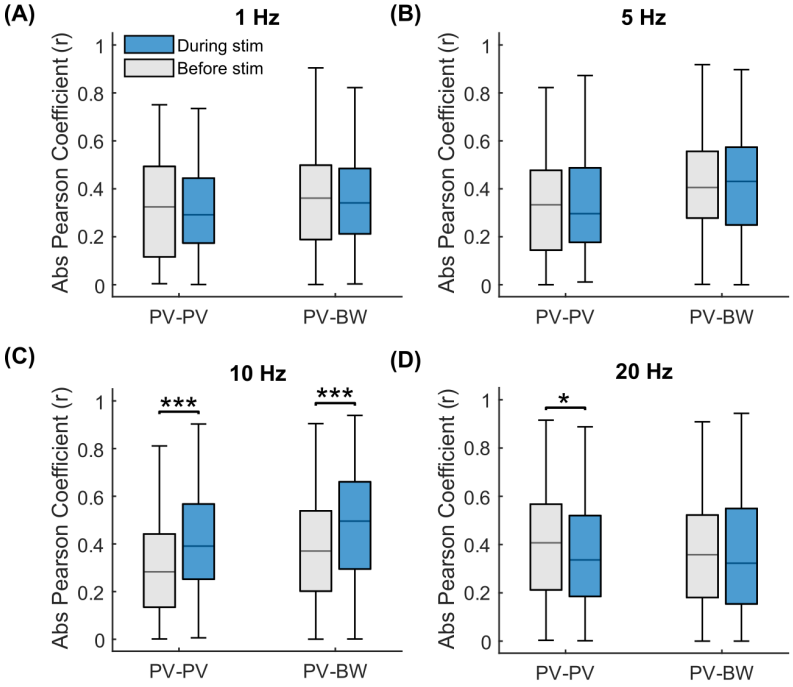

Figure 5.14: Effects of optogenetic activation of DRN 5-HT neurons on spike count correlation betweeen neuron pairs in the mPFC of ChR2-eYFP mice. PV-PV (both putative PVINs, n = 183) and PV-BW (one putative PVIN and one broad waveform unit, n = 1052) pairs were examined. Bar charts showing the correlation strength, in terms of absolute median Pearson correlation coefficient (r), before and after light stimulation at (A) 1 Hz, (B) 5 Hz, (C) 10 Hz, and (D) 20 Hz. Data are represented as median ± interquartile range. *p<0.05, ***p<0.001.

5.4 Discussion

Experiments in this chapter investigated the *in vitro* and *in vivo* effects of optogenetically evoked release of 5-HT on the activity of mPFC neurons. Using the transgenic SERT-Cre mouse line, ChR2-eYFP was selectively expressed in DRN 5-HT neurons to enable the light-driven release of 5-HT in the mPFC. Although experiments in Chapter 4 successfully optogenetically activated 5-HT neurons *in vitro*, slice recording experiments were inconclusive as light stimuli did not evoke detectable responses in any mPFC neuron tested. However, *in vivo* recordings demonstrated clear and frequency-dependent effects of optical activation of 5-HT neurons on neural activity in the mPFC, including PVINs, at multiple levels.

5.4.1 Validity of optogenetic activation of 5-HT neurons

The marked *in vivo* effects of optogenetic activation of 5-HT neurons on mPFC activity observed in the current study were most likely mediated by 5-HT, given the lack of response in control mice as well as results from Chapter 4 that verified the selective targeting of ChR2 to DRN 5-HT neurons. Although the expression of ChR2 in 5-HT neurons was not quantified in this thesis, previous work by Sengupta et al. (2017) utilising the same viral construct and transgenic mouse line showed a 100% co-localisation rate of ChR2-eYFP and 5-HT in the DRN. Importantly, experiments in Chapter 4 demonstrated light-driven action potentials by DRN ChR2-expressing 5-HT neurons *in vitro* and *in vivo*, in keeping with reports by Liu et al. (2014) and Grandjean et al. (2019) that ChR2-expressing 5-HT neurons faithfully fired action potentials with light stimuli *in vitro*. Further *in vivo* microdialysis evidence confirmed an increase in extracellular 5-HT levels in the mouse hippocampus following light stimulation of ChR2-expressing 5-HT neurons (Ohmura et al., 2014). As reviewed in Section 5.1, 5-HT-mediated postsynaptic effects following light stimulation of ChR2-expressing 5-HT terminals have also been pharmacologically verified in slices of the mouse mPFC (Athilingam et al., 2017), ventral tegmental area and nucleus accumbens (Liu et al., 2014), olfactory bulb (Kapoor et al., 2016), amygdala (Sengupta et al., 2017). Finally, the *in vivo* neurophysiological effects of optogenetically evoked 5-HT in the mPFC reported here closely replicated those reported by previous studies utilising electrical stimulation of the DRN (further discussed in the following subsections), providing added confidence that effects observed in the current study were indeed mediated by 5-HT.

5.4.2 Effects of optogenetic activation of 5-HT axons on cortical activity *in vitro*

To determine the *in vitro* effects of optogenetic activation of 5-HT terminals on mPFC neuron activity, whole-cell patch-clamp recordings were performed in mPFC slices obtained from SERT-Cre mice, in which DRN 5-HT neurons were virally transfected with ChR2-eYFP. These recordings were initially performed between 4 to 6 weeks after injection of the viral vector, as histological evidence showed abundant ChR2-eYFP expression in 5-HT cell bodies in the DRN and the presence of ChR2-eYFP-expressing 5-HT terminals in the mPFC at this time point. This timing was also consistent with previous studies by our lab that optogenetically activated ChR2-expressing 5-HT afferents in amygdala slices of SERT-Cre mice 4 weeks after viral injection (Sengupta et al., 2017). Despite extensive testing in 39 neurons from 12 mice, light pulses applied during current-clamp sessions did not evoke any responses in mPFC neurons, although the presence of ChR2-eYFP in the DRN was confirmed *post hoc*.

Experiments similar to those reported here were carried out by Athilingam et al. (2017), and optogenetically evoked 5-HT_{2A} receptor-mediated responses in putative PVINs of the mPFC were reported. It is important to note that these whole-cell patch-clamp experiments were carried out 5 to 15 months after viral injection (Athilingam et al., 2017), but the timeframe of the current project did not allow for experiments of such a long duration. It is, therefore, possible that ChR2 expression in the mPFC was insufficient to produce detectable responses in the current study. The successful optogenetic activation of 5-HT axons in the amygdala (Sengupta et al., 2017) might be due to the dense 5-HT input in the amygdala compared to the mPFC and the shorter distance for ChR2 trafficking. Whatever the explanation, it seems likely that the amount of 5-HT released from DRN afferents was insufficient to evoke a measurable response in mPFC neurons

under current conditions.

5.4.3 Effects of optogenetic activation of 5-HT neurons on cortical activity *in vivo*

Given the findings in Chapter 4 that 5-HT cell bodies could be optogenetically activated, experiments here determined the effects of optogenetic activation of DRN 5-HT neurons on mPFC activity *in vivo*. LFP recordings showed that optogenetic stimulation of DRN 5-HT neurons caused a frequency-dependent suppression of SWA in the mPFC and simultaneously increased the time spent in UP states. Importantly, this effect was observed in mice expressing ChR2-eYFP and not control mice, suggesting that these effects were specific and 5-HT-mediated. In keeping with these observations, Puig et al. (2010) previously reported that electrical stimulation of the DRN ($1 - 100$ Hz) caused a frequency-dependent suppression of SWA in the rat frontal cortex.

The effects of optogenetic activation of DRN 5-HT neurons on SWA were supported by evidence that multi-unit activity in the mPFC also changed. Moreover, at the single-unit level, optogenetic activation of 5-HT neurons evoked significant changes in the firing rates of about a third of the mPFC neurons sampled. The predominant effect was a frequency-dependent decrease in firing rate, although a small number of neurons were also activated. These results are strikingly similar to previous studies that electrically stimulated the DRN (Hajós et al., 2003; Amargós-Bosch et al., 2004; Puig et al., 2005), and in keeping with a recent fMRI study that reported a reduction in cerebral blood volume in the mouse mPFC following the optogenetic activation of 5-HT neurons in the DRN (Grandjean et al., 2019).

Peri-stimulus time histogram analysis of the ChR2-eYFP dataset showed that optogenetic activation of DRN 5-HT neurons at 1 Hz resulted in different types of responses in mPFC neurons: inhibition, slow excitation, biphasic (i.e. inhibition

followed by slow excitation), fast excitation, and both slow and fast excitations. Of these post-stimulus response types, inhibition, slow excitation, and biphasic responses have been reported in mPFC pyramidal neurons in response to electrical stimulation of the DRN at 1 Hz (Amargós-Bosch et al., 2004; Puig et al., 2005). The inhibitory responses were reported to be mediated by the 5-HT_{1A} receptor and local GABAergic interactions (Puig et al., 2005; Schweimer et al., 2022). The latency of inhibitory responses observed here (<50 ms) was consistent with previous reports of 5-HT_{1A} receptor-mediated inhibition (22 ms; Puig et al., 2010) as well as the conduction velocity of 5-HT axons to the mPFC (24 ms; Puig et al., 2010). Slow excitation responses were previously blocked by MDL-100907, indicating a 5-HT_{2A} receptor-mediated mechanism (Amargós-Bosch et al., 2004). These responses were reported to have a latency of $71 - 77$ ms (Amargós-Bosch et al., 2004; Puig et al., 2010), also consistent with the current findings (<100 ms). On the other hand, fast excitation responses have been observed in 5-HT_3R-expressing interneurons in the mPFC (Puig et al., 2004; Schweimer et al., 2022). These responses of short latency (<50 ms) could be mediated by the 5-HT_3 receptor as previously reported ($36 - 39$ ms; Puig et al., 2004; Schweimer et al., 2022) or glutamatergic receptors (10 ms; Varga et al., 2009). However, more extensive pharmacological analyses are needed to determine the receptor subtypes involved in these responses.

5.4.4 Optogenetic activation of DRN 5-HT neurons altered the activity of mPFC PVINs

Putative PVINs were then identified by their waveform characteristics, as discussed in Chapter 3, allowing the examination of their responses to optogenetically evoked 5-HT. Heterogeneous and frequency-dependent changes in firing rate were detected in putative PVINs. As the light stimulation frequency increased, the number of

inhibited neurons increased, but that of activated neurons decreased. The frequency-dependent effects of 5-HT on putative PVIN firing are of particular interest, as it has previously been shown that 5-HT afferents in the mouse amygdala co-released glutamate when optogenetically activated at 1 Hz but not 20 Hz (Sengupta et al., 2017). Informed by optotagging results in Chapter 4, a light-independent subpopulation of DRN 5-HT neurons with more irregular spike discharge patterns did not spike with light stimuli at higher frequencies. Therefore, it is likely that the inhibitory changes in putative PVIN activity observed at higher frequency stimulation were mediated by the light-dependent and regular-firing 5-HT neuron population.

While the *in vitro* results from Chapter 2 and Athilingam et al. (2017) predicted that mPFC PVINs would be activated by the optogenetically evoked release of 5-HT in a 5-HT_{2A} receptor-dependent manner, *in vivo* results here instead demonstrated primarily inhibitory effects in that 16 out of 43 putative PVINs decreased in firing rate at 20 Hz stimulation. Although a minor subpopulation of putative PVINs was activated and increased in firing rate (2/43), the *in vitro* results demonstrated an increase in firing rate in response to bath applied 5-HT in all PVINs tested. An earlier immunocytochemistry study reported that 5-HT_{2A} receptor localisation rarely overlapped with 5-HT terminal varicosities in the rat cortex (Jansson et al., 2001), suggesting that the release of endogenous 5-HT may not act directly on 5-HT_{2A} receptors under physiological conditions. Another possibility is that the inhibitory effects of 5-HT on putative PVINs were amplified by 5-HT_3R- and VIP-expressing interneurons that preferentially targeted PVINs (Schweimer et al., 2022).

Finally, peri-stimulus time histograms of putative PVINs indicated a lack of biphasic responses, in agreement with a previous *in situ* hybridisation report that they do not co-express 5-HT_{1A} and 5-HT_{2A} receptors (Puig et al., 2010). Interestingly, a recent study by the lab detected short-latency excitation PVINs evoked by electrical stimulation of the DRN that was not blocked by vortioxetine,

a selective 5-HT_3 receptor antagonist, and was putatively mediated by co-released glutamate (Schweimer et al., 2022). A subpopulation of putative PVINs here might have responded to 5-HT stimulation with glutamate-dependent fast excitatory responses, although this has not been pharmacologically confirmed.

5.4.5 Optogenetic activation of DRN 5-HT neurons disrupted excitatory/inhibitory balance in the mPFC

Lastly, correlation analysis was used to understand the effects of optogenetically evoked 5-HT on neuronal interactions and network dynamics in the mPFC. A clear finding was that the optogenetic activation of DRN 5-HT neurons significantly altered the correlation strength between simultaneously recorded neuron pairs, specifically those comprising putative PVINs. Stimulation at 10 Hz increased the correlation strength between PV-PV and PV-BW pairs, whereas 20 Hz stimulation decreased the correlation strength between PV-PV pairs.

Interestingly, 20 Hz stimulation suppressed SWA to the largest extent, accompanied by a marked increase in multi-unit activity in the mPFC. As mentioned in Chapter 3, PVINs act as key regulators of local circuits and are essential in the balance of UP/DOWN states during SWA. Fast-spiking interneurons, including juxtacellularly labelled PVINs, have been shown to be coupled to UP states in the rat PFC in two distinct manners (Puig et al., 2008). One subgroup of fast-spiking interneurons fired early during UP states, whereas another subgroup fired preferentially near the end of UP states (Puig et al., 2008). Another study reported that PV-expressing basket cells increased in firing rate earlier than PV-expressing chandelier cells during transitions from DOWN to UP states in the rat mPFC (Massi et al., 2012), possibly representing the two subpopulations of fast-spiking interneurons observed by Puig et al. (2008). Using a transgenic mouse line with GAD67 depleted from PVINs, Kuki et al. (2015) reported a reduction in UP state

duration during anaesthesia-induced slow oscillations, suggesting that PVINs are crucial in the maintenance of UP states. Cortical PVINs may also be necessary for UP-to-DOWN state transitions, as the optogenetic activation of PVINs in the mouse PFC during an ongoing UP state was sufficient to trigger the transition to a DOWN state, whereas optogenetic inhibition of PVINs had the opposite effect (Zucca et al., 2017). It is, therefore, possible that optogenetic activation of DRN 5-HT neurons at 20 Hz inhibited the firing of PVINs and disrupted the correlation between PVIN pairs, effectively prolonging the duration of UP states and desynchronising cortical neuron output, leading to a local increase in activity and suppression of SWA (Zucca et al., 2017).

5.4.6 Conclusions

Altogether, experiments in this chapter demonstrated significant effects of optogenetically evoked 5-HT on the neural activity in the mPFC *in vivo* at multiple levels, despite inconclusive *in vitro* results. Optogenetic activation of DRN 5-HT neurons suppressed SWA in the mPFC and evoked changes in population activity and the firing of individual neurons. While LFP results indicated that 5-HT modulation of the mPFC was frequency-dependent, multi-unit and single-unit data suggested that the relationship between stimulation frequency and mPFC neuronal activity was more complex. Interestingly, the effects of optogenetic activation of 5-HT neurons on putative PVINs were primarily inhibitory. Such inhibition of putative PVINs could potentially contribute to the overall activation of mPFC neural activity by physiological 5-HT via the desynchronisation of neuronal activity and disruption of the UP/DOWN state balance.

6 General Discussion

6.1 Summary of main findings

The central aim of this thesis was to characterise interactions between the 5-HT system and the neural microcircuitry of the mPFC, and particularly PVINs, using modern neuroscience techniques such as multi-unit silicon probe recording and optogenetics that are lacking in the literature. While it is well-known that 5-HT is critically involved in cognition and mood regulation, and that microcircuitry in the mPFC plays a key role, interactions between the two are poorly understood.

Interactions between bath applied 5-HT and genetically labelled PVINs in the mouse mPFC *in vitro* were characterised in Chapter 2. Bath applied 5-HT increased the excitability of PVINs primarily via the 5-HT_{2A} receptor as they were blocked by the selective 5-HT_{2A} receptor antagonist MDL-100907. However, experiments also suggested that the 5-HT_{2C} and putatively 5-HT_{1A} receptors were involved to a lesser extent, likely through an indirect mechanism.

It was subsequently determined whether these 5-HT_{2A} receptor-mediated excitatory effects on PVINs and other neurons in the mPFC could be detected *in vivo* following systemic application of the 5-HT_{2A} receptor agonists DOI and psilocin to urethane-anaesthetised mice (Chapter 3). Using multi-unit silicon probe technology and a waveform-based clustering approach supported by optotagging evidence in

the literature, putative PVINs as well as other neurons were identified from the dataset. Indeed, the 5-HT_{2A} receptor agonists DOI and psilocin evoked excitatory responses in putative PVINs that were blocked by MDL-100907, although inhibitory responses and non-responding putative PVINs were also detected, perhaps due to the involvement of other 5-HT receptor subtypes. DOI and psilocin were also shown to enhance multi-unit activity and suppress SWA in the mPFC via the 5-HT_{2A} receptor. Importantly, DOI and psilocin disrupted pair-wise spike correlations between putative PVINs and neighbouring neurons via a 5-HT_{2A} receptor-mediated mechanism, potentially desynchronising cortical activity and contributing to their actions on multi-unit and LFP levels.

With the effects of pharmacological 5-HT_{2A} receptor activation on mPFC PVINs investigated *in vitro* and *in vivo*, it was next sought to determine the effects of physiologically released 5-HT on mPFC PVINs, utilising an optogenetic approach. Experiments in Chapter 4 verified the optogenetic methodology *in vitro* and *in vivo* by demonstrating reliable light-evoked action potentials in ChR2-expressing 5-HT neurons in the DRN of SERT-Cre mice. The *in vivo* results demonstrated heterogeneity in the baseline firing properties of optotagged 5-HT neurons that went beyond the widely reported slow and regular characteristics of 5-HT neurons (Aghajanian and Vandermaelen, 1982; Vandermaelen and Aghajanian, 1983; Li et al., 2001; Allers and Sharp, 2003). Specifically, some optotagged neurons were slow and regular firing as expected, but others were slow and irregular firing as well as fast-firing. Interestingly, while all patch-clamped 5-HT neurons faithfully discharged action potentials up to 20 Hz light stimulation, *in vivo* optotagging experiments revealed a population of 5-HT neurons that could follow stimulation frequencies up to 20 Hz, whereas another population could not. The former 5-HT neurons exhibited a more regular baseline firing compared to those that showed

light-independent firing, suggesting two electrophysiologically distinct 5-HT neuron populations in the mouse DRN.

Finally, experiments in Chapter 5 determined the effects of optogenetic activation of DRN 5-HT neurons on neural activity in the mPFC, including that of putative PVINs, both *in vitro* and *in vivo*. Despite much effort, optogenetic stimulation failed to elicit changes in the activity of mPFC nuerons *in vitro*, likely due to insufficient ChR2 expression and 5-HT release in the slice. In contrast, *in vivo* experiments demonstrated marked effects of optogenetic activation of DRN 5-HT neurons on mPFC activity at multiple levels. Thus, optogenetic activation of 5-HT neurons strongly suppressed SWA and increased UP state duration in the mPFC, with the magnitude of effect scaling with light stimulation frequency. Single-unit analysis revealed clear-cut but heterogeneous effects of optogenetic activation of 5-HT neurons on the firing rate of mPFC neurons, including putative PVINs. Specifically, the effects of optogenetic activation were mainly inhibitory, although excitatory effects and non-responders were also detected. These effects of optogenetic activation of DRN 5-HT neurons in the mPFC were very similar to those previously reported following electrical stimulation of the DRN in rats (Gartside et al., 2000; Amargós-Bosch et al., 2004; Puig et al., 2005, 2010). Interestingly, the number of light-inhibited putative PVINs increased with stimulation frequency while the number of light-excited putative PVINs decreased with stimulation frequency. Also, optogenetic activation of 5-HT neurons at 20 Hz decreased the correlation between putative PVIN pairs. The latter result has similarities with the finding in Chapter 3 in that administration of DOI and psilocin also decreased the correlation between putative PVIN pairs. This reduction in synchrony between putative PVIN pairs may be a common mechanism underlying the desynchronisation of cortical neuron activity and disruption of the excitatory/inhibitory balance.

6.2 Discussion of main findings

6.2.1 Differential subpopulations of DRN 5-HT neurons

Optotagging experiments in Chapter 4 represent, to our knowledge, the first comprehensive analysis of the *in vivo* baseline firing properties of identified 5-HT neurons in the mouse DRN. Subpopulations of 5-HT neurons with different baseline firing properties as well as different response to increasing stimulation freqeuncy were detected. Many optotagged 5-HT neurons had slow regular firing characteristics, but others were slow-firing but less regular and some were fast-firing. These results are consistent with a number of previous *in vivo* juxtacellular labelling studies in rats (Allers and Sharp, 2003; Kocsis et al., 2004; Schweimer et al., 2011). Despite being widely reported as slow-firing, identified 5-HT neurons in both mouse and rat DRN are reported to engage in phasic firing at $15 - 20$ Hz under rewarding and aversive conditions (Schweimer and Ungless, 2010; Cohen et al., 2015; Li et al., 2016). Interestingly, in the current study, a subpopulation of slow and regular optotagged 5-HT neurons were able to follow stimulation frequencies up to 20 Hz, whereas less regular optotagged 5-HT neurons could not. The present data are in accord with the idea that 5-HT transmission operates on multiple timescales; while low-frequency firing 5-HT neurons may oscillate around the sleep-wake cycle and signal arousal (Jacobs and Fornal, 1999; Sakai, 2011), 5-HT neurons with the capacity to fire at higher frequencies may encode and signal emotionally salient stimuli. These distinct firing and signalling properties of 5-HT neurons potentially correspond to the light-dependent and light-independent subpopulations identified here.

Interestingly, frequency-dependence in 5-HT/glutamate co-transmission was recently reported in an optogenetic study using mouse amygdala slices (Sengupta et al., 2017). Specifically, optogenetic activation of 5-HT terminals at 1 Hz caused glutamate-mediated fast responses that diminished with increasing frequency,

whereas 5-HT-mediated responses increased linearly up to 20 Hz, indicating that 5-HT is preferentially released at higher freqeuncies (Sengupta et al., 2017). It is reasonable to propose that the release of 5-HT at higher frequencies arises from light-dependent 5-HT neurons, whereas the release of glutamate at lower frequencies arises from light-independent 5-HT neurons.

It is noteworthy that, in Chapter 4, comparison of baseline firing properties of DRN neurons in mice with a 5-HT neuron targeted genetic deletion of VGLUT3 expression found evidence that DRN neurons had decreased firing rates and increased regularity. This fits with the idea that VGLUT3-expressing DRN 5-HT neurons may be the light-independent and irregular-firing 5-HT neurons. On the other hand, the regular-firing and light-dependent 5-HT neurons may preferentially release 5-HT and could be the source of the effects on mPFC activity of high-frequency optogenetic activation of 5-HT neurons reported in Chapter 5.

6.2.2 Modulation of mPFC PVINs by optogenetically evoked 5-HT

Results from the optogenetic study in Chapter 5 showed that the main effect of optogenetic activation of 5-HT neurons at 20 Hz on the firing rates of individual mPFC neurons, including putative PVINs, was inhibitory, albeit with minor excitatory responses and non-responders also detected. The effects of optogenetic activation of 5-HT neurons on network activity in the mPFC, however, were excitatory, as demonstrated in the suppression of SWA and increased duration of UP states.

While these actions of 5-HT seemingly contradict each other, similar effects have been observed in response to electrical stimulation of the DRN (Puig et al., 2010), and a dual-action model has been proposed to explain the phenomenon (Puig and Gulledge, 2011). Specifically, *in vivo* recording studies show that LFP measurements represent the summation of post-synaptic potentials at the soma (Oren et al., 2010;

Gulyás et al., 2010) and dendrites (Monosov et al., 2008; Nielsen et al., 2006), rather than action potential generation. Puig and Gulledge (2011) suggest that 5-HT modulates cortical activity by inhibiting action potential generation via 5-HT_{1A} receptors located at axon initial segments (DeFelipe et al., 2001) and, at the same time, enhancing excitatory post-synaptic potentials via 5-HT_{2A} receptors localised on dendrites (Jansson et al., 2001; Amargós-Bosch et al., 2004). While this model is consistent with evidence that cortical pyramidal neurons co-express 5-HT_{1A} and 5-HT_{2A} receptors (Puig et al., 2010), the role of inhibitory neurons is unclear and requires consideration. Since PVINs preferentially target the soma, proximal dendrites, and axon initial segments of pyramidal neurons (Tremblay et al., 2016), they possess the ability to modulate both pyramidal neuron action potential output and local network oscillations.

The present finding that putative PVINs were inhibited by optogenetically evoked 5-HT release agrees with the reported effects of electrical stimulation of the DRN on putative PVINs (Puig et al., 2010), and were likely mediated by an action of 5-HT on 5-HT_{1A} receptor-expressing PVINs. Such inhibition of PVINs would in turn likely disinhibit pyramidal cells, contributing to the generation of post-synaptic potentials at the soma and an excitatory effect on network oscillations. This scenario is consistent with the reduction in SWA and increase in UP state duration observed in the current study, as well as previous optogenetic evidence that the selective inhibition of PVINs leads to prolonged UP states (Zucca et al., 2017). On the other hand, putative PVINs that were excited by the optogenetic activation of 5-HT neurons, although infrequently observed, likely represents 5-HT_{2A} receptor-expressing PVINs. The latter PVINs would likely inhibit pyramidal cells, perhaps contributing to the suppression of action potential generation at axon initial segments and producing the decrease in individual mPFC neuron firing rates observed here.

PVINs act as key regulators of excitatory/inhibitory balance in the cortex and are important for PFC-dependent behaviours, especially behavioural flexibility in emotionally salient environments (Ferguson and Gao, 2018). For instance, optogenetic activation of PVINs in the mouse prelimbic cortex was shown to enhance reward-related behavioural flexibility (Sparta et al., 2014). Moreover, RNA interference-based downregulation of PVINs in the rat PFC showed that a 25% decrease in PV during adolescence was sufficient to disrupt cortical excitatory/inhibitory balance and reduce extinction learning in fear conditioning tasks (Caballero et al., 2021). Fear extinction was also shown to be impaired in transgenic mice with a selective knockdown of GAD67 expression in PVINs (Brown et al., 2015). Altogether, evidence in the literature suggests that high PVIN activity in the mPFC correlates with accelerated extinction of behaviour associated with rewards, whereas low PVIN activity in the mPFC impairs extinction learning in fear-associated contexts. This is important to the current study, as it was demonstrated that the optogenetic activation of 5-HT neurons at frequencies physiologically relevant during rewarding and aversive conditions ($10 - 20$ Hz; Schweimer and Ungless, 2010; Cohen et al., 2015) inhibited the activity of a putative PVIN subpopulation and significantly altered mPFC neurophysiology.

5-HT availability in the brain has long been implicated in emotional learning mechanisms such as fear conditioning and extinction. For instance, 5-HTT-KO mice have been shown to exhibit impaired fear extinction retrieval (Wellman et al., 2007) and increased acquisition of fearful memories (Lima et al., 2019). Moreover, a recent optogenetic study demonstrated that selective activation of DRN 5-HT projections to the basal amygdala impaired fear extinction in mice (Sengupta and Holmes, 2019). This idea that elevated 5-HT neurotransmission results in impaired fear extinction is in agreement with (i) the inhibition of putative PVIN activity in the mPFC by high-frequency optogenetic activation of DRN 5-HT neurons as reported

here, and that (ii) inhibited PVIN activity is associated with deficits in extinction learning (Caballero et al., 2021; Brown et al., 2015). It is, therefore, plausible that a functional relationship exists between the high-frequency recruitment of DRN 5-HT neurons and the inhibition of PVINs in the mPFC during emotionally-driven events such as fear.

6.2.3 Modulation of mPFC PVINs by 5-HT_{2A} receptor agonists

Pharmacological experiments in Chapter 3 showed that systemic administration of the 5-HT_{2A} receptor agonists, DOI and psilocin, increased the firing of a subpopulation of mPFC neurons, including putative PVINs. Notably, correlated activity between putative PVINs and other neurons was also disrupted via a 5-HT_{2A} receptor-mediated mechanism, and it was proposed that the resulting desynchronisation of neuronal output ultimately led to the suppression of low-frequency oscillations in the mPFC. These findings are in agreement with reports that asynchrony in cortical neuron firing potentially underlies the psychotropic action of these 5-HT_{2A} receptor agonists (Muthukumaraswamy et al., 2013). Specifically, results presented in Chapter 3 suggest that the disruption of PVIN interaction with neighbouring neurons may act as the neural substrate for such desynchronisation of cortical activity.

In a recent review by Smausz et al. (2022), it was hypothesised that 5-HT_{2A} receptor agonists might exert opposite effects on neuronal firing in the mPFC compared to physiologically released 5-HT. Indeed, this thesis demonstrated that 5-HT_{2A} receptor agonists greatly increased the firing rate of a subpopulation of mPFC neurons (Chapter 3), whereas optogenetically evoked release of 5-HT primarily inhibited mPFC neuron firing (Chapter 5). These differences could be explained by DOI and psilocin's selectivity for 5-HT_{2A} receptors over 5-HT_{1A} receptors, in contrast

to 5-HT that instead binds 5-HT_{1A} receptors at a higher affinity (see summary of K_i values in Table 1.2). Additionally, the localisation of 5-HT_{1A} receptors on axon initial segments (DeFelipe et al., 2001) allows for more potent inhibition of action potential generation by physiologically released 5-HT. Finally, immunocytochemistry reports of little overlap between the localisation of rat cortical 5-HT_{2A} receptors and 5-HT varicosities (Jansson et al., 2001) suggest that systemically administered 5-HT_{2A} receptor agonists are more likely to bind and act at 5-HT_{2A} receptors on mPFC neurons compared to physiologically released 5-HT, which may need to diffuse over a distance to interact with 5-HT_{2A} receptors.

Importantly, psilocin was chosen for pharmacological experiments in this thesis in part because of the therapeutic potential of its prodrug, psilocybin, in psychiatric disorders (Nutt et al., 2020; Vollenweider and Preller, 2020). Psilocybin has also been shown to facilitate fear extinction in rodents alongside its antidepressant effects (Catlow et al., 2013; Du et al., 2023). There is a possibility that this is mediated by an action on PVINs in the mPFC, which would be consistent with both observations in Chapter 3 that psilocin activated a putative PVIN subpopulation via the 5-HT_{2A} receptor, and reports that elevated PVIN activity in the mPFC is associated with enhanced behavioural flexibility (Sparta et al., 2014).

The importance of PVINs has been highlighted in the antidepressant actions of ketamine, an NMDA receptor antagonist commonly used as an anaesthetic agent. Much like psilocybin, a single subanaesthetic dose of ketamine has been shown to produce rapid and sustained antidepressant actions in clinical trials (Berman et al., 2000; aan het Rot et al., 2010; Murrough et al., 2013). Interestingly, subanaesthetic doses of ketamine with antidepressant actions were shown to selectively activate PVINs in the mouse PFC (Ng et al., 2018). *In vivo* electrophysiology and imaging experiments showed that ketamine enhanced the activity of mouse cortical PVINs under stress, and rescued the stress-induced loss of PV axonal boutons (Ng et al.,

2018). In addition, the antidepressant actions of ketamine were abolished in a genetic mouse model with selective knockdown of GluN2B, an NMDA receptor subunit, in PVINs but not pyramidal neurons of the mPFC (Gerhard et al., 2020).

Given the crucial role of PVINs in ketamine's antidepressant actions, they might also act as key mediators in the antidepressant effects of psilocybin. Indeed, as shown in Chapter 3, psilocin altered the activity of putative PVINs in the mPFC and disrupted their spiking dynamic with neighbouring neurons. Moreover, it is possible that after the delayed onset of SSRI action, due to desensitisation of 5-HT_{1A} autoreceptors (Gray et al., 2013), the resultant elevation in extracellular 5-HT in the mPFC could modulate PVIN activity and contribute to the antidepressant effects of SSRIs.

6.3 Future directions

One of the main assumptions in the current study is that the waveform-based classification of putative PVINs in multi-unit recordings is highly reliable (Section 3.3.5 and 5.3.6). An essential next step would be to perform optotagging experiments in PV-Cre mice to test the baseline firing properties and waveform characteristics of optotagged PVINs and verify the current classification method, as previously achieved by Kvitsiani et al. (2013), Cardin et al. (2009), Royer et al. (2012) and Senzai et al. (2019).

Building on the hypothesis that light-dependent, slow and regular firing 5-HT neurons mediate the effects of optogenetically evoked 5-HT release on mPFC PVINs, this could be tested in a further optotagging study that utilises retrograde rather anterograde viral vectors to specifically target ChR2 to 5-HT neurons that project to the mPFC. These experiments would shed light on the firing properties and identity of 5-HT neurons in the DRN that project to the mPFC. In spite of clear

evidence that the effects of optogenetic activation of 5-HT neurons on mPFC activity reported in Chapter 5 were mediated by a local release of 5-HT, it is possible that indirect effects via subcortical circuits, such as the thalamus, were involved. To better understand the direct effects of optogenetically evoked 5-HT release on mPFC activity, experiments could directly activate 5-HT terminals in the mPFC instead of 5-HT cell bodies in the DRN. Pilot experiments of this nature have been conducted, although the data analysis has yet to be completed.

While experiments in this thesis explored the interactions between 5-HT and mPFC neurons in the slice and in anaesthetised mice, 5-HT interactions with the mPFC under non-anaesthetised conditions are not well-characterised. Although the anaesthetised mouse provides a useful model and features cortical slow oscillations that are prominent during sleep, it is not equivalent to natural sleep. Studying the effects of optogenetically evoked 5-HT release on mPFC neurons in non-anaesthetised conditions would serve as a key next step in understanding 5-HT modulation of mPFC neural activity under natural sleep and wake conditions. Finally, given the crucial role of PVINs in high-level cognitive tasks such as behavioural flexibility and extinction learning, further work should be conducted to investigate the functional relationship between the 5-HT system and mPFC PVINs in awake mice during behaviour. In particular, the role of 5-HT modulation of mPFC PVINs in the context of fear and aversion could be studied by optogenetically activating the DRN-mPFC 5-HT pathway during fear conditioning and extinction learning, much like the aforementioned study by Sengupta and Holmes (2019).

6.4 Conclusions

In summary, this thesis used multi-unit silicon probe recording technology combined with optogenetic tools to investigate interactions between 5-HT and the mPFC.

Data presented here highlight PVINs in the mPFC as a key part of the cortical microcircuitry that is targeted by the ascending 5-HT system. Initial experiments found that bath applied 5-HT evoked powerful and 5-HT_{2A} receptor-mediated excitatory effects on mPFC PVINs *in vitro*. As a follow up, subsequent experiments showed that both systemic administration of 5-HT_{2A} receptor agonists and optogenetically evoked release of 5-HT had marked effects on the neurophysiology of mPFC neurons, including putative PVINs. Effects were detected at multiple levels ranging from changes in the firing rate of individual neurons and spiking correlations between neuron pairs to altered aggregate network activity and local oscillations. As part of these experiments, optotagging of DRN 5-HT neurons revealed an interesting subpopulation of 5-HT neurons that are slow and regular firing but able to follow stimulation frequencies in the physiological range likely to impact mPFC microcircuits. Finally, findings of the present study support the concept that 5-HT-mediated desynchronisation of putative PVIN spiking with neighbouring neurons may serve as a key underlying mechanism for 5-HT's actions on the excitatory/inhibitory balance and local oscillations in the mPFC.

Bibliography

M. aan het Rot, K. A. Collins, J. W. Murrough, A. M. Perez, D. L. Reich, D. S. Charney, and S. J. Mathew. Safety and efficacy of repeated-dose intravenous ketamine for treatment-resistant depression. *Biological Psychiatry*, 67:139–145, 1 2010. ISSN 00063223. doi: 10.1016/j.biopsych.2009.08.038.

G. Aghajanian. Electrophysiology of serotonin receptor subtypes and signal transduction pathways. *Psychopharmacology: The Fourth Generation of Progress.*, pages 1451–1459, 1995.

G. K. Aghajanian and G. J. Marek. Serotonin, via 5-ht receptors, increases epscs in layer v pyramidal cells 2a of prefrontal cortex by an asynchronous mode of glutamate release. *Brain Research*, 825:161–171, 1999.

G. K. Aghajanian and C. P. Vandermaelen. Intracellular identification of central noradrenergic and serotonergic neurons by a new double labeling procedure. *The Journal of Neuroscience*, 2: 1786–1792, 1982.

K. A. Allers and T. Sharp. Neurochemical and anatomical identification of fast- and slow-firing neurones in the rat dorsal raphe nucleus using juxtacellular labelling methods in vivo. *Neuroscience*, 122:193–204, 11 2003. ISSN 03064522. doi: 10.1016/S0306-4522(03)00518-9.

M. Amargós-Bosch, A. Bortolozzi, M. V. Puig, J. Serrats, A. Adell, P. Celada, M. Toth, G. Mengod, and F. Artigas. Co-expression and in vivo interaction of serotonin1a and serotonin2a receptors in pyramidal neurons of pre-frontal cortex. *Cerebral Cortex*, 14:281–299, 3 2004. ISSN 10473211. doi: 10.1093/cercor/bhg128.

B. Amilhon, Ève Lepicard, T. Renoir, R. Mongeau, D. Popa, O. Poirel, S. Miot, C. Gras, A. M. Gardier, J. Gallego, M. Hamon, L. Lanfumey, B. Gasnier, B. Giros, and S. E. Mestikawy. Vglut3 (vesicular glutamate transporter type 3) contribution to the regulation of serotonergic transmission and anxiety. *Journal of Neuroscience*, 30:2198–2210, 2 2010. ISSN 02706474. doi: 10.1523/JNEUROSCI.5196-09.2010.

P. G. Anastasiades and A. G. Carter. Circuit organization of the rodent medial prefrontal cortex. *Trends in Neurosciences*, 44:550–563, 7 2021. ISSN 1878108X. doi: 10.1016/j.tins.2021.03.006.

R. Andrade. Serotonergic regulation of neuronal excitability in the prefrontal cortex. *Neuropharmacology*, 61:382–386, 9 2011. ISSN 00283908. doi: 10.1016/j.neuropharm.2011.01.015.

I. Antoniadou, M. Kouskou, T. Arsiwala, N. Singh, S. R. Vasudevan, T. Fowler, E. Cadirci, G. C. Churchill, and T. Sharp. Ebselen has lithium-like effects on central 5-ht 2a receptor function. *British Journal of Pharmacology*, 175:2599–2610, 7 2018. ISSN 14765381. doi: 10.1111/bph.14179.

P. Antonoudiou, Y. L. Tan, G. Kontou, A. L. Upton, and E. O. Mann. Parvalbumin and somatostatin interneurons contribute to the generation of hippocampal gamma oscillations. *Journal of Neuroscience*, 40:7668–7687, 9 2020. ISSN 15292401. doi: 10.1523/JNEUROSCI.0261-20.2020.

R. Araneda and R. Andrade. 5-hydroxytryptamine2 and 5-hydroxytryptaminela receptors mediate opposing responses on membrane excitability in rat association cortex. *Neuroscience*, 40:399–412, 1991.

B. V. Atallah, W. Bruns, M. Carandini, and M. Scanziani. Parvalbumin-expressing interneurons linearly transform cortical responses to visual stimuli. *Neuron*, 73:159–170, 1 2012. ISSN 08966273. doi: 10.1016/j.neuron.2011.12.013.

J. C. Athilingam, R. Ben-Shalom, C. M. Keeshen, V. S. Sohal, and K. J. Bender. Serotonin enhances excitability and gamma frequency temporal integration in mouse prefrontal fast-spiking interneurons. *eLife*, 6, 2017. doi: doi.org/10.7554/eLife.31991.001.

M. Avermann, C. Tomm, C. Mateo, W. Gerstner, and C. C. H. Petersen. Microcircuits of excitatory and inhibitory neurons in layer 2/3 of mouse barrel cortex. *J Neurophysiol*, 107: 3116–3134, 2012. doi: 10.1152/jn.00917.2011.-Synaptic.

D. Avesar and A. T. Gulledge. Selective serotonergic excitation of callosal projection neurons. *Frontiers in Neural Circuits*, 2 2012. ISSN 16625110. doi: 10.3389/fncir.2012.00012.

A. Baker, B. Kalmbach, M. Morishima, J. Kim, A. Juavinett, N. Li, and N. Dembrow. Specialized subpopulations of deep-layer pyramidal neurons in the neocortex: Bridging cellular properties to functional consequences. *Journal of Neuroscience*, 38:5441–5455, 6 2018. ISSN 15292401. doi: 10.1523/JNEUROSCI.0150-18.2018.

S. J. Bang and K. G. Commons. Forebrain gabaergic projections from the dorsal raphe nucleus identified by using gad67-gfp knock-in mice. *Journal of Comparative Neurology*, 520:4157–4167, 12 2012. ISSN 00219967. doi: 10.1002/cne.23146.

N. M. Barnes and T. Sharp. A review of central 5-ht receptors and their function. *Neuropharmacology*, 38:1083–1152, 1999.

J. M. Barry. Axonal activity in vivo: Technical considerations and implications for the exploration of neural circuits in freely moving animals, 2015. ISSN 1662453X.

P. Barthó, H. Hirase, L. Monconduit, M. Zugaro, K. D. Harris, and G. Buzsáki. Characterization of neocortical principal cells and interneurons by network interactions and extracellular features. *Journal of Neurophysiology*, 92:600–608, 7 2004. ISSN 00223077. doi: 10.1152/jn.01170.2003.

M. Bartos, I. Vida, M. Frotscher, J. Rg, R. P. Geiger, and P. Jonas. Rapid signaling at inhibitory synapses in a dentate gyrus interneuron network. *The Journal of Neuroscience*, 21:2687–2698, 2001.

S. G. Beck, Y. Z. Pan, A. C. Akanwa, and L. G. Kirby. Median and dorsal raphe neurons are not electrophysiologically identical. *Journal of Neurophysiology*, 91:994–1005, 2 2004. ISSN 00223077. doi: 10.1152/jn.00744.2003.

R. M. Berman, A. Cappiello, A. Anand, D. A. Oren, G. R. Heninger, D. S. Charney, and J. H. Krystal. Brief reports antidepressant effects of ketamine in depressed patients. *Biol Psychiatry*, 47:351–354, 2000.

M. Blatow, A. Rozov, I. Katona, S. G. Hormuzdi, A. H. Meyer, M. A. Whittington, A. Caputi, and H. Monyer. A novel network of multipolar bursting interneurons generates theta frequency oscillations in neocortex. *Neuron*, 38:805–817, 2003.

L. Blazquez-Llorca, A. Woodruff, M. Inan, S. A. Anderson, R. Yuste, J. DeFelipe, and A. Merchan-Perez. Spatial distribution of neurons innervated by chandelier cells. *Brain Structure and Function*, 220:2817–2834, 9 2015. ISSN 18632661. doi: 10.1007/s00429-014-0828-3.

M. Bocchio, G. Fucsina, L. Oikonomidis, S. B. McHugh, D. M. Bannerman, T. Sharp, and M. Capogna. Increased serotonin transporter expression reduces fear and recruitment of parvalbumin interneurons of the amygdala. *Neuropsychopharmacology*, 40:3015–3026, 12 2015. ISSN 1740634X. doi: 10.1038/npp.2015.157.

S. A. Booker, J. Song, and I. Vida. Whole-cell patch-clamp recordings from morphologically- and neurochemically-identified hippocampal interneurons. *Journal of visualized experiments : JoVE*, page e51706, 2014. ISSN 1940087X. doi: 10.3791/51706.

L. J. Boothman, K. A. Allers, K. Rasmussen, and T. Sharp. Evidence that central 5-ht 2a and 5-ht 2b/c receptors regulate 5-ht cell firing in the dorsal raphe nucleus of the anaesthetised rat. *British Journal of Pharmacology*, 139:998–1004, 7 2003. ISSN 00071188. doi: 10.1038/sj.bjp.0705328.

J. A. Brown, T. S. Ramikie, M. J. Schmidt, R. Báldi, K. Garbett, M. G. Everheart, L. E. Warren, L. Gellért, S. Horváth, S. Patel, and K. Mirnics. Inhibition of parvalbumin-expressing interneurons results in complex behavioral changes. *Molecular Psychiatry*, 20:1499–1507, 12 2015. ISSN 14765578. doi: 10.1038/mp.2014.192.

G. Buzsáki and A. Draguhn. Neuronal oscillations in cortical networks. *Science*, 306:1926–1929, 2004.

G. Buzsáki, E. Stark, A. Berényi, D. Khodagholy, D. R. Kipke, E. Yoon, and K. D. Wise. Tools for probing local circuits: High-density silicon probes combined with optogenetics, 4 2015. ISSN 10974199.

G. Buzśaki and X. J. Wang. Mechanisms of gamma oscillations. *Annual Review of Neuroscience*, 35:203–225, 7 2012. ISSN 0147006X. doi: 10.1146/annurev-neuro-062111-150444.

J. C. Béïque, B. Campbell, P. Perring, M. W. Hamblin, P. Walker, L. Mladenovic, and R. Andrade. Serotonergic regulation of membrane potential in developing rat prefrontal cortex: Coordinated expression of 5-hydroxytryptamine (5-ht)1a, 5-ht2a, and 5-ht7 receptors. *Journal of Neuroscience*, 24:4807–4817, 5 2004. ISSN 02706474. doi: 10.1523/JNEUROSCI.5113-03.2004.

A. Caballero, A. Orozco, and K. Y. Tseng. Developmental regulation of excitatory-inhibitory synaptic balance in the prefrontal cortex during adolescence. *Seminars in Cell and Developmental Biology*, 118:60–63, 10 2021. ISSN 10963634. doi: 10.1016/j.semcdb.2021.02.008.

X. Cai, Z. Gu, P. Zhong, Y. Ren, and Z. Yan. Serotonin 5-ht1a receptors regulate ampa receptor channels through inhibiting ca2+/calmodulin-dependent kinase ii in prefrontal cortical pyramidal neurons. *Journal of Biological Chemistry*, 277:36553–36562, 9 2002. ISSN 00219258. doi: 10.1074/jbc.M203752200.

A. E. Calder and G. Hasler. Towards an understanding of psychedelic-induced neuroplasticity. *Neuropsychopharmacology*, 48:104–112, 1 2023. ISSN 1740634X. doi: 10.1038/s41386-022-01389-z.

L. H. Calizo, A. Akanwa, X. Ma, Y. Z. Pan, J. C. Lemos, C. Craige, L. A. Heemstra, and S. G. Beck. Raphe serotonin neurons are not homogenous: Electrophysiological, morphological and neurochemical evidence. *Neuropharmacology*, 61:524–543, 9 2011. ISSN 00283908. doi: 10.1016/j.neuropharm.2011.04.008.

C. E. Canal, R. G. Booth, and D. Morgan. Support for 5-ht2c receptor functional selectivity in vivo utilizing structurally diverse, selective 5-ht2c receptor ligands and the 2,5-dimethoxy-4-iodoamphetamine elicited head-twitch response model. *Neuropharmacology*, 70:112–121, 7 2013. ISSN 00283908. doi: 10.1016/j.neuropharm.2013.01.007.

J. A. Cardin. Inhibitory interneurons regulate temporal precision and correlations in cortical circuits. *Trends in Neurosciences*, 41:689–700, 10 2018. ISSN 1878108X. doi: 10.1016/j.tins.2018.07.015.

J. A. Cardin, M. Carlén, K. Meletis, U. Knoblich, F. Zhang, K. Deisseroth, L. H. Tsai, and C. I. Moore. Driving fast-spiking cells induces gamma rhythm and controls sensory responses. *Nature*, 459:663–667, 6 2009. ISSN 00280836. doi: 10.1038/nature08002.

B. J. Catlow, S. Song, D. A. Paredes, C. L. Kirstein, and J. Sanchez-Ramos. Effects of psilocybin on hippocampal neurogenesis and extinction of trace fear conditioning. *Experimental Brain Research*, 228:481–491, 8 2013. ISSN 14321106. doi: 10.1007/s00221-013-3579-0.

P. Celada, M. V. Puig, L. Díaz-Mataix, and F. Artigas. The hallucinogen doi reduces low-frequency oscillations in rat prefrontal cortex: Reversal by antipsychotic drugs. *Biological Psychiatry*, 64:392–400, 9 2008. ISSN 00063223. doi: 10.1016/j.biopsych.2008.03.013.

P. Celada, M. V. Puig, and F. Artigas. Serotonin modulation of cortical neurons and networks. *Frontiers in Integrative Neuroscience*, 4 2013. ISSN 16625145. doi: 10.3389/fnint.2013.00025.

C. Challis and O. Berton. Top-down control of serotonin systems by the prefrontal cortex: A path toward restored socioemotional function in depression. *ACS Chemical Neuroscience*, 6: 1040–1054, 7 2015. ISSN 19487193. doi: 10.1021/acschemneuro.5b00007.

F. S. Chance. Receiver operating characteristic (roc) analysis for characterizing synaptic efficacy. *Journal of Neurophysiology*, 97:1799–1808, 2 2007. ISSN 00223077. doi: 10.1152/jn.00885.2006.

F. J. Chaure, H. G. Rey, and R. Q. Quiroga. A novel and fully automatic spike-sorting implementation with variable number of features. *J Neurophysiol*, 120:1859–1871, 2018. doi: 10.1152/jn.00339.2018.-The.

K. K. Cho, R. Hoch, A. T. Lee, T. Patel, J. L. Rubenstein, and V. S. Sohal. Gamma rhythms link prefrontal interneuron dysfunction with cognitive inflexibility in dlx5/6+/- mice. *Neuron*, 85:1332–1343, 3 2015. ISSN 10974199. doi: 10.1016/j.neuron.2015.02.019.

D. A. Clemett, T. Punhani, M. S. Duxon, T. P. Blackburn, and K. C. F. Fone. Immunohistochemical localisation of the 5-ht 2c receptor protein in the rat cns, 2000.

J. Y. Cohen, M. W. Amoroso, and N. Uchida. Serotonergic neurons signal reward and punishment on multiple timescales. *eLife*, 4, 2015. doi: 10.7554/eLife.06346.001.

P. J. Cowen and M. Browning. What has serotonin to do with depression? *World Psychiatry*, 14: 158–160, 6 2015. ISSN 20515545. doi: 10.1002/wps.20229.

A. Dahlström and K. Fuxe. Localization of monoamines in the lower brain stem. *Experientia*, 20: 398–399, 7 1964. ISSN 0014-4754. doi: 10.1007/BF02147990.

J. Daniel and M. Haberman. Clinical potential of psilocybin as a treatment for mental health conditions. *Mental Health Clinician*, 7:24–28, 1 2017. ISSN 21689709. doi: 10.9740/mhc.2017.01.024.

J. DeFelipe, J. I. Arellano, A. Gómez, E. C. Azmitia, and A. Muñoz. Pyramidal cell axons show a local specialization for gaba and 5-ht inputs in monkey and human cerebral cortex. *Journal of Comparative Neurology*, 433:148–155, 4 2001. ISSN 00219967. doi: 10.1002/cne.1132.

E. Deneris and P. Gaspar. Serotonin neuron development: shaping molecular and structural identities. *Wiley Interdisciplinary Reviews: Developmental Biology*, 7, 1 2018. ISSN 17597692. doi: 10.1002/wdev.301.

J. Deubner, P. Coulon, and I. Diester. Optogenetic approaches to study the mammalian brain. *Current Opinion in Structural Biology*, 57:157–163, 8 2019. ISSN 1879033X. doi: 10.1016/j.sbi.2019.04.003.

A. Domonkos, L. N. Ledri, T. Laszlovszky, C. Cserép, Z. Borhegyi, E. Papp, G. Nyiri, T. F. Freund, and V. Varga. Divergent in vivo activity of non-serotonergic and serotonergic vglut3–neurones in the median raphe region. *Journal of Physiology*, 594:3775–3790, 7 2016. ISSN 14697793. doi: 10.1113/JP272036.

I. P. Dorocic, D. Fürth, Y. Xuan, Y. Johansson, L. Pozzi, G. Silberberg, M. Carlén, and K. Meletis. A whole-brain atlas of inputs to serotonergic neurons of the dorsal and median raphe nuclei. *Neuron*, 83:663–678, 8 2014. ISSN 10974199. doi: 10.1016/j.neuron.2014.07.002.

H. C. Dringenberg and C. H. Vanderwolf. 5-hydroxytryptamine (5-ht) agonists: effects on neocortical slow wave activity after combined muscarinic and serotonergic blockade, 1996.

Y. Du, Y. Li, X. Zhao, Y. Yao, B. Wang, L. Zhang, and G. Wang. Psilocybin facilitates fear extinction in mice by promoting hippocampal neuroplasticity. *Chinese Medical Journal*, 2023. doi: 10.1097/CM9.0000000000002647.

E. Eldar, J. D. Cohen, and Y. Niv. The effects of neural gain on attention and learning. *Nature Neuroscience*, 16:1146–1153, 8 2013. ISSN 10976256. doi: 10.1038/nn.3428.

I. Erkizia-Santamaría, R. Alles-Pascual, I. Horrillo, J. J. Meana, and J. E. Ortega. Serotonin 5-ht2a, 5-ht2c and 5-ht1a receptor involvement in the acute effects of psilocybin in mice. in vitro pharmacological profile and modulation of thermoregulation and head-twich response. *Biomedicine and Pharmacotherapy*, 154, 10 2022. ISSN 19506007. doi: 10.1016/j.biopha.2022.113612.

B. R. Ferguson and W. J. Gao. Pv interneurons: critical regulators of e/i balance for prefrontal cortex-dependent behavior and psychiatric disorders. *Frontiers in Neural Circuits*, 12, 5 2018. ISSN 16625110. doi: 10.3389/fncir.2018.00037.

G. Fishell and A. Kepecs. Interneuron types as attractors and controllers. *Annual Review of Neuroscience*, 43:1–30, 7 2020. ISSN 15454126. doi: 10.1146/annurev-neuro-070918-050421.

P. J. Fitzgerald and B. O. Watson. Gamma oscillations as a biomarker for major depression: an emerging topic. *Translational Psychiatry*, 8, 12 2018. ISSN 21583188. doi: 10.1038/s41398-018-0239-y.

R. Fiáth, A. L. Márton, F. Mátyás, D. Pinke, G. Márton, K. Tóth, and I. Ulbert. Slow insertion of silicon probes improves the quality of acute neuronal recordings. *Scientific Reports*, 9, 12 2019. ISSN 20452322. doi: 10.1038/s41598-018-36816-z.

R. C. Foehring, J. F. M. V. Brederode, G. A. Kinney, and W. J. Spain. Serotonergic modulation of supragranular neurons in rat sensorimotor cortex. *J Neurosci*, 22:8238–8250, 2002.

J. Francis-Oliveira, O. Leitzel, and M. Niwa. Are the anterior and mid-cingulate cortices distinct in rodents? *Frontiers in Neuroanatomy*, 16, 6 2022. ISSN 16625129. doi: 10.3389/fnana.2022.914359.

K. B. J. Franklin and G. Paxinos. *The Mouse Brain in Stereotaxic Coordinates*. 4th edition, 2013.

P. Fries. Neuronal gamma-band synchronization as a fundamental process in cortical computation. *Annual Review of Neuroscience*, 32:209–224, 6 2009. ISSN 0147006X. doi: 10.1146/annurev.neuro.051508.135603.

S. Fujisawa, A. Amarasingham, M. T. Harrison, and G. Buzsáki. Behavior-dependent short-term assembly dynamics in the medial prefrontal cortex. *Nature Neuroscience*, 11:823–833, 7 2008. ISSN 10976256. doi: 10.1038/nn.2134.

S. Funahashi and J. M. Andreau. Prefrontal cortex and neural mechanisms of executive function. *Journal of Physiology Paris*, 107:471–482, 12 2013. ISSN 09284257. doi: 10.1016/j.jphysparis.2013.05.001.

I. Férézou, B. Cauli, E. L. Hill, J. Rossier, E. Hamel, and B. Lambolez. 5-ht 3 receptors mediate serotonergic fast synaptic excitation of neocortical vasoactive intestinal peptide/cholecystokinin interneurons. *The Journal of Neuroscience*, 22:7389–7393, 2002.

M. G. Garcia-Garcia, C. Marquez-Chin, and M. R. Popovic. Operant conditioning of motor cortex neurons reveals neuron-subtype-specific responses in a brain-machine interface task. *Scientific Reports*, 10, 12 2020. ISSN 20452322. doi: 10.1038/s41598-020-77090-2.

S. E. Gartside, E. Hajós-Korscsok, E. Bagdy, L. G. H. Jr., S. T, and M. Hajós. Neurochemical and electrophysiological studies on the functional significance of burst firing in serotonergic neurons. *Neuroscience*, 98:295–300, 2000.

P. Gaspar and C. Lillesaar. Probing the diversity of serotonin neurons. *Philosophical Transactions of the Royal Society B: Biological Sciences*, 367:2382–2394, 2012. ISSN 14712970. doi: 10.1098/rstb.2011.0378.

T. Gener, A. Tauste-Campo, M. Alemany-González, P. Nebot, C. Delgado-Sallent, J. Chanovas, and M. V. Puig. Serotonin 5-ht1a, 5-ht2a and dopamine d2 receptors strongly influence prefronto-hippocampal neural networks in alert mice: Contribution to the actions of risperidone. *Neuropharmacology*, 158, 11 2019. ISSN 18737064. doi: 10.1016/j.neuropharm.2019.107743.

D. M. Gerhard, S. Pothula, R. J. Liu, M. Wu, X. Y. Li, M. J. Girgenti, S. R. Taylor, C. H. Duman, E. Delpire, M. Picciotto, E. S. Wohleb, and R. S. Duman. Gaba interneurons are the cellular trigger for ketamine's rapid antidepressant actions. *Journal of Clinical Investigation*, 130:1336–1349, 3 2020. ISSN 15588238. doi: 10.1172/JCI130808.

C. T. Golden and P. Chadderton. Psilocybin reduces low frequency oscillatory power and neuronal phase-locking in the anterior cingulate cortex of awake rodents. *Scientific Reports*, 12, 12 2022. ISSN 20452322. doi: 10.1038/s41598-022-16325-w.

G. Gonzalez-Burgos, R. Y. Cho, and D. A. Lewis. Alterations in cortical network oscillations and parvalbumin neurons in schizophrenia. *Biological Psychiatry*, 77:1031–1040, 6 2015. ISSN 18732402. doi: 10.1016/j.biopsych.2015.03.010.

J. González-Maeso, N. V. Weisstaub, M. Zhou, P. Chan, L. Ivic, R. Ang, A. Lira, M. Bradley-Moore, Y. Ge, Q. Zhou, S. C. Sealfon, and J. A. Gingrich. Hallucinogens recruit specific cortical 5-ht2a receptor-mediated signaling pathways to affect behavior. *Neuron*, 53: 439–452, 2 2007. ISSN 08966273. doi: 10.1016/j.neuron.2007.01.008.

G. M. Goodwin, S. T. Aaronson, O. Alvarez, P. C. Arden, A. Baker, J. C. Bennett, C. Bird, R. E. Blom, C. Brennan, D. Brusch, L. Burke, K. Campbell-Coker, R. Carhart-Harris, J. Cattell, A. Daniel, C. DeBattista, B. W. Dunlop, K. Eisen, D. Feifel, M. Forbes, H. M. Haumann, D. J. Hellerstein, A. I. Hoppe, M. I. Husain, L. A. Jelen, J. Kamphuis, J. Kawasaki, J. R. Kelly, R. E. Key, R. Kishon, S. K. Peck, G. Knight, M. H. Koolen, M. Lean, R. W. Licht, J. L. Maples-Keller, J. Mars, L. Marwood, M. C. McElhiney, T. L. Miller, A. Mirow, S. Mistry, T. Mletzko-Crowe, L. N. Modlin, R. E. Nielsen, E. M. Nielson, S. R. Offerhaus, V. O'Keane, T. Páleníček, D. Printz, M. C. Rademaker, A. van Reemst, F. Reinholdt, D. Repantis, J. Rucker, S. Rudow, S. Ruffell, A. J. Rush, R. A. Schoevers, M. Seynaeve, S. Shao, J. C. Soares, M. Somers, S. C. Stansfield, D. Sterling, A. Strockis, J. Tsai, L. Visser, M. Wahba, S. Williams, A. H. Young, P. Ywema, S. Zisook, and E. Malievskaia. Single-dose psilocybin for a treatment-resistant episode of major depression. *New England Journal of Medicine*, 387: 1637–1648, 11 2022. ISSN 0028-4793. doi: 10.1056/nejmoa2206443.

M. A. Gradwell, K. A. Boyle, T. J. Browne, A. M. Bell, J. Leonardo, F. S. P. Reyes, A. C. DIckie, K. M. Smith, R. J. Callister, C. V. Dayas, D. I. Hughes, and B. A. Graham. Diversity of inhibitory and excitatory parvalbumin interneuron circuits in the dorsal horn. *Pain*, 163: E432–E452, 3 2022. ISSN 18726623. doi: 10.1097/j.pain.0000000000002422.

M. Graf, A. Nair, K. L. Wong, Y. Tang, and G. J. Augustine. Identification of mouse claustral neuron types based on their intrinsic electrical properties. *eNeuro*, 7:1–29, 7 2020. ISSN 23732822. doi: 10.1523/ENEURO.0216-20.2020.

J. Grandjean, A. Corcoba, M. C. Kahn, A. L. Upton, E. S. Deneris, E. Seifritz, F. Helmchen, E. O. Mann, M. Rudin, and B. J. Saab. A brain-wide functional map of the serotonergic responses to acute stress and fluoxetine. *Nature Communications*, 10, 12 2019. ISSN 20411723. doi: 10.1038/s41467-018-08256-w.

S. Granon and B. Poucet. Involvement of the rat prefrontal cortex in cognitive functions: A central role for the prelimbic area. *Psychobiology*, 28:229–237, 2000.

N. A. Gray, M. S. Milak, C. Delorenzo, R. T. Ogden, Y. Y. Huang, J. J. Mann, and R. V. Parsey. Antidepressant treatment reduces serotonin-1a autoreceptor binding in major depressive disorder. *Biological Psychiatry*, 74:26–31, 7 2013. ISSN 00063223. doi: 10.1016/j.biopsych.2012.11.012.

S. Gretenkord, A. Rees, M. A. Whittington, S. E. Gartside, and F. E. N. Lebeau. Dorsal vs. ventral differences in fast up-state-associated oscillations in the medial prefrontal cortex of the urethane-anesthetized rat. *J Neurophysiol*, 117:1126–1142, 2017. doi: 10.1152/jn.00762.2016.-Cortical.

A. I. Gulyás, G. G. Szabó, I. Ulbert, N. Holderith, H. Monyer, F. Erdélyi, G. Szabó, T. F. Freund, and N. Hájos. Parvalbumin-containing fast-spiking basket cells generate the field potential oscillations induced by cholinergic receptor activation in the hippocampus. *Journal of Neuroscience*, 30:15134–15145, 11 2010. ISSN 02706474. doi: 10.1523/JNEUROSCI.4104-10.2010.

M. Hajós and T. Sharp. Burst-firing activity of presumed 5-ht neurones of the rat dorsal raphe nucleus: electrophysiological analysis by antidromic stimulation, 1996.

M. Hajós, S. E. Gartside, A. E. P. Villa, and T. Sharp. Evidence for a repetitive (burst) firing pattern in a sub-population of 5-hydroxytryptamine neurons in the dorsal and median raphe nuclei of the rat, 1995.

M. Hajós, C. D. Richards, A. D. Szekelly, and T. Sharp. An electrophysiological and neuroanatomical study of the medial prefrontal cortical projection to the midbrain raphe nuclei in the rat. *Neuroscience*, 87:95–108, 1998.

M. Hajós, S. E. Gartside, V. Varga, and T. Sharp. In vivo inhibition of neuronal activity in the rat ventromedial prefrontal cortex by midbrain-raphe nuclei: Role of 5-ht1a receptors. *Neuropharmacology*, 45:72–81, 2003. ISSN 00283908. doi: 10.1016/S0028-3908(03)00139-4.

N. Hajós, J. Pálhalini, E. O. Mann, B. Nèmeth, O. Paulsen, and T. F. Freund. Spike timing of distinct types of gabaergic interneuron during hippocampal gamma oscillations in vitro. *Journal of Neuroscience*, 24:9127–9137, 10 2004. ISSN 02706474. doi: 10.1523/JNEUROSCI.2113-04.2004.

X. Han. In vivo application of optogenetics for neural circuit analysis. *ACS Chemical Neuroscience*, 3:577–584, 8 2012. ISSN 19487193. doi: 10.1021/cn300065j.

K. Hara and R. A. Harris. The anesthetic mechanism of urethane: The effects on neurotransmitter-gated ion channels. *Anesthesia Analgesia*, 94:313–318, 2002.

S. Hardung, R. Epple, Z. Jäckel, D. Eriksson, C. Uran, V. Senn, L. Gibor, O. Yizhar, and I. Diester. A functional gradient in the rodent prefrontal cortex supports behavioral inhibition. *Current Biology*, 27:549–555, 2 2017. ISSN 09609822. doi: 10.1016/j.cub.2016.12.052.

C. J. Harmer, R. S. Duman, and P. J. Cowen. How do antidepressants work? new perspectives for refining future treatment approaches. *The Lancet Psychiatry*, 4:409–418, 5 2017. ISSN 22150374. doi: 10.1016/S2215-0366(17)30015-9.

A. Hasenstaub, Y. Shu, B. Haider, U. Kraushaar, A. Duque, and D. A. McCormick. Inhibitory postsynaptic potentials carry synchronized frequency information in active cortical networks. *Neuron*, 47:423–435, 8 2005. ISSN 08966273. doi: 10.1016/j.neuron.2005.06.016.

L. Helboe, J. Egebjerg, and I. E. de Jong. Distribution of serotonin receptor 5-ht6 mrna in rat neuronal subpopulations: A double in situ hybridization study. *Neuroscience*, 310:442–454, 12 2015. ISSN 18737544. doi: 10.1016/j.neuroscience.2015.09.064.

D. A. Henze, Z. Borhegyi, J. Csicsvari, A. Mamiya, K. D. Harris, O. Buzs, and G. Buzsáki. Intracellular features predicted by extracellular recordings in the hippocampus in vivo. *J Neurophysiol*, 84:390–400, 2000.

C. S. Herrmann and T. Demiralp. Human eeg gamma oscillations in neuropsychiatric disorders. *Clinical Neurophysiology*, 116:2719–2733, 12 2005. ISSN 13882457. doi: 10.1016/j.clinph.2005.07.007.

S. Hestrin and M. Galarreta. Electrical synapses define networks of neocortical gabaergic neurons. *Trends in Neurosciences*, 28:304–309, 2005. ISSN 01662236. doi: 10.1016/j.tins.2005.04.001.

H. Hioki, H. Nakamura, Y. F. Ma, M. Konno, T. Hayakawa, K. C. Nakamura, F. Fujiyama, and T. Kaneko. Vesicular glutamate transporter 3-expressing nonserotonergic projection neurons constitute a subregion in the rat midbrain raphe nuclei. *Journal of Comparative Neurology*, 518:668–686, 3 2010. ISSN 00219967. doi: 10.1002/cne.22237.

S. Hippenmeyer, E. Vrieseling, M. Sigrist, T. Portmann, C. Laengle, D. R. Ladle, and S. Arber. A developmental switch in the response of drg neurons to ets transcription factor signaling. *PLoS Biology*, 3:0878–0890, 2005. ISSN 15457885. doi: 10.1371/journal.pbio.0030159.

G. R. Holt, W. R. Softky, C. Koch, and R. J. Douglas. Comparison of discharge variability in vitro and in vivo in cat visual cortex neurons, 1996.

D. Hoyer, J. P. Hannon, and G. R. Martin. Molecular, pharmacological and functional diversity of 5-ht receptors. *Pharmacology, Biochemistry and Behavior*, 71:533–554, 2002.

H. Hu, J. Gan, and P. Jonas. Fast-spiking, parvalbumin + gabaergic interneurons: From cellular design to microcircuit function. *Science*, 345:1255263, 2014.

K. W. Huang, N. E. Ochandarena, A. C. Philson, M. Hyun, J. E. Birnbaum, M. Cicconet, and B. L. Sabatini. Molecular and anatomical organization of the dorsal raphe nucleus. *eLife*, 8: e46464, 2019. doi: 10.7554/eLife.46464.001.

N. Insel and C. A. Barnes. Differential activation of fast-spiking and regular-firing neuron populations during movement and reward in the dorsal medial frontal cortex. *Cerebral Cortex*, 25:2631–2647, 9 2015. ISSN 14602199. doi: 10.1093/cercor/bhu062.

B. L. Jacobs and C. A. Fornal. Activity of serotonergic neurons in behaving animals. *Neuropsychopharmacology*, 21:9–15, 1999.

M. P. Jankowski and S. R. Sesack. Prefrontal cortical projections to the rat dorsal raphe nucleus: Ultrastructural features and associations with serotonin and -aminobutyric acid neurons. *Journal of Comparative Neurology*, 468:518–529, 1 2004. ISSN 00219967. doi: 10.1002/cne.10976.

A. Jansson, B. Tinner, M. Bancila, D. Vergé, H. W. M. Steinbusch, L. F. Agnati, and K. Fuxe. Relationships of 5-hydroxytryptamine immunoreactive terminal-like varicosities to 5-hydroxytryptamine-2a receptor-immunoreactive neuronal processes in the rat forebrain. *Journal of Chemical Neuroanatomy*, 22:185–203, 2001.

K. A. Jennings, W. J. Sheward, A. J. Harmar, and T. Sharp. Evidence that genetic variation in 5-ht transporter expression is linked to changes in 5-ht2a receptor function. *Neuropharmacology*, 54:776–783, 4 2008. ISSN 00283908. doi: 10.1016/j.neuropharm.2007.12.001.

M. D. Johnson. Synaptic glutamate release by postnatal rat serotonergic neurons in microculture. *Neuron*, pages 433–442, 1994.

M. T. Jones, M. T. Strassnig, and P. D. Harvey. Emerging 5-ht receptor antagonists for the treatment of schizophrenia. *Expert Opinion on Emerging Drugs*, 25:189–200, 2020. doi: 10.1080/14728214.2020.1773792. PMID: 32449404.

F. Jung and M. Carlén. Neuronal oscillations and the mouse prefrontal cortex. *International review of neurobiology*, 158:337—372, 2021. ISSN 0074-7742. doi: 10.1016/bs.irn.2020.11.005.

V. Kapoor, A. C. Provost, P. Agarwal, and V. N. Murthy. Activation of raphe nuclei triggers rapid and distinct effects on parallel olfactory bulb output channels. *Nature Neuroscience*, 19: 271–282, 11 2016. ISSN 15461726. doi: 10.1038/nn.4129.

Y. Kawaguchi and Y. Kubota. Correlation of physiological subgroupings of nonpyramidal cells with parvalbumin- and calbindind28k-immunoreactive neurons in layer v of rat frontal cortex. *Journal of Neurophysiology*, 70:387–396, 7 1993. ISSN 0022-3077. doi: 10.1152/jn.1993.70.1.387.

F. B. Kayarian, A. Jannati, A. Rotenberg, and E. Santarnecchi. Targeting gamma-related pathophysiology in autism spectrum disorder using transcranial electrical stimulation: Opportunities and challenges. *Autism Research*, 13:1051–1071, 7 2020. ISSN 19393806. doi: 10.1002/aur.2312.

J. H. Kehne, B. M. Baron, A. A. Carr, S. F. Chaney, J. Elands, D. J. Feldman, R. A. Frank, P. L. van Giersbergen, T. C. McCloskey, M. P. Johnson, D. R. McCarty, M. Poirot, Y. Senyah, B. W. Siegel, and C. Widmaier. Preclinical characterization of the potential of the putative atypical antipsychotic mdl 100,907 as a potent 5-ht2a antagonist with a favorable cns safety profile. *Journal of Pharmacology and Experimental Therapeutics*, 277:968–981, 1996. ISSN 0022-3565.

T. Kendrick and S. Collinson. Antidepressants and the serotonin hypothesis of depression. *The BMJ*, 2022. ISSN 17561833. doi: 10.1136/bmj.o1993.

G. A. Kennett, M. Wood, F. Bright, B. Trail, G. Riley, V. Holland, K. Avenell, T. Stean, N. Upton, S. Bromidge, I. Forbes, A. Brown, D. Middlemiss, and T. Blackburn. Sb 242084, a selective and brain penetrant 5-ht 2c receptor antagonist. *Neuropharmacology*, 36:609–620, 4 1997. ISSN 00283908. doi: 10.1016/S0028-3908(97)00038-5.

H. Kim, S. Ährlund Richter, X. Wang, K. Deisseroth, and M. Carlén. Prefrontal parvalbumin neurons in control of attention. *Cell*, 164:208–218, 1 2016. ISSN 10974172. doi: 10.1016/j.cell.2015.11.038.

V. Kiyasova, P. Bonnavion, S. Scotto-Lomassese, V. Fabre, I. Sahly, F. Tronche, E. Deneris, P. Gaspar, and S. P. Fernandez. A subpopulation of serotonergic neurons that do not express the 5-ht1a autoreceptor. *ACS Chemical Neuroscience*, 4:89–95, 1 2013. ISSN 19487193. doi: 10.1021/cn300157s.

T. Klausberger and P. Somogyi. Neuronal diversity and temporal dynamics: The unity of hippocampal circuit operations. *Science*, 321:53–57, 7 2008. ISSN 00368075. doi: 10.1126/science.1149381.

B. Kocsis, V. Varga, L. Dahan, and A. Sik. Serotonergic neuron diversity: Identification of raphe neurons with discharges time-locked to the hippocampal theta rhythm, 2004. URL `www.pnas.orgcgidoi10.1073pnas.0508360103`.

E. Krediet, T. Bostoen, J. Breeksema, A. van Schagen, T. Passie, and E. Vermetten. Reviewing the potential of psychedelics for the treatment of ptsd. *International Journal of Neuropsychopharmacology*, 23:385–400, 2020. ISSN 14695111. doi: 10.1093/ijnp/pyaa018.

T. Kuki, K. Fujihara, H. Miwa, N. Tamamaki, Y. Yanagawa, and H. Mushiake. Contribution of parvalbumin and somatostatin-expressing gabaergic neurons to slow oscillations and the balance in beta-gamma oscillations across cortical layers. *Frontiers in Neural Circuits*, 9, 2 2015. ISSN 16625110. doi: 10.3389/fncir.2015.00006.

K. Kullander and L. Topolnik. Cortical disinhibitory circuits: cell types, connectivity and function. *Trends in Neurosciences*, 44:643–657, 8 2021. ISSN 1878108X. doi: 10.1016/j.tins.2021.04.009.

D. Kvitsiani, S. Ranade, B. Hangya, H. Taniguchi, J. Z. Huang, and A. Kepecs. Distinct behavioural and network correlates of two interneuron types in prefrontal cortex. *Nature*, 498: 363–366, 2013. ISSN 00280836. doi: 10.1038/nature12176.

A. C. Kwan, D. E. Olson, K. H. Preller, and B. L. Roth. The neural basis of psychedelic action. *Nature Neuroscience*, 25:1407–1419, 11 2022. ISSN 15461726. doi: 10.1038/s41593-022-01177-4.

M. Laubach, L. M. Amarante, K. Swanson, and S. R. White. What, if anything, is rodent prefrontal cortex? *eNeuro*, 5, 9 2018. ISSN 23732822. doi: 10.1523/ENEURO.0315-18.2018.

D. Levenstein, J. Gornet, R. Huszár, G. Girardeau, A. Grosmark, A. Peyrache, Y. Senzai, B. O. Watson, K. Mizuseki, J. Rinzel, and G. Buzsáki. Distinct ground state and activated state modes of firing in forebrain neurons. *bioRxiv*, 2022. doi: 10.1101/2021.09.20.461152.

D. A. Lewis, A. A. Curley, J. R. Glausier, and D. W. Volk. Cortical parvalbumin interneurons and cognitive dysfunction in schizophrenia. *Trends in Neurosciences*, 35:57–67, 1 2012. ISSN 01662236. doi: 10.1016/j.tins.2011.10.004.

B. Li, B. N. Routh, D. Johnston, E. Seidemann, and N. J. Priebe. Voltage-gated intrinsic conductances shape the input-output relationship of cortical neurons in behaving primate v1. *Neuron*, 107:185–196.e4, 7 2020. ISSN 10974199. doi: 10.1016/j.neuron.2020.04.001.

Y. Li, W. Zhong, D. Wang, Q. Feng, Z. Liu, J. Zhou, C. Jia, F. Hu, J. Zeng, Q. Guo, L. Fu, and M. Luo. Serotonin neurons in the dorsal raphe nucleus encode reward signals. *Nature Communications*, 7, 1 2016. ISSN 20411723. doi: 10.1038/ncomms10503.

Y.-Q. Li, H. Li, T. Kaneko, and N. Mizuno. Morphological features and electrophysiological properties of serotonergic and non-serotonergic projection neurons in the dorsal raphe nucleus an intracellular recording and labeling study in rat brain slices, 2001.

L. Lim, D. Mi, A. Llorca, and O. Marín. Development and functional diversification of cortical interneurons. *Neuron*, 100:294–313, 10 2018. ISSN 10974199. doi: 10.1016/j.neuron.2018.10.009.

J. Lima, T. Sharp, D. M. Bannerman, and S. B. McHugh. Enhanced discriminative aversive learning and amygdala responsivity in 5-ht transporter mutant mice. *Translational Psychiatry*, 9, 12 2019. ISSN 21583188. doi: 10.1038/s41398-019-0476-8.

S. Liu, M. J. Bubar, M. F. Lanfranco, G. R. Hillman, and K. A. Cunningham. Serotonin2c receptor localization in gaba neurons of the rat medial prefrontal cortex: Implications for understanding the neurobiology of addiction. *Neuroscience*, 146:1677–1688, 6 2007. ISSN 03064522. doi: 10.1016/j.neuroscience.2007.02.064.

Z. Liu, J. Zhou, Y. Li, F. Hu, Y. Lu, M. Ma, Q. Feng, J. en Zhang, D. Wang, J. Zeng, J. Bao, J. Y. Kim, Z. F. Chen, S. ElMestikawy, and M. Luo. Dorsal raphe neurons signal reward through 5-ht and glutamate. *Neuron*, 81:1360–1374, 3 2014. ISSN 10974199. doi: 10.1016/j.neuron.2014.02.010.

A. Llorca and R. Deogracias. Origin, development, and synaptogenesis of cortical interneurons. *Frontiers in Neuroscience*, 16, 6 2022. ISSN 1662453X. doi: 10.3389/fnins.2022.929469.

S. Lohani, A. K. Martig, K. Deisseroth, I. B. Witten, and B. Moghaddam. Dopamine modulation of prefrontal cortex activity is manifold and operates at multiple temporal and spatial scales. *Cell Reports*, 27:99–114.e6, 4 2019. ISSN 22111247. doi: 10.1016/j.celrep.2019.03.012.

E. Lottem, M. L. Lörincz, and Z. F. Mainen. Optogenetic activation of dorsal raphe serotonin neurons rapidly inhibits spontaneous but not odor-evoked activity in olfactory cortex. *Journal of Neuroscience*, 36:7–18, 1 2016. ISSN 15292401. doi: 10.1523/JNEUROSCI.3008-15.2016.

L. Madisen, T. A. Zwingman, S. M. Sunkin, S. W. Oh, H. A. Zariwala, H. Gu, L. L. Ng, R. D. Palmiter, M. J. Hawrylycz, A. R. Jones, E. S. Lein, and H. Zeng. A robust and high-throughput cre reporting and characterization system for the whole mouse brain. *Nature Neuroscience*, 13:133–140, 1 2010. ISSN 10976256. doi: 10.1038/nn.2467.

A. Mahrach, G. Chen, N. Li, C. van Vreeswijk, and D. Hansel. Mechanisms underlying the response of mouse cortical networks to optogenetic manipulation. *eLife*, 9, 1 2020. ISSN 2050084X. doi: 10.7554/eLife.49967.

E. O. Mann and O. Paulsen. Role of gabaergic inhibition in hippocampal network oscillations. *Trends in Neurosciences*, 30:343–349, 7 2007. ISSN 01662236. doi: 10.1016/j.tins.2007.05.003.

N. Mansouri-Guilani, V. Bernard, E. Vigneault, V. Vialou, S. Daumas, S. E. Mestikawy, and G. Gangarossa. Vglut3 gates psychomotor effects induced by amphetamine. *Journal of Neurochemistry*, 148:779–795, 3 2019. ISSN 14714159. doi: 10.1111/jnc.14644.

J. Mantz, R. Godbout, J.-P. Tassin, J. Glowinski, and A.-M. Thierry. Inhibition of spontaneous and evoked unit activity in the rat medial prefrontal cortex by mesencephalic raphe nuclei. *Brain Research*, 512:22–30, 1990.

H. Markram, M. Toledo-Rodriguez, Y. Wang, A. Gupta, G. Silberberg, and C. Wu. Interneurons of the neocortical inhibitory system. *Nature Reviews Neuroscience*, 5:793–807, 10 2004. ISSN 1471003X. doi: 10.1038/nrn1519.

J. P. Marquis, S. Killcross, and J. E. Haddon. Inactivation of the prelimbic, but not infralimbic, prefrontal cortex impairs the contextual control of response conflict in rats. *European Journal of Neuroscience*, 25:559–566, 1 2007. ISSN 0953816X. doi: 10.1111/j.1460-9568.2006.05295.x.

R. Martín-Ruiz, M. V. Puig, P. Celada, D. A. Shapiro, B. L. Roth, G. Mengod, and F. Artigas. Control of serotonergic function in medial prefrontal cortex by serotonin-2a receptors through a glutamate-dependent mechanism. *Journal of Neuroscience*, 21:9856–9866, 2001.

J. J. Martínez, B. Rahsepar, and J. A. White. Anatomical and electrophysiological clustering of superficial medial entorhinal cortex interneurons. *eNeuro*, 4, 9 2017. ISSN 23732822. doi: 10.1523/ENEURO.0263-16.2017.

L. Massi, M. Lagler, K. Hartwich, Z. Borhegyi, P. Somogyi, and T. Klausberger. Temporal dynamics of parvalbumin-expressing axo-axonic and basket cells in the rat medial prefrontal cortex in vivo. *Journal of Neuroscience*, 32:16496–16502, 11 2012. ISSN 02706474. doi: 10.1523/JNEUROSCI.3475-12.2012.

D. J. McKenna and S. J. Peroutka. Differentiation of 5=hydroxytryptamine, receptor subtypes using 125l-r-(-)2,5-dimethoxy-4-iodo-phenylisopropylamine and 3h-ketanserin. *The Journal of Neuroscience*, 9:34823490, 1989.

L. Medrihan, Y. Sagi, Z. Inde, O. Krupa, C. Daniels, A. Peyrache, and P. Greengard. Initiation of behavioral response to antidepressants by cholecystokinin neurons of the dentate gyrus. *Neuron*, 95:564–576.e4, 8 2017. ISSN 10974199. doi: 10.1016/j.neuron.2017.06.044.

G. Mengod, R. C. S, M. T. Vilar, and D. Hoyer. Distribution of 5-ht receptors in the central nervous system. *ACS Chemical Neuroscience*, 6:1089–1098, 2015. doi: 10.1016/B978-0-12-374634-4.00006-X.

P. L. Merre, S. Ährlund Richter, and M. Carlén. The mouse prefrontal cortex: Unity in diversity. *Neuron*, 109:1925–1944, 6 2021. ISSN 10974199. doi: 10.1016/j.neuron.2021.03.035.

H. S. Meyer, D. Schwarz, V. C. Wimmer, A. C. Schmitt, J. N. Kerr, B. Sakmann, and M. Helmstaedter. Inhibitory interneurons in a cortical column form hot zones of inhibition in layers 2 and 5a. *Proceedings of the National Academy of Sciences of the United States of America*, 108:16807–16812, 10 2011. ISSN 00278424. doi: 10.1073/pnas.1113648108.

K. A. Michelsen, C. Schmitz, and H. W. Steinbusch. The dorsal raphe nucleus-from silver stainings to a role in depression. *Brain Research Reviews*, 55:329–342, 2007. ISSN 01650173. doi: 10.1016/j.brainresrev.2007.01.002.

E. K. Miller and J. D. Cohen. An integrative theory of prefrontal cortex function. *Annual Review of Neuroscience*, 2001.

J. Moncrieff, R. E. Cooper, T. Stockmann, S. Amendola, M. P. Hengartner, and M. A. Horowitz. The serotonin theory of depression: a systematic umbrella review of the evidence. *Molecular Psychiatry*, 2022. ISSN 14765578. doi: 10.1038/s41380-022-01661-0.

I. E. Monosov, J. C. Trageser, and K. G. Thompson. Measurements of simultaneously recorded spike and local field potentials suggest that spatial selection emerges in the frontal eye field. *Neuron*, 57:614–625, 2008.

J. Monti, G. Piñeyro, C. Orellana, M. Boussard, H. Jantos, and P. Labraga. 5-ht receptor agonists 1-(2,5-dimethoxy-4-iodophenyl)-2-aminopropane (doi) and 8-oh-dpat increase wakefulness in the rat. *Biog Amines*, 7:145–151, 1990.

A. K. Moore and M. Wehr. Parvalbumin-expressing inhibitory interneurons in auditory cortex are well-tuned for frequency. *Journal of Neuroscience*, 33:13713–13723, 2013. ISSN 02706474. doi: 10.1523/JNEUROSCI.0663-13.2013.

M. Mukovski, S. Chauvette, I. Timofeev, and M. Volgushev. Detection of active and silent states in neocortical neurons from the field potential signal during slow-wave sleep. *Cerebral Cortex*, 17:400–414, 2 2007. ISSN 10473211. doi: 10.1093/cercor/bhj157.

J. W. Murrough, A. M. Perez, S. Pillemer, J. Stern, M. K. Parides, M. A. H. Rot, K. A. Collins, S. J. Mathew, D. S. Charney, and D. V. Iosifescu. Rapid and longer-term antidepressant effects of repeated ketamine infusions in treatment-resistant major depression. *Biological Psychiatry*, 74:250–256, 8 2013. ISSN 00063223. doi: 10.1016/j.biopsych.2012.06.022.

S. D. Muthukumaraswamy, R. L. Carhart-Harris, R. J. Moran, M. J. Brookes, T. M. Williams, D. Errtizoe, B. Sessa, A. Papadopoulos, M. Bolstridge, K. D. Singh, A. Feilding, K. J. Friston, and D. J. Nutt. Broadband cortical desynchronization underlies the human psychedelic state. *Journal of Neuroscience*, 33:15171–15183, 2013. ISSN 02706474. doi: 10.1523/JNEUROSCI.2063-13.2013.

A. Muzerelle, S. Scotto-Lomassese, J. F. Bernard, M. Soiza-Reilly, and P. Gaspar. Conditional anterograde tracing reveals distinct targeting of individual serotonin cell groups (b5–b9) to the forebrain and brainstem. *Brain Structure and Function*, 221:535–561, 1 2014. ISSN 18632661. doi: 10.1007/s00429-014-0924-4.

G. Nagel, T. Szellas, W. Huhn, S. Kateriya, N. Adeishvili, P. Berthold, D. Ollig, P. Hegemann, and E. Bamberg. Channelrhodopsin-2, a directly light-gated cation-selective membrane channel. *PNAS*, 100:13940–13945, 2003.

A. Naka and H. Adesnik. Inhibitory circuits in cortical layer 5. *Frontiers in Neural Circuits*, 10, 5 2016. ISSN 16625110. doi: 10.3389/fncir.2016.00035.

D. L. Nelson, V. L. Lucaites, D. B. Wainscott, and R. A. Glennon. Ht 2 receptor subpopulations comparisons of hallucinogenic phenylisopropylamine binding affinities at cloned human 5-ht 2a , 5-ht 2b and 5-ht 2c receptors. *Naunyn-Schmiedeberg's Arch Pharmacol*, 359:1–6, 1999.

C. B. Nemeroff and M. J. Owens. Treatment of mood disorders. *Nature Neuroscience*, 5: 1068–1070, 2002. ISSN 15461726. doi: 10.1038/nn943.

L. H. L. Ng, Y. Huang, L. Han, R. C. C. Chang, Y. S. Chan, and C. S. W. Lai. Ketamine and selective activation of parvalbumin interneurons inhibit stress-induced dendritic spine elimination. *Translational Psychiatry*, 8, 12 2018. ISSN 21583188. doi: 10.1038/s41398-018-0321-5.

K. J. Nielsen, N. K. Logothetis, and G. Rainer. Dissociation between local field potentials and spiking activity in macaque inferior temporal cortex reveals diagnosticity-based encoding of complex objects. *Journal of Neuroscience*, 26:9639–9645, 9 2006. ISSN 02706474. doi: 10.1523/JNEUROSCI.2273-06.2006.

M. J. Nigro, H. Kirikae, K. Kjelsberg, R. R. Nair, and M. P. Witter. Not all that is gold glitters: Pv-ires-cre mouse line shows low efficiency of labeling of parvalbumin interneurons in the perirhinal cortex. *Frontiers in Neural Circuits*, 15, 11 2021. ISSN 16625110. doi: 10.3389/fncir.2021.781928.

D. Nutt, D. Erritzoe, and R. Carhart-Harris. Psychedelic psychiatry's brave new world. *Cell*, 181: 24–28, 4 2020. ISSN 10974172. doi: 10.1016/j.cell.2020.03.020.

Y. Ohmura, K. F. Tanaka, T. Tsunematsu, A. Yamanaka, and M. Yoshioka. Optogenetic activation of serotonergic neurons enhances anxiety-like behaviour in mice. *International Journal of Neuropsychopharmacology*, 17:1777–1783, 11 2014. ISSN 14695111. doi: 10.1017/S1461145714000637.

B. W. Okaty, N. Sturrock, Y. E. Lozoya, Y. Chang, R. A. Senft, K. A. Lyon, O. V. Alekseyenko, and S. M. Dymecki. A single-cell transcriptomic and anatomic atlas of mouse dorsal raphe pet1 neurons. *eLife*, 9:1–44, 6 2020. ISSN 2050084X. doi: 10.7554/eLife.55523.

I. Oren, N. Hájos, and O. Paulsen. Identification of the current generator underlying cholinergically induced gamma frequency field potential oscillations in the hippocampal ca3 region. *Journal of Physiology*, 588:785–797, 3 2010. ISSN 00223751. doi: 10.1113/jphysiol.2009.180851.

M. Pachitariu, N. Steinmetz, S. Kadir, M. Carandini, and K. D. Harris. Kilosort: realtime spike-sorting for extracellular electrophysiology with hundreds of channels. *bioRxiv*, 2016. doi: 10.1101/061481.

E. A. Pehek, C. Nocjar, B. L. Roth, T. A. Byrd, and O. S. Mabrouk. Evidence for the preferential involvement of 5-ht2a serotonin receptors in stress- and drug-induced dopamine release in the rat medial prefrontal cortex. *Neuropsychopharmacology*, 31:265–277, 2 2006. ISSN 0893133X. doi: 10.1038/sj.npp.1300819.

N. J. Penington and J. S. Kelly. Serotonin receptor activation reduces calcium current in an acutely dissociated adult central neuron. *Neuron*, 4:751–758, 1990.

G. Perlman, A. Tanti, and N. Mechawar. Parvalbumin interneuron alterations in stress-related mood disorders: A systematic review. *Neurobiology of Stress*, 15, 11 2021. ISSN 23522895. doi: 10.1016/j.ynstr.2021.100380.

Q. Perrenoud, C. M. Pennartz, and L. J. Gentet. Membrane potential dynamics of spontaneous and visually evoked gamma activity in v1 of awake mice. *PLoS Biology*, 14, 2 2016. ISSN 15457885. doi: 10.1371/journal.pbio.1002383.

A. Peyrache and A. Destexhe. Electrophysiological monitoring of inhibition in mammalian species, from rodents to humans. *Neurobiology of Disease*, 130:104500, 2019. doi: 10.1016/j.nbd.2019.104500Ãŕ.

R. Peñas-Cazorla and M. T. Vilaró. Serotonin 5-ht4 receptors and forebrain cholinergic system: receptor expression in identified cell populations. *Brain Structure and Function*, 220:3413–3434, 11 2015. ISSN 18632661. doi: 10.1007/s00429-014-0864-z.

H. J. Pi, B. Hangya, D. Kvitsiani, J. I. Sanders, Z. J. Huang, and A. Kepecs. Cortical interneurons that specialize in disinhibitory control. *Nature*, 503:521–524, 2013. ISSN 00280836. doi: 10.1038/nature12676.

V. M. Pogorelov, R. M. Rodriguiz, J. Cheng, M. Huang, C. M. Schmerberg, H. Y. Meltzer, B. L. Roth, A. P. Kozikowski, and W. C. Wetsel. 5-ht2c agonists modulate schizophrenia-like behaviors in mice. *Neuropsychopharmacology*, 42:2163–2177, 10 2017. ISSN 1740634X. doi: 10.1038/npp.2017.52.

M. V. Puig and T. Gener. Serotonin modulation of prefronto-hippocampal rhythms in health and disease. *ACS Chemical Neuroscience*, 6:1017–1025, 7 2015. ISSN 19487193. doi: 10.1021/cn500350e.

M. V. Puig and A. T. Gulledge. Serotonin and prefrontal cortex function: neurons, networks, and circuits. *Molecular neurobiology*, 44:449–464, 2011. ISSN 15591182. doi: 10.1007/s12035-011-8214-0.

M. V. Puig, P. Celada, L. Díaz-Mataix, and F. Artigas. In vivo modulation of the activity of pyramidal neurons in the rat medial prefrontal cortex by 5-ht2a receptors: Relationship to thalamocortical afferents. *Cerebral Cortex*, 13:870–882, 2003.

M. V. Puig, N. Santana, P. Celada, G. Mengod, and F. Artigas. In vivo excitation of gaba interneurons in the medial prefrontal cortex through 5-ht3 receptors. *Cerebral Cortex*, 14: 1365–1375, 12 2004. ISSN 10473211. doi: 10.1093/cercor/bhh097.

M. V. Puig, F. Artigas, and P. Celada. Modulation of the activity of pyramidal neurons in rat prefrontal cortex by raphe stimulation in vivo: Involvement of serotonin and gaba. *Cerebral Cortex*, 15:1–14, 1 2005. ISSN 10473211. doi: 10.1093/cercor/bhh104.

M. V. Puig, M. Ushimaru, and Y. Kawaguchi. Two distinct activity patterns of fast-spiking interneurons during neocortical up states. *PNAS*, 105:8428–8433, 2008.

M. V. Puig, A. Watakabe, M. Ushimaru, T. Yamamori, and Y. Kawaguchi. Serotonin modulates fast-spiking interneuron and synchronous activity in the rat prefrontal cortex through 5-ht1a and 5-ht2a receptors. *Journal of Neuroscience*, 30:2211–2222, 2 2010. ISSN 02706474. doi: 10.1523/JNEUROSCI.3335-09.2010.

M. E. Ragozzino, S. Detrick, and R. P. Kesner. Involvement of the prelimbic-infralimbic areas of the rodent prefrontal cortex in behavioral flexibility for place and response learning. *The Journal of Neuroscience*, 19:4585–4594, 1999.

J. Ren, D. Friedmann, J. Xiong, C. D. Liu, B. R. Ferguson, T. Weerakkody, K. E. DeLoach, C. Ran, A. Pun, Y. Sun, B. Weissbourd, R. L. Neve, J. Huguenard, M. A. Horowitz, and L. Luo. Anatomically defined and functionally distinct dorsal raphe serotonin sub-systems. *Cell*, 175:472–487.e20, 10 2018. ISSN 10974172. doi: 10.1016/j.cell.2018.07.043.

A. A. Robbins, S. E. Fox, G. L. Holmes, R. C. Scott, and J. M. Barry. Short duration waveforms recorded extracellularly from freely moving rats are representative of axonal activity. *Frontiers in neural circuits*, 7:181, 2013. ISSN 16625110. doi: 10.3389/fncir.2013.00181.

T. W. Robbins. Chemistry of the mind: Neurochemical modulation of prefrontal cortical function. *Journal of Comparative Neurology*, 493:140–146, 12 2005. ISSN 00219967. doi: 10.1002/cne.20717.

J. J. Rodríguez, H. N. Noristani, W. B. Hoover, S. B. Linley, and R. P. Vertes. Serotonergic projections and serotonin receptor expression in the reticular nucleus of the thalamus in the rat. *Synapse*, 65:919–928, 9 2011. ISSN 08874476. doi: 10.1002/syn.20920.

S. Royer, B. V. Zemelman, A. Losonczy, J. Kim, F. Chance, J. C. Magee, and G. Buzsáki. Control of timing, rate and bursts of hippocampal place cells by dendritic and somatic inhibition. *Nature Neuroscience*, 15:769–775, 5 2012. ISSN 10976256. doi: 10.1038/nn.3077.

B. Rudy, G. Fishell, S. H. Lee, and J. Hjerling-Leffler. Three groups of interneurons account for nearly 100gabaergic neurons. *Developmental Neurobiology*, 71:45–61, 1 2011. ISSN 19328451. doi: 10.1002/dneu.20853.

K. Sakai. Sleep-waking discharge profiles of dorsal raphe nucleus neurons in mice. *Neuroscience*, 197:200–224, 12 2011. ISSN 03064522. doi: 10.1016/j.neuroscience.2011.09.024.

N. Santana, A. Bortolozzi, J. Serrats, G. Mengod, and F. Artigas. Expression of serotonin1a and serotonin2a receptors in pyramidal and gabaergic neurons of the rat prefrontal cortex. *Cerebral Cortex*, 14:1100–1109, 10 2004. ISSN 10473211. doi: 10.1093/cercor/bhh070.

J. V. Schweimer and M. A. Ungless. Phasic responses in dorsal raphe serotonin neurons to noxious stimuli. *Neuroscience*, 171:1209–1215, 12 2010. ISSN 03064522. doi: 10.1016/j.neuroscience.2010.09.058.

J. V. Schweimer, N. Mallet, T. Sharp, and M. A. Ungless. Spike-timing relationship of neurochemically-identified dorsal raphe neurons during cortical slow oscillations. *Neuroscience*, 196:115–123, 11 2011. ISSN 03064522. doi: 10.1016/j.neuroscience.2011.08.072.

J. V. Schweimer, J. T. Brouard, Y. Li, C. Sánchez, and T. Sharp. In vivo electrophysiological study of the targeting of 5-ht3 receptor-expressing cortical interneurons by the multimodal antidepressant, vortioxetine. *European Journal of Neuroscience*, 55:1409–1423, 3 2022. ISSN 14609568. doi: 10.1111/ejn.15623.

A. Sengupta and A. Holmes. A discrete dorsal raphe to basal amygdala 5-ht circuit calibrates aversive memory. *Neuron*, 103:489–505.e7, 8 2019. ISSN 10974199. doi: 10.1016/j.neuron.2019.05.029.

A. Sengupta, M. Bocchio, D. M. Bannerman, T. Sharp, and M. Capogna. Control of amygdala circuits by 5-ht neurons via 5-ht and glutamate cotransmission. *Journal of Neuroscience*, 37: 1785–1796, 2 2017. ISSN 15292401. doi: 10.1523/JNEUROSCI.2238-16.2016.

Y. Senzai, A. Fernandez-Ruiz, and G. Buzsáki. Layer-specific physiological features and interlaminar interactions in the primary visual cortex of the mouse. *Neuron*, 101:500–513.e5, 2 2019. ISSN 10974199. doi: 10.1016/j.neuron.2018.12.009.

T. Sharp and N. M. Barnes. Central 5-ht receptors and their function; present and future. *Neuropharmacology*, 177, 10 2020. ISSN 18737064. doi: 10.1016/j.neuropharm.2020.108155.

T. Sharp and P. J. Cowen. 5-ht and depression: Is the glass half-full? *Current Opinion in Pharmacology*, 11:45–51, 2011. ISSN 14714892. doi: 10.1016/j.coph.2011.02.003.

M. J. Sharpe and S. Killcross. The prelimbic cortex uses higher-order cues to modulate both the acquisition and expression of conditioned fear. *Frontiers in Systems Neuroscience*, 8, 1 2015. ISSN 16625137. doi: 10.3389/fnsys.2014.00235.

H. Shikanai, T. Yoshida, K. Konno, M. Yamasaki, T. Izumi, Y. Ohmura, M. Watanabe, and M. Yoshioka. Distinct neurochemical and functional properties of gad67-containing 5-ht neurons in the rat dorsal raphe nucleus. *Journal of Neuroscience*, 32:14415–14426, 10 2012. ISSN 02706474. doi: 10.1523/JNEUROSCI.5929-11.2012.

J. H. Siegle, A. C. López, Y. A. Patel, K. Abramov, S. Ohayon, and J. Voigts. Open ephys: An open-source, plugin-based platform for multichannel electrophysiology. *Journal of Neural Engineering*, 14, 6 2017. ISSN 17412552. doi: 10.1088/1741-2552/aa5eea.

A. Sik, M. Penttonen, A. Ylinen, and G. Buzsiki. Hippocampal ca1 interneurons: An in vivo intracellular labeling study. *The Journal of Neuroscience*, 75:6651–6665, 1995.

A. Sirota, S. Montgomery, S. Fujisawa, Y. Isomura, M. Zugaro, and G. Buzsáki. Entrainment of neocortical neurons and gamma oscillations by the hippocampal theta rhythm. *Neuron*, 60: 683–697, 11 2008. ISSN 08966273. doi: 10.1016/j.neuron.2008.09.014.

R. Smausz, J. Neill, and J. Gigg. Neural mechanisms underlying psilocybin's therapeutic potential – the need for preclinical in vivo electrophysiology. *Journal of Psychopharmacology*, 36:781–793, 7 2022. ISSN 14617285. doi: 10.1177/02698811221092508.

V. S. Sohal, F. Zhang, O. Yizhar, and K. Deisseroth. Parvalbumin neurons and gamma rhythms enhance cortical circuit performance. *Nature*, 459:698–702, 6 2009. ISSN 00280836. doi: 10.1038/nature07991.

P. Somogyi and T. Klausberger. Defined types of cortical interneurone structure space and spike timing in the hippocampus. *Journal of Physiology*, 562:9–26, 1 2005. ISSN 00223751. doi: 10.1113/jphysiol.2004.078915.

D. R. Sparta, N. Hovelsø, A. O. Mason, P. A. Kantak, R. L. Ung, H. K. Decot, and G. D. Stuber. Activation of prefrontal cortical parvalbumin interneurons facilitates extinction of reward-seeking behavior. *Journal of Neuroscience*, 34:3699–3705, 2014. ISSN 02706474. doi: 10.1523/JNEUROSCI.0235-13.2014.

T. Spellman, M. Svei, J. Kaminsky, G. Manzano-Nieves, and C. Liston. Prefrontal deep projection neurons enable cognitive flexibility via persistent feedback monitoring. *Cell*, 184: 2750–2766.e17, 5 2021. ISSN 10974172. doi: 10.1016/j.cell.2021.03.047.

E. Stark, R. Eichler, L. Roux, S. Fujisawa, H. G. Rotstein, and G. Buzsáki. Inhibition-induced theta resonance in cortical circuits. *Neuron*, 80:1263–1276, 12 2013. ISSN 08966273. doi: 10.1016/j.neuron.2013.09.033.

N. A. Steinmetz, C. Koch, K. D. Harris, and M. Carandini. Challenges and opportunities for large-scale electrophysiology with neuropixels probes, 6 2018. ISSN 18736882.

K. T. Sultan and S. H. Shi. Generation of diverse cortical inhibitory interneurons. *Wiley Interdisciplinary Reviews: Developmental Biology*, 7, 3 2018. ISSN 17597692. doi: 10.1002/wdev.306.

C. Tanahira, S. Higo, K. Watanabe, R. Tomioka, S. Ebihara, T. Kaneko, and N. Tamamaki. Parvalbumin neurons in the forebrain as revealed by parvalbumin-cre transgenic mice. *Neuroscience Research*, 63:213–223, 3 2009. ISSN 01680102. doi: 10.1016/j.neures.2008.12.007.

H. Taniguchi. Genetic dissection of gabaergic neural circuits in mouse neocortex. *Frontiers in Cellular Neuroscience*, 8, 1 2014. ISSN 16625102. doi: 10.3389/fncel.2014.00008.

C. W. Thomas, C. Blanco-Duque, B. J. Bréant, G. M. Goodwin, T. Sharp, D. M. Bannerman, and V. V. Vyazovskiy. Psilocin acutely alters sleep-wake architecture and cortical brain activity in laboratory mice. *Translational Psychiatry*, 12, 12 2022. ISSN 21583188. doi: 10.1038/s41398-022-01846-9.

M. Titeler, R. A. Lyon, and R. A. Glennon. Radioligand binding evidence implicates the brain 5-ht2 receptor as a site of action for lsd and phenylisopropylamine hallucinogens. *Psychopharmacology*, 94:213–216, 1988.

R. Tremblay, S. Lee, and B. Rudy. Gabaergic interneurons in the neocortex: From cellular properties to circuits. *Neuron*, 91:260–292, 7 2016. ISSN 10974199. doi: 10.1016/j.neuron.2016.06.033.

L. Trudeau. Glutamate co-transmission as an emerging concept in monoamine neuron function. *Rev Psychiatr Neurosci*, 29:296–310, 2004.

H. A. Tseng and X. Han. Distinct spiking patterns of excitatory and inhibitory neurons and lfp oscillations in prefrontal cortex during sensory discrimination. *Frontiers in Physiology*, 12, 2 2021. ISSN 1664042X. doi: 10.3389/fphys.2021.618307.

P. J. Uhlhaas and W. Singer. Abnormal neural oscillations and synchrony in schizophrenia. *Nature Reviews Neuroscience*, 11:100–113, 2 2010. ISSN 1471003X. doi: 10.1038/nrn2774.

C. T. Unal, D. Pare, and L. Zaborszky. Impact of basal forebrain cholinergic inputs on basolateral amygdala neurons. *Journal of Neuroscience*, 35:853–863, 1 2015. ISSN 15292401. doi: 10.1523/JNEUROSCI.2706-14.2015.

I. van Welie, A. Roth, S. S. Ho, S. Komai, and M. Häusser. Conditional spike transmission mediated by electrical coupling ensures millisecond precision-correlated activity among interneurons in vivo. *Neuron*, 90:810–823, 5 2016. ISSN 10974199. doi: 10.1016/j.neuron.2016.04.013.

C. P. Vandermaelen and G. K. Aghajanian. Electrophysiological and pharmacological characterization of serotonergic dorsal raphe neurons recorded extracellularly and intracellularly in rat brain slices. *Brain Research*, 289:109–119, 1983.

V. Varga, A. D. Szèkely, A. Csillag, T. Sharp, and M. S. Hajós. Evidence for role of gaba interneurones in the cortical modulation of midbrain 5-hydroxytryptamine neurones. *Neuroscience*, 106:783–792, 2001.

V. Varga, B. Kocsis, and T. Sharp. Electrophysiological evidence for convergence of inputs from the medial prefrontal cortex and lateral habenula on single neurons in the dorsal raphe nucleus. *European Journal of Neuroscience*, 17:280–286, 1 2003. ISSN 0953816X. doi: 10.1046/j.1460-9568.2003.02465.x.

V. Varga, A. Losonczy, B. V. Zemelman, Z. Borhegyi, G. Nyiri, A. Domonkos, B. Hangya, N. Holderith, J. C. Magee, and T. F. Freund. Fast synaptic subcortical control of hippocampal circuits. *Science*, 326:445–449, 10 2009. ISSN 00368075. doi: 10.1126/science.1174481.

M. Vascak, X. Jin, K. M. Jacobs, and J. T. Povlishock. Mild traumatic brain injury induces structural and functional disconnection of local neocortical inhibitory networks via parvalbumin interneuron diffuse axonal injury. *Cerebral Cortex*, 28:1625–1644, 5 2018. ISSN 14602199. doi: 10.1093/cercor/bhx058.

F. X. Vollenweider and K. H. Preller. Psychedelic drugs: neurobiology and potential for treatment of psychiatric disorders. *Nature Reviews Neuroscience*, 21:611–624, 11 2020. ISSN 14710048. doi: 10.1038/s41583-020-0367-2.

F. X. Vollenweider, M. F. I. Vollenweider-Scherpenhuyzen, A. Bäbler, H. Vogel, and D. Hell. Psilocybin induces schizophrenia-like psychosis in humans via a serotonin-2 agonist action. *NeuroReport*, 9:3897–3902, 1998.

D. B. Wainscott, V. L. Lucaites, J. D. Kursar, M. Baez, and D. L. Nelson. Pharmacologic characterization of the human 5-hydroxytryptamine2b receptor: evidence for species differences. *Journal of Pharmacology and Experimental Therapeutics*, 276:720–727, 1996. ISSN 0022-3565.

J. A. Waltz. The neural underpinnings of cognitive flexibility and their disruption in psychotic illness. *Neuroscience*, 345:203–217, 3 2017. ISSN 18737544. doi: 10.1016/j.neuroscience.2016.06.005.

E. T. Weber and R. Andrade. Htr2a gene and 5-ht2a receptor expression in the cerebral cortex studied using genetically modified mice. *Frontiers in Neuroscience*, 4, 2010. ISSN 16624548. doi: 10.3389/fnins.2010.00036.

B. Weissbourd, J. Ren, K. E. DeLoach, C. J. Guenthner, K. Miyamichi, and L. Luo. Presynaptic partners of dorsal raphe serotonergic and gabaergic neurons. *Neuron*, 83:645–662, 8 2014. ISSN 10974199. doi: 10.1016/j.neuron.2014.06.024.

C. L. Wellman, A. Izquierdo, J. E. Garrett, K. P. Martin, J. Carroll, R. Millstein, K. P. Lesch, D. L. Murphy, and A. Holmes. Impaired stress-coping and fear extinction and abnormal corticolimbic morphology in serotonin transporter knock-out mice. *Journal of Neuroscience*, 27: 684–691, 1 2007. ISSN 02706474. doi: 10.1523/JNEUROSCI.4595-06.2007.

J. Wood, Y. Kim, and B. Moghaddam. Disruption of prefrontal cortex large scale neuronal activity by different classes of psychotomimetic drugs. *Journal of Neuroscience*, 32:3022–3031, 2 2012. ISSN 02706474. doi: 10.1523/JNEUROSCI.6377-11.2012.

A. Woodruff, Q. Xu, S. A. Anderson, and R. Yuste. Depolarizing effect of neocortical chandelier neurons. *Frontiers in Neural Circuits*, 3, 10 2009. ISSN 16625110. doi: 10.3389/neuro.04.015.2009.

L. J. Wu, X. Li, T. Chen, M. Ren, and M. Zhuo. Characterization of intracortical synaptic connections in the mouse anterior cingulate cortex using dual patch clamp recording. *Molecular Brain*, 2, 2009. ISSN 17566606. doi: 10.1186/1756-6606-2-32.

J. Yu, H. Hu, A. Agmon, and K. Svoboda. Principles governing the dynamics of gabaergic interneurons in the barrel cortex. *bioRxiv*, 2019. doi: 10.1101/554949.

P. Zhong and Z. Yan. Differential regulation of the excitability of prefrontal cortical fast-spiking interneurons and pyramidal neurons by serotonin and fluoxetine. *PLoS ONE*, 6, 2011. ISSN 19326203. doi: 10.1371/journal.pone.0016970.

P. Zhong, E. Y. Yuen, and Z. Yan. Modulation of neuronal excitability by serotonin-nmda interactions in prefrontal cortex. *Molecular and Cellular Neuroscience*, 38:290–299, 6 2008. ISSN 10447431. doi: 10.1016/j.mcn.2008.03.003.

F.-M. Zhou and J. J. Hablitz. Activation of serotonin receptors modulates synaptic transmission in rat cerebral cortex. *J. Neurophysiol.*, 82:2989–2999, 1999.

S. Zucca, G. D'Urso, V. Pasquale, D. Vecchia, G. Pica, S. Bovetti, C. Moretti, S. Varani, M. Molano-Mazón, M. Chiappalone, S. Panzeri, and T. Fellin. An inhibitory gate for state transition in cortex. *eLife*, 6, 5 2017. ISSN 2050084X. doi: 10.7554/eLife.26177.001.